Scattering Studies of Self-Assembling Processes of Polymer Blends in Spinodal Decomposition

A Dissertation Presented

by

MIKIHITO TAKENAKA

Scattering Studies of Self-Assembling Processes of Polymer Blends in Spinodal Decomposition

A Dissertation Presented

by

MIKIHITO TAKENAKA

Contents

General Introduction

1. Self-assembly in spinodal decomposition

When a system, such as binary fluids, binary metallic alloys or binary polymer mixtures, is quenched from a single-phase state to a two-phase state inside its miscibility gap, concentration fluctuation of the system grows with time in terms of both its spatial scale and amplitude toward a new equilibrium. This unmixing mechanism is classically[1] classified into two different types, depending on the nature of thermodynamic instability to the concentration fluctuation. One is the case when a system is quenched into a metastable region between the coexisting curve and the the spinodal curve. It has the instability only against the large amplitude of the concentration fluctuation which is close to the composition difference between the coexisting composition at a given quench state. This first one is called *nucleation and growth.* The other is the case when a system is quenched inside the spinodal curve. It has the instability even against the infinitesimal amplitude of concentration fluctuations. This second one is called *spinodal decomposition.*

A new structure is self-organized or self-assembled in the system undergoing spinodal decomposition. The self-assembling process, mechanism, dynamics and structure, generally called self-assembly, is generally described by a nonlinear time-evolution equation[2]. The self-assembly in spinodal decomposition of the mixtures is a fascinating subject both from industrial and academic view points. From the industrial view point the study contributes to a development of a methodology to control the self-assembling structures having various spatial scales and various composition difference between two coexisting phases. This development leads to control the physical

properties of materials. From an academic view point, the theoretical and experimental studies of the subject contribute to a development and understanding of nonlinear and nonequilibrium statistical physics[2].

2. General results in earlier studies

Theoretical and experimental investigation have been developed in the field of polymer mixtures[3] as well as of mixtures of small molecules, such as metallic alloys[4], inorganic glasses[5], and simple liquid mixtures[6]. As for the results of earlier studies using the scattering techniques, two main important features were found.

One feature is that the self-assembling process of spinodal decomposition in the critical mixture is divided into three stages, the early stage, intermediate and late stage spinodal decomposition and the other is concerning with scaling laws for the self-assembling structure.

In the early stage spinodal decomposition, the time-evolution of the concentration fluctuation can be described by Cahn's linearized theory[6]. According to the theory,

(i) the scattered intensity at wavenumber q and time t , S(q,t), grows with time exponentially as given by

$$S(q,t) = S(q,t = 0)\exp[2R(q)t]$$

where R(q) is the growth rate of q-Fourier mode. R(q) is given by

$$R(q) = D_{app}(T)q^2\{1 - q^2/[2q_m(0)^2]\}$$

where $D_{app}(T)$ and $q_m(0)$ are the mutual diffusion coefficient and the wavenumber of dominant mode of the concentration fluctuation, respectively.

(ii) The dominant mode of concentration fluctuations has q given by $q=q_m(0)$, for which R(q) becomes maximum. This $q_m(0)$ is constant with time.

The process occuring after this early stage spinodal decomposition is called the later-stage spinodal decomposition which comprises the intermediate stage and the late stage. In the later-stage spinodal decomposition, the phase-separating structure coarsens with time. The coarsening of the structure is characterized by a shift of the peak wavenumber of scattering function $q_m(t)$ toward smaller q and by an increase of the peak intensity of the scattering function $I_m(t)$ with time. $q_m(t)$ is related to $\Lambda_m(t)$, the (characteristic) wavelength of the dominant mode of the phase-separating structure by

$$\Lambda_m(t) = 2\pi/q_m(t).$$

The time-evolution of $q_m(t)$ and that of $I_m(t)$ have been traditionally characterized by scaling law

$$q_m(t) \sim t^{-\alpha},$$

and

$$I_m(t) \sim t^{\beta},$$

where α and β are the scaling exponents characterizing the time evolution of the structure.

In the intermediate stage spinodal decomposition, both the wavelength and the amplitude of the concentration fluctuation grow with time. Hence the exponents α and β have a relationship given by[3]

$$\beta > 3\alpha.$$

In the late stage spinodal decomposition, the amplitude of the concentration fluctuation reaches the equilibrium value determined by the coexistence curve of the blends and the phase separation temperature, but the characteristic wavelength of the concentration fluctuation continues to grow with time. The growth of the concentration fluctuation or structure with time has been found to occur with dynamical self-similarity[7] such that the phase separating structures at different times have statistically identical shape, only their characteristic sizes increasing with time. Thus in this case the phase-separating structures at different times can be scaled with the characteristic length $\Lambda_m(t)$, and the structures scaled with $\Lambda_m(t)$ become statistically identical. In terms of the scattering function, the dynamical self-similarity means that the scaled structure factor F(x,t) defined by

$$F(x,t) \equiv q_m(t)^3 I(x,t)$$

in which

$$x \equiv q/q_m(t)$$

becomes universal with time t. If this dynamical scaling hypothesis is valid, the relation between α and β is given by[3]

$$\beta = 3\alpha.$$

The scaling postulate was proposed by Chou and Goldburg[8] on the time changes of $q_m(t)$ and $I_m(t)$. Reduced dimensionless quantities $Q_m(\tau)$, $\tilde{I}_m(\tau)$ and τ are defined by

$$Q_m(\tau) \equiv q_m(\tau)/q_m(0)$$

$$\tilde{I}_m(\tau)=I_m(\tau;T)q_m(0;T)^3 \Big/ \int_0^{\infty} q^2 I(q,\tau;T)dq \ ,$$

and

$$\tau \equiv t/t_c$$

where

$$t_c = [q^2{}_m(0)D_{app}]^{-1}.$$

If the results obtained at various quench depth fall onto master curves in the reduced plots of Q_m vs. τ and $\tilde{I}_m(\tau)$ vs. τ, then the phase-separating structure is proven to grow according to the same coarsening mechanism at these quench depthes and the difference of the quench depth affects only the time scale [through $t_c(T)$] and spatial scale [through $q_m(0)$] of the phase-separating structure. This results is called dynamical scaling postulate.

3. Unique features of polymer mixtures

Linear polymers consist of many monomer units (corresponding to small-molecules) connected by covalent bonds and hence they have usually the large size of order of 100 Å. This fact gives polymer mixtures such unique features as follows which do not exist in small-molecule systems;

(i) The spatial scale ($1/q_m(t)$ or $\Lambda_m(t)$) of the concentration fluctuation developed by spinodal decomposition in polymer mixtures is larger than that in small-molecule mixtures when the two kinds of the mixtures are compared for the same quench depth and at the same reduced time[9].

(ii) The characteristic time t_c of spinodal decomposition in polymer mixtures is larger than that in the small-molecule mixtures[9].

(iii) Static and dynamical behavior of polymer mixtures, such as Flory-Huggins theory, can be adequately described by the mean-field theory even near critical point[10]. However the static and kinetic behavior of small-molecule mixtures can not be adequately described by the mean-field theory, such as the theory of van der Waals or the Bragg-Williams approximation, near critical region. This is because the Ginzburg criterion[10] for the critical region is much narrower in polymer mixtures than in small molecule mixtures. As an example of static behavior of the mixtures in one-phase region, the scattering intensity at q=0, S(q=0), and the thermal correlation length ξ diverge according to the scaling laws given by

$$S(q=0) \sim |1-T/T_c|^{-\gamma}$$

and

$$\xi \sim |1-T/T_c|^{-\upsilon},$$

where T_c is the critical temperature of the mixture. The exponents γ and υ are 0.63 and 1.26, respectively, in the critical region for the systems three-dimensional kinetic Ising universality class[11], whereas they are 0.5 and 1.0, respectively, for the systems belonging to the mean-field universality class.

(iv) In polymers with high molecular weight, the molecular entanglements cause a unique molecular-weight dependence of the parameters characterizing their physical properties. For examples, viscosity η is proportion to $M^{3.4}$, and self-diffusion constant is proportion to M^2 in the case of $M>M_e$, where M is the molecular weight of polymers and M_e is that between the entanglements[12].

(v) The effect of hydrodynamic interactions on the coarsening of the phase-separating domains, introduced by Kawasaki and Ohta[13] and Siggia[14] tends to be suppressed at least in the initial stage of the spinodal decomposition because of high viscosity resulting from entanglement coupling[15].

The features (i) and (ii) facilitate in-situ or real-time observation of the self-assembling process with light scattering and optical microscopy even at an initial stage of the spinodal decomposition, the feature (iii) makes the theoretical treatment of kinetics of the spinodal decomposition easy, and the features (iv) and (v) are expected to give the kinetics of the spinodal decomposition new aspects.

4. Objectives and contents of this thesis

Taking advantages of studying polymers which have those unique features (i) to (v) as described above, I would expect to find features common for dynamics of spinodal decomposition in polymer systems and that in small-molecules systems (*universality*) and features unique to polymer systems (*polymer effects*).

The fundamental study of the *universality* and the *polymer effects* would contribute to a progress of nonlinear and nonequilibrium statistical physics in the field of polymer and small-molecules systems as well as to a progress of technology in terms of controlling the physical properties of polymeric materials.

Hence I aimed to study the *universality* and the *polymer effects* on kinetics of spinodal decomposition of some polymer mixtures by using time-resolved light-scattering.

This thesis has three main parts. Part I consists of chapters 1 and 2 concerning with time-evolution of the interfacial structure in the spinodal decomposition of polymer mixtures with a near critical composition. Part II

consists of chapters 3 and 4 for molecular-weight dependence on kinetics of the spinodal decomposition with near critical mixtures. A unique feature (polymer effect) in the Chou-Goldburg scaling postulate will be discussed in chapter 4. Part III consists of chapters 5 and 6, concerned with a polymer effect of the kinetics in the spinodal decomposition of the polymer mixtures with off-critical compositions.

The parameters characterizing the phase separating structure in the late stage was found to be divided into two kinds. One is the parameters characterizing the global structure of phase separating structure such as $q_m(t)$ and $I_m(t)$. The other is those characterizing the interfacial structure. In chapter 1, I investigated the time-evolution of the interfacial structure, such as the interfacial thickness $t_I(t)$ and the interfacial area density $\Sigma(t)$ of the phase-separating structure in the late stage of spinodal decomposition, at a particular phase separation temperature. As a result of this investigation, the parameters of the interfacial structure, $\Sigma(t)$ and $t_I(t)$, are found to be characterized by

$$\Sigma(t) \sim t^{-\gamma}$$

and

$$t_I(t) \sim t^{-\delta},$$

and the late stage of spinodal decomposition is subdivided into two regions, the late stage I and the late stage II. In the late stage I, the time-evolution of the interfacial area density $\Sigma(t)$ does not scale with that of global the parameter $q_m(t)$ i.e., the exponent γ is larger than α and the scaled structure factor are found to be nonuniversal at higher x ($x \geq 2$). In the late stage II, the time-evolution of the local structure i.e., $\Sigma(t)$ is found to obey the same scaling law as that of the global structure, i.e. $q_m(t)$, The exponents γ and α become identical, the scaled structure factor become universal even at higher

x, and the true self-similar growth is attained. The universal scaled structure factor obtained in the late stage II then is compared with that obtained from the results of a theory[16] and a computer simulation[17].

In chapter 2 the time-evolution of the interfacial structure at a given temperature was further explored as a function of temperature. The validity of the dynamical scaling postulate[8] on the time changes of the interfacial structure, $\Sigma(t)$, was examined at various temperatures. The universal scaled structure factor in the late stage II was investigated at various temperatures and was found to be independent of temperature. The experimental result of $Q_m(\tau)$ and the scaled structure factor in the late stage II were compared with those obtained by computer simulation[18].

In chapter 3 effects of the molecular weight on early stage spinodal decomposition was discussed. The kinetics of the early stage spinodal decomposition was investigated as a function of molecular weight using a particular mixtures in which one component has a fixed molecular weight but the other has different molecular weights. The experimental result was analyzed with the linearized theory[6] and the characteristic parameters characterizing the early stage of spinodal decomposition were obtained as a function of molecular weight. By analyzing these parameters, the transport mechanism in the early stage of spinodal decomposition were explored.

In chapter 4 effects of molecular weight on later-stage of spinodal decomposition was discussed. The coarsening behavior of four mixtures which is used in chapter 3 were investigated. The time changes of $q_m(t)$ and $I_m(t)$ of the mixtures were subjected to the reduced plot to examine the validity of the dynamical scaling postulate. For each mixture the reduced quantities $Q_m(\tau)$ and $\tilde{I}_m(\tau)$ obtained at different quench depthes were found to fall onto correspomding master curves on the reduced plot. However those master curves obtained for the mixtures with different molecular weights were found not to fall onto a master curve but rather shows a branching on

the reduced plot (*N-branching*) indicating that the scaling postulate is not valid for the systems with different molecular weight.

The study of the self-assembly was further extended to off-critical mixtures. In chapter 5 I investigated the coarsening behavior in the spinodal decomposition of the off-critical polymer mixtures with high molecular weights. I found *spontaneous pinning* on growth of the self-assembling structure. This is a new phenomenon that the wavelength of the dominant mode of concentration fluctuation does not continue to increase as found for the critical mixture but rather stops increasing and becomes constant at $t>t_p$, time for the pinning. The spontaneous pinning in the coarsening behavior was investigated as a function of the composition of mixtures and the phase separation temperature. The pinning was proposed to be associated with the dynamical percolation-cluster transition and with the extremely slow growth of the cluster structure due to a heavily suppressed mutual diffusion process as will be discussed in detail in the text.

In chapter 6, the time change of the scaled structure factors of the off-critical polymer mixtures discussed in chapter 5 were investigated. The scaled structure factor was found to be nonuniversal with time, and the nonuniversality was analyzed as a function of phase separation temperature and composition of the mixtures. The time change in the scaled structure factor before and after the pinning suggested that the dynamical percolation-cluster transition occurs in the coarsening process.

References

1 J.W. Cahn, and J.E. Hilliard, J.Chem.Phys., **28**, 258(1958); J.W. Cahn, ibid., **30**, 1121(1959); J.W. Cahn, and J.E. Hilliard, ibid., **31**, 688(1959)

2 J. D. Gunton, M. Miguel and P. P. Sahni, *Phase Transition and Critical Phenomena*, edited by C. Domb and J. L. Lebowitz (Academic Press, N.Y., 1983), Vol. 8, p. 269.

3 T.Nose,Phase Transitions, **8**, 245(1987).
T. Hashimoto, Phase Transitions, **12**, 47 (1988).

4 S.Komura, K.Osamura, H.Fujii and T.Takeda, Phys.Rev.B **31**,1278 (1985).

5 A.F.Craievich, J.M.Sanchez, and C.E.Williams, Phys.Rev.B **34**,2762 (1986).

6 J. W. Cahn, J.Chem.Phys. **42**, 93 (1965).

7 K. Binder and D. Stauffer, Phys.Rev.Lett. **33**, 1006 (1974).
K. Binder, Phys.Rev. **B15**, 4425 (1977).
H. Furukawa, Phys.Lett.Sect. **A98**, 28 (1983).

8 Y. C. Chou and W. I. Goldburg, Phys.Rev.A **20**, 2105 (1979).
Y. C. Chou and W. I. Goldburg, Phys.Rev.A **23**, 858 (1980).

9 P. G. de Gennes, *Scaing Concepts in Polymer Physics*, Ithaca, Cornell University Press, (1979).

10 K.Binder, J.Chem.Phys., **79**, 6387 (1983).

11 H.L. Stanley, *Phase Transitions and Critical Phenomena*, Oxford University Press, New York, (1971).

12 M. Doi and S. F. Edwards, *The Theory of Polymer Dynamics*, Clarendon Press, London, (1986).

13 K. Kawasaki, Progr.Theor.Phys. **57**, 826 (1977).
K. Kawasaki and T. Ohta, Progr.Theor.Phys. **59**, 362 (1978).

14 E. D. Siggia, Phys.Rev.A **20**, 595 (1979).

15 T.Takebe, R.Sawaoka and T.Hashimoto, J.Chem.Phys. **91**, 4369(1989)

16 T. Ohta and H. Nozaki, in the book of *Space-Time Organization in Macromolecular Fluids*, edited by F. Tanaka, M. Doi and T. Ohta (Springer, Berlin, 1989), p. 51-57.

17 A. Chakrabarti, A. Toral, J. D. Gunton and M. Muthukumar, Phys.Rev.Lett. **63**, 2072 (1989).

18 T. Koga and K. Kawasaki, Phys.Rev.A. **44**, R817 (1991).

Chapter 1 : Ordering Process of Polymer Blends via Spinodal Decomposition -Dynamical Scaling on Global and Local Structure

1-1. Introduction

The mechanism and dynamics of spinodal decomposition (SD) processes of polymer blends have been extensively investigated from both theoretical[1] and experimental[2] sides. We have classified the SD of a critical mixture of polystyrene (PS) and poly(vinylmethylether) (PVME) into three stages which we named early, intermediate, and late[3]. The spatial composition distributions in these stages for a mixture of polymer A and B are shown in Figure 1-1, where ϕ_A is the composition of polymer A. In the early stage, the composition distribution is well described by the linearized theory[4,5,6]. The wavelength $\Lambda_m(t)$ of the dominant mode of composition variation is essentially independent of time t, while the amplitude of composition fluctuation, $\Delta\phi_A(t)$, grows exponentially with increasing t. The quantitative definition of $\Lambda_m(t)$ is given below. The composition fluctuation continuously grows as time goes on, and nonlinear effects become important. Thus, there occurs an increase in $\Lambda_m(t)$ (from Λ_1 to Λ_2 in Figure 1-1)[7,8]. We called this stage of SD the later stage. It can be divided into two substages, intermediate and late. In the intermediate stage, the growth of $\Delta\phi_A$ is substantial, but its rate is progressively suppressed and eventually becomes negligible. In this last state, $\Delta\phi_A$ is no longer distinguishable from its equilibrium value $\Delta\phi_e$ determined by the coexistence curve[9], and the system enters the late stage. In this stage, well-defined interfaces develop between two coexisting phases having the equilibrium compositions, and $\Lambda_m(t)$ characterizing the global size of the structure thus self-assembled increases with time.

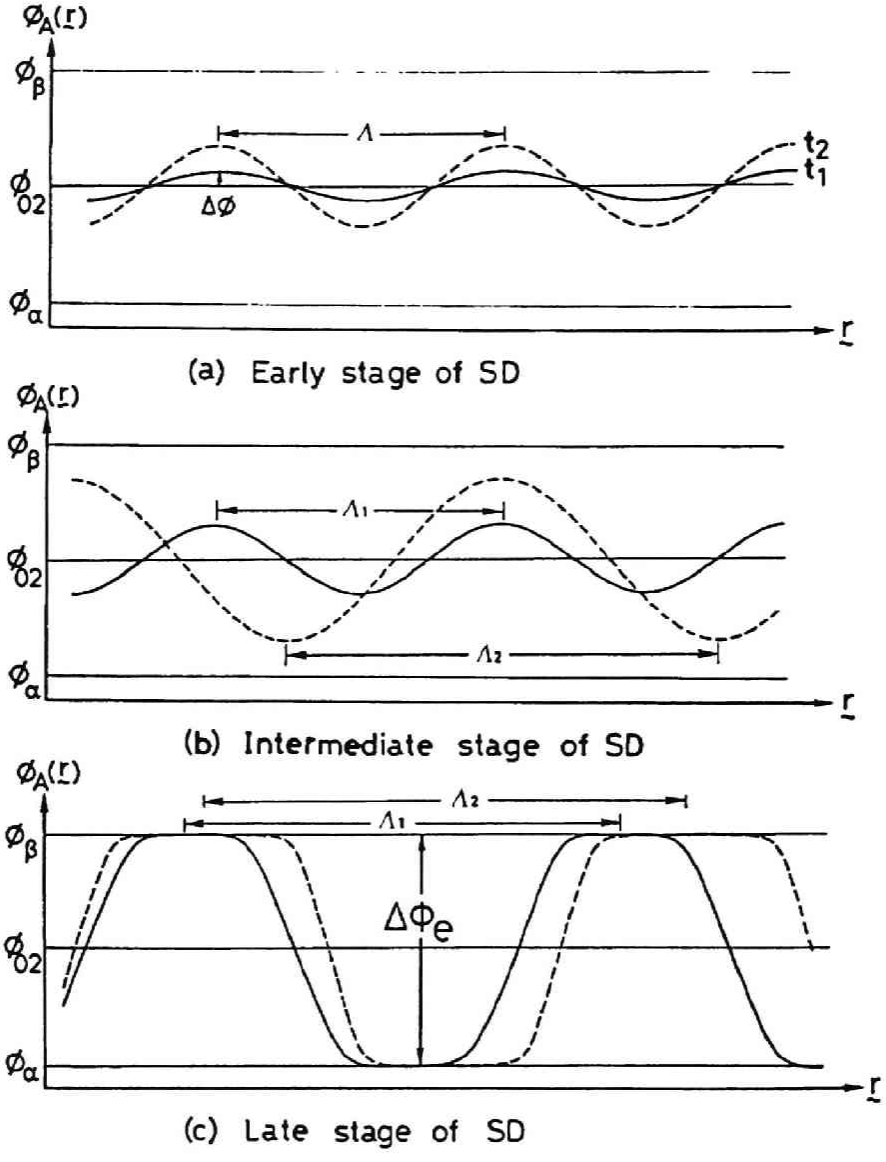

Fig.1-1. Schematic diagram showing the spatial segmental density profile of component A in early (a), intermediate (b), and late stage (c) of spinodal decomposition.

As usual, we define $\Lambda_m(t)$ by $2\pi/q_m(t)$, where $q_m(t)$ is the scattering vector q at which the scattered intensity I(q, t) shows a maximum $I_m(t)$. It can be shown by scaling analysis of $q_m(t)$, $I_m(t)$ and the scaled structure factor F(x, t) that if SD reaches the stage where F(x, t) for different t are superimposable (i.e., universal for t) over the entire range of x, the following relation holds:

$$\beta = 3\alpha. \tag{1-1}$$

Here, α and β are the exponents defined by

$$q_m(t) \sim t^{-\alpha} \tag{1-2}$$

$$I_m(t) \sim t^{-\beta} \tag{1-3}$$

and F(x, t) is defined by

$$F(x) \equiv I(q,t)q_m(t)^3 \tag{1-4}$$

with

$$x \equiv q/q_m(t). \tag{1-5}$$

As usual, q is defined as $q = (4\pi/\lambda) \sin(\theta/2)$, with λ and θ being the wavelength in the medium and the scattering angle, respectively.

Our data on the time-evolution of self-assembled structure at q comparable to $q_m(t)$, i.e., $x \sim 1$, for the critical mixture of PS and PVME were consistent with those reported for other polymer mixtures[1,10,11,12,13,14]. The study reported in this paper was undertaken to look at the scattering behavior of a spinodal-decomposing polymer blend over a longer period of

time and a wider range of x than before. It is expected that data from such work makes a more rigorous check of Eq 1-1 possible and those at large x provide information about how the mean radius $R_m(t)$ of wavy phase-phase interfaces and the interface thickness $t_I(t)$ (see Figure 1-2) vary with time in the late stage of SD. We note that $R_m(t)$ is proportional to the inverse of the interfacial area density $\Sigma(t)$.

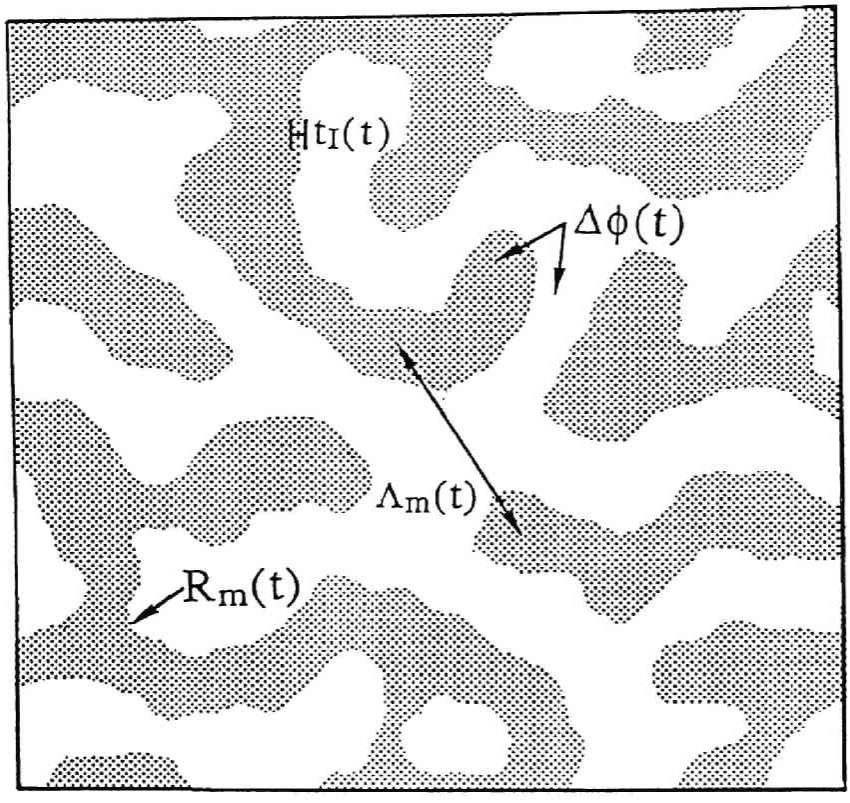

Fig.1-2. Model for the self-assembling process in the late stage. The model involves various length scales such as $\Lambda_m(t)$, $R_m(t)$ (or $1/\Sigma(t)$), and $t_I(t)$, where $\Lambda_m(t)$ is the wavelength of the dominant mode of the concentration fluctuations, $R_m(t)$ is the mean radius of wavy interfaces, $\Sigma(t)$ is the interfacial area density, and t_I is the characteristic interface thickness.

1-2. Experimental

A binary mixture of polybutadiene (PB) and polyisoprene (PI) with a near critical composition (50/50 wt/wt) was chosen for this work. Molecular characteristics of PB and PI are summarized in Table I. The polymer mixture was dissolved in toluene to prepare a homogeneous solution containing 10 wt % polymer. The solution was first filtered through a Milipore film having an average pore size of 0.2μm, and then cast to thin films in a petri dish by evaporating solvent slowly for four days. Each film obtained was further dried in a vacuum oven at room temperature until its weight became constant (about three days were needed). The as-cast film thus prepared was transferred onto a glass plate of 0.5 mm thick and 13 × 13 mm^2 wide, degassed under vacuum at room temperature for about 12 h, and seal-covered with a glass plate. Both PB and PI had N/N_e about 20, where N and N_e are the polymerization degrees of the polymer chain and the chain between entangling points, respectively[15].

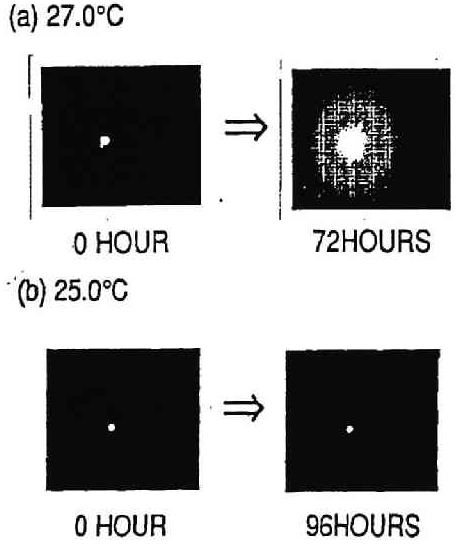

Fig.1-3. Scattering pattern leading to determination of the spinodal temperature.

Table 1-I. Molecular characteristics of polybutadiene (PB) and polyisoprene (PI) used for this study.

Sample Code	$M_w \times 10^{-4}$	M_w/M_n[a)]	Microstructure[b)]			
			cis-1,4	trans-1,4	1,2	3,4
PB	5.8	1.2	28	56	16	-
PI	10.1	1.3	70.4	22.1	-	7.5

a) measured using size exclusion chromatography equipped with a light scattering apparatus.
b) measured by IR spectroscopy.

Our polymer mixture was found to show phase separation behavior of the LCST (the lower critical solution temperature) type, with the spinodal temperature $T_S = 26 \pm 1$ °C. This T_S was determined from the following observations. Temperature jump to T = 25° C from a lower temperature caused no measurable increase in scattered intensity over a period of time up to 4 days (see Figure 1-3b), while there appeared a spinodal ring at $q_m = 1.0 \times 10^{-4}$ nm^{-1} three days after the temperature jump to 27 °C (Figure 1-3a). The data reported below are concerned with the SD behavior of our polymer blend observed by the previously described time-resolved light scattering method for a temperature jump from 25 to 33 °C, i.e., for a quench depth of $\Delta T_S \equiv T - T_S = 7$ °C.

1-3. Experimental results

Time-evolution of light scattering profiles after the temperature-jump mentioned above is shown in Figure 1-4, where part b concerns the change from the early to the intermediate stage of SD and part a the change from the intermediate to the late stage. An intensity maximum appears some time after the onset of SD, and it shifts toward smaller q while the peak intensity increases. The early stage SD went on for about 20 min or about 2 in the reduced time τ, which is defined below by eq 9.

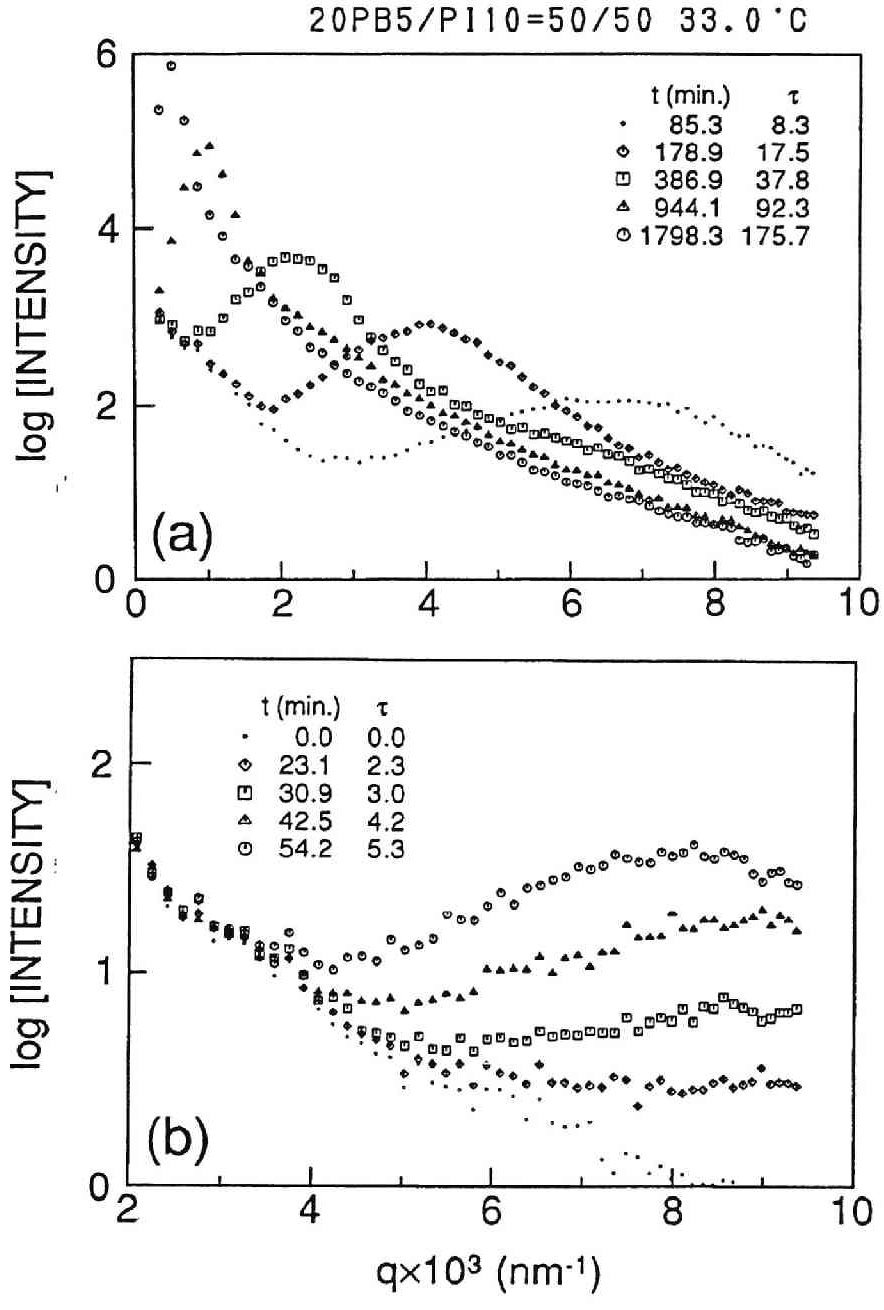

Fig.1-4. Time-evolution of light scattering profiles after a temperature jump from 22°C in the single phase state to 33°C inside the spinodal phase boundary; $\varepsilon_T = |1/T-1/T_S|/(1/T_S) = 2.29\times10^{-2}$. (a) the late stage and (b) the early and intermediate stages. The intensity is in arbitrary unit.

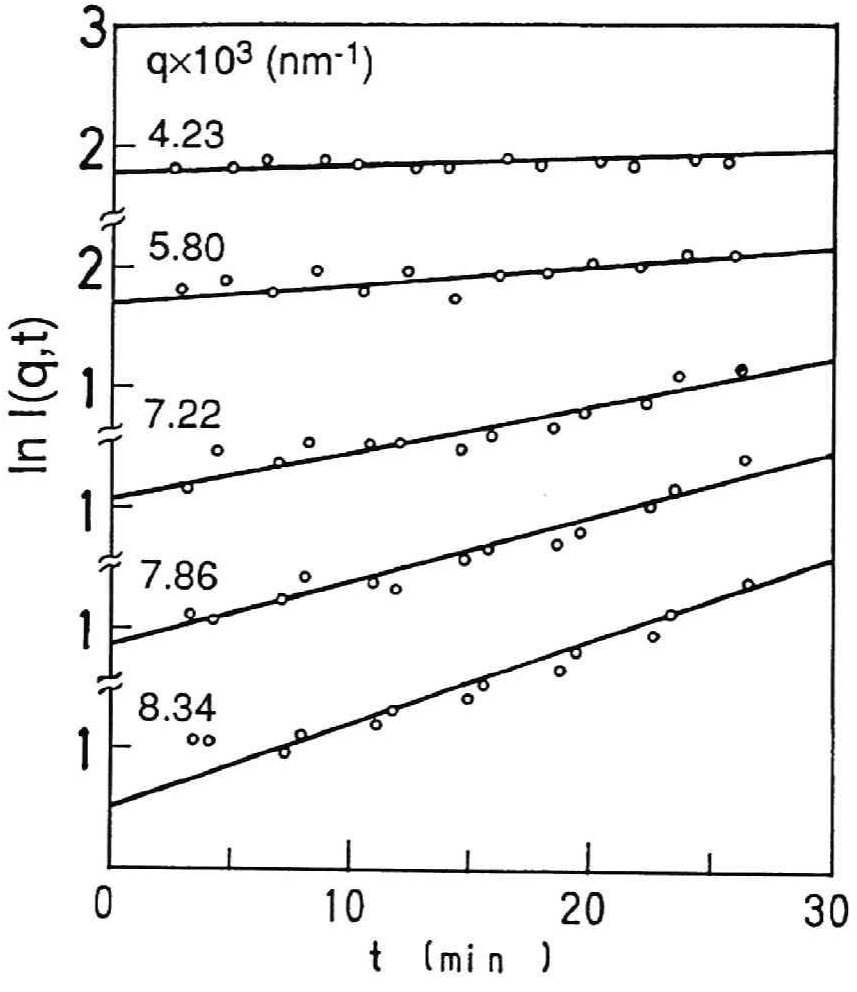

Fig.1-5. ln I(q,t) vs. t in the early stage SD at various scattering vectors q. The intensity I is in arbitrary unit.

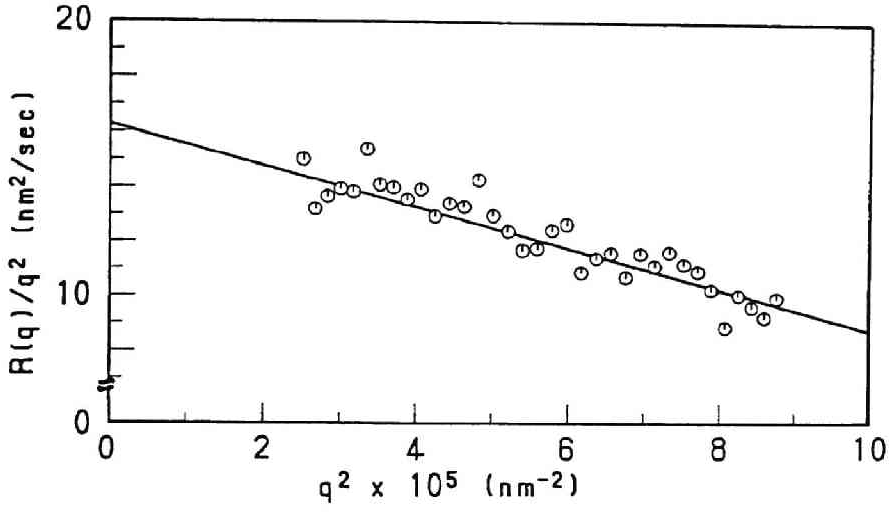

Fig.1-6. Plots of $R(q)/q^2$ vs q^2, where R(q) is the growth rate of the q-Fourier mode of fluctuations in the early stage SD.

Figure 1-5 shows time changes in the scattered intensity I(q, t) at various q values in the early stage SD. It is seen that ln I(q, t) at fixed q increases linearly with t at a q-dependent growth rate R(q), yielding

$$I(q, t) = I(q, 0)\exp[2R(q)t]. \qquad (1\text{-}6)$$

This behavior agrees with the prediction from Cahn's linearized theory[4]. Departure of the data points from Eq 1-6 after some period of time reflects nonlinear effects which arise from the increased amplitude of composition fluctuation.

Figure 1-6 illustrates $R(q)/q^2$ plotted against q^2, and the behavior of the data points is consistent with the theoretically predicted relation

Table 1-II. Characteristic parameters for spinodal decomposition

$q_m(0)$[a] (nm^{-1})	D_{app}[b] (nm^2/s)	t_c[c] (s)	$t_{cr,1}$[d] (s)	$t_{cr,2}$[e] (s)	$\tau_{cr,1}$[f]	$\tau_{cr,2}$[g]
1.0×10^{-2}	16.3	613	9.2×10^3	5.5×10^4	15	90

a) wavenumber of the dominant mode of fluctuations in the early stage SD as determined from $R(q)/q^2$ vs. q^2.
b) collective diffusivity in the early stage SD as determined from $R(q)/q^2$ vs. q^2.
c) characteristic time for the early stage SD, $t_c = [q_m^2(0)D_{app}]^{-1}$.
d) crossover time from the intermediate stage to the late stage I.
e) crossover time from the late stage I to the late stage II.
f) reduced crossover time $\tau_{cr,1} \equiv t_{cr,1}/t_c$.
g) reduced crossover time $\tau_{cr,2} \equiv t_{cr,2}/t_c$.

$$R(q)/q^2 = D_{app}\{1 - q^2/[2q_m(0)^2]\}. \qquad (1\text{-}7)$$

Table II shows the values of the characteristic parameters D_{app} (the collective diffusivity) and $q_m(0)$ determined by fitting Eq 1-7 to the data of Figure 1-6. This table also gives the value of the characteristic time t_c defined by

$$t_c = [q_m^2(0)D_{app}]^{-1}. \qquad (1\text{-}8)$$

In Figure 1-7, the time changes in $q_m(t)$ and $I_m(t)$ are shown. Hear, the arrow for $t_{cr,1}$ indicates the crossover between the intermediate stage in which β was larger than 3α and the late stage in which β became equal to 3α (actually, these conditions are our definition for the intermediate and late stages). Table 1-II includes the value of $t_{cr,1}$. The arrow for another crossover time $t_{cr,2}$ points to the boundary between the late stage I and the late stage II, which are defined in the following section. At the longest time limit that could be attained by the present experiment, the exponent α reached 0.92. We believed the system would ultimately go into the regime where α is equal to unity. In fact, we have observed this regime at higher temperatures[16].

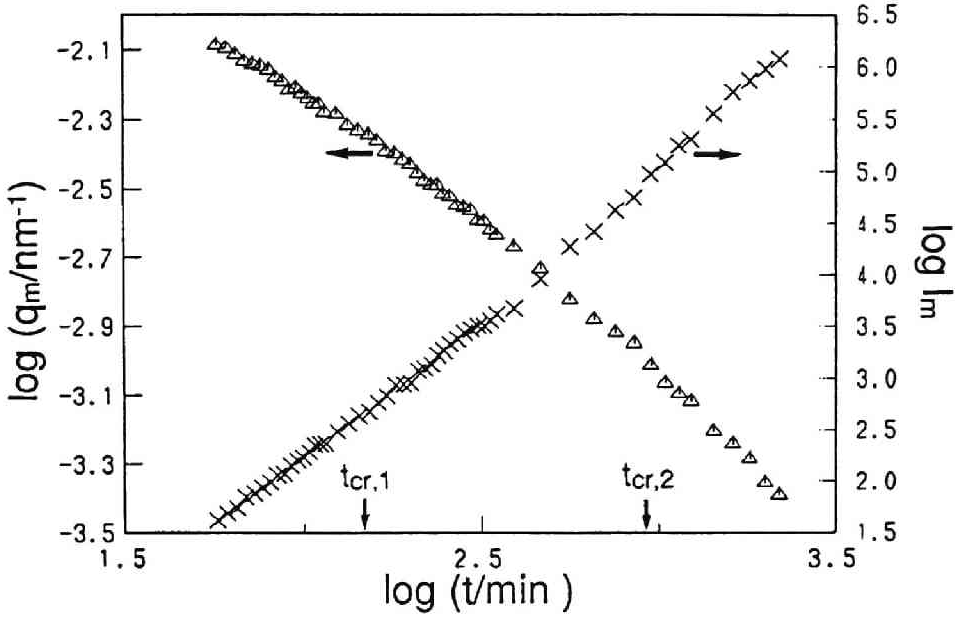

Fig.1-7. Time changes in the peak wavenumber $q_m(t)$ and the peak scattered intensity $I_m(t)$.

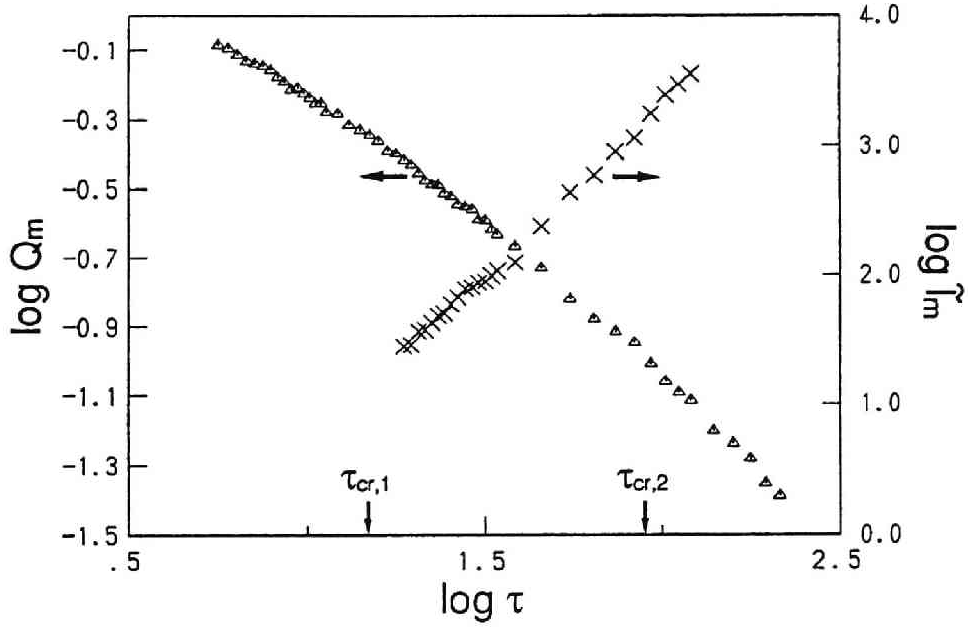

Fig.1-8. Reduced wavenumber Q_m and reduced scattered intensity $\tilde{I}_m$ plotted against reduced time τ .

1-4. Scaling analysis

The time changes in $q_m(t)$ and $I_m(t)$ are replotted in Figure 1-8 using the reduced variables defined by

$$\tau \equiv t/t_c \ , \tag{1-9}$$

$$Q_m(\tau) \equiv q_m(\tau)/q_m(0) \ , \tag{1-10}$$

$$\tilde{I}_m(\tau) = I_m(\tau) q_m(0)^3 / \int_{q'}^{q''} I(q, \tau) q^2 dq \ , \tag{1-11}$$

where q' and q" denote the q values at which I(q, t) almost vanishes. The arrows in the figure indicate the reduced times $\tau_{cr,1}$ and $\tau_{cr,2}$ corresponding to $t_{cr,1}$ and $t_{cr,2}$, respectively, and give $\tau_{cr,1} \simeq 15$ and $\tau_{cr,2} \simeq 90$. In the time scale of our experiment, α varied from 0.56 to 0.92 and β from 2.4 to 2.8 as τ increased. In the long time limit of SD, the theory predicts either $\alpha = 1/3$ and $\beta = 1$ (bulk diffusion) or $\alpha = 1/4$ and $\beta = 3/4$ (surface diffusion) in the nonhydrodynamic regime, and $\alpha = 1$ and $\beta = 3$ in the hydrodynamic regime[1]. Thus, our results suggest that, in the period from the intermediate stage to an early time of the late stage I, the hydrodynamic interaction is less significant, while, in the late stage II, the system enters the hydrodynamic regime.

Figure 1-9 presents the data for the scaled structure factor F(x, t) (Eq. 1-4) in the intermediate stage (a), the late stage I (b) and the late stage II (c). The scattered intensity I(q, t) can be generally expressed as

$$I(q, t) \sim \langle \eta^2 \rangle \Lambda_m(t)^3 S(x, t) \tag{1-12}$$

where $\langle \eta^2 \rangle$ is the mean square of refractive index fluctuations and S(x, t) is a scaling function which varies between zero and unity when x is increased from zero to infinity. This characterizes the q dependence of the scattered

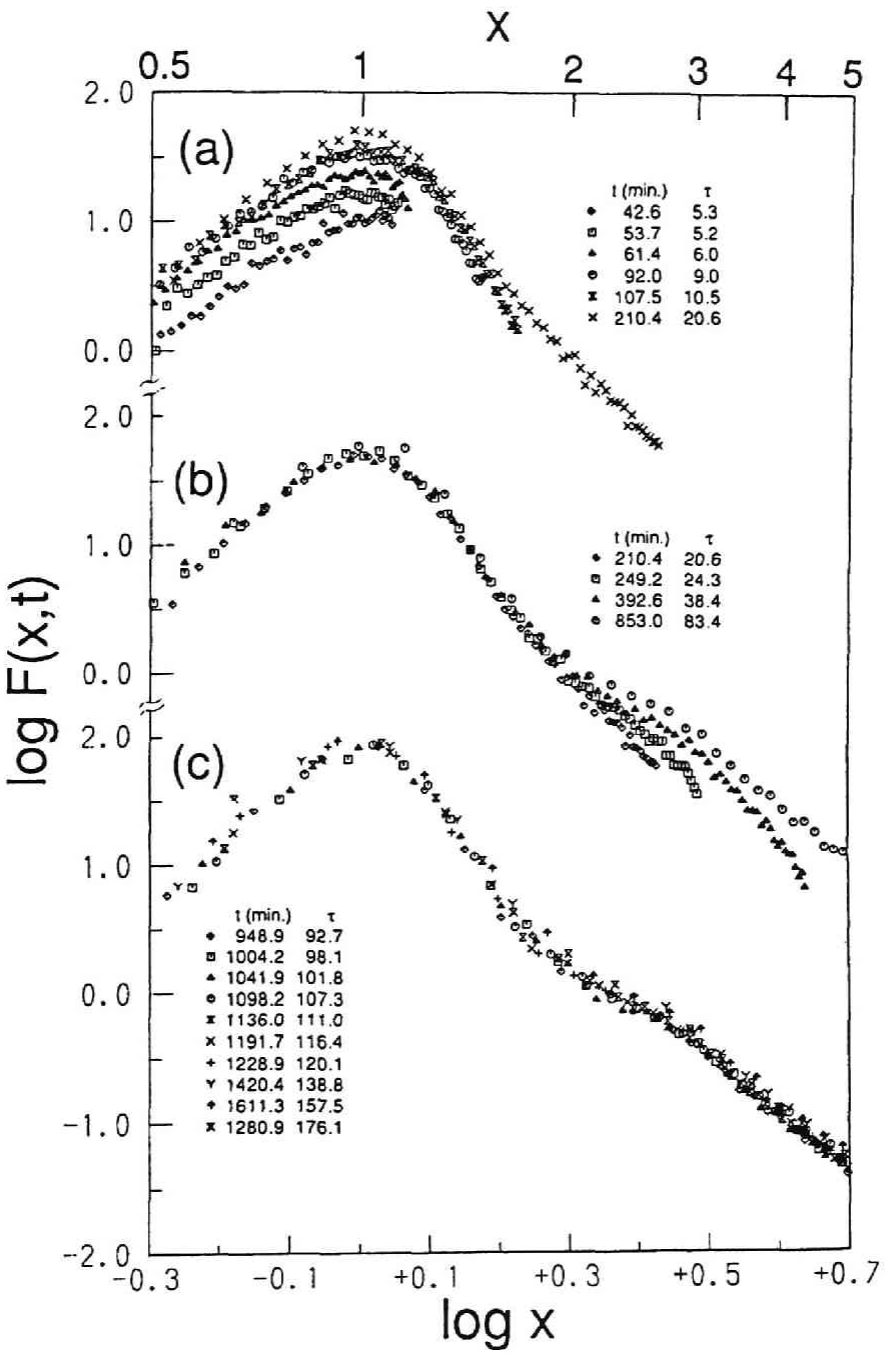

Fig.1-9. Scaled structure factor F(x, t) in (a) intermediate stage, (b) late stage I, and (c) late stage II.

intensity and hence the pattern self-assembled during SD. $\langle\eta^2\rangle$ is proportional to $\Delta\phi(t)^2$ and can be experimentally determined from the integrated scattered intensity,

$$\langle\eta^2\rangle = \int_{q'}^{q''} I(q, t)q^2\, dq \quad .$$

The scaling function may generally depend on time, because the self-assembling pattern may change with time. However, in the late stage SD in which the pattern grows with the dynamical self-similarity, the function becomes independent of time.

Comparing Eq 1-12 with Eq 1-4 and noting the definition of $q_m(t)$, we find that the scaling function S(x, t) is related to F(x, t) by

$$F(x, t) = \langle\eta^2\rangle\, S(x, t) \, . \qquad (1\text{-}13)$$

In the intermediate stage F(x, t) increases with time, primarily due to an increase of $\Delta\phi(t)^2$ and hence $\langle\eta^2\rangle$. At the same time F(x, t) becomes sharper with increasing time. This sharpening is clearly observed by vertically shifting the profiles F(x, t) at different times. The sharpening of F(x, t) reflects that of S(x, t). Thus, in the intermediate stage, $\langle\eta^2\rangle$ increases and S(x, t) becomes sharper with time, so that F(x, t) becomes nonuniversal with time.

Figure 1-9(b) shows that when SD enters the late stage, F(x, t) at x comparable to 1 becomes time-independent. This implies that the global structure corresponding to $q \simeq q_m(t)$ becomes scalable with a single time-dependent length parameter $\Lambda_m(t)$ $(= 2\pi/q_m(t))$. However, this figure reveals that F(x, t) for x above 2 (i.e., $q > 2q_m(t)$) differs for different t. We define the late stage I as the interval of time in which F(x, t) for high q remains unscalable with $\Lambda_m(t)$ only. Thus, though self-similar globally, the self-assembled structure at different times is not yet self-similar locally. Figure

1-9(c) shows that F(x, t) at $\tau > 90$ turned to be scalable only with $\Lambda_m(t)$ over the entire range of x covered in the present work. We define the late stage II as the time interval in which this complete universality of F(x, t) is observed.

Interestingly, F(x, t) in the late stage exhibits a shoulder or a second order maximum at $x \simeq 3$. In another work on a mixture of PB and styrene-butadiene random copolymer (SBR), we observed a similar shoulder in F(x, t) at $x \simeq 2$ [17,18]. We tentatively consider that such a shoulder has something to do with a local structure probably consisting of stacked lamella type domains. According to this idea, depending on whether the effective volume fractions of A-rich and B-rich domains are 50/50 or deviate from them, the shoulder should appear at either $x \simeq 3$ or $x \simeq 2$ [19,20]. We note that the shoulder was found, almost at the same time, experimentally by Nose[21] and Bates and Wiltzius[22], and predicated by simulations by Puri and Ohno[23] and Chakrabarti et al.[24], and theoretically by Ohta and Nozaki[25].

In the late stage I, if the data for F(x, t) at $x > 2$ are fitted to a relation

$$F(x, t) \sim x^{-n}, \qquad (1\text{-}14)$$

the exponent n decreases from 7.2 to 4 with increasing time. This is a kind of dynamical crossover. A similar change in n is expected to occur for F(x, t) at a given time when x is increased. This may be referred to spatial crossover. In fact this spatial crossover is confirmed in the late stage II. The origin of these crossover phenomena has been discussed elsewhere[18].

Bates and Wiltzius[22] studied the SD on a nearly symmetric critical mixture of deuterated and protonated polybutadiene, and divided the observed process into four stages: early, intermediate, transition and final. It is worth comparing their four stage classification with ours, early, intermediate, late I, late II.

(i) In both, the early stage ($0 < \tau < 2$ in our case) refers to the time interval in which the SD dynamics follows Cahn's linearized theory.

(ii) In both, the relation $\beta > 3\alpha$ ($\alpha \sim 0.77$ and $\beta \sim 2.5$ in our system) holds in the intermediate stage ($2 < \tau < 15$ in our case). In the experiment of Bates and Wiltzius, α depends on phase separation temperature, so that plots of $Q_m(\tau)$ vs τ at different temperatures do not fall on a single curve, differing from our PB/PI mixture for which they definitely fell onto a master curve.

(iii) Either in our late stage I ($15 < \tau < 89$) or in the Bates-Wiltzius transition stage ($15 < \tau < 200$), the amplitude of concentration fluctuation reaches equilibrium. However, in the former, the relation $\beta = 3\alpha$ holds ($\alpha = 0.91 \sim 0.92$ and $\beta = 2.7 \sim 2.8$), while, in the latter, β is still larger than 3α and, in addition, α is not only independent of temperature but also surprisingly as small as 0.28. Bates and Wiltzius consider that even after the amplitude of composition fluctuation reaches equilibrium, the interface thickness is initially comparable to $\Lambda_m(t)$ and decreases to an equilibrium value while $\Lambda_m(t)$ increases. This substantial decrease in the interface thickness must have considerable effect on the dynamics in which the global structure is self-assembled during SD and hence on the relation between α and β. Thus, Bates and Wiltzius conclude that the relation $\beta = 3\alpha$ will not be established soon after the amplitude of composition fluctuation reaches equilibrium. We directly evaluate the interface thickness as a function of time and found it to be about 350 nm in the initial period of the late stage I. This value is only one seventh the value of $\Lambda_m(t)$ at the same time, suggesting that the local dynamic process toward the equilibrium interface does not much affect the self-assembling of the global structure so that the relation $\beta = 3\alpha$ will hold to a good approximation once the amplitude of composition fluctuation reaches equilibrium.

Thus, our late stage I is not always the same as what Bates and Wiltzius call the transition stage.

(iv) Our late stage II ($89 < \tau < 210$) and the final stage of Bates and Wiltzius are the same thing. In both, SD is characterized by a single length parameter $\Lambda_m(t)$, and the composition distribution self-similariy varies with time, with its amplitude maintained at the equilibrium value.

(v) Finally, though interesting, the paper of Bates and Wiltzius did not go into a detailed discussion either the time change in the scaled structure factor F(x, t) or the nonuniversality of F(x, t) at large $x \geq 2$. Thus, it is difficult to judge there is a one-to-one correspondence between our late stage I and their transition stage.

1-5. Time evolution of interface structure

The scattered intensity I(q, t) at large q for a self-assembled structure with a diffuse interface approaches the so-called Porod region, in which we have

$$I(q, t) \sim \langle \eta(t)^2 \rangle \Sigma(t)\, q^{-4} \exp[-\sigma(t)^2 q^2] \qquad (1\text{-}15)$$

Here, $\sigma(t)$ is a time-dependent parameter characterizing the spread of the segmental density profile $\rho(z)$ across the interface, which is described by

$$\rho(z) = \rho_o(z) * h(z) \qquad (1\text{-}16)$$

with

$$h(z) = (2\pi\sigma^2)^{-1/2} \exp(-z^2/2\sigma^2) \qquad (1\text{-}17)$$

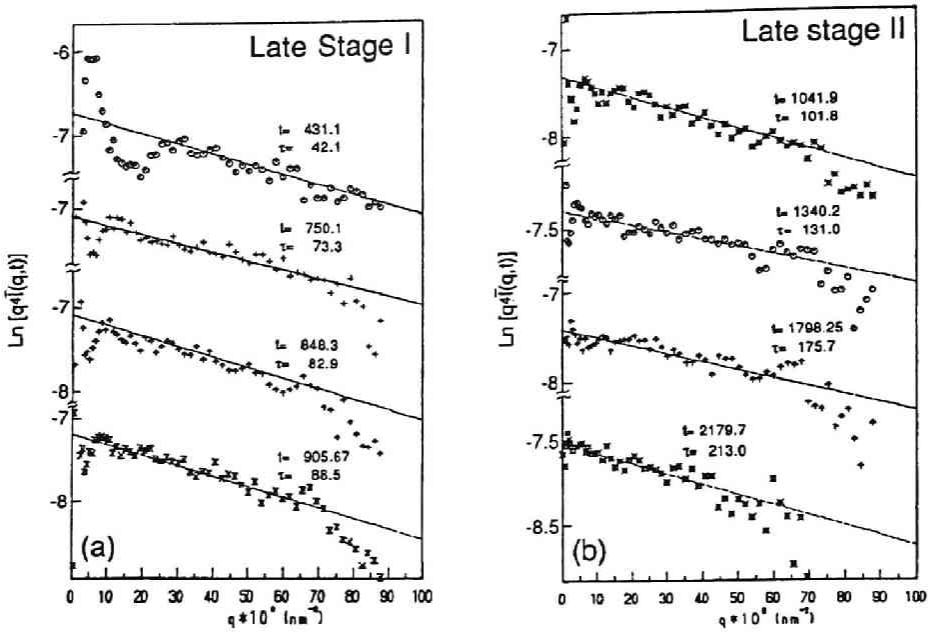

Fig.1-10. Plots of ln qI(q) vs q^2 at different times in the late stages I and II.

where z is a coordinate normal to the interface, $\rho_o(z)$ is the segmental density profile for the sharp interface, and the asterisk signifies a convolution product. We note that σ is related to the characteristic interface thickness t_I defined as the integral width of the Gaussian curve h(z) by

$$t_I \equiv \int_{-\infty}^{\infty} h(z)\, dz \;\Big/ h(z=0)$$

$$= \sqrt{2\pi}\,\sigma \qquad (1\text{-}18)$$

With Eq 1-15 we obtain

$$\bar{I}(q, t) \equiv I(q, t) \Big/ \int_{q'}^{q''} I(q, t) q^2\, dq$$

$$\sim \Sigma(t)\, q^{-4} \exp[-\sigma(t)^2 q^2] \qquad (1\text{-}19)$$

Table 1-III. Time-evolution of Interfacial Structure in Late Stages I and II

time t (min.)	reduced time τ[a]	$\Sigma(t)\times10^{2}$[b] (nm^{-1})	σ[c] (nm)	t_I[d] (nm)	Remark
336.5	32.9	1.29	138.6	347.4	Late stage I
363.8	35.5	1.08	137.5	344.7	
392.6	38.4	1.06	125.0	313.3	
431.1	42.1	0.75	112.2	281.2	
465.6	45.5	0.69	96.5	242.0	
750.1	73.3	0.33	102.5	257.0	
848.3	82.9	0.27	108.2	271.2	
905.6	88.5	0.24	106.8	267.7	
948.9	92.7	0.24	112.2	281.2	Late Stage II
1000.2	97.7	0.22	109.5	274.5	
1041.9	101.8	0.22	110.9	278.0	
1136.0	111.0	0.17	109.5	274.5	
1228.9	120.1	0.18	102.5	256.9	
1340.2	131.0	0.16	86.6	217.1	
1420.4	138.8	0.16	99.5	249.4	
1535.0	150.0	0.14	110.9	278.0	
1611.3	157.5	0.15	103.9	260.4	
1725.5	168.6	0.13	101.0	253.2	
1798.2	175.7	0.12	96.4	241.7	
1916.1	187.2	0.11	91.6	229.7	
1992.3	194.7	0.11	105.4	264.2	
2179.7	213.0	0.10	108.2	271.2	

a) $\tau=t/t_C$

b) interfacial area density

c) parameter characterizing the interface thickness (see eq.1-16)

d) characteristic interface thickness (see eq.1-18)

which shows that ln $[\bar{I}(q,t)q^4]$ at fixed t plotted against q^2 follows a straight line and the parameters $\Sigma(t)$ and $\sigma(t)$ can be evaluated from the intercept at q = 0 and the slope of the line. Figure 1-10 presents this plot at various t in the late stages I and II. we observe that the data points at relatively small t exhibit a minimum. This feature is associated with the appearance of a shoulder in F(x, t) at $x \simeq 3$ and makes the determination of the parameters

somewhat ambiguous. However, as time elapses, the shoulder shifts to lower q and, as a result, the linear region is expanded and the parameters can be evaluated more accurately. The resulting value of $\Sigma(t)$ and $\sigma(t)$ are listed in Table III, along with those of t_I. Figure 1-11 shows how $\Sigma(t)$ and t_I vary with time. The interface thickness decreases with time in the late stage I but stays constant at $t_{Ie} = 256 \pm 20$ nm in the late stage II. If we fit the $\Sigma(t)$ data to a power law

$$\Sigma(t) \sim t^{-\gamma}, \tag{1-20}$$

we find that γ decreases systematically in the late stage I and stays at about 1 in the late stage II (note the location for $t_{cr,2}$ indicated by an arrow on the horizontal axis). Since, as has been shown above, the exponent α was found to be 0.77 - 0.90 in the late stage I and 0.9 - 0.92 in the late stage II, we see $\gamma > \alpha$ throughout the late stage. This inequality implies that, in the late stage, the local structure corresponding to higher q modes relaxes to the equilibrium faster than the global structure corresponding to lower q modes. It should be noted here that our previous analysis of the late stage SD for a near critical mixture of PB and SBR yielded $\gamma < \alpha$, i.e., a conclusion quite opposite to that obtained here[18]. We considered this to be reexamined, because the previous analysis was based on the assumption $\sigma(t)\, q_m(t) << 1$.

Figure 1-12 illustrates the changes with time in $\Sigma(t) / q_m(t)$, i.e., the interfacial area density relative to $q_m(t)$ scaling the global structure, and also in $t_I(t)\Sigma(t)$, i.e., the volume fraction of the interface region. With Eqs. 1-2 and 1-20, we can write

$$\Sigma(t)/q_m(t) \sim t^{-(\gamma - \alpha)} \tag{1-21}$$

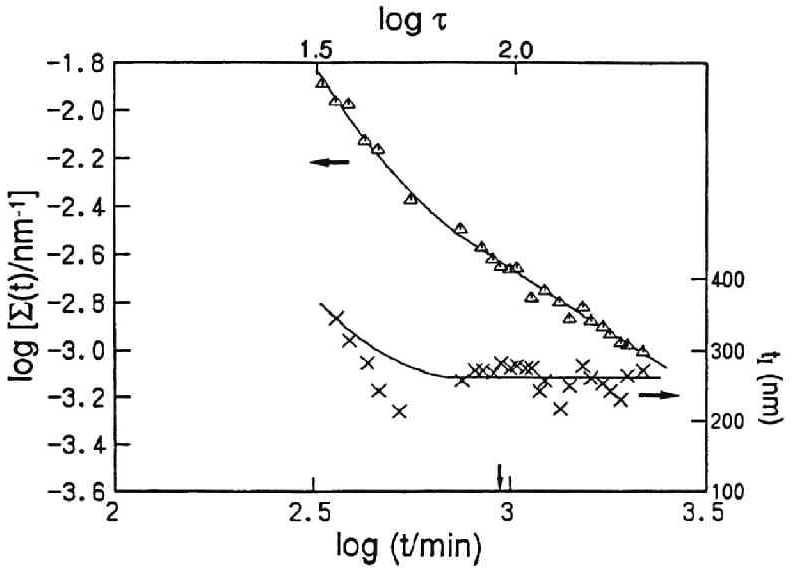

Fig.1-11 Time changes in the interfacial area density $\Sigma(t)$ and the characteristic interface thickness $t_I(t)$. t and τ are real and reduced times, respectively.

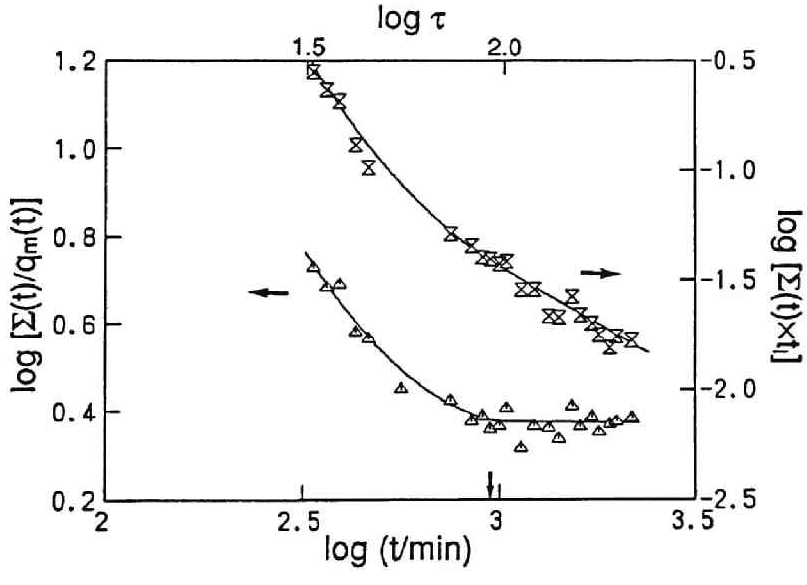

Fig.1-12. Time changes in the interfacial area density per characteristic wavenumber $\Sigma(t)/q_m(t)$ and the interface volume fraction $t_I(t)\Sigma(t)$.

and find $\gamma - \alpha$ to be 0.23 and 0 for the late stages I and II, respectively. On the other hand, the power law

$$\Sigma(t)t_I(t) \sim t^{-\delta} \qquad (1\text{-}23)$$

gives $\delta \sim 1.3$ and 1.0 for the late stages I and II, respectively.These results lead us to the following conclusion. (i) In the late stage I, the time change in $\Sigma(t)$ and $q_m(t)$ follow different laws and $t_I(t)$ keeps decreasing with time. (ii) In the late stage II, the time change in $\Sigma(t)$ and $q_m(t)$ follow the same power law and $t_I(t)$ reaches an equilibrium value. Thus, in the late stage II, it turns that the time-evolution of the self-assembled structure is scaled with a single length parameter over the entire length scale from local to global. The radii of gyration of our PB and PI samples can be estimated to be 8.8 and 10.4 nm, respectively, so that if their arithmetic mean is denoted by R_g, t_{Ie} / R_g is 27 at $\Delta T = 7$ °C or $\varepsilon_T \equiv (1/T - 1/T_s) / (1/T_s) \simeq 2.29 \times 10^{-2}$.

1-6. Universal nature of F(x, t) and crossover

As mentioned above, the nonuniversality of F(x, t) at large x (> 2) in the late stage I can be attributed to the fact that $q_m(t)$ and $\Sigma(t)$ follow different dynamical scaling laws and $t_I(t)$ still decreases in the late stage I. From Eqs. 1-4 and 15 it follows that F(x, t) at large x in the late stage, where $\langle\eta^2\rangle$ becomes independent of time, is represented by

$$F(x, t) \sim \Sigma(t)\, q_m(t)^{-1} x^{-4} \exp[-\sigma(t)^2\, q_m(t)^2\, x^2] \qquad (1\text{-}23)$$

or

$$F(x, t) \sim t^{-(\gamma-\alpha)}\, x^{-4} \exp[-\sigma(t)^2\, q_m(t)^2\, x^2]. \qquad (1\text{-}24)$$

Since the term $t^{-(\gamma-\alpha)}$ decreases and the exponential term in this equation increases with time, the increase in F(x, t) at x > 2 in the late stage I can be

explained as due to the outweighting of the latter over the former. The crossover from the nonuniversal to universal F(x, t) occurs at $t > t_{cr,2}$ at which $\gamma = \alpha$ and $\sigma_e q_m(t) << 1$, where σ_e is the equilibrium interface thickness.

We compare our value for t_{Ie} with the theoretical prediction by Joanny and Leibler[26] for a polymer/polymer mixture near the critical point. On the assumption of the hyperbolic tangent type segment density profile across the interface, they derived

$$t_{Ie} = 2L \tag{1-25}$$

where

$$L = \sqrt{2}\xi = [9\overline{N}\varepsilon_T / N_A N_B \overline{a^2}]^{-1/2} \tag{1-26}$$

with ξ is the thermal correlation length, and

$$\overline{N} = N_A\phi_{A,C} + N_B(1-\phi_{A,C}) \tag{1-27}$$

$$\overline{a^2} = a_A^2 (1-\phi_{A,C}) + a_B^2 \phi_{A,C} \tag{1-28}$$

$$\varepsilon_T = (\chi - \chi_s) / \chi_s \, . \tag{1-29}$$

Here, $\phi_{K,C}$, a_K, and N_K denotes the volume fraction at the critical point, the Kuhn statistical segment length, and the degree of polymerization of polymer K (K = A or B), and χ the Flory interaction parameter, with the subscript s specifying the value at the spinodal point. We assume our 50/50 wt/wt mixture of PB and PI to have the critical composition. Then, since N_{PB} = 1070, a_{PB} = 0.656 nm, N_{PI} = 1490, a_{PI} = 0.656 nm, and , as noted above, ε_T = 2.29×10^{-2}, we get $t_{Ie,theory}$ = 102 nm from Eq 1-25. Though our experimental value is larger than this by a factor 2, the agreement may be considered satisfactory.

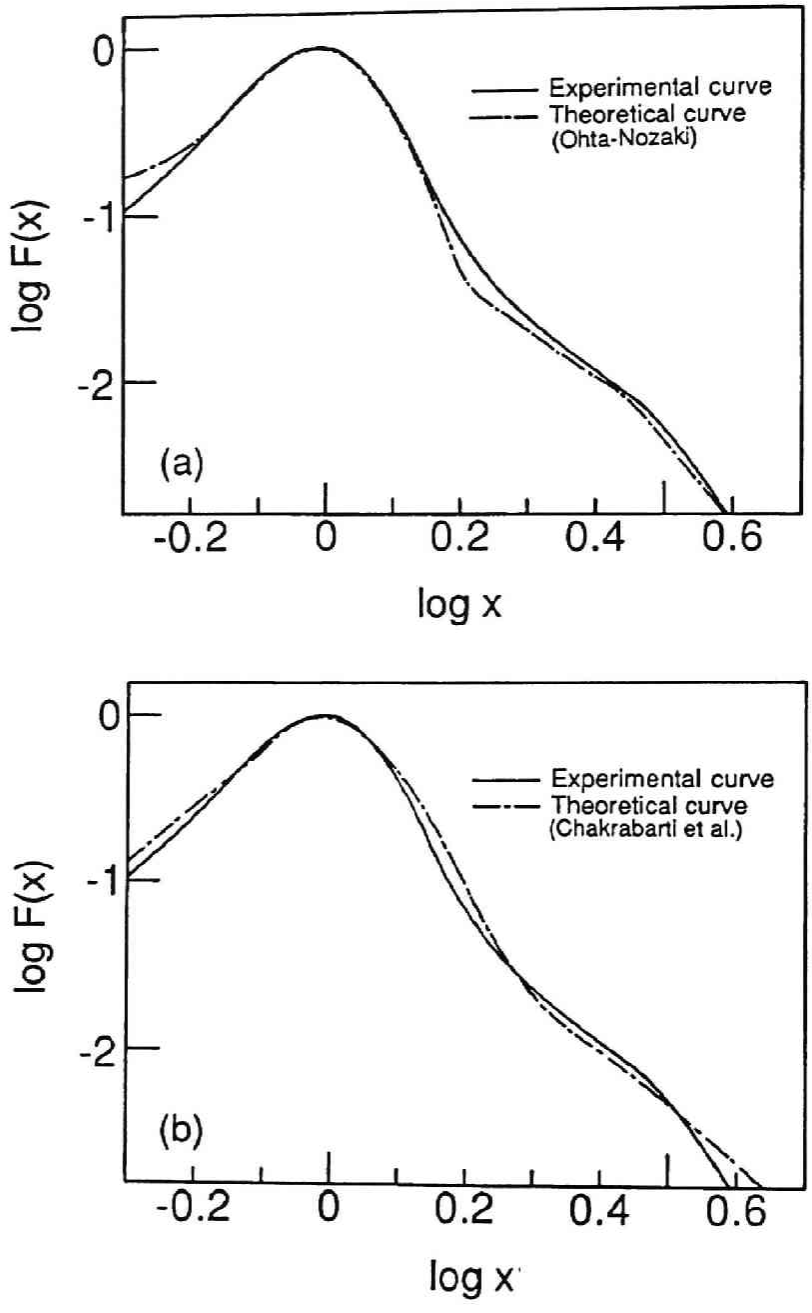

Fig.1-13. Comparison of experimental and theoretical scaled structure factors: (a) theoretical curve by Ohta et al. (dash-dot line) and experimental curve (solid line) and (b) numerical results by Chakrabarti et al. (dash-dot line) and experimental curve (solid line).

1-7. Comparison with theoretical scaled structure factors

Theories so far presented for F(x, t) are all concerned with the non-hydrodynamic regime (α = 1/3 in eq 2), and thus not applicable to the late stage in our experiment (α = 1). Nonetheless, in Figure 1-13, our experimental F(x, t) curve in the late stage II is compared with the theory of Ohta and Nozaki[25] (Figure 1-13(a)) and the simulation work of Chakrabarti et al.[24] (Figure 1-13(b)). Though not shown here, the latter gives nonuniversal F(x, t) for x > 2, which decreases with increasing time. We interpret this behavior as due to the overweighting of the term $t^{-(\gamma-\alpha)}$ over the term $\exp[-\sigma(t)^2 q_m(t)^2 x^2]$ (see Eq 1-24).

The agreement of the experimental curve with the calculated one of Ohta and Nozaki is quite good. It is worth noting that both show a shoulder at $x \simeq 3$. The experimental result is also consistent with the numerical one of Chakrabarti et al., though the shoulder is less apparent in the latter. This fine agreement between the experimental curve obtained in the hydrodynamic regime ($\alpha \simeq 1$) and the calculated ones obtained in the nonhydrodynamic regime ($\alpha \simeq 1/3$) may imply that the behavior of F(x, t) is rather insensitive to the detailed coarsening mechanism. On the contrary, the time change in the characteristic length scale $\Lambda_m(t)$ (or $1/q_m(t)$) is quite sensitive to the mechanism. Bates and Wiltzius[22] made a similar comparison for a mixture of deuterated and protonated polybutadiene. Though exhibiting a shoulder at $x \simeq 2$ instead of 3, their data are also consistent with the curve of Ohta and Nozaki[25].

1-8. Concluding remarks

The demixing processes occurring in a spinodally decomposing mixture PB and PI with a near critical composition was studied over wide ranges of time scale and length scale by a time-resolved light scattering. It was found that the process consists of four stages we call early, intermediate,

late I, and late II and that the self-assembled structure scalable over the entire length scale appears in the late stage II. In this stage, the interface thickness becomes independent of time and the global and local self-assembled structures follow the same dynamical scaling law. Further work will be required to check the present conclusion by changing the quench depth[16].

References

1 J. D. Gunton, M. Miguel and P. P. Sahni, *Phase Transition and Critical Phenomena*, edited by C. Domb and J. L. Lebowitz (Academic Press, N.Y., 1983), Vol. 8, p. 269.

2 T. Hashimoto, Phase Transitions **12**, 47 (1988).

3 T. Hashimoto, M. Itakura and H. Hasegawa, J.Chem.Phys. **85**, 6118 (1986).

4 J. W. Cahn, J.Chem.Phys. **42**, 93 (1965).

5 P. G. de Gennes, J.Chem.Phys. **72**, 4756 (1980).

6 K. Binder, J.Chem.Phys. **79**, 6387 (1983).

7 J. S. Langer, M. Bar-on and H. D. Miller, Phys.Rev.A. **11**, 1417 (1975).

8 M.Grant, M. San Miguel, J.Viñals and J.D.Gunton,Phys.Rev.B **31**,3027(1983).

9 H. Jinnai, H. Hasegawa, T. Hashimoto and C. C. Han, Macromolecules **24**, 282 (1991).

10 T. Hashimoto, M. Itakura and N. Shimidzu, J.Chem.Phys. **85**, 6773 (1986).

11 S. Nojima, K. Tsutsumi and T. Nose, Poly.J. **14**, 225 (1982).

12 T. Kyu and J. M. Saldanha, Macromolecules **21**, 1021 (1988).

13 H. L. Snyder, P. Meakin and S. Reich, Macromolecules **16**, 757 (1983).

14 P. E. Tomlins and J. S. Higgins, J.Chem.Phys. **90**, 6691 (1989).

15 J. D. Ferry, *Viscoelastic Properties of Polymers*, (John Willey & Sons, New York, 1980).

16 M.Takenaka and T.Hashimoto, in preparation.

17 T. Hashimoto, M. Takenaka and T. Izumitani, Polym. Commun. **30**, 45 (1989).

18 M. Takenaka, T. Izumitani and T. Hashimoto, J.Chem.Phys. **92**, 4566 (1990).

19 T.Hashimoto, K.Nagatoshi, A.Todo, H.Hasegawa,and H.Kawai, Macromolecules, **7**, 364(1974).

20 T.Hashimoto, M.Shibayama, and H.Kawai, Macromolecules, **13**, 1237(1980).

21 T. Nose, *Kinetics of phase separation in polymer mixtures*, edited by 1987), Vol. 8, p. 245.

22 F. S. Bates and P. Wiltzius, J. Chem. Phys. **91**, 3258 (1989).

23 S. Puri and Y. Oono, Phys.Rev.A. **38**, 1542 (1988).

24 A. Chakrabarti, A. Toral, J. D. Gunton and M. Muthukumar, Phys.Rev.Lett. **63**, 2072 (1989).

25 T.Ohta and H.Nozaki,In *Space-Time Organization in Macromolecular Fluids*, edited by F. Tanaka; M. Doi and T. Ohta, Springer. pp. 51-57. Berlin:(1989)

26 J.F.Joanny and L.Leibler, J.Phys. (Paris) **39**, 951(1978).

Chapter 2 : Further Investigation of Dynamical Scaling as a Function of Temperature

2-1. Introduction

In the previous chapter, we reported that the early-to-late stage SD at a given quench depth $\Delta T = T - T_s = 7.5$ K for the critical mixture of polybutadiene (PB) and polyisoprene (PI) can be classified into, at least, the following four stages : (i) early stage, (ii) intermediate stage, (iii) late stage I and (iv) late stage II, where T is the phase separation temperature inside the spinodal phase boundary and T_s is T at the spinodal point.

In the early stage SD, the time-evolution of the concentration fluctuations is well approximated by linearized theory[7-9]. Here the wavenumber $q_m(t;T)$ at time t and T of the dominant mode of the fluctuations is independent of t, but depends only on T,

$$q_m(t;T) = q_m(0;T) \tag{2.1}$$

and the amplitude of the spatial concentration fluctuation $\Delta\phi(\underset{\sim}{r},t)$ grows exponentially with t where $\underset{\sim}{r}$ is the position vector. In the intermediate stage, the nonlinear terms in the time-evolution equation of $\Delta\phi(\underset{\sim}{r},t)$ become increasingly important[10], giving rise to a decrease of $q_m(t;T)$ as well as a further increase of $\Delta\phi(\underset{\sim}{r},t)$. In the late stage SD, the interfaces between two coexisting domains are well developed, and the local concentration of each component in the domains reaches equilibrium values determined by the coexistence curve and T for the mixture[11]. Although the amplitude of the concentration of fluctuation $\Delta\phi(\underset{\sim}{r},t)$ has reached the equilibrium $\Delta\phi_e$, the size of the domains are still growing and hence $q_m(t;T)$ is decreasing to reduce the

excess free energy associated with the interfacial area[1]. The interfacial area density $\Sigma(t;T)$ is also decreasing toward its equilibrium value[6,12].

The time-evolution of the global structure in the later stage SD (the intermediate and late stages) has been characterized by $q_m(t;T)$, the maximum scattered intensity $I_m(t:T)$ occuring at a magnitude of the scattering vector $q = [(4\pi/\lambda)\sin(\theta/2)] = q_m(t;T)$, and the scaled structure factor $F(x,t)$ defined by

$$F(x,t) \equiv I(q,t;T)q_m^3(t;T) \tag{2.2}$$

and

$$x \equiv q/q_m(t;T). \tag{2.3}$$

where θ and λ are the scattering angle and the wavelength of the incident beam in the medium, respectively. The time-evolutions of $q_m(t;T)$ and $I_m(t;T)$ have been traditionally characterized by such scaling laws as[2]

$$q_m(t;T) \sim t^{-\alpha} \tag{2.4}$$

and

$$I_m(t;T) \sim t^{\beta}. \tag{2.5}$$

The scaling exponents, β and α, in the intermediate stage have been found to show the relationship of[13]

$$\beta > 3\alpha. \tag{2.6}$$

This relationship changes into[13]

$$\beta = 3\alpha \qquad (2.7)$$

in the late stage SD in the case when the contribution of the interfacial thickness $t_I(t;T)$ to $I_m(t;T)$ is negligible, as found previously[6] or as is expected to be valid for most of the cases (see the criterion given below by eq.(2.15)). The crossover of the behavior from eqs. (2.6) to (2.7) has been used to find the crossover between the intermediate and late stages[13,15]. The scaled structure factor F(x,t) at $x \cong 1$ was found to increase and sharpen with t in the intermediate stage[12,14]. However, in the late stage, F(x,t) at $x \leq 2$ reaches a time-independent universal scaling function S(x)[12,14,16], supporting the dynamical scaling hypothesis[17] for the time-evolution of the global structure , in that the growth of the global structure occurs with dynamical self-similarity and is scaled with a time-dependent single length parameter $1/q_m(t;T)$. This change in F(x,t) has been applied also to identify the crossover from the intermediate to late stage[12,14].

Recently the structure factor F(x,t) has been more closely investigated[3-6,12,18-23], viz., investigation of F(x,t) up to a larger reduced scattering vector x or down to a low intensity level has elucidated the following interesting features in the time-evolution of the local structures : (i) F(x,t) at large x (> 2) is not universal but rather increasing with t in early times of the late stage, implying that the local structure of such an interfacial structure cannot be scaled with the length parameter $1/q_m(t;T)$ characterizing the global structure[6,12,18], i.e., relevant parameters such as $\Sigma(t;T)$ and $t_I(t;T)$ characterizing the time-evolution of the local structure change with different scaling laws[6,12],

$$\Sigma(t;T) \sim t^{-\gamma}, \qquad (2.8)$$

and

$$t_I(t) \sim t^{-\delta}, \tag{2.9}$$

where Σ and t_I are the interfacial area density and characteristic interfacial thickness, respectively. (ii) F(x) shows a higher order maximum at x = $2^{12,18,20}$ or $3^{3\text{-}6,21}$, and (iii) F(x) shows a crossover in its asymptotic behavior with $x^{3\text{-}6,12,18,20,22,23}$,

$$F(x,t) \sim x^{-n} \tag{2.10}$$

where

$$n \equiv 6 - 7 \text{ for critical mixtures at } 1<x < x_c \tag{2.11}$$

and

$$n \equiv 4 \quad \text{at } x > x_c \tag{2.12}$$

where x_c is the crossover x ($\equiv$ 2). Our previous analyses[6] elucidated that

$$\gamma > \alpha \qquad \text{(in the late stage I)} \tag{2.13}$$

but that

$$\gamma = \alpha = 1 \quad \text{(in the late stage II).} \tag{2.14}$$

The relation given by eq.(2.13) and a non negligible contribution of the interfacial thickness to F(x,t) at large x were found to give the nonuniversality of F(x,t) at large x [6]. Furthermore we proposed from eq. (2.13) that the local structures relax and approach toward equilibrium faster than the global

structure[6]. In the later time of the late stage (i.e., the late stage II), we found[6] that eq.(2.14) and the experimental finding of

$$t_I(t;T)/[1/q_m(t;T)] << 1 \qquad (2.15)$$

assure the dynamical scaling hypothesis and hence a universal F(x,t) even at large x.

Such new pieces of evidence as described above on F(x,t) were implied in the studies of a polymer mixture of PB and poly(styrene-ran-butadiene) (SBR)[12] at various T's and were clearly indicated in the studies of the critical mixture of PB and PI at 33°C[6]. In this study we aimed to confirm whether the previous observations and conclusions obtained on the PB/PI mixtures at the given temperature were valid at other temperatures. Thus in this chapter we investigated the SD process at various temperatures, corresponding to $\Delta T = T - T_s$ = 5.5 to 34.5 or $\varepsilon_T = 4.50\times10^{-2}$ to 2.79×10^{-1}, where the mixture has a phase diagram of lower critical solution temperature (LCST), T_s is the spinodal temperature, and ε_T is defined by

$$\varepsilon_T = (\chi - \chi_s)/\chi_s. \qquad (2.16)$$

The quantities χ and χ_s are the Flory interaction parameter per segment at T and T_s, respectively.

This chapter is composed as follows. After describing experimental methods (sec. 2-2) and experimental results (sec. 2-3), we first present the analyses on the early stage SD (sec. 2-4-1), the results of which will be utilized on the scaling analyses of $q_m(t;T)$ and $I_m(t;T)$ for the test of the Chou-Goldburg scaling hypothesis[24] (sec. 2-4-2). We then present the analyses of F(x,t) over a wide range of x at various T's (sec. 2-4-3), which are followed by the analyses on the interfacial structures such as $\Sigma(t;T)$ and

TABLE I. Molecular characteristics of polybutadiene (PB) and polyisoprene (PI) used for this study.

Sample Code	$M_w \times 10^{-4}$ a)	M_w/M_n a)	Microstructure b)			
			cis-1,4	trans-1,4	vinyl-1,2	vinyl-3,4
PB	5.8	1.2	28	56	16	-
PI	10.1	1.3	70.4	22.1	-	7.5

a) measured using size exclusion chromatography equipped with a light scattering apparatus.

b) measured by IR spectroscopy.

$t_1(t;T)$ at various T (sec. 2-4-4). We further test and extend the Chou-Goldburg scaling postulate on $I_m(t;T)$ and $q_m(t;T)$ to the a new quantities $\Sigma(t;T)$ and $\Sigma(t;T)/q_m(t;T)$ and discuss the origin of nonuniversality in F(x,t) in the late stage I (sec. 2-4-5). In sec. 2-4-6, we compare the universal scaling function F(x,t) in the late stage II with F(x,t) obtained by other experiments and computer simulations. Finally in sec. V we give our summary and a possible model for the local structure giving rise to the higher-order maximum in F(x,t).

2-2. Experimental Methods

Molecular characteristics of PB and PI used in this work were summarized in TABLE I. A mixture of PB/PI with a near critical composition (50/50 wt./wt.) was dissolved in toluene and a homogeneous solution containing 10 wt% polymer was filtered through a Milipore film having an average pore size of 0.2 μm. Then the solution was cast to thin films in a petri dish by slowly evaporating the solvent for a few days at room temperature. The films obtained were further dried in a vacuum oven at room temperature until their weights became constant. The as-cast film thus

prepared was stacked inside a glass cell of 0.5 mm thickness and 13 mm^2 area, degassed under vacuum at room temperature for about 12 h, and sealed by covering with a glass plate. PB and PI have N/N_e about 23 and 29, respectively, where N and N_e are the weight-average degrees of polymerization of the entire polymer chain and the chain between entanglement points, respectively. Our critical mixture was shown to have the LCST type phase diagram with T_S higher than 298 K (25°C) but lower than 300 K (27°C)[6]. The time-resolved light scattering experiments were carried out by quenching the specimens from 20°C to the phase separation temperatures T = 31, 33, 35, 40, 45, 50, 55, and 60 °C, corresponding to the quench depth of ΔT = 5.5 to 34.5 K and $\varepsilon_T = 4.50\times10^{-2}$ to 2.79×10^{-1}. The light scattering apparatus and time-resolved experiment were described elsewhere[25]. In the previous paper[6] we reported our results, analyses and conclusions obtained from the experiments only at 33 °C.

PB and PI have T_g's well below the phase separation temperatures, and the mixture behaves as a liquid at a long time scale.

It should be noted that a new correction factor which has been ignored in our earlier experimental results[6,12,18] was introduced to obtain the true scattered intensity I(q,t;T). This is the correction factor C_n discussed by Keane and Stein[26] which is associated with the change of the solid angle Ω subtended by a detector when the scattering angle θ is changed. This change of Ω occurs owing to refraction of the scattered light beam at the film-air interface, and C_n is given by

$$C_n = \frac{\left\{1 - \left[\frac{\sin(\theta-\phi)}{n}\right]^2\right\}^{1/2}}{\cos(\theta-\phi)}, \qquad (2.17)$$

where n is the refractive index of the sample, and θ and ϕ are the scattering angle and the angle between the film normal and the propagation direction of

the incident light beam, respectively. In our experiment $\phi = 0$ because of normal incidence. This correction factor C_n was experimentally obtained also by measuring inelastic light scattering from aqueous solutions of methylene blue[28] with the same light scattering photometer and the same optical setup as those used for the time-resolved LS experiments. For this purpose the aqueous solution containing 1.0×10^{-4} and 30×10^{-4} mol/l methylene blue with PH 3.4 was prepared and put into the sample cell used for the blend study. A satisfactory agreement was obtained between the experimental and theoretical correction factors. The factor C_n thus determined was used to correct the measured scattered intensity distribution to obtain I(q,t;T). The correction gave a substantial effect in the large q
region (typically $q > 5\times10^{-3}$ nm^{-1}) but negligible effect in the small q region (typically $q < 5\times10^{-3}$ nm^{-1}) as will be demonstrated in sec. 2-4-3 (see Fig. 2-9(b) and (c)).

2-3. Results

Figure 2-1 shows a change of the time-sliced light scattering profiles after the onset of SD at 35°C where part b covers the profiles at t = 0.0 to 57.7 min. (τ = 0 to 9.4), corresponding to the early-to-intermediate stage SD, and part a the profiles at t = 72.6 to 1215 min. (τ = 11.8 to 197.0), corresponding to the intermediate-to-late stage SD. Here τ is the reduced time defined by

$$\tau \equiv t/t_c(T) \qquad (2.18)$$

where $t_c(T)$ is the temperature-dependent characteristic time of the mixture as will be discussed in sec. 2-4-1. It is clearly observed that, as time elapses, a

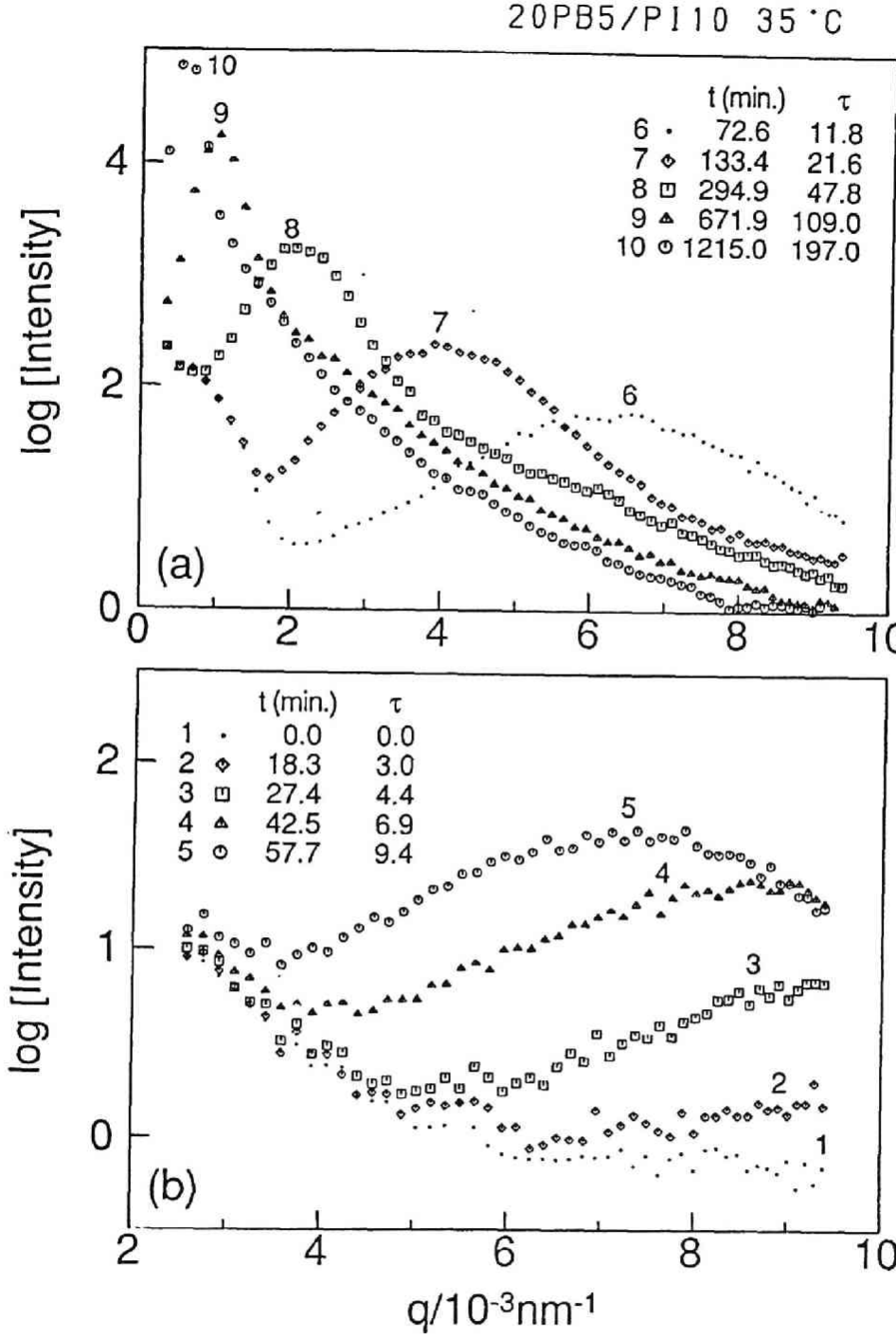

Figure 2-1 Time-evolution of light scattering profiles after a temperature jump from 295 K in the single phase state to 308 K inside the spinodal phase boundary. (a) The late stage and (b) the early and intermediate stage.

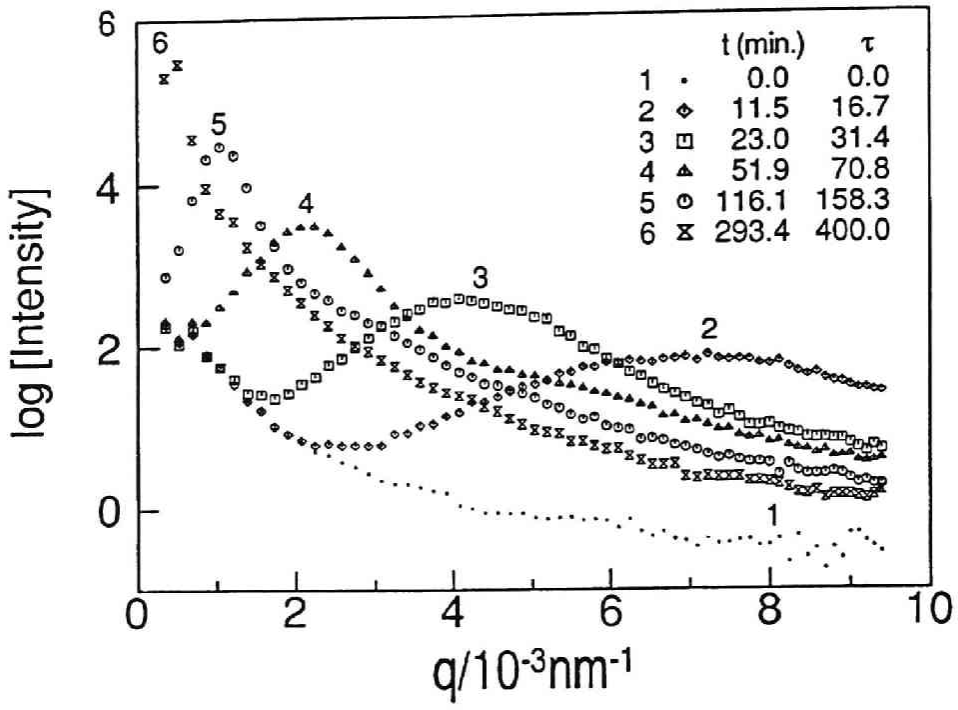

Figure 2-2 Time-evolution of the light scattering profile after a temperature jump from 295 K to 328 K.

scattering maximum appears inside the experimental q-window, the maximum intensity $I_m(t;T)$ increases and the corresponding $q_m(t;T)$ shifts toward smaller q.

Figure 2-2 shows the change in the time-sliced light scattering profiles at a higher temperature 50°C. The time change is similar to that in Figure 2-1, except for the fact that it occurs much faster here. The early stage SD occurs in the time scale earlier than 11.53 min., and hence the profiles obtained at t = 0.0 to 293.4 min. (τ = 0 to 400) correspond to those relevant to the early-to-late stage SD.

The profiles obtained at the later stage SD clearly manifest the higher order maximum or shoulder, e.g., at q = 6, 3, and 2×10^{-3} nm^{-1} for the curves 8 to 10 in Figure 2-1(a), respectively, and at q = 6, 3 and 1.5×10^{-3} nm^{-1} for

the curves 4 to 6 in Figure 2-2, respectively. These curves will be shown to become identical after a proper scaling as shown in sec. 2-4-3. The time-sliced scattering profiles obtained at various T's will be analyzed in the next section 2-4.

2-4. Analyses and Discussion

2-4-1. Early stage spinodal decomposition

The time-change of the scattering profiles I(q,t;T) obtained in the early stage, in the small q-range, and at T's covered in this experiment were found to be described well by Cahn's linearized theory[7-9] of SD with a negligible contribution of the random thermal noise[8,9,27,28]. Thus they are given by

$$I(q,t;T) = I(q,t = 0;T)\exp[2R(q;T)t], \tag{2.19}$$

where R(q;T) is the growth rate for the q-Fourier mode of the fluctuation at T. The rate was shown to be given by

$$R(q;T) = q^2 D_{app}(T)[1 - q^2/\{2q^2_m(0;T)\}] , \tag{2.20}$$

where $D_{app}(T)$ is the collective diffusivity at T and $q_m(0;T)$ was defined in eq.(2.1). The characteristic time for the phase separation at T, $t_c(T)$, is given by

$$t_c(t) = [D_{app}(T)q^2_m(0;T)]^{-1}. \tag{2.21}$$

At 31,33, and 35°C, the plots of ln[I(q,t;T)] vs t were found to be linear in the early time (though not shown here) as shown in previous papers[13,25,29], from the slopes of which R(q;T) were estimated. Figure 2-3 shows a so called Cahn's plot to determine $D_{app}(T)$ and $q^2_m(0;T)$ on the basis of

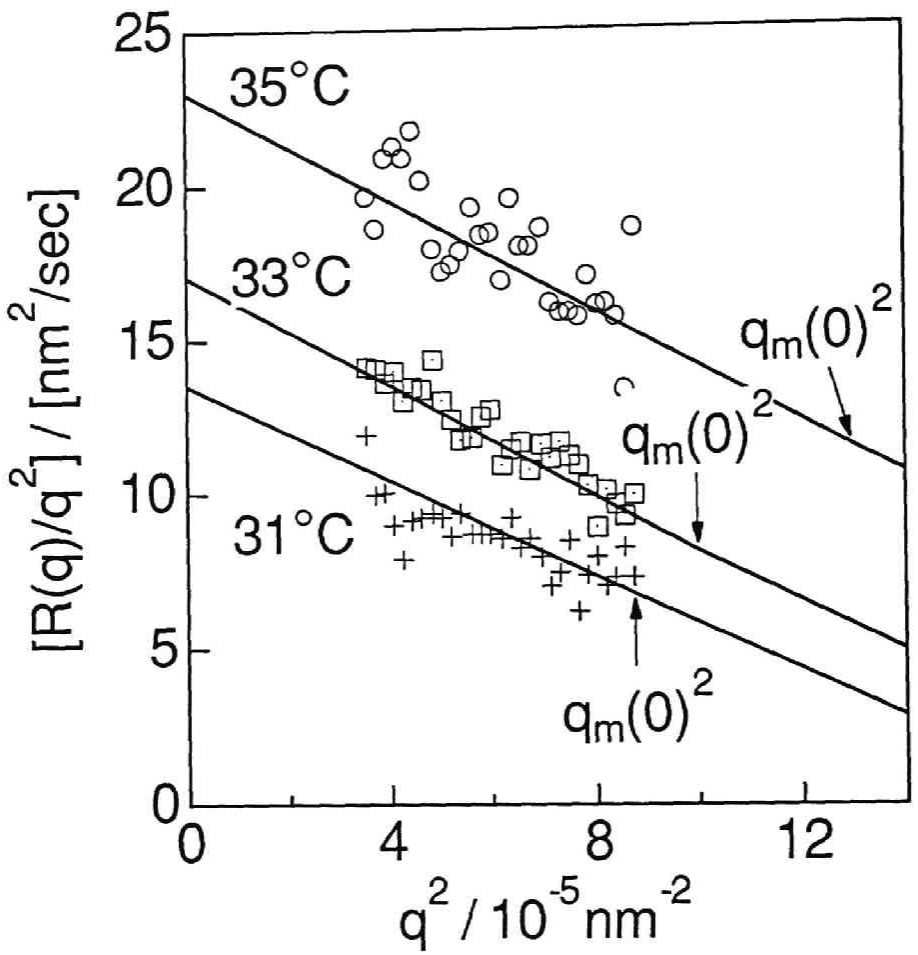

Figure 2-3 Plots of $R(q)/q^2$ vs. q^2 at 31,33, and 35°C in the early stage of spinodal decomposition.

eq.(2.20). The results of $D_{app}(T)$ and $q_m(0;T)$ thus estimated are summarized in TABLE 2-II along with $t_c(T)$ and $D_{app}(T)/q^2_m(0;T)$, i.e., a quantity proportional to the Onsager kinetic coefficient $\Lambda(T)$[8,9,30].

The spinodal decomposition at higher temperatures is very rapid, so that the analyses of the early stage SD become increasingly difficult. Instead of directly determining $D_{app}(T)$ and $q_m(0;T)$ at higher temperatures, we determined them by extrapolating the data at the three lower temperatures by the method as described below. The determination of $q^2_m(0;T)$ at higher temperatures was made using information on T_s separately obtained[6] ($25 < T_s < 27$ °C) and using its temperature dependence as given by

$$q^2_m(0;T) \sim \varepsilon_T \sim 1/T - 1/T_s, \tag{2.22}$$

since this mixture obeys the mean-field behavior over T's covered in this experiment. Figure 2-4 shows the three data points on $q^2_m(0;T)$ (filled circles) and the predetermined T_s (a range of the values being shown by the arrow in the T^{-1} axis), together with the expected temperature dependence of $q^2_m(0;T)$ (solid line) and the values at the five higher temperatures read off from this line (open circles). These five data points on $q_m(0;T)$ were also included in TABLE 2-II. The temperature dependence of $\Lambda(T)$ was assumed to be given by an Arrhenius behavior,

$$\Lambda(T) \sim D_{app}(T)/q^2_m(0;T) \sim \exp(-\Delta H/RT), \tag{2.23}$$

as T's covered in this experiment are much higher than the T_g of the mixture, where ΔH is the activation energy and R is the ideal gas constant. Figure 2-5 shows the Arrhenius plot where the filled circles represent the measured data points, the solid line represents the temperature dependence of $\Lambda(T)$ as extrapolated from the three data points, and the open circles represent the

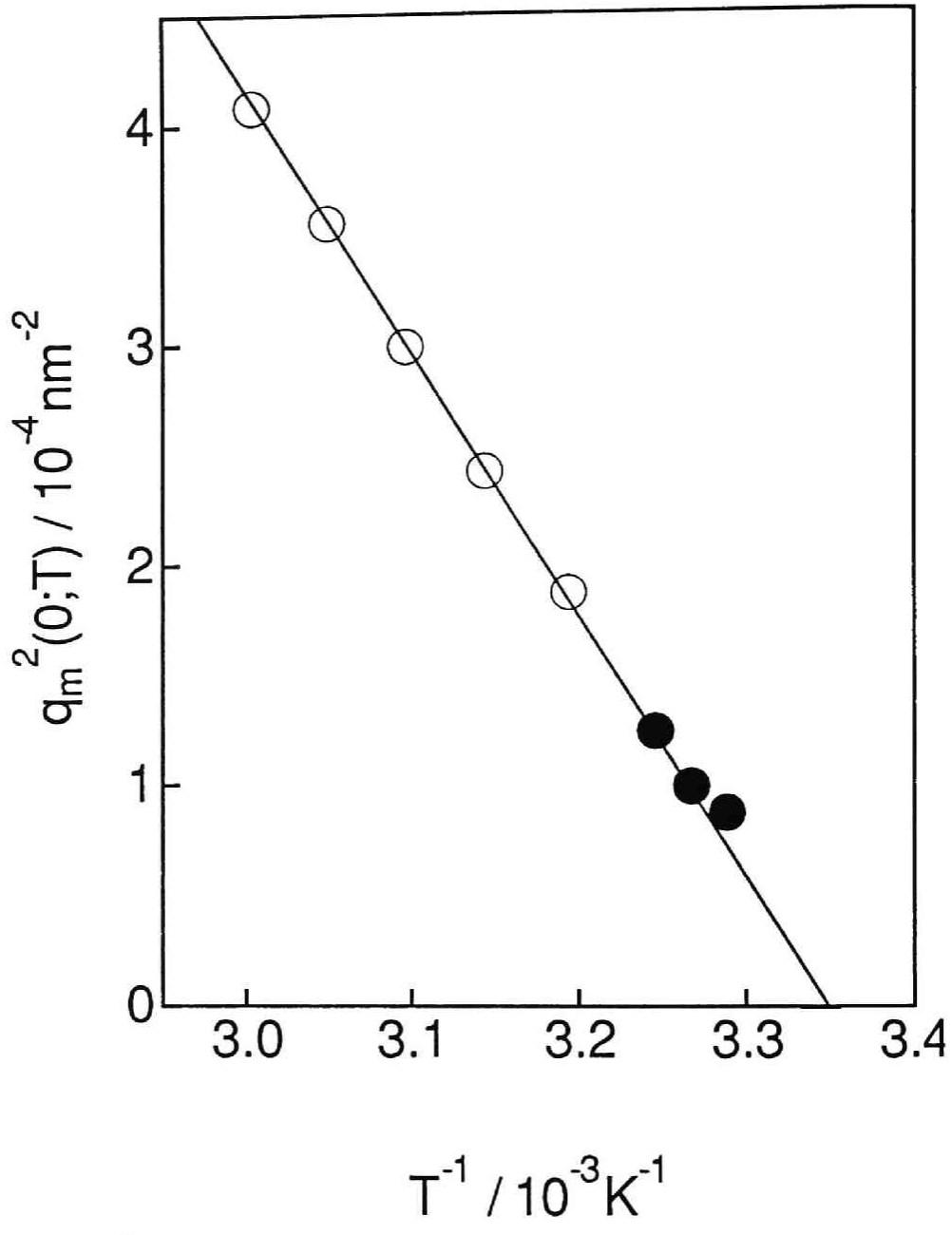

Figure 2-4 Plot of $q_m^2(0;T)$ vs. 1/T. The filled circles are obtained from Figure 3 and the open circle are the read off data at 40,45,50,55, and 60°C from the line obtained by the extrapolation of the three lower temperature data.

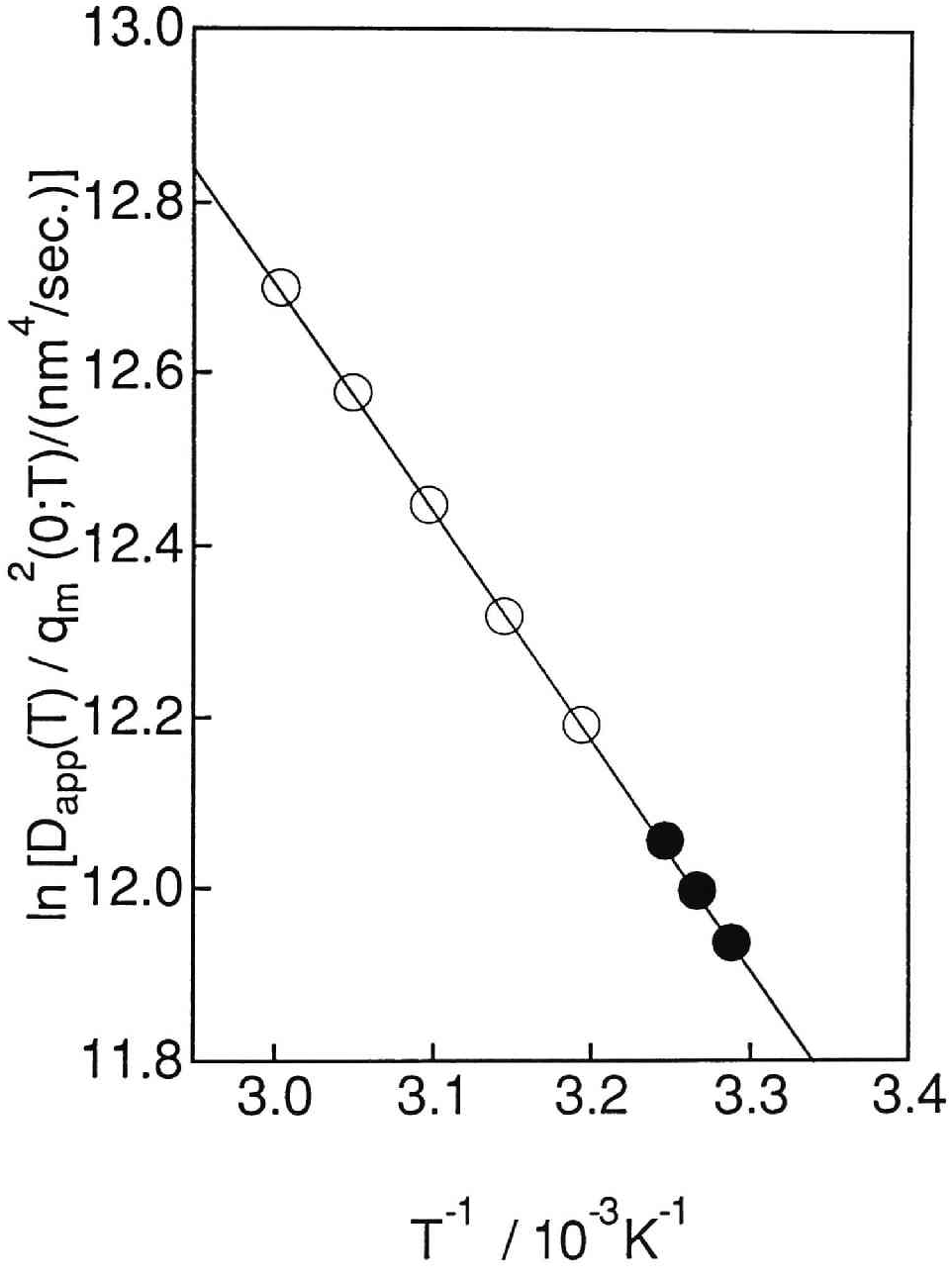

Figure 2-5 Plot of $D_{app}(T)/q_m^2(0;T)$ vs 1/T. The filled circles are obtained from Figure 3 and the open circles are those read off at 40,45,50,55, and 60°C from the line obtained by the extrapolation of the three lower temperature data.

TABLE 2-II. Parameters characterizing the early stage of spinodal decomposition

Temp. (°C)	ΔT (°C)	ε_T	$D_{app}(T)$ (nm^2/sec)	$q_m(0;T)\times10^3$ (nm^{-1})	$t_c\times10^{-1}$ (sec)	$D_{app}(T)/q_m^2(0;T)\times10^{-5}$ (nm^4/sec)
31	5.5	0.045	13.5	9.38	84.2	1.53
33	7.5	0.063	16.3	10.0	61.3	1.63
35	9.5	0.079	23.0	11.4	37.0	1.73
40*	14.5	0.122	37.0	13.7	14.4	1.97
45*	19.5	0.163	54.7	15.6	7.49	2.24
50*	24.5	0.203	75.8	17.3	4.40	2.53
55*	29.5	0.242	103	19.4	2.72	2.88
60*	34.5	0.279	134	20.2	1.82	3.28

*The parameters at these temperatures were obtained by extrapolating the data at the three lower temperatures (see Figs.2-4 and 2-5).

points read off from this line. The values for $\Lambda(T)$ thus determined were also included in TABLE 2-II. We determined the values $D_{app}(T)$ at 40 to 60 °C from the extrapolated values of $D_{app}(T)/q_m^2(0;T)$ and $q_m^2(0;T)$. The corresponding values of $t_c(T)$ were determined using eq.(2.21).

The data $q_m(0;T)$ and $t_c(T)$ thus determined will be used for the scaling analyses on the later stage SD. Uncertainty involved in the determination of the $q^2_m(0;T)$ and $\Lambda(T)$ at higher temperatures from 40 to 60°C causes uncertainty in $q_m(0;T)$ and $t_c(T)$. However we found that this uncertainty gave surprisingly little effect on the reduced plots shown later in Figures 2-8, 2-12 and 2-15.

2-4-2. Scaling analyses of $q_m(t;T)$ and $I_m(t,T)$ in the later stage and test of the scaling postulate

The time changes of $q_m(t;T)$ and $I_m(t;T)$ at various T's in the later stage SD were plotted double logarithmically in Figures 2-6 and 2-7, respectively. The higher the temperature the faster the growth of the pattern (domains), hence giving rise to smaller $q_m(t;T)$ and higher $I_m(t;T)$ at a given

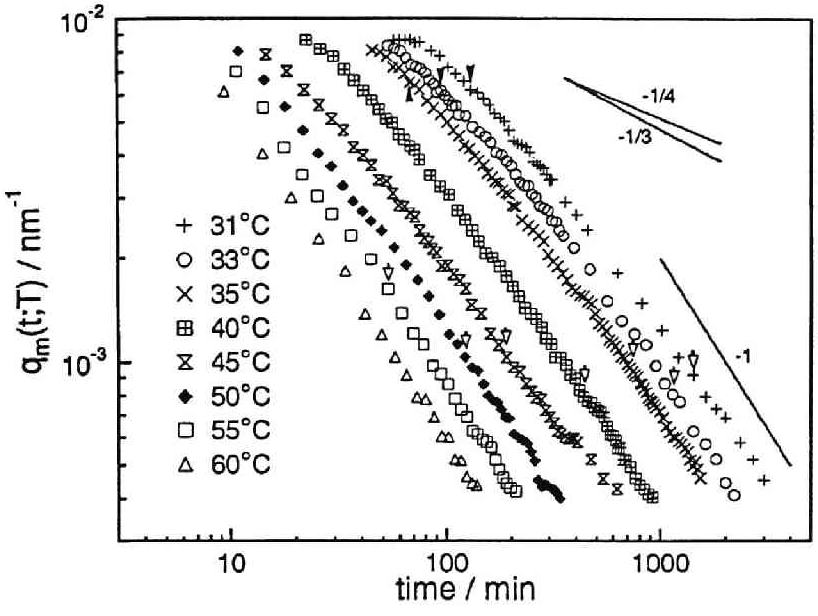

Figure 2-6 Time change of $q_m(t;T)$ at various temperatures. The filled arrows and open arrows indicate the crossover time from the intermediate stage to late stage I ($t_{cr,1}$) and that from the late stage I to late stage II ($t_{cr,2}$), respectively.

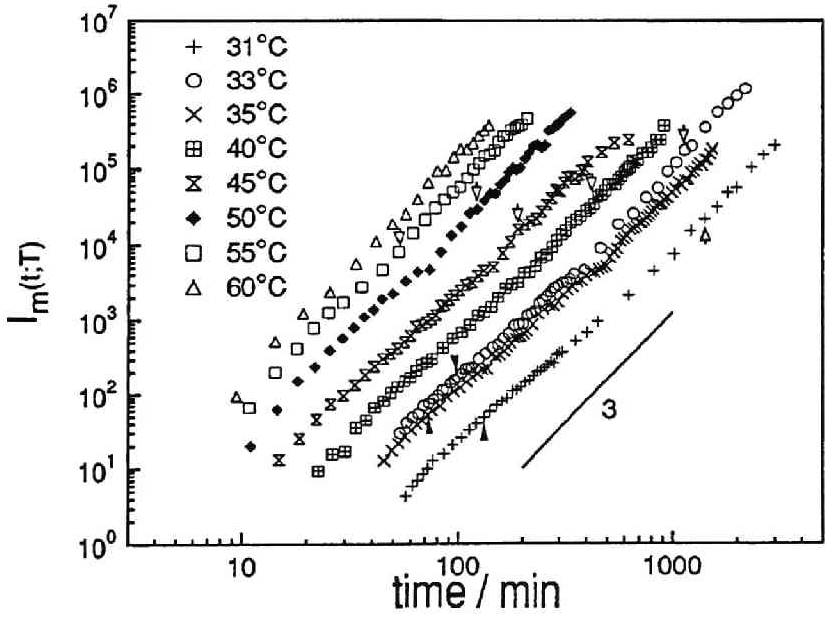

Figure 2-7 Time change of $I_m(t;T)$ at various temperatures.The arrows have the same significance as in Figure 6.

TABLE 2-III. The scaling exponents characterizing time-evolution of the global (α,β) and local structures (γ) at long time limit of the experiments and the crossover reduced times $\tau_{cr,1}$ and $\tau_{cr,2}$.

Temp. (°C)	α	β	β/α	γ	$\tau_{cr,1}$	$\tau_{cr,2}$
31	0.90	2.70	3.0	1.1	9	95
33	0.92	2.78	3.0	1.0	11	118
35	0.92	2.76	3.0	1.0	10	115
40	0.89	2.73	3.1	1.0	-	176
45	0.93	2.67	2.9	1.0	-	139
50	0.95	2.79	2.9	1.0	-	163
55	0.95	2.85	3.0	1.1	-	130
60	1.02	3.03	3.0	1.0	-	-

and $t_{cr,2}$ shown by filled and open arrows , respectively, indicate the crossovers from the intermediate stage to the late stage I and from the late stage I to the late stage II. The crossover $t_{cr,1}$ was determined from eqs.(2.6) and (2.7) as well as from the time change of F(x,t) as will be discussed later (sec. 2-4-3). The crossover $t_{cr,2}$ will be also discussed later in sec. 2-4-5. The scaling exponents at the long time limits covered in the experiment are summarized in TABLE 2-III where α and β are shown to be close to 1 and 3, respectively, in accord with the coarsening law proposed by Siggia[31].

The time changes of $q_m(t;T)$ and $I_m(t;T)$ were, respectively, reduced to dimensionless quantities, $Q_m(\tau)$ and $\tilde{I}_m(\tau)$, and plotted as a function of the reduced time τ in order to test the scaling postulate proposed by Chou and Goldburg[24]. $Q_m(\tau)$ and $\tilde{I}_m(\tau)$ are defined by

$$Q_m(\tau) \equiv q_m(t;T)/q_m(0;T), \tag{2.24}$$

and

$$\tilde{I}_m(\tau)=I_m(t;T)q_m(0;T)^3 \Big/ \int_{q'}^{q''} q^2 I(q;t;T)dq, \qquad (2.25)$$

where q' and q" are the lower and upper bounds of q beyond which the integrand effectively becomes zero. The reduced wavenumber $Q_m(\tau)$ and the reduced maximum scattered intensity $\tilde{I}_m(\tau)$ were plotted double logarithmically against the reduced time τ in Figure 2-8. The results obtained at various T's are found to fall onto the respective master curves, supporting validity of the Chou-Goldburg scaling postulate as reported for other polymer blend systems[13,15,32-35]. Thus temperature affects the time scale [through $t_c(T)$] and the spatial scale [through $q_m(0;T)$] of the growing pattern, but the mechanism of the pattern growth is independent of T covered in this experiment. This result is consistent with previous experimental reports except for one reported by Bates et al.[20]. The arrows indicate the crossover reduce times $\tau_{cr,1}$ and $\tau_{cr,2}$ given by

$$\tau_{cr,1} = t_{cr,1}/t_c(T), \quad \tau_{cr,2} = t_{cr,2}/t_c(T) \qquad (2.26)$$

which are found to be approximately 10 and 120, respectively, independent of T as shown in TABLE 2-III. The results are consistent with those previously reported[6]. TABLE 2-IV summarizes the ranges of α and β as well as γ and δ in each regime which will be discussed later.

2-4-3. Scaled Structure Factor

If the time evolution of the pattern at a given T obeys the dynamical scaling law[17] and the pattern evolved is independent of T, then the time evolution of the scattering function I(q,t;T) corresponding to that of the pattern is given in terms of the universal scaling function S(x),

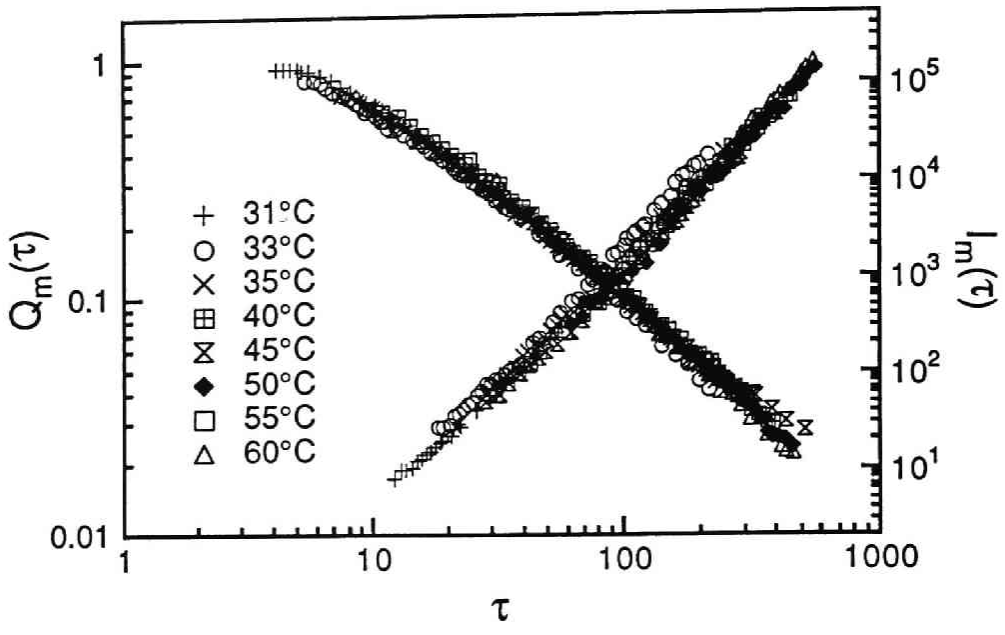

Figure 2-8 Reduced wavenumber $Q_m(\tau)$ and reduced intensity $\tilde{I}_m(\tau)$ plotted against reduced time τ at various temperatures. $\tau_{cr,1}$ and $\tau_{cr,2}$ are the crossover reduced times corresponding to $t_{cr,1}$ and $t_{cr,2}$, respectively.

TABLE 2-IV.The range of values for the characteristic parameters τ,α,β,γ, and δ in each regime of the spinodal decomposition

Parameters	regime of SD		
	Intermediate	Late I	Late II
τ	2 ~ 9	9 ~ 120	120 ~ 450
α	0 ~ 0.6	0.6 ~ 0.96	0.96 ~ 1.0
β	1.2 ~ 1.8	1.8 ~ 2.9	2.9 ~ 3.0
γ	-	1.0	1.0
δ	-	~0	~0

τ,α,β,γ, and δ are defined in eqs.(2.18),(2.4),(2.5),(2.8) and (2.9),respectively.

$$I(q,t;T) \sim \langle \eta^2(t;T) \rangle q^{-3}{}_m(t;T) S(x) \qquad (2.27)$$

where $\langle \eta^2(t;T) \rangle$ is the mean square fluctuation of the refractive index relevant to the pattern at t and T. Thus from eqs.(2.2) and (2.27), the scaled structure factor F(x,t) is related to S(x) by

$$F(x,t) \sim \langle \eta^2(t;T) \rangle S(x). \qquad (2.28)$$

In the late stage in which the interface contribution to $\langle \eta^2(t;T) \rangle$ is negligible or when the interface thickness $t_I(t;T)$ reaches an equilibrium value, $\langle \eta^2(t;T) \rangle$ becomes the equilibrium value $\langle \eta^2(T) \rangle_e$ determined by the phase diagram and T,

$$\langle \eta^2(t;T) \rangle = \langle \eta^2(T) \rangle_e \, . \qquad (2.29)$$

Thus in this case F(x;t) at a given t becomes universal with t. Furthermore the reduced $\overline{F}(x,t)$ defined by

$$\overline{F}(x,t) \equiv F(x,t) \Big/ \int_{q'}^{q_m} q^2 I(q;t;T) dq \sim F(x,t)/\langle \eta^2(T) \rangle_e \qquad (2.30)$$

becomes universal with T also, i.e.,

$$\overline{F}(x,t) = S(x). \qquad (2.31)$$

In this section we test the dynamical scaling law[17] and investigate whether such a universal scaling function S(x) exists for our system.

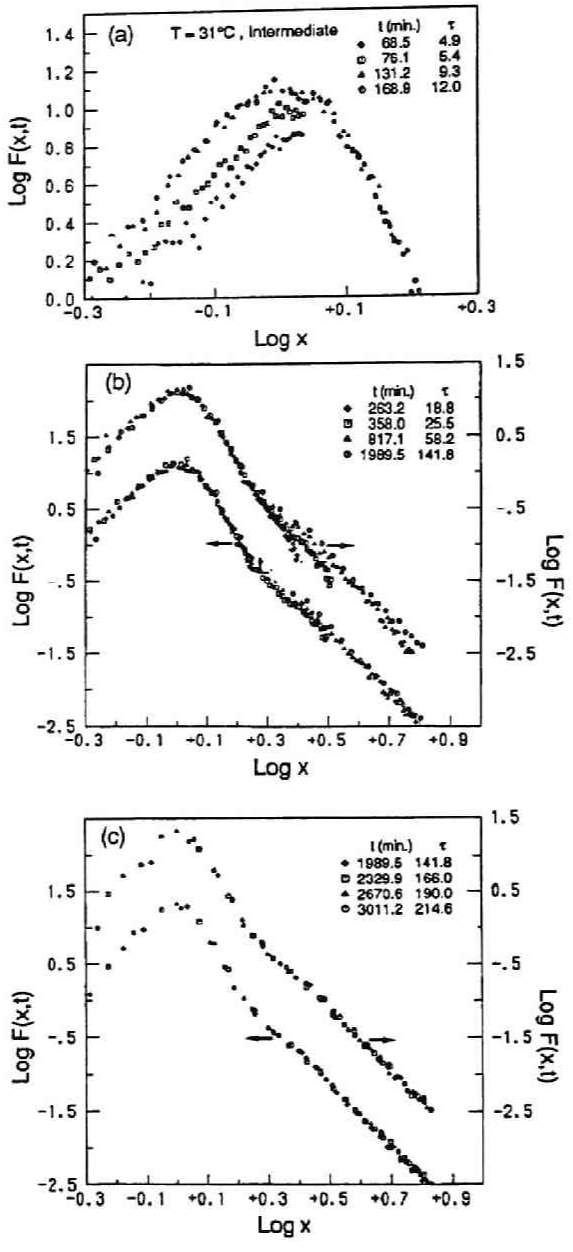

Figure 2-9 Scaled structure factor F(x,t) in (a) the intermediate stage, (b) the late stage I, and (c) the late stage II. In parts (b) and (c), the profiles marked by A and B correspond to those with and without the correction given by eq.(2.17), respectively.

Figure 2-9 shows the time change of F(x) at T = 31°C. At $\tau < 12$ (as in part a), F(x) is not universal with t but increases with t, primarily due to the increase of $<\eta^2(t;T)>$. Thus this behavior is relevant to the intermediate stage. At $10 < \tau < 120$ (as in part b), F(x) is universal with t at small x ($x < 2$) but nonuniversal at large x ($x > 2$), as reported in previous papers[6,12,18] (see only the profile marked A here). The features at the large x region are the same as those previously reported. (i) F(x) increases with t, (ii) the asymptotic behavior of F(x) at large x (eq.(2.10)) has a crossover , n changing from 6 ~ 7 to 4, and (iii) F(x) has a higher order maximum at x = 2 or 3 (x=3 for this sample). The features (ii) and (iii) were reported also by theoretical[21,36], experimental[6,12,18-20] and computer simulation work[3-5,22,23]. The maximum at x = 2 was reported by Bates et.al.[20] and Hashimoto et.al.[14,18] and that x = 3 was reported by Hashimoto et.al.[6] , Ohta et.al.,[21] Chakrabarti et.al.,[5,22] Oono et.al.,[3,23] and Koga et.al.[4]. At $\tau > 120$ (as in part c), F(x,t) becomes universal with t for all the x range covered in this experiment, confirming the previous result in the late stage II (see the profile marked A)[6]. Although not shown here, such a crossover such as the one observed in F(x,t) with t in Figure 2-9 was observed also at the other temperatures covered in this experiment.

It should be noted here that the nonuniversality at large x in the late stage I (in the profile A) is less pronounced than that reported earlier[6,12,18]. This is due to the newly incorporated correction given by eq.(2.17) which was ignored in our previous work. The profiles obtained by ignoring this correction were also shown in part b and c in Figure 2-9 for comparison (see the profiles marked by B).

Figure 2-10 shows the scaled structure factors $\overline{F}(x,t)$ reduced for the temperature effect on $<\eta^2(t;T)>$ at the eight temperatures studied and in the late stage II. It is clearly seen that $\overline{F}(x,t)$ is essentially independent of T at $x \lesssim 2$ representing the universal scaling function S(x) relevant to the global

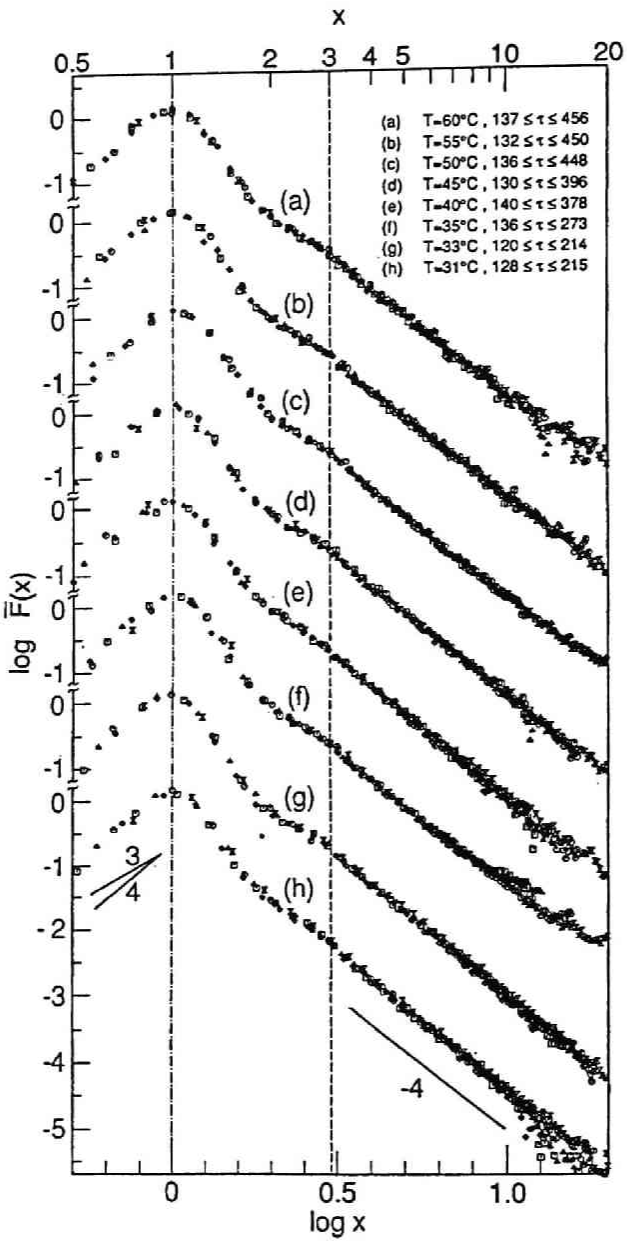

Figure 2-10 Reduced scaled structure factor $\bar{F}(x,t)$ in the late stage II at various temperatures. The curves (a) to (h) were obtained in the following condition; (a) T=60°C, 137≤τ≤456, (b) T=55°C, 136≤τ≤462, (c) T=50°C, 140≤τ≤461, (d) T=45°C, 132≤τ≤401, (e) T=40°C, 141≤τ≤381, (f) T=35°C, 136≤τ≤273, (g) T=33°C, 120≤τ≤214, (h) T=31°C, 128≤τ≤215.

pattern in our system. Such a clear universality of F(x,t) with T as shown here has not been reported earlier, though F(x,t) observed for PB/SBR showed approximately the universality with T[12]. Nonuniversalilty of F(x,t) or $\overline{F}(x,t)$ with T was found for PS/PVME[14], PS/PB[16], and PMES/PMDS[19]. In the case of PS/PVME[14] and probably the case of PMES/PMDS[19] as well, the nonuniversality is due to the asymmetry of their phase diagrams, which causes the relative volume fraction of each domain depends strongly on T. This effect in turn causes the change of the structure factor in the late stage with T. $\overline{F}(x,T)$ slightly depends on T at x>2 even for our mixture, which is due to the temperature change of the equilibrium interfacial thickness.

2-4-4. Scaling analysis on time evolution of local structure

2-4-4-1. Experimental Analyses

In our previous analysis[12], we have shown that the crossover in the asymptotic behavior of F(x,t) as given by eqs.(2.10) to (2.12) occurs at $q_c = 1/R_m$ where q_c and R_m are, respectively, the mean curvature and radius of the local curvature of the interface[36]. At $q < q_c$, the interface is sufficiently curved, generating tortuous, intersecting, tangled interfaces, so that F(x,t) has the asymptotic form given by eqs.(2.10) and (2.11). However at $q > q_c$ or at $r < R_m$, the interface is sufficiently flat so that F(x,t) has the asymptotic form given by eqs.(2.10) and (2.12), relevant to that in the Porod's law regime[37]. Of course as time elapses R_m increases and hence q_c decreases, i.e., $R_m = R_m(t;T) = 1/q_c(t;T)$.

We analyze the time evolution of the interfacial structure according to the method described previously[6]. Although we previously analyzed $\Sigma(t;T)$ and $t_I(t;T)$ as a function of t only, here we analyzed them as a function of T as well. The reduced scattered intensity $\overline{I}(q,t;T)$ defined as

$$\bar{I}(q,t;T)=I(q,t;T)\Big/\int_{q_*}^{q^*} q^2 I(q;t;T)dq \qquad (2.32)$$

is given, in the Porod's law[6,37,38] regime, by

$$\bar{I}(q,t;T) = [\pi\phi(1-\phi)]^{-1}\Sigma(t;T)q^{-4}\exp[-\sigma(t;T)^2q^2], \qquad (2.33)$$

where $\sigma(t;T)$ is the parameter related to $t_I(t;T)$ by[39]

$$t_I(t;T) = \sqrt{2\pi}\sigma(t;T). \qquad (2.34)$$

As shown previously[6], the plot of $\ln[q^4\bar{I}(q,t;T)]$ vs q^2 showed a good linear relation over a wide range of q in the late stage SD, though not shown here. The plots yielded $\sigma(t;T)$ and $\Sigma(t;T)$ from the slopes and the intercepts at $q = 0$, respectively.

Figure 2-11(a) shows a double logarithmic plot of $\Sigma(t;T)$ thus determined as a function of t at the eight different temperatures. It is clearly shown that $\Sigma(t;T)$ obeys the scaling law given by eq.(2.8), and that the value of γ is 1 at the long time limit covered in our experiment. The higher the temperature, the faster the pattern growth and hence the faster the decay of $\Sigma(t;T)$.

$\Sigma(t;T)$ has a dimension of wavenumber, and hence we designate it as "*local wavenumber*" in contrast to the $q_m(t;T)$ characterizing "*global wavenumber*". We attempted to scale $\Sigma(t;T)$ with the characteristic wavenumber $q_m(0;T)$ and characteristic time $t_c(T)$. Similarly to the analysis of $q_m(t;T)$, we defined the dimensionless quantities $\bar{\Sigma}(t;T)$ by

$$\bar{\Sigma}(t;T)=\Sigma(t;T)/q_m(0;T). \qquad (2.35)$$

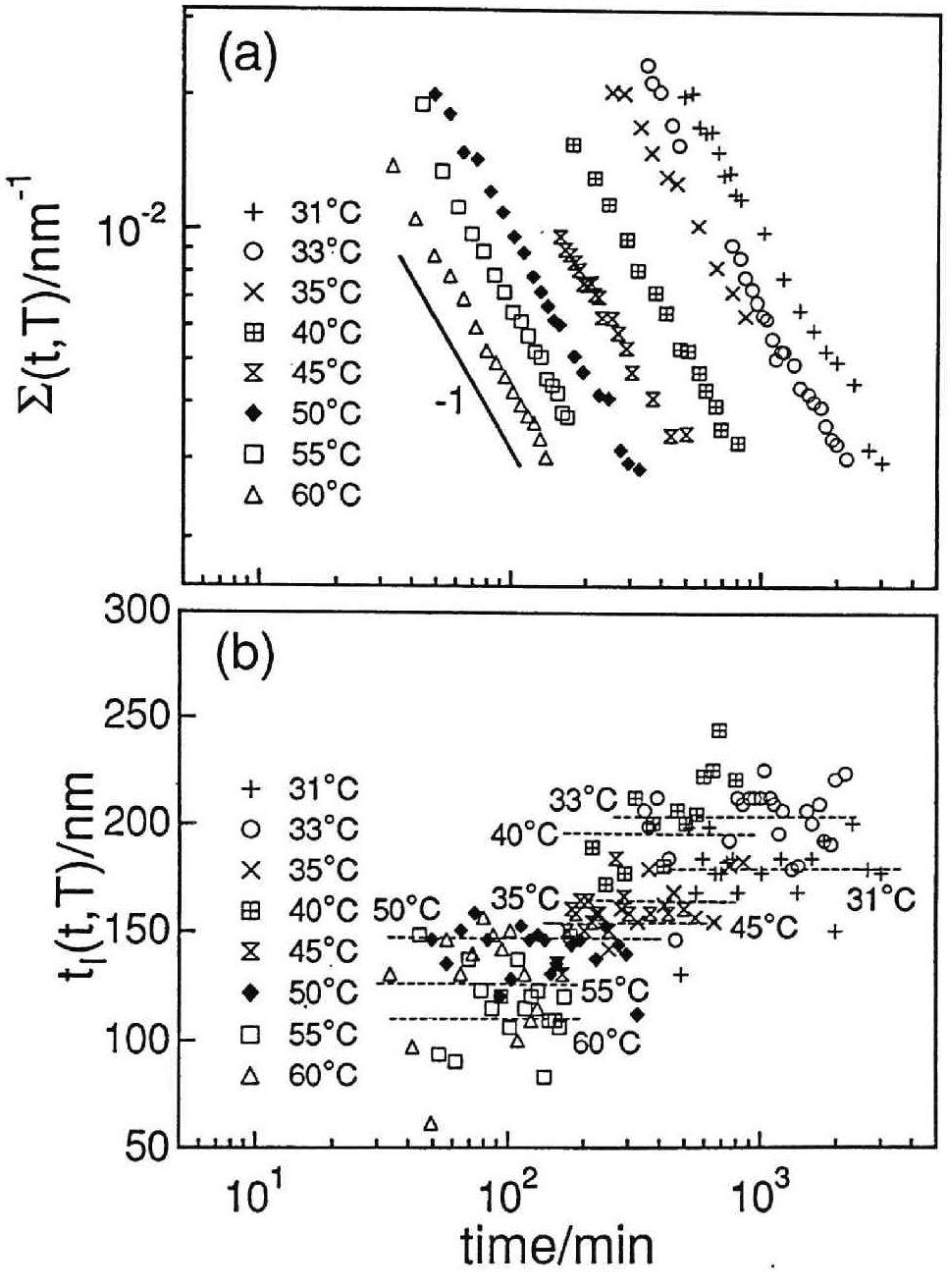

Figure 2-11 Time change of (a) the interfacial area density $\Sigma(t;T)$ and (b) the interfacial thickness $t_I(t;T)$ at various temperatures.

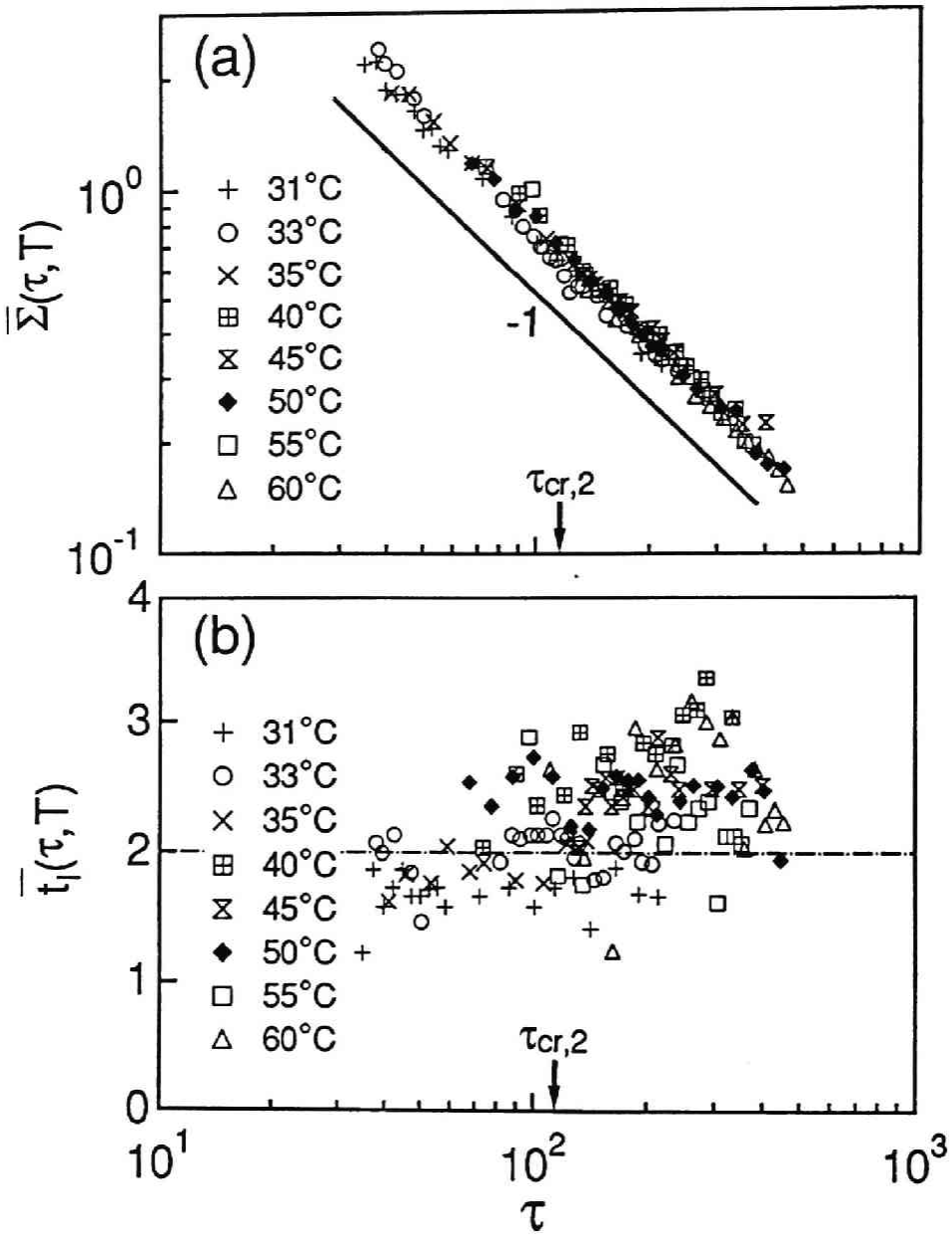

In order to extend the scaling postulate by Chou and Goldburg[24] on the global

Figure 2-12 (a) Reduced interfacial area density $\overline{\Sigma}(\tau;T)$ and (b) reduced interfacial thickness $\overline{t_I}(\tau;T)$ plotted as a function of reduced time τ.

structure to the local structure, $\bar{\Sigma}(\tau;T)$ is plotted double logarithmically as a function of τ in Figure 2-12(a). Each plot, at various T's, falls onto a master curve. This fact suggests that temperature affects only the spatial scale [through $1/q_m(0;T)$] and time scale [thorough $t_c(T)$] in the time evolution of the local structure $\Sigma(t;T)$, supporting an extension of the Chou-Goldburg scaling postulate also to the time evolution of the local pattern. Again $\gamma = 1.0$ is observed for a sufficiently wide time scale , i.e., for $30 < \tau < 500$, covered in our experiment.

Figure 2-11(b) show the time-evolution of the interfacial thickness $t_I(t;T)$ at various T's. As shown in the figure, in the time scale where the local structure can be assessed with a good accuracy, $t_I(t;T)$ tends to reach an equilibrium value $t_{Ie}(T)$ which depends only on T, as shown by the horizontal line corresponding to each T, although the data points are much scattered. Figure 2-12(b) shows the reduced interfacial thickness $\bar{t}_I(t;T)$ defined by

$$\bar{t}_I(t;T) \equiv t_I(t;T)q_m(0;T) \tag{2.36}$$

plotted as a function of the reduced time τ. Although the data points obtained at different T's are scattered, $\bar{t}_I(t;T)$ is constant with τ and approximately equal to 2 as predicted by Joanny-Leibler's theory[40] combined with the linearized theory of SD[8] (see eq.(2.43) below). The relationship between $t_{Ie}(T)$ and $q_m(0;T)$ (= 1/L in ref. 40 for asymmetric blends) will be given later. Thus we have *causality* such that the amplitude of $\Delta\phi(\underset{\sim}{r},t)$ first reaches equilibrium, which is followed by equilibration of $t_I(t;T)$, while the local and global wavenumbers are still decreasing toward equilibrium.

We reported previously[6] that $t_I(t;T)$ decreases with t in the late stage I and reaches to $t_{Ie}(T)$ in the late stage II. We could not confirm this tendency in our experiment this time, which is probably due to the change of I(q,t;T)

TABLE 2-V. The temperature dependence of the equilibrium characteristic interfacial thickness t_{Ie}

Temp. (°C)	$1/T\times10^3$ (K^{-1})	t_{Ie} (nm)	$t_{Ie,Theory}$ [a] (nm)
31	3.288	178±35	64
33	3.266	203±23	56
35	3.245	167±15	51
40	3.193	197±27	44
45	3.143	157±27	37
50	3.095	147±27	33
55	3.047	110±27	30
60	3.002	127±31	29

a) obtained using eqs.(2.37)-(2.41) and (2.43)-(2.46).

at large q involved by the correction newly incorporated in this chapter (eq.(2.17)). Temperature dependence of $t_{Ie}(T)$ was also summarized in TABLE 2-V. Although the experimental values for $t_{Ie}(T)q_m(0;T)$ is consistent with the theoretical value 2 (Fig.2-12(b)), the experimental values for t_{Ie} themselves are approximately a factor of 3 larger than those predicted by the theory as will be discussed later in conjunction with eqs. (2.37) to (2.39). This implies that the experimental values for $q_m(0;T)$ are also smaller than the theoretical values by the same factor as that for t_{Ie} if eq.(2.43) below is correct. We shall discuss later comparisons of the experimental and theoretical values of $t_{Ie}(T)$ and $\bar{t}_{Ie}(T) \equiv t_{Ie}(T)q_m(0;T)$. Let us first discuss below the theoretical determination of $t_{Ie}(T)$ and $\bar{t}_{Ie}(T)$.

2-4-4-2. Comparison between Experimental and Theoretical Interfacial Thickness

The interfacial thickness $t_{Ie}(T)$ was estimated on the basis of the following mean-field theory by Joanny and Leibler (JL)[40]. Our characteristic interfacial thickness t_{Ie} is related to L given by JL,

$$t_{Ie}(T) = 2L \qquad (2.37)$$

where

$$L = \sqrt{2}\xi(T) \tag{2.38}$$

and $\xi(T)$ is the thermal correlation length. $\xi(T)$ for the asymmetric polymer blend in the mean-field regime is given by

$$\xi(T) = (9\bar{N}/2N_AN_Bv_0\bar{a^2})^{-1/2}\varepsilon_T^{-1/2} \tag{2.39}$$

where

$$\bar{N} = N_Av_A\phi_A + N_Bv_B(1 - \phi_A), \tag{2.40}$$

$$v_0\bar{a^2} = v_Aa_A^2(1 - \phi_A) + v_Ba_B^2\phi_A. \tag{2.41}$$

Furthermore the linearized theory[8] gives a relationship between $\xi(T)$ and $q_m(0;T)$ as given by

$$\xi(T) = [\sqrt{2}q_m(0;T)]^{-1}. \tag{2.42}$$

Then from eqs. (2.37),(2.38) and (2.42), it follows that

$$t_{Ie}(T) = 2/q_m(0;T). \tag{2.43}$$

Therefore the result obtained in Fig.2-12(b),i.e., $\bar{t}_{Ie}(T) = 2$, is consistent with the theoretical result of eq. (2.43).

Here v_K, ϕ_K, a_K, and N_K denote the segment volume, the volume fraction, the Kuhn statistical segment length, and the degree of polymerization of polymer K(K = A or B), respectively, and $v_0 = [\phi_A/v_A + \phi_B/v_B]^{-1}$. In our

PB/PI mixture, A and B correspond to PB and PI, respectively; ϕ_{PB} =0.51 and ϕ_{PI} = 0.49, and a_{PB} = a_{PI} = 0.656 nm. The determination of the absolute value of $t_{Ie}(T)$, however, requires ε_T, (eq.(2.39)) which, in turn, requires $\chi(T)$ (see eq.(2.16)). If $\chi(T)$ for the PB/PI mixture is given by[41]

$$\chi = A_H + B_H/T \tag{2.44}$$

then

$$\varepsilon_T = B_H(1/T - 1/T_S)/\chi_S \tag{2.45}$$

where χ_S is given by the Flory-Huggins theory

$$\frac{\chi_S}{v_0} = \frac{1}{2}\left(\frac{1}{N_{Aw}v_A\phi_A} + \frac{1}{N_{Bw}v_B\phi_2}\right) \tag{2.46}$$

with N_{Kw} the weight-average degree of polymerization of the K-th constituent polymer (K=A or B). Since B_H is not known, we assumed that $B_H \cong B_D$ for deuterated PB (DPB) and PI mixtures with essentially equivalent microstructures[41], i.e.,

$$B_H \cong B_D = -1.333. \tag{2.47}$$

An error in B_H gives an identical error on both $t_{Ie}(T)$ and $q_m(0;T)^{-1}$. If we rely on ε_T estimated by $q_m(0;T)$, then the experimental and theoretical $t_{Ie}(T)$'s are in good agreement.

Figure 2-13 shows a plot of $t_{Ie}(T)^{-2}$ vs. T^{-1}, based upon the JL mean-field theory (see eqs.(2.37)-(2.39) and (2.43)). The solid line in Fig.2-13 obtained by a least squares fit shows the results predicted by the mean-field theory. The absolute values of the experimental t_{Ie}'s are different from the theoretical values given by the JL theory with ε_T given by eqs.(2.44) to (2.47).

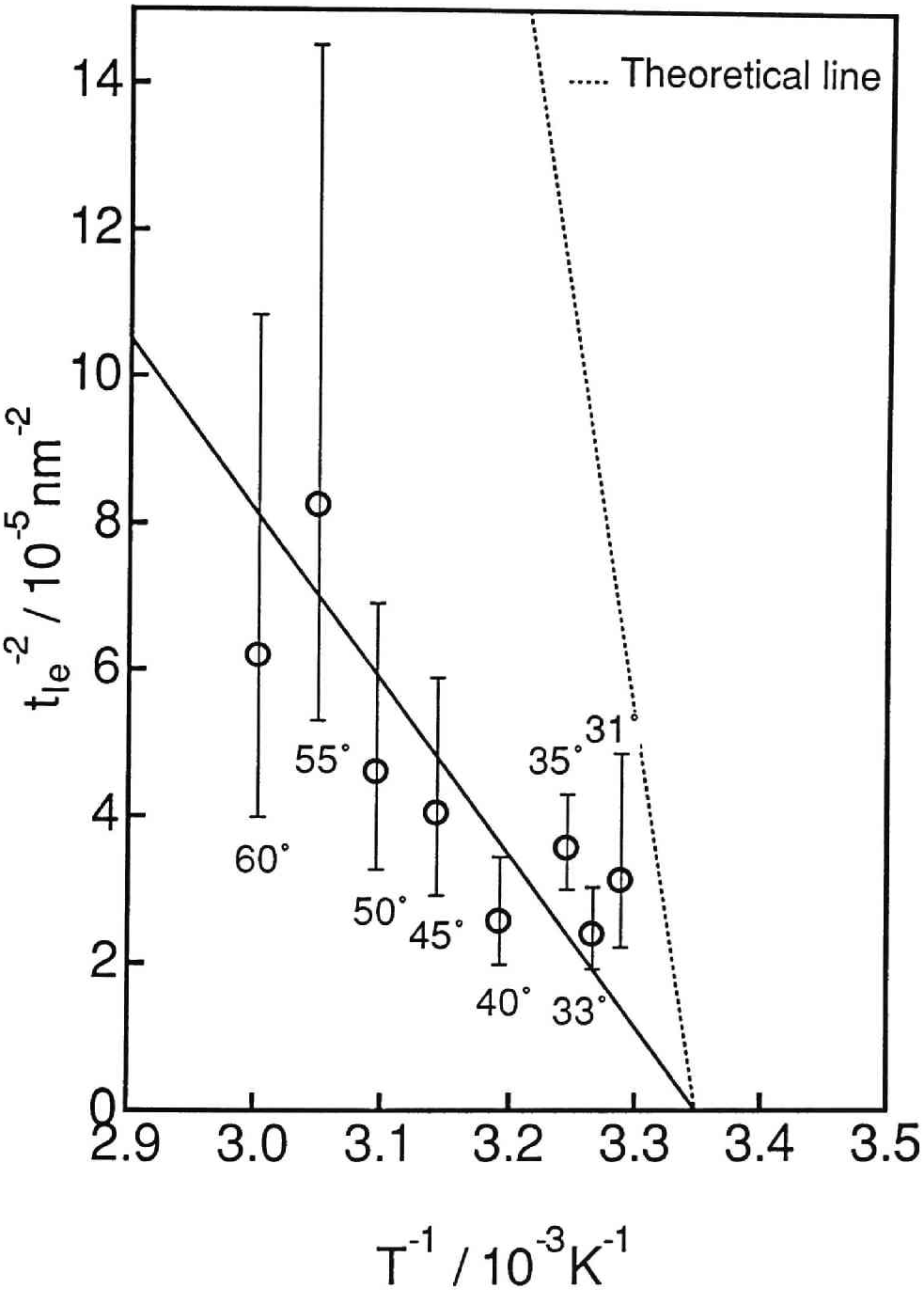

Figure 2-13 Plots of $t_{Ie}(T)^{-2}$ vs T^{-1}. The solid line is that obtained by the least squares method and the broken line is the theoretical curve given by Eqs. (2.37) to (2.39).

Now let us discuss the comparison between the experimental and theoretical values of $t_{Ie}(T)$ and $\bar{t}_{Ie}(T)$. The discrepancies between the theoretical and experimental results in $t_{Ie}(T)$ (and $q_m(0;T)$) may arise either from (i) experimental difficulties in assessing these quantities in the q-range accessible to our light scattering (LS) experiment or from (ii) error involved in the estimation of $\chi(T)$. The values $q_m(0;T)$ exist outside the largest q-range covered in our LS experiment and were indirectly determined only from the Cahn's plot as shown in Fig.2-3. The values of $t_I(t;T)$ were determined from the analysis of LS data in the Porod's law region. i.,e., at $q>q_c(t) = 1/R_m(t)$, so that the values determined should be , in principle, free from the interface waviness. Yet there may exist fine interface waviness with the radius of the curvature $R(t) < R_m(t)$. Such fine waviness may tend to make the estimated t_{Ie} larger than the true value. In this sense it is desirable to estimate t_{Ie} as a function of q, including the high q-region outside the LS experiment, which is attained by small-angle neutron or X-ray scattering. The information may then be useful to decouple the effects of the interface thickness $t_{Ie}(t)$ and the waviness R(t) on the scattering functions and hence to a rigorous estimation of $t_{Ie}(t)$. The latter reason (ii) is interpreted as follows.

As shown in eq.(2.22), $q_m(0;T) \sim \varepsilon_T^{1/2}$, while as shown in eqs.(2.37)-(2.39) $t_{Ie}(T) \sim \varepsilon_T^{-1/2}$. Thus the experimentally assessed quantity $\bar{t}_{Ie}(T) \equiv t_{Ie}(T)q_m(0;T)$ is independent of ε_T and hence of $\chi(T)$ and can be directly compared with the theoretical prediction without having information of ε_T or $\chi(T)$. The discrepancies on $t_{Ie}(T)$ and $q_m(0;T)$ described earlier may be due to an error in estimating $\varepsilon_T^{-1/2}$ by the factor of ca.3. However this error in $\varepsilon_T^{-1/2}$ does not obviously affect the value of $\bar{t}_{Ie}(T)$.

Now if the discrepancy in $t_{Ie}(T)$ is due to the latter reason (ii), then the observation $\bar{t}_{Ie}(T) = 2$ consistent with the theory, has a sound physical basis, proving the JL theory and the linearized theory. However if the discrepancy is due to the former reason (i), then the observation $\bar{t}_{Ie}(T) = 2$ is just accidental.

There might be a third possibility that the expression (2.39) for $\xi(T)$ is theoretically inadequate to describe the quantities $t_{Ie}(T)$ [$= 2\sqrt{2}\xi(T)$] and $q_m(0;T)$ [$= [\sqrt{2}\xi(T)]^{-1}$] in a two-phase state. If this is the case one can account for the discrepancy in $t_{Ie}(T)$ and the consistency in $\overline{t_{Ie}}(T) = 2$. At present we feel the reason (ii) is more probable than the others. However further clarification of the discrepancies is left as a future important investigation.

2-4-5. Scaling analysis of $\Sigma(t;T)/q_m(t;T)$

The time-evolution of the local wavenumber $\Sigma(t;T)$ in the late stage was compared with that of the global wavenumber $q_m(t;T)$. A result of the analysis is shown in Figure 2-14 where the time change of $\Sigma(t;T)/q_m(t;T)$ is plotted on a double logarithmic scale. It is clearly observed that at a given T the ratio of $\Sigma(t;T)/q_m(t;T)$ tends to decrease with t toward a constant value which appears to be independent of T within experimental accuracy. It is also observed that the higher the temperature the shorter the time required for achieving the constant value. These results suggest that $\gamma > \alpha$ in the earlier time of the late stage (the late stage I) but $\gamma = \alpha$ in the later time of the late stage (the late stage II) (eqs.(2.4) and (2.8)) and that this crossover occurs at an earlier time as temperature is raised.

As the ratio $\Sigma(t;T)/q_m(t;T)$ is a dimensionless quantity, the ratios obtained at different T's are scaled simply by reducing the time scale. The reduced plot is shown in Figure 2-15. Although the data points are much scattered, the reduced plot tends to show such a tendency that

$$\gamma - \alpha = 0.25 \qquad \text{at } \tau < \tau_{cr,2} = 120 \quad \text{(the late stage I).} \tag{2.48}$$

and

$$\gamma - \alpha = 0 \qquad \text{at } \tau > \tau_{cr,2} \quad \text{(the late stage II).} \tag{2.49}$$

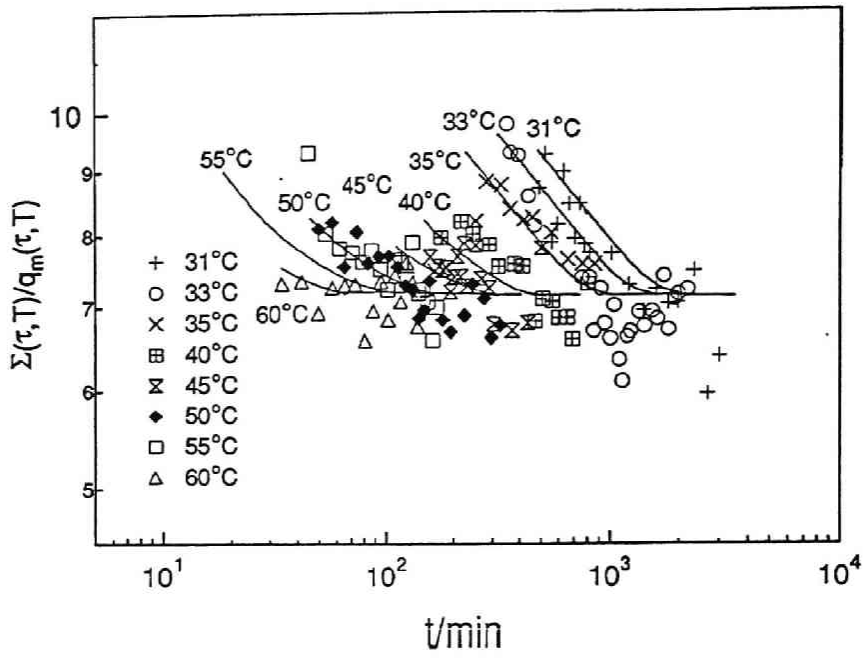

Figure 2-14 Double logarithmic plots of $\Sigma(t;T)/q_m(t;T)$ vs. t at various temperatures.

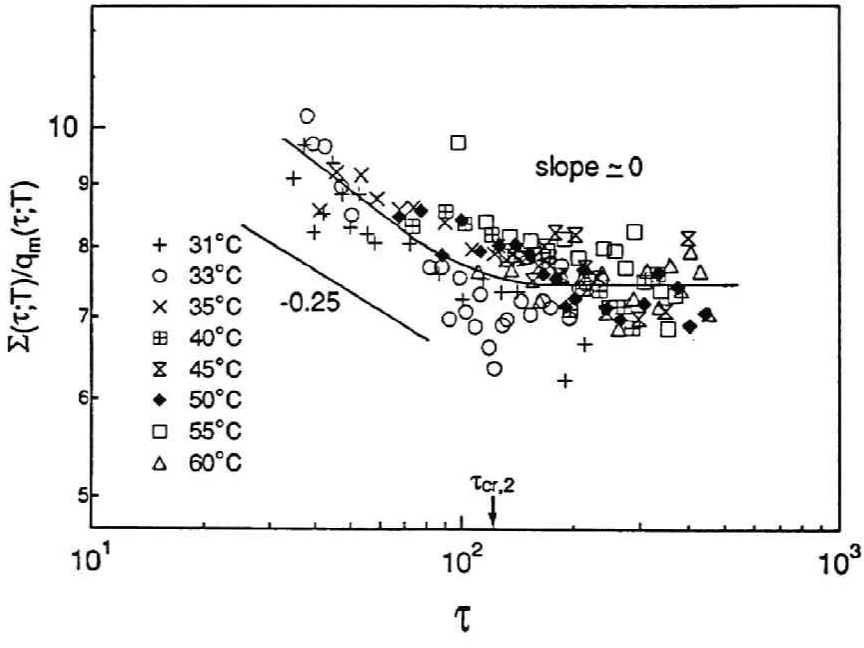

Figure 2-15 $\Sigma(\tau;T)/q_m(\tau;T)$ plotted as a function of τ in a double logarithmic scale. $\tau_{cr,2}$ is the crossover reduced time from the late stage I to the late stage II.

This result is consistent with that previously obtained[6] at 33°C. Thus we could confirm our previous conclusion on the origin of the nonuniversality in F(x,t) at large x > 2 and in the late stage I. F(x,t) at large x is given by

$$F(x,t) \sim [\Sigma(t;T)/q_m(t;T)]x^{-4}\exp[-\sigma(t;T)^2 q_m(t;T)^2 x^2] \qquad (2.50)$$

from eqs.(2.2),(2.3) and (2.33). Thus the time-dependence of F(x,t) results from the two competing factors: the decrease of $\Sigma(t;T)/q_m(t;T)$ and the increase of the exponential term due to the decrease of the relative interfacial thickness $\sigma(t;T)q_m(t;T)$. The increase of F(x,t) is due to the outweighing of the latter over the former. However in the late stage II, $\Sigma(t;T)/q_m(t;T)$ becomes independent of time and $\sigma(t;T)q_m(t;T)x << 1$ over the range of x covered in this experiment, hence the structure factor becomes truly universal with t, assuring the dynamical scaling hypothesis[17]. The value $\sigma(t;T)q_m(t;T)$ varies between 0.07 and 0.02 in the late stage II.

2-4-6. Comparisons of Scaled Structure Factors

Here we compare our universal scaled structure factor S(x) obtained in the late stage II (which is shown to be independent of t and T in sec. 2-4-3) with those obtained by computer simulations[3-5,22,23] (Fig. 2-16) and other experiments[20,42] (Fig. 2-17). The structure factor S(x) obtained in this work was confirmed to be essentially identical to that (previously) obtained at a particular temperature of 33°C (see F(x) in Fig. 13 of ref. 6). Thus our previous discussion on the comparisons of our S(x) with the theoretical one reported by Ohta-Nozaki[21] and the one obtained by a computer simulation by Chakrabarti et al.[5] are still valid. Though the theory and simulation mentioned above have been developed without incorporation of the hydrodynamic interaction, they are still found to be in good agreement.

Further progress in the computer simulations has been achieved since then, and in Fig.2-16, we compared our S(x) (the solid line) at T=55°C with

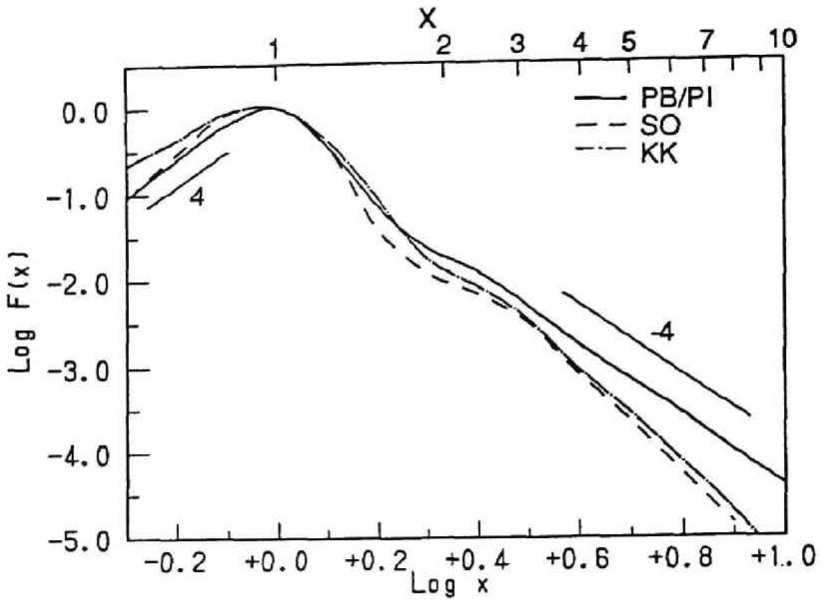

Figure 2-16 Comparison of our F(x,t) in the late stage II at T=55°C with those obtained by computer simulations. PB/PI;our data, KK;Koga-Kawasaki[4], SO;Shinozaki-Oono[3].

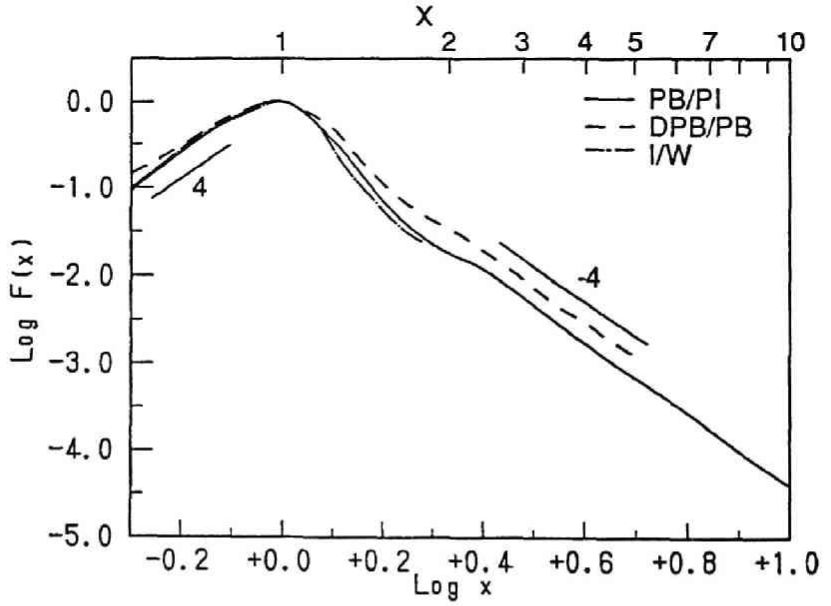

Figure 2-17 Comparison of our F(x,t) in the late stage II at T=55°C with those of other experiments. PB/PI;our data, I/W;isobutyric acid / water mixture[42], DPB/PB;deuterated polybutadiene / polybutadiene mixture[20].

two of them, both obtained in 3-d space. The broken curve shows a result obtained by Shiozaki and Ohno[3] without incorporating the hydrodynamic interactions, while the dash-dot curve by Koga-Kawasaki[4] with incorporating the hydrodynamic interactions. The two results obtained by the computer simulation are in agreement with our S(x) in that S(x) has a higher-order maximum at $x = 3$ and an asymptotic behavior of x^{-n}, $n \cong 4$ at $x > 2$. They are in agreement with our S(x) at $x<1$ in that S(x) at $x<1$ has an asymptotic behavior of x^n, $n \cong 4$. This x^4 dependence also agrees with some theoretical results[43]. However the following subtle differences may be also discernible: (i) S(x) reported by SO agrees well with our result at $x < 1$, but deviates at $x > 1$, as manifested by the fact that their S(x) is sharper than ours and (ii) S(x) reported by KK agrees with our result at $1< x < 3$ but deviates at $x < 1$ in terms of the absolute intensity. This deviation at $x < 1$ is due to the effect of the finite size of their system. The functions S(x) at $x \geq 3$ given by KK and SO has a larger exponent n than that obtained by our results. This may be due to the fact that the effect of σ or t_{le} on S(x) given by KK and SO is greater than that obtained by our results. It is interesting and important to note that the late-stage pattern itself is insensitive to the detailed coarsening processes, i.e., independent on whether the hydrodynamic interactions are active or inactive, though the coarsening rate is much affected by the hydrodynamic interactions, i.e., $\alpha = 1$ and 1/3 if they are active and inactive, respectively.

Figure 2-17 shows comparisons of our result with the two experimental results on a critical mixture of polymers (deuterated polybutadiene DPB and PB, designated by DPB/PB) by Wiltzius and Bates[20] and that of small molecules (isobutyric acid and water, designated by I/W) by Chou and Goldburg[42]. The three experimental results are similar except for the fact that the I/W mixture has the sharpest profile at $x \leq 2$ while the DPB/PB mixture has the broadest one. It is also noted that the DPB/PB mixture shows the broad higher order maximum as does the SBR/PB mixture reported

previously[30] but our mixture shows it at x = 3 instead of at x ≅ 2. The origin of this higher order maximum will be discussed in the next section.

Figure 2-18 shows comparisons of our $Q_m(\tau)$ with that reported by the computer simulation of KK[4]. It is very impressive that the 3-d computer simulation with the hydrodynamic interactions gives the time-evolution of $Q_m(\tau)$ close to that found by our experiments, though the simulation covered only the limited ranges of Q_m and τ. The hydrodynamic interactions tend to suppress the time scale where α=1/3 or 1/4 is legitimate. The theory[21] and simulations[3,5,22,23] without the hydrodynamic interactions naturally give $Q_m(\tau) \sim \tau^{-1/3}$ at the long time limit of $\tau > 10$ and hence cannot reproduce our result.

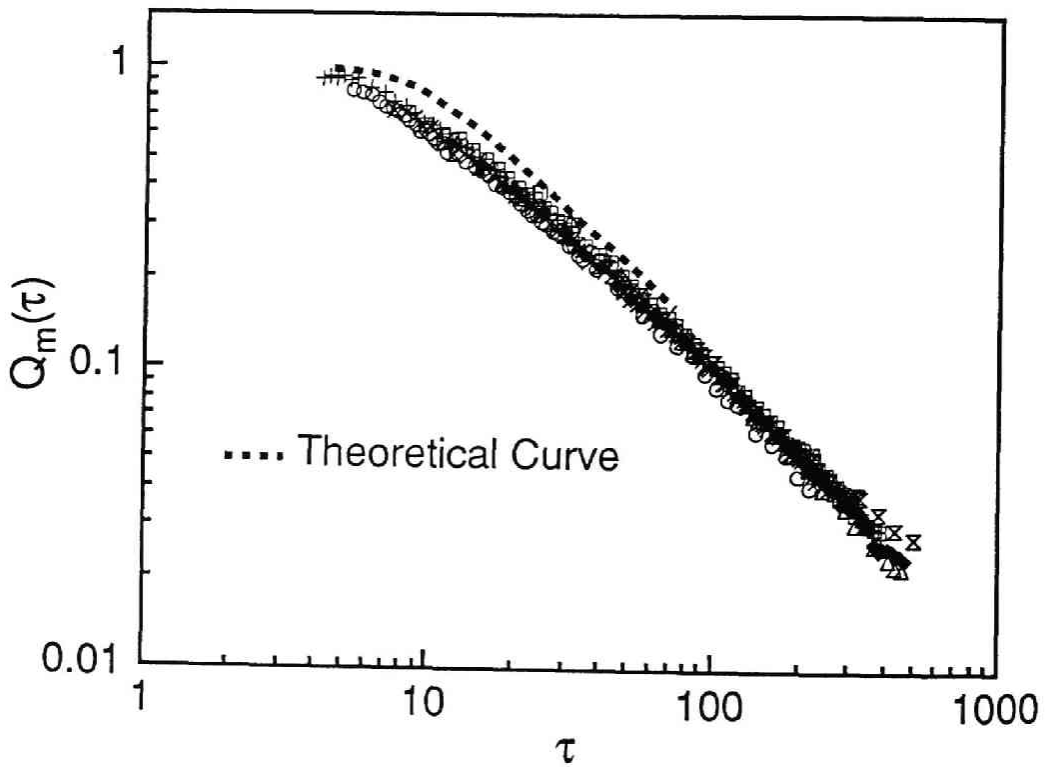

Figure 2-18 Comparison of $Q_m(\tau)$ with that obtained from computer simulation by KK[4].

2-5. Conclusion

Self-assembly of a critical mixture of PB/PI in the spinodal decomposition (SD) process was investigated as a function of ΔT (= 5.5 - 34.5) or ε_T (= 4.50×10^{-2} - 2.79×10^{-1}) using a time-resolved light scattering method. The SD process was found to be classified into four stages: early, intermediate, late I, and late II stages. One may try to classify further the early stage SD into the *very early stage* and the *early stage*. The very early stage is the one in which the thermal concentration fluctuations change from those at the initial temperature in the single phase state to those which start to be described by the linearized theory. In this case the SD can be classified into five stages. This crossover from the very early stage to the early stage was not discussed in this chapter but will be described elsewhere[44]. It is worth noting that this crossover was previously analyzed theoretically by Strobl[45] and implied experimentally by Schwahn et al.[46] to some extent.

In the intermediate- and late-stage SD, we could confirm the Chou-Goldburg scaling postulate[24] on the reduced wavenumber $Q_m(\tau)$ and the maximum scattered intensity $\tilde{I}_m(\tau)$ as a function of the reduced time τ , as we did previously for other systems, viz., the data on $Q_m(\tau)$ and $\tilde{I}_m(\tau)$ obtained at different T's or ε_T's fall onto the respective master curves on the reduced plot.

The scaled structure F(x;t) was found to be non-universal with t in the intermediate stage, primarily due to an increase of the amplitude of the concentration fluctuation $\Delta\phi(\underset{\sim}{r},t)$. In the late stage I, we found that F(x;t) becomes universal with t and that $\overline{F}(x;t)$ defined by eq.(2.30) does so with t and T at the small reduced wavenumber $x < 2$. However at the large $x > 2$, F(x,t) and $\overline{F}(x;t)$ are not universal but increasing with t. In this regime, the local wavenumber $\Sigma(t;T)$ relaxes faster than the global wavenumber ($\gamma > \alpha$), and the interfacial thickness $t_I(t;T)$ still makes a nonnegligible contribution to F(x,t) or $\overline{F}(x;t)$. Hence the pattern growth involves the time-change of the three length parameters, at least, i.e., $1/q_m(t;T)$, $1/\Sigma(t;T) \sim R_m(t;T)$, and

$t_I(t;T)$. In the late stage II, $\gamma = \alpha$, and $t_I(t;T) = t_{Ie}(T) << 1/q_m(0;T)$. Thus the interfacial thickness hardly contributes to $F(x,t)$ or $\bar{F}(x;t)$, and hence the pattern growth is scaled with the time- and temperature-dependent single length-parameter $1/q_m(t;T)$, assuring the dynamical scaling hypothesis[17] and the time- and temperature-independent universal scale function $\bar{F}(x;t) = S(x)$, except for the small temperature dependence of $\bar{F}$ at large x associated with $t_{Ie}(T)$.

Throughout the late stage, it was found that $\Sigma(t;T) \sim t^{-1}$ and the time dependence of $\Sigma(t;T)$'s at different T's is scaled with the temperature dependent characteristic parameters $q_m(0;T)$ and $t_c(T)$, viz., $\Sigma(t;T)/q_m(0;T)$ being independent of T, and the data obtained at different T's fall onto a single master curve with the reduced plot. This result naturally leads also to temperature-independent $\Sigma(t;T)/q_m(t;T)$. Thus the Chou-Goldburg scaling postulate was found to be applicable to the local structure.

It is interesting to note the following causality on the pattern growth: the composition difference $\Delta\phi(\underset{\sim}{r},t)$ first reaches an equilibrium value in the beginning of the late stage, which is followed by equilibration of $t_I(t;T)$, though the local and global structure are still changing with time toward equilibrium. In the late stage I, the local structure relaxes faster toward equilibrium than the global structure ($\gamma > \alpha$), but in the late stage II the two structures eventually relax at the same rate ($\gamma = \alpha$).

The universal scaling function $\bar{F}(x;t)$ or $S(x)$ which has a higher order maximum at $x = 3$ may suggest that the local structure at the length scale $r < r_c = R_m$ comprises a stack of alternating lamellae rich in PB and PI with such a regularity as to give the third-order maximum. The fact that the higher order maximum at $x = 2$ is not seen may be attributed to the fact that the volume fraction of each lamella is very close to 1/2 [39]. At $r > r_c$ the lamellae are curved, branched or intersected resulting in tangled, tortuous, bicontinuous, interconnected domain structure with a mean spacing

$2\pi/q_m(t;T)$. If this is the case, the mixtures having a composition biased from 1/2 are expected to show the second order peak at x = 2, as inferred in our previous report[6,12]. This point, however, should be further confirmed in the future.

References

1 T. Hashimoto, Phase Transitions **12**, 47 (1988).

2 J. D. Gunton, M. San Miguel and P. S. Sahni, *Phase Transition and Critical Phenomena*, edited by C. Domb and J. L. Lebowitz (Academic Press, N.Y., Vol. 8, p. 269.

3 A. Shinozaki and Y. Oono, Phys. Rev. Lett. **66**, 173 (1991).

4 T. Koga and K.Kawasaki Phys.Rev.A. **44**,.R817 (1991).

5 A. Chakrabarti, A. Toral, J. D. Gunton and M. Muthukumar, J.Chem.Phys. **92**, 6899 (1990).

6 T. Hashimoto, T. Takenaka and H. Jinnai, J.Appl.Cryst. **24**, 457 (1991).

7 J. W. Cahn, J.Chem.Phys. **42**, 93 (1965).

8 P. G. de Gennes, J.Chem.Phys. **72**, 4756 (1980).

9 K. Binder, J.Chem.Phys. **79**, 6387 (1983).

10 J. S. Langer, M. Bar-on and H. D. Miller, Phys.Rev.A. **11**, 1417 (1975).

11 H. Jinnai, H. Hasegawa, T. Hashimoto and C. C. Han, Macromolecules **24**, 282 (1991).

12 M. Takenaka, T. Izumitani and T. Hashimoto, J.Chem.Phys. **92**, 4566 (1990).

13 T. Hashimoto, M. Itakura and N. Shimidzu, J.Chem.Phys. **85**, 6773 (1986).

14 T. Hashimoto, M. Itakura and H.Hasegawa, J.Chem.Phys. **85**, 6773 (1986).

15 T. Izumitani, M.Takenaka and T. Hashimoto, J. Chem. Phys. **92**, 3213, (1990).

16 P. E. Tomlins and J. S. Higgins, J.Chem.Phys. **90**, 6691 (1989).

17 K. Binder and D. Stauffer, Phys.Rev.Lett. **33**, 1006 (1974).K. Binder, Phys.Rev. **B15**, 4425 (1977).

18 T. Hashimoto, M. Takenaka and T. Izumitani, Polym. Commun. **30**, 45 (1989).

19 T. Nose, in book of "Space-Time Organization in Macromolecular Fluids", edited by F. Tanaka, M. Doi and T. Ohta Springer, Berlin, (1989), p. 40.

20 F. S. Bates and P. Wiltzius, J. Chem. Phys. **91**, 3258 (1989).

21 T. Ohta and H. Nozaki, in book of "Space-Time Organization in Macromolecular Fluids", edited by F. Tanaka, M. Doi and T. Ohta Springer, Berlin (1989), p. 51.

22 R. Toral, A. Chakrabarti and J. D. Gunton, Phys.Rev.Lett. **60**, 2311 (1988); A.Chakrabarti and J.D. Gunton,Phys.Rev.B **37**, 3798 (1988).

23 S. Puri and Y. Oono, Phys.Rev.A. **38**, 434 (1988); S. Puri and Y. Oono, Phys.Rev.A. **38**, 1542 (1988); Y. Oono and S. Puri, Phys.Rev.Lett. **58**, 863 (1987).

24 Y. Chou and W. I. Goldburg, Phys.Rev.A **20**, 2105 (1979).

25 T. Hashimoto, J. Kumaki and H. Kawai, Macromolecules **16**, 641 (1983).

26 R. S. Stein and J. J. Keane, J.Polymer Sci. **13**, 21 (1955).

27 H. E. Cook, Acta. Met. **18**, 297 (1970).

28 T. Sato and C. C. Han, J.Chem.Phys. **88**, 2057 (1988).

29 T. Izumitani and T. Hashimoto, J. Chem. Phys. **83**, 3694 (1985).

30 M. Takenaka, T. Izumitani and T. Hashimoto, J.Chem.Phys. **92**, 4566 (1990).

31 E.D. Siggia, Phys.Rev.A **20**, 595 (1979).

32 H. Yang, M. Shibayama, R. S. Stein, N. Shimidzu and T. Hashimoto, Macromolecules **19**, 1667 (1986).

33 T. Kyu and J. M. Saldanha, Macromolecules **21**, 1021 (1988).

34 N. Inaba, K. Sato, S. Suzuki and T. Hashimoto, Macromolecules **19**, 1690 (1986).

35 S. Nojima, K. Tsutsumi and T. Nose, Poly.J. **14**, 907 (1982).

36 H.Tomita,Progr.Theor.Phys.Progr.Lett.,**72**,656(1984); Progr.Theor.Phys.,**72**,482(1986).

37 G. Porod, Koll. Z.,**124**,83(1951); ibid,**125**,51(1952); ibid,**125**,108(1952).

38 W. Ruland, J.Appl. Cryst.,**4**,70 (1971).

39 T. Hashimoto, M. Shibayama and H. Kawai, Macromolecules **13**, 1237 (1980).

40 J. F. Joanny and L. Leibler, J.Phys.(Paris) **39**, 951 (1978).

41 S.Sakurai, H.Hasegawa, T.Hashimoto, and C.C.Han, Macromolecules **24**, 24,(1991).

42 Y. C. Chou and W. I. Goldburg, Phys.Rev.A **23**, 858 (1980).

43 C. Yeung, Phys.Rev.Lett. **61**, 1135 (1988).
H. Furukawa, Phys.Rev.B **40**, 2341 (1989); J.Phys.Soc.Jpn. **58**, 216 (1989).

44 M.Motowoka, C.C. Han, and T.Hashimoto,in preparation ; H.Jinnai, T.Hashimoto, and C.C.Han, in preparation.

45 G. R. Strobl, Macromolecules **18**, 558 (1985).

46 D. Schwahn, K. Hahn and T. Springer, J.Chem.Phys. **93**, 8383 (1990).

Chapter 3 : Effect of Molecular Weight on Early Stage Spinodal Decomposition

3-1. Introduction

In this chapter we investigate an early stage of SD as a function of molecular weight of one of the constituent polymers, polyisoprene (PI), and the applicability of the linearized theory. The parameters characterizing the early stage SD will be obtained as a function of the molecular weight, from which transport mechanism of polymer chains in bulk in the ordering process at the phase transition will be discussed.

In the previous paper[1] a very slow spinodal decomposition was reported for the binary liquid mixtures of polybutadiene (PB) and styrene-butadiene random copolymer (SBR) at temperatures well above the glass transition temperatures (T_g's) of the constituent polymers. The time scale where the early stage of the spinodal decomposition (SD) can be described with a good accuracy by the linearized theory of Cahn[2] was found to extend over more than one hour at 40°C, for example, which is due to the system having a very long characteristic time t_c as defined by

$$t_c = \xi^2/D_{app} \tag{3.1}$$

where ξ and D_{app} are the thermal correlation length andmutual diffusivity of the mixture at a given temperature T.

Since the characteristic times of the mixtures are expected to vary very much depending on the systems, it is quite useful to compare the time-evolution of the fluctuations during unmixing of the systems with a reduced time scale τ , a dimensionless time defined by

$$\tau = t/t_c \tag{3.2}$$

where t is real time. The critical reduced time τ_c where the spinodal decomposition is described by the linearized theory with a good accuracy was shown to be a universal constant and was found to be approximately equal to 2 for some polymer systems[4]. Thus the long characteristic time t_c of the systems expands the real time scale where the early stage SD occurs. Polymer systems realize beautifully this situation[1,5,8,35].

The polymer systems to be considered in this paper have advantages of (i) a relatively narrow molecular weight distribution as they are prepared by living anionic polymerization, and of (ii) being liquid well above T_g's at the measuring temperatures. Moreover the systems can be studied in the dissipative limit where $t > t_R/\varepsilon^2$ and consequently growth of fluctuations occur as a consequence of translational diffusion of center-of-mass of polymer molecules. Here the quantity t_R is time required for the center-of-mass of the polymer chains to translate over its end-to-end distance R_o (called "reptation time" when the diffusion obeys the reptation mechanism[9,10]),

$$t_R \simeq R_o^2/D_c \tag{3.3}$$

and D_c is the self-diffusivity. The quantity ε is the thermodynamic driving force for the fluctuations to grow as defined by

$$\varepsilon = (\chi - \chi_s)/\chi_s \simeq \frac{1}{\chi_s}\left(\frac{\partial \chi}{\partial T}\right)_{T_s} \Delta T + \vartheta(\Delta T^2) \tag{3.4}$$

where χ is the thermodynamic interaction parameter between the two polymers, χ_s is the χ-parameter at spinodal point, T_s is the spinodal temperature, and T is the quench depth as defined by

$$\Delta T = |T_S - T| \tag{3.5}$$

The analyses of the early stage SD where the linearized theory works yield the characteristic parameters[1,2,4-7,11-13] such as D_{app} and q_m, the wavenumber of the dominant mode of the fluctuations. If the constituent polymers are symmetric, having identical D_c and R_o, these parameters are given by[11]

$$D_{app} = D_c \varepsilon \tag{3.6}$$

$$q_m^2 = \frac{9}{R_0^2}\varepsilon \tag{3.7}$$

Thus the ratio of the two parameters

$$q_m^2/D_{app} \sim D_c^{-1} R_o^{-2} \tag{3.8}$$

is independent of and purely depends upon the dynamical variable D_c and hence upon dynamics of the polymers at the phase transition. If the dynamics obeys reptation mode[9,10], one finds

$$q_m^2/D_{app} \sim N^1 \tag{3.9}$$

since $D_c \sim N^{-2}$ and $R_o^2 \sim N$ where N is the polymerization index. However if the dynamics obeys Rouse mode, one finds

$$q_m^2/D_{app} \sim N^0 \tag{3.10}$$

Thus the molecular-weight dependence of q_m^2/D_{app} can be a good measure to probe molecular dynamcis and transport mechanism.

Gelles and Frank[14] also investigated the effect of molecular weight on the kinetics of phase separation in polystyrene (PS) and poly(vinyl methyl ether) blends by using the technique of excimer fluorescence. By assuming that the unmixing occurs by SD, they found the growth rate of the fluctuations to decrease with increasing PS molecular weight but the observed effect was weaker than that expected from the scaling theory based upon reptation mechanism.[11,12,15] Objectives of our studies are along the same line as theirs, but we believe that the time-resolved light scattering analysis during the isothermal unmixing process would give much more quantitative information as to the spinodal decomposition and transport mechanism. The use of the polymers with narrow molecular weight distributions would give further advantages in our analyses on molecular dynamics.

3-2. Theoretical background: *spinodal decomposition of asymmetric blends*

We consider here linearized theory of spinodal decomposition for the asymmetric polymer mixtures A and B with polymerization indices N_A and N_B, statistical segment lengths a_A and a_B, self-diffusivities D_A and D_B, polymerization indices between entanglement coupling N_{eA} and N_{eB},and volume fraction of each component $\phi_A=\phi$ and $\phi_B=1-\phi$.The growth rate of q-Fourier mode of the concentration fluctuations R(q) is given by de Gennes[11], Pincus[12] and Binder[13] theories

$$R(q) = \Lambda(q)q^2\left\{2\chi - \left(\frac{1}{\phi N_A} + \frac{1}{(1-\phi)N_B}\right) - \frac{a_A^2(1-\phi)+a_B^2\phi}{18\phi(1-\phi)}q^2\right\} \quad (3\text{-}11)$$

where q is the wavenumber of a particular Fourier component of the concentration fluctuations. The equation was obtained for the small q-regime

where $qR_{gA}<<1$ and $qR_{gB}<<1$ (R_{gK} being the gyration radius of K-polymer, K = A or B) and for the time and ε regime where the effects of thermal fluctuating force on time evolution of scattering is negligible. In Eq.(3.1) $\Lambda(q)$ is the Onsager kinetic coefficient describing the mutual diffusion of the two types of chains given by[11]

$$\frac{1}{\Lambda(q)} = \frac{1}{\Lambda_{AA}(q)} + \frac{1}{\Lambda_{BB}(q)} \tag{3.12}$$

where Λ_{KK} is the coefficient for the K-th polymer (K = A or B), and Λ_{KK} in the small q-regime is given by[11]

$$\Lambda_{KK}(q\rightarrow 0) = D_K N_K \phi_K \tag{3.13}$$

From Eqs.(3.11) to (3.13), one obtains for small q-regime

$$R(q)=q^2 D_{app}\left[1 - \frac{q^2}{2q_{m2}}\right] \tag{3.14}$$

where

$$D_{app} = \frac{D_A D_B \bar{N}}{D_A N_A \phi + D_B N_B (1-\phi)}\varepsilon \tag{3.15}$$

$$q_m^2 = \frac{9\bar{N}}{N_A N_B \bar{a}^2}\varepsilon \tag{3.16}$$

$$2\chi_S = \frac{1}{\phi N_A} + \frac{1}{(1-\phi)N_B} \tag{3.17}$$

$$\bar{N} \equiv \phi N_A + (1-\phi)N_B \tag{3.18}$$

and

$$\bar{a}^2 \equiv a_A^2(1-\phi) + a_B^2\phi \tag{3.19}$$

The equations reduce to the ones derived by deGennes[11] for the symmetric blends with $N_A = N_B = N$, $a_A = a_B = a$, and $D_A = D_B = D_C$. It is clear from Eqs.(3.15) and (3.16) that the ratio q_m^2/D_{app} is independent of but depends only upon dynamical variables and hence upon dynamics.

$$\frac{q_m^2}{D_{app}} = \frac{9[D_A N_A \phi + D_B N_B(1-\phi)]}{D_A D_B N_A N_B \bar{a}^2} \tag{3.20}$$

If the diffusion occurs via reptation[9,10],

$$D_K = D_{1K} N_{eK} N_K^{-2} \quad (K = A \text{ or } B) \tag{3.21}$$

where D_{1K} is the microscopic diffusion coefficient. From Eqs.(3.20) and (3.21),

$$\frac{q_m^2}{D_{app}} = \frac{9[D_{1A} N_{eA} \phi N_B + D_B N_B(1-\phi) N_A]}{D_{1A} D_{1B} N_{eA} N_{eB} \bar{a}^2} \quad \text{(for repation)} \tag{3.22}$$

If the two polymers have identical polymerization indices, $N = N_A = N_B$, the ratio is simply proportional to N

$$\frac{q_m^2}{D_{app}} \sim N \tag{3.23}$$

If the two polymers have asymmetry in the polymerization indices but satisfy the condition

$$D_{1A}N_{eA} \simeq D_{1B}N_{eB} \equiv D_1N_e \tag{3.24}$$

as in our experimental systems (see section V), then

$$\frac{q_m^2}{D_{app}} = \frac{9[\phi N_B+(1-\phi)N_A]}{D_1N_e\bar{a}^2} \tag{3.25}$$

Comparisons of Eqs.(3.22), (3.23), and (3.25) clearly suggest that the mixtures with identical N_A and N_B are the most ideal and straight forward to judge the transport mechanism.

On the other hand if the diffusion occurs in the Rouse mode

$$D_K = D_{1K}N_K^{-1} \tag{3.26}$$

then

$$\frac{q_m^2}{D_{app}} = \frac{9[\phi D_{1A}+(1-\phi)D_{1B}]}{D_{1A}D_{1B}\bar{a}^2} \sim N_A^0N_B^0 \tag{3.27}$$

3-3. Experimental method

3-3-1. Specimens

The samples used in this studies are listed in Table 3-I together with their number average molecular weight M_n, weight average molecular weight M_w and heterogeneity M_w/M_n index measured by GPC. The weight fraction of styrene monomers in the SBR (designated as SBR1) was measured by using the Infra Red (IR) absorption at 699 cm^{-1}. The SBR sample and the PB samples (designated as PI20, PI55, PI122 and PI273) were prepared by living anionic polymerization with butyllithium as a catalyst and cyclohexane as the solvent. In Table 3-I, N and N_e are the polymerization index of entire

Table 3-I. Characterization of polymers used in this study

sample	$M_n \times 10^{-4}$	$M_w \times 10^{-4}$	Mw/Mn	PS, wt%	N/N_e[a)]
SBR1	10.0	11.8	1.18	20	32.8
PI20	17.7	20.5	1.16	0	58.6
PI55	53.5	54.6	1.02	0	156
PI122	114	122	1.07	0	349
PI273	219	273	1.25	0	780

a)N_e for SBR1 was measured to be 56.1 and that for PI was taken to be 51 for the literature.[16]

polymer and that between entanglement coupling, respectively. The value N_e for SBR1 was determined to be

$$N_e = 56.1 \quad \text{for SBR1} \tag{3.28}$$

by rheology measurement by using the relationship

$$G_{eN}{}^{o} \simeq 3.56\, G_{max}'' = \rho RT/M_e \tag{3.29}$$

where $G_{eN}{}^{o}$ is equilibrium plateau modulus, G_{max}'' is the maximum loss modulus with respect to frequency at a given temperature T, is the mass density, R is gas constant, and M_e is the molecular weight between the entanglements. The value G_{max}'' was 1.56×10^6 dynes/cm^2 at 323 K, and was 0.92g/cm^3, from which M_e was estimated to be 4.5×10^3 and N_e to be 56.1. The value N_e for PI was taken from Ferry's book[16] to be 51.5 by finding the value for PI sample having microstructure close to our PI.

The fractions of cis, trans, 1,2-vinyl and 3,4-vinyl linkages of the butadiene or isoprene part were measured by IR. They are summerized in Table 3-I.

3-3-2. Preparation of the mixtures

Mixtures of SBR1/PI20, SBR1/PI55, SBR1/PI122, and SBR1/PI273 were prepared as follows. All the mixtures studied were 50/50 wt/wt, and they were dissolved into 7 wt% toluene solution. Toluene is a neutrally good solvent for PI and SBR. The solution containing 7 wt% of total amount of polymer was homogeneous and was cast into film specimens by slowly evaporating the solvent. The solvent was completely evaporated until a constant weight was attained.

The films thus obtained were further mechanically mixed by holding and pressing repeatedly (typically 30 times) in order to make **homogenized films** immediately before the use for the studies of the phase separation kinetics. Significance of the **mixing or mechanical homogenization** was discussed in previous papers[1,17] and will be discussed extensively in a forthcoming paper[18]. Light scattering studies on the homogenized films showed that the homogenization brings the mixtures to a state corresponding to in the single phase region near the spinodal point[18].

3-3-3. Time-resolved light scattering technique

Isothermal unmixing process from the homogenized mixtures was analyzed in real time and *in situ* with an automated laser-light scattering photometer constructed in our laboratory[5]. The photometer utilizes a photomultiplier with a rapid step-scanning device and data acquisition into microcomputor as a function of time during the unmixing process. The further details of the apparatus were described elsewhere[5].

3-4. Experimental results and discussion

3-4-1. Time-evolution of light scattered intensity I(q, t)

Figure 3-1 shows typically time-evolution of light scattering profiles during isothermal phase separation at 60°C from the homogenized mixtures of (a) SBR1/PI20, (b) SBR1/PI55, (c) SBR1/PI122, and (d) SBR1/PI273

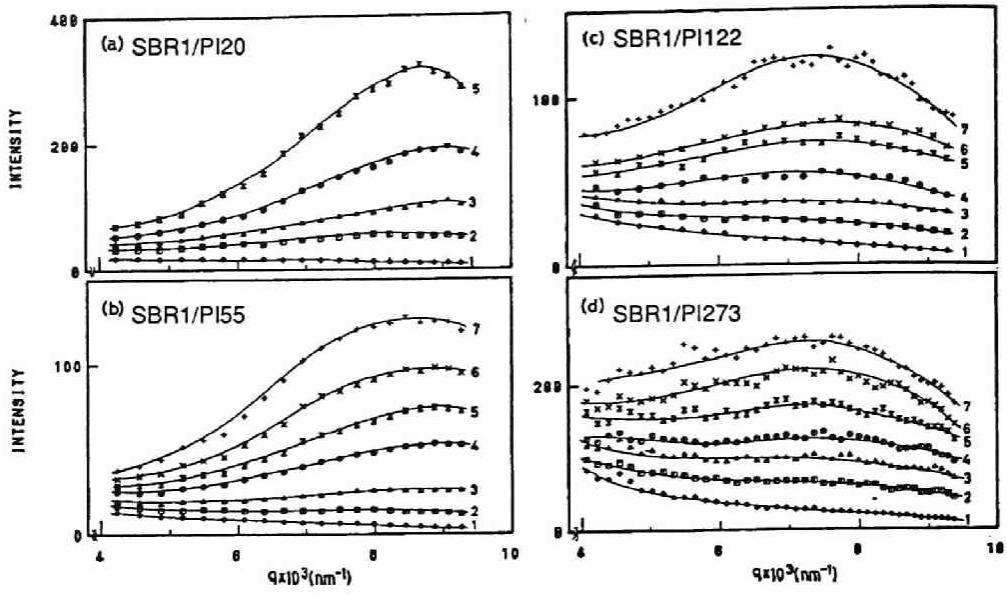

Fig.3-1 Time evolution of light scattering profiles during isothermal phase separation at 60°C for the binary mixtures of (a) SBR1/PI20, (b) SBR1/PI55, (c) SBR1/PI122, (d) SBR1/PI273. Each scattering profile was obtained at times in minutes, as indicated below,after phase separation ; (a) 1 : 2.27, 2 : 11.5, 3 : 16.1, 4 : 20.7, 5 : 25.3, (b) 1 : 2.27, 2 : 11.5, 3 : 20.7, 4 : 29.9, 5 : 34.6, 6 : 39.1, 7 : 43.8, (c) 1 : 2.27, 2 : 17.5, 3 : 32.7, 4 : 48.0, 5 : 63.2, 6 : 70.8, 7 : 92.4, (d) 1 : 4.69, 2 : 32.7, 3 : 61.2, 4 : 89.7, 5 : 132.4, 6 : 171.6, 7 : 210.9.

where some but not all of the time-sliced profiles only in the early stage unmixing process were shown. The ordinate in each figure is relative intensity so that the intensity level can be compared only within each figure but not between different figures. The abscissa is the scattering vector q defined by

$$q = (4\pi/\lambda)\sin(\theta/2) \tag{3.30}$$

where λ and θ are the wavelength of light in the medium and the scattering angle in the medium, respectively. It should be noted that the scattered intensity at the scattering vector q is related to the intensity of the q-Fourier component of the fluctuations.

Each mixture gives rise to similar time-evolution behavior of scattering : increase of scattered intensity and appearance of the scattering maximum at the high q region covered in this experiment. The q-value at which the scattered intensity reaches maximum, q_m, appears to be independent of time in the early stage unmixing process for each mixture,

$$q_m(t) = q_m(0)t^0 \tag{3.31}$$

Comparisons of Figures 3-1 and 3-2 will reveal that the early stage of unmixing process can be described with a good accuracy by the linearized theory of SD and that the profiles numbered 1 to 4 in Figure 3-1(a), those numbered 1 to 4 in Figure 3-1(b), those numbered 1 to 4 in Figure 3-1(c) and those numbered 1 to 4 in Figure 3-1(d) should correspond to the linear SD regime. The behavior given by Eq.(3.31) may be clearly seen for the mixtures having higher molecular weights (e.g. Figures 3-1(b) to 3-1(d)). The values $q_m(0)$ appear to decrease with increasing the molecular weight, so that the wavelength Λ_m of the dominant mode of concentration fluctuations increases with increasing molecular weight. Moreover the larger the molecular weight, the longer the time limit defined as t_{max} where the linear SD behavior is observed. In other words, the larger the molecular weight the slower the spinodal decomposition rate.

The rate of SD and t_{max} may be more quantitatively investigated in Figure 3-2 where logarithums of relative scattered intensity I(q,t) were plotted as a function of time t after initiation of isothermal unmixing at 60°C for each mixture (a)for SBR1/PI20, (b) for SBR1/PI55, (c) for SBR/PI122 and (d) for SBR/PI273. Each figure shows ln I(q,t) vs. t at same q values (but not all q values measured in this experiments); the curves numbered 1 to 6 for each mixture were obtained ,respectively, at q-values of 9.08×10^{-3}, 8.23×10^{-3}, 7.22×10^{-3}, 6.39×10^{-3}, 5.50×10^{-3}, and 4.24×10^{-3} nm^{-1}.

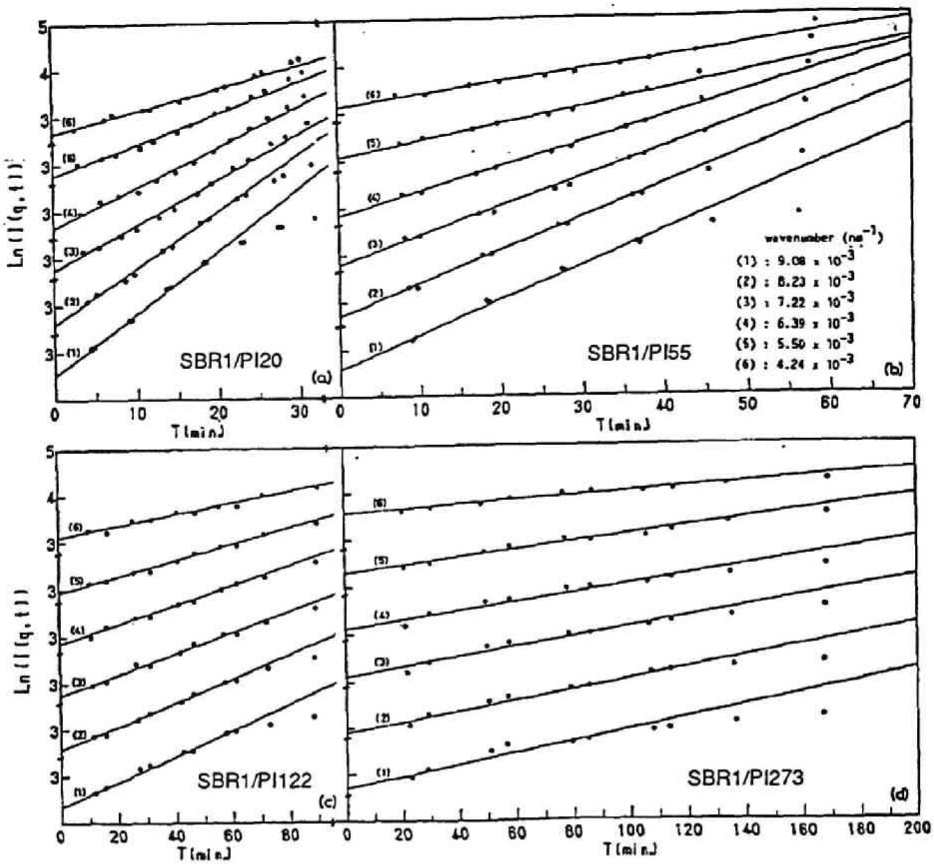

Fig.3-2 Time evolution of light scattering intensity at various q's during the isothermal phase separation at 60°C for the binary mixtures of (a) SBR1/PI20, (b) SBR1/PI55, (c) SBR1/PI122, (d) SBR1/PI273. The logarithm of the intensity was plotted as function of time t (min.).The curves numbered 1 to 6 in parts (a) to (d) were obtained at q = 9.08×10^{-3}, 8.23×10^{-3}, 7.22×10^{-3}, 6.39×10^{-3}, 5.50×10^{-3}, 4.24×10^{-3}, nm^{-1}, respectively.

Each figure shows clearly that, in the early stage unmixing process, ln I(q,t) at a given q linearly increases with t, indicating the exponential growth of the concentration fluctuations of all q-Fourier modes and of the associated scattered intensity for the q-range covered in this experiment,

$$I(q,t) = I(q,0)\exp[2R(q)t] \qquad (3.32)$$

$$S(q,t) = S(q,0)\exp[R(q)t] \tag{3.33}$$

where S(q,t) is the time-evolution of order parameter conjugated with the scattered intensity,

$$I(q,t) = \langle |S(q,t)|^2 \rangle_T \tag{3.34}$$

where $\langle\rangle_T$ denotes the average over all possible probability distribution of the order parameter. The observations given by Eqs.(3.31) to (3.33) strongly suggest that the unmixing behavior is approximated by the linearized theory of SD, as reported also for other polymer systems[1,4,8,19,20].

From the slope of each straight line one can determine the growth rate R(q) for each mixture. Comparisons of the time evolution behavior of the scattered intensity for the mixtures shown in Figure 3-2 clearly indicate that R(q) and t_{max} strongly depends on molecular weight. The larger the molecular weight the slower the growth, i.e., the smaller the value R(q) and the larger the value t_{max}.

It should be pointed out that in the later stage of unmixing (e.g. in the time scale of t > 30 min. in Figure 2(a), t > 60 min. in Figure 2(b), t > 90 min. in Figure 2(c), and t > 125 min. in Figure 2(d)), the intensity increase with time deviates from the exponential behavior at all q's due to the onset of various coarsening mechanisms[4,21-31]. In the later stage the growth rates become much slower than that of the exponential behavior as predicted by Eq.(3-32), the data points thus falling below the straight lines at all q's. The deviations of the data points in the time scale of 25 < t < 30 min. in Figure 2(a) and 45 < t < 60 min. in Figure 2(b), for example, are not yet those as described above. The upward deviation at small q's from the straight line and downward deviations at large q's from the straight line in that time scale may be due to the effect of thermal fluctuating force as described by Okada and

Han[8], brief discussions related to this point will be given in section 3-4-3. In the larger time scale the deviations from the straight lines occur always downward at all q's. The analyses in these late stage unmixing process are given elsewhere[4,23,32].

3-4-2. Growth rate for q-Fourier mode of fluctuations

Figure 3-3 shows the growth rates R(q) as a function of q for the four mixtures with different molecular weights as determined from the analyses shown in Figure 3-2 . The growth rates R(q) for all q-Fourier modes covered in this studies decrease with increasing molecular weights of the mixtures. The q-dependence of R(q) has a functional form as given by Eq.(3.14), the curves drawn by the solid lines being the best-fitted results of the The q-dependence of R(q) has a functional form as given by Eq.(3.14), the curves drawn by the solid lines being the best-fitted results of the experimental R(q) with Eq.(3.14). It should be noted that the best-fitted curves give also the straight lines in the plots as shown in Figures 4 and 5. The growth rates R(q)'s for the mixtures appear to have a maximum R_m at $q = q_m$. The growth rate R_m and the wavenumber q_m of the dominant mode of the concentration fluctuations seem to depend strongly and moderately upon the molecular weight of the mixture, respectively. The larger the molecular weight the smaller the values R_m and q_m.

3-4-3. Test of linearized theory of spinodal decomposition

Figures 3-4 and 3-5 show the plots of $R(q)/q^2$ vs. q^2 for the four mixtures which provide a critical test of Eq.(3.14) obtained by the linearized theory of SD. All the experimental results seem to exhibit with agood accuracy, the linearity as predicted by Eq.(3.14). This evidence together with the evidence given by Eqs.(3.31) and (3.32). suggest that the linearized theory of SD describes the early stage unmixing behavior of the real systems with a good approximation over the q-range covered in this studies. In the previous paper[1] the mixture SBR1/PI20 was found to have $T_S \simeq 400°C$. Hence the phase

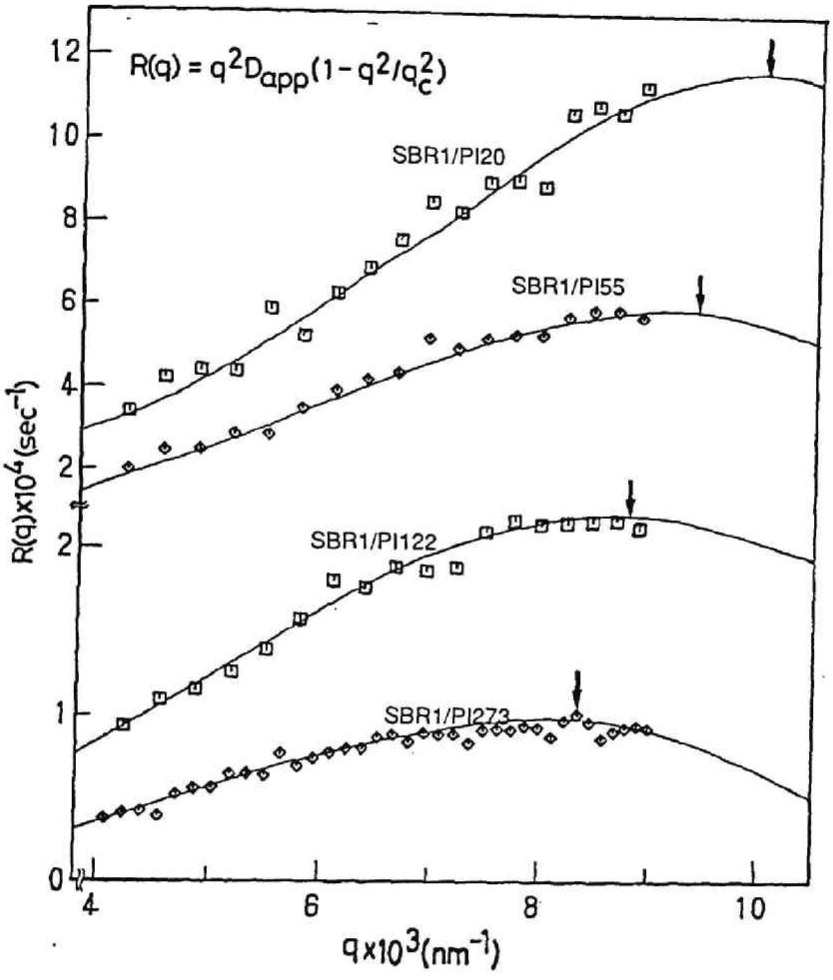

Fig.3-3 Growth rate R(q) as a function of q at 60°C for the binary mixtures.

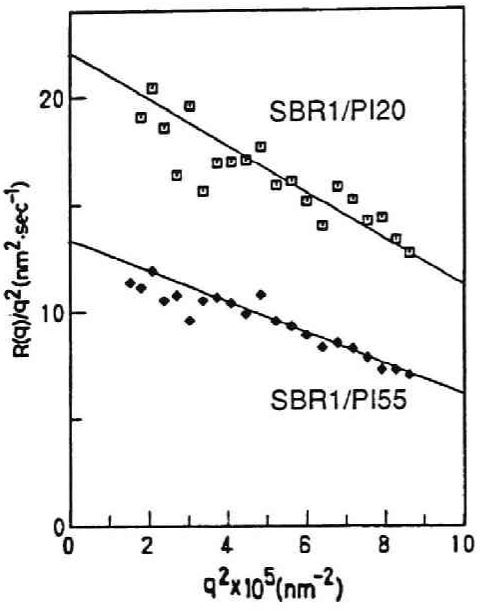

Fig.3-4 Plots of $R(q)/q^2$ vs. q^2 at 60°C for the binary mixtures of SBR1/PI20 and SBR1/PI55.

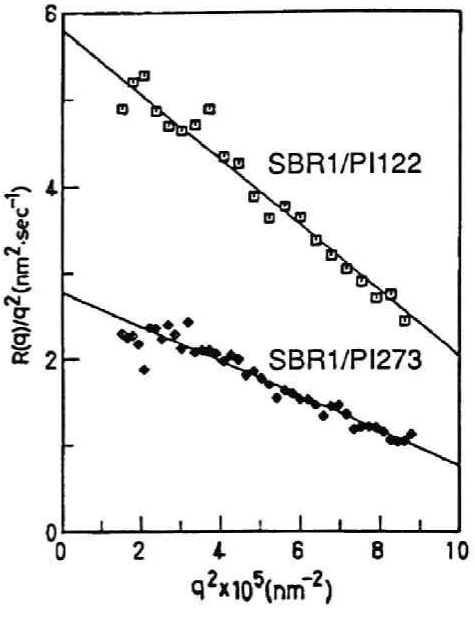

Fig.3-5 Plots of $R(q)/q^2$ vs. q^2 at 60°C for the binary mixtures of SBR1/PI122 and SBR1/PI273.

separation at 60°C corresponds to the phase separation under apparently large quench depth. It will be shown later in section 3-4 that the "effective quench depth" is not so large as the actual quench depth appears to be so.

The thermal fluctuation force[33] is one physical factor which causes the deviation from the behavior as predicted by the linearized theory of SD. Its effect is especially important at high q's near q_c where $R(q=q_c)=0$

$$q_c^2=2q_m^2 \tag{3.35}$$

Unfortunately our light scattering technique cannot cover the high q-regime of $q\simeq q_c$ but can only cover the low q regime satisfying $q<<q_m$. Hence we are observing the q-regime where the effects of thermal fluctuating force is relatively weak. Even in small q-regime the effects should be detected if the

effective quench depth is small enough. In fact Okada and Han[8] observed the effects clearly for the quench depth as large as 0.29°C but not for the quench depth as large as 0.44°C for their polymer mixtures composed of polystyrene and poly(vinyl methyl ether). In our earlier paper[4] we analized the effects of thermal fluctuatuation force on the time-evolution of scattered intensity at small q and found the effects are greater for the mixtures with larger molecular weights under a given ϵ . Under a given ϵ the effects are greater in polymer mixtures than in small molecular fluids by a faster on N (degree of polymerization)[4], which may be a possible reason why the effects were observed at the large quench depth T of 0.29°C in the studies of Okada and Han[8], much larger than those normally employed inthe small molecular fluids (T of the order of 10^{-3}°C being employed). For agiven Nthe effects decrease with increasing as well-known from the earlier studies[8,13.33]. The "effective quench depths" or ϵ's of our systems are much larger than 0.29°C, and hence the effects would hardly be seen or be small, if they exist, in the small q-regime for our system. This factor appears to act in favor of the linearized theory of SD.

The plots of Figures 3-4 and 3-5 will yield the parameters characterizing the early stage SD such as D_{app} and q_m or R_m and Λ_m as defined by

$$R_m = R(q_m(0)) \tag{3.36}$$

and

$$\Lambda_m = 2\pi/q_m(0) \tag{3.37}$$

The quantity R_m and Λ_m are the maximum growth rate of the fluctuations and the wavelength of the dominant mode of the fluctuations. The parameters

Table 3-II. Paramters characterizing ealy stage spinodal decomposition

sample	D_{app}[a]	$R_m \times 10^{4}$[b]	$q_m(0) \times 10^{3}$[c]	$\Lambda_m \times 10^{-2}$[d]	$\tau_m \times 10^{-3}$[e]	$t_c \times 10^{-3}$[f]	τ_c
	$nm^2/sec.$	sec^{-1}	nm^{-1}	nm	sec.	sec.	
SBR1/PI20	22	11	10	6.3	0.92	0.46	2.4
SBR1/PI55	13	6.0	9.5	6.7	1.7	0.84	2.5
SBR1/PI122	5.8	2.2	8.8	7.2	4.6	2.3	1.8
SBR1/PI273	2.8	0.96	8.4	7.5	10	5.2	1.4

[a]Eq.(3-14). [b]Eq.(3-36). [c]Eq.(3-31). [d]Eq.(3-37). [e]Eq.(3-38). [f]Eqs.(3-1) and (3-39).

thus estimated are summarized in Table 3-II. In Table 3-II, the parameters τ_m is defined by

$$\tau_m = R_m^{-1} \tag{3.38}$$

and t_c is the characteristic time of the mixture as defined by Eq.(3.1) where ξ is given by

$$\xi = q_m(0)^{-1} \tag{3.39}$$

3-4-4. Parameters characterizing early stage of spinodal decomposition

The apparent or mutual diffusivity D_{app} and the wavenumber $q_m(0)$ of the dominant mode of the fluctuations decrease with increasing molecular weight of one-component, e.g., PI (see Table 3-II). The value D_{app} depends both upon ε , the thermodynamic driving force which depends on N_K at given temperature ,and D_K, the transport terms which depend also on N_K (see Eq.(3-15)). Similarly $q_m(0)$ depends upon and chain dimension R_{gK} which also depends upon N_K. Generally N-dependences of D_{app} and $q_m(0)$ are a consequence of N-dependences of D_K, R_{gK} and ε. From Eq.(3.17), the value χ_S for our mixtures is given by

$$\chi_S \simeq \frac{1}{N_{PB}} + \frac{1}{N_{SBR}} \tag{3.40}$$

simply because $\phi \simeq 1/2$, where N_{PI} and N_{SBR} are the polymerization indices for PI and SBR , respectively. Now that the decrease of χ_S with increasing N_{PI} given by

$$d\chi_S/dN_{PI} = N_{PI}^{-2} \tag{3.41}$$

is small for large N_{PI}, the increase of ε with increasing N_{PI} is also expected to be small. Hence the N-dependences of D_{app} and $q_m(0)$ may be primarily be determined by those of D_K and R_{gK}. Since D_{app}/ε and q_m^2/ε are expected to decrease with increasing N_{PI}, the trends found in the experiments appear to be justified by the mean field predictions given by Eqs.(3.4) to (3.6). Likewise the N-dependences of other parameters also should primarily deterimned by the N-dependences of R_{gK} and D_K rather than that of ε.

It is interesting to note that the characteristic time t_c increases by about 10 times, from about 500 to 5000 s, by increasing N_{PI}. Similar increase of the relaxation time τ_m (from about 900 to 10000 s) for the dominant mode of fluctuations to grow was also found. The wavelength of the dominant mode of fluctuations Λ_m seems to be much larger than the molecular sizes themselves R_{gK}'s by one order of magnitude for all the mixtures (i.e., $\Lambda_m/R_{gK} \simeq 10$), a possible interpretation of which will be given in section VI.

3-4-5. τ_c

In previous papers[1,4] we indicated that the critical reduce time τ_c below which the unmixing behavior can be approximated by the linearized theory of SD is a universal constant[4] approximately equal to 2.

$$\tau_c = t_{max}/t_c \simeq 2$$

The universality was tested also for the mixtures studied here. The value t_{max}'s were estimated to be 1.2×10^3 , 2.1×10^3 , 4.2×10^3 and 7.2×10^3 s for

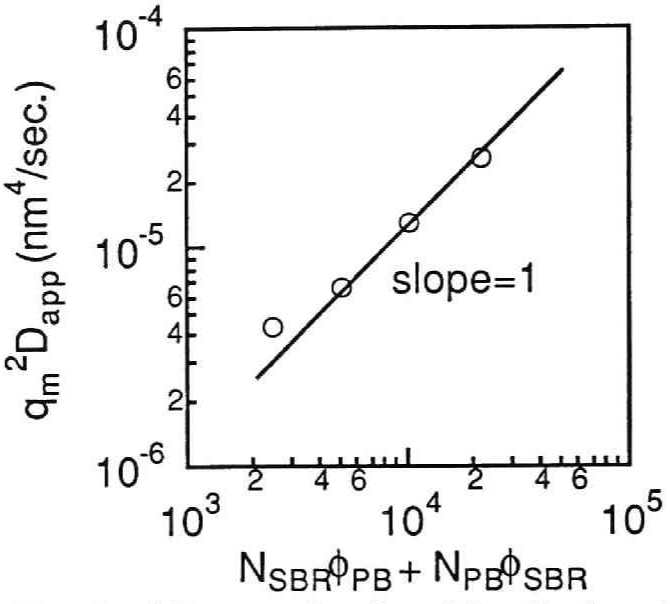

Fig.3-6 Plot of q_m^2/D_{app} as a function of the effectivepolymerzation index, $\phi_{PI}N_{SBR} + \phi_{SBR}N_{PI}$. If the mutual diffusion occurs through reptation, the slope 1 should be observed.

SBR1/PI20, SBR1/PI55, SBR1/PI122, and SBR1/PI273, respectively from the plots as shown in Figures 2 (see table III). For SBR1/PI20 and SBR1/PI55, t_{max}'s were determined at the highest accessible q's which are still slightly smaller than the corresponding q_m's, but for SBR1/PI122 and SBR1/PI273, they were determined at corresponding q_m's. The estimated values τ_c are also included in Table 3-II. The results approximately assure the relationship of $\tau_c \simeq 2$.

3-5. Transport mechanism

As already discussed in 3-2, the ratio q_m^2/D_{app} is a good probe to investigate the dynamics and transport mechanism of polymer molecules in the mixtures undergoing the phase transition. The ratios were plotted in Figure 3-6 as a function of the effective polymerization index N_{eff}

$$N_{eff} \equiv \phi_{PI}N_{SBR} + (1 - \phi_{PI})N_{PI} \qquad (3.42)$$

where ϕ_{PI} is volume fraction of PI in the mixture of PI and SBR. As is clearly seen from the Figure 6, the experimental results obtained at the three mixtures with larger molecular weights tend to support N_{eff}^{1}

$$q_m^2/D_{app} \sim N_{eff}^{1} \tag{3.43}$$

and hence the reptation mechanism. In these three mixtures N/N_e for SBR is about 33 and N/N_e for PI is from about 150 to 770(Table 3-I). However for the mixture with the smallest molecular weight (SBR1/PI20), there is a deviation from the behavior as given by Eq.(3.43).

Uncertainty of our conclusion results from inequality of N_{SBR} and N_{PI} which involves detailed information of $D_{1A}N_{eA}$ and $D_{1B}N_{eB}$ as is obvious from Eq.(3.22). Further investigation along this line which use SBR and PI specimens having about equal N_{PI} and N_{SBR} are in progress. Before closing this section we will make a rough estimation on accuracy of our assumption of Eq.(3-24) or a ratio of $(N_e/\zeta)_{SBR}$ to $(N_e/\zeta)_{PI}$ where ζ_K is the monomeric friction coefficient of K (K = SBR or PI).

From the Table 12-III of Ferry's book[16] one can estimate monomeric friction coefficients ζ_{SBR} and ζ_{PI} at 60°C by using WLF equation[16]. For example SBR has the values of log ζ (dynes·s/cm) -6.11, -7.93, and -8.25 at 298, 373 and 398 K, respectively, from which one obtains the constants C_1 and C_2 in WLF equation

$$\log\left(\frac{\zeta_0 T_0}{\zeta T}\right)_{SBR} = \frac{C_1(T-T_0)}{C_2+T-T_0} \tag{3.44}$$

where T_0 is the reference temperature (298 K) and ζ_0 is ζ at 298 K.

$$C_1 = 4.07 \quad \text{and} \quad C_2 = 102.4 \tag{3.45}$$

Hence one can estimate ζ_{SBR} at 60°C (= 333 K) as

$$\zeta_{SBR} = 6.31\times10^{-8} \qquad \text{dynes·s/cm} \tag{3.46}$$

Similarly by using the tabluated values for poly-1,4-isoprene in Table 12-III of Ferry's book[16], C_1 and C_2 for PI can be estimated as

$$C_1 = 3.15 \quad \text{and} \quad C_2 = 176.5 \tag{3.47}$$

for T_o = 298 K, from which one can estimate ζ_{PI} at 60°C as

$$\zeta_{PI} = 4.79\times10^{-8} \qquad \text{dynes·s/cm} \tag{3.48}$$

It should be noted that the microstructure for Poly-1,4-isoprene in the Table 12-III of Ferry's book[16] is different from that of our PI, hence ζ_{PI} for our PI is not necessarily the same as that given by Eq.(3.48). However the value ζ_{PI} given by Eq.(3.48) should be much closer to ζ_{PI} for our PI than that expected for poly-1,2-butadiene. Thus we use the value given by Eq.(3.48) for our PI. The value $(N_e)_{SBR}$ measured was 56.1 and that taken from the Table 13-I of the Ferry's book[16] was 45.8. The value $(N_e)_{PI}$ was 51.0 from the Table 13-I of Ferry's book[16]. By using these values one can estimate the ratio

$$(D_1N_e)_{SBR} : (D_1N_e)_{PI} = (N_e/\zeta)_{SBR} : (N_e/\zeta)_{PI}$$

$$= 1 : 1.16 \quad \text{or} \quad 1.05 : 1 \tag{3.49}$$

by using $(N_e)_{SBR}$ = 45.8 or 56.1, respectively. Thus the assumption of Eq.(3.24) and hence Eq.(3.25) may be assured.

References

1 T.Izumitani, T.Hashimoto, J.Chem.Phys. 1985, **83**, 3694.

2 J.W. Cahn, J.Chem.Phys. 1965, **42**, 93.

3 Y.C. Chou, and W.I.Goldburg,Phys.Rev. A, 1979, **23**, 2105.

4 T.Hashimoto, M.Itakura, and N.Shimizu, J.Chem.Phys. 1986, **85**, 6773.

5 T.Hashimoto, J.Kumaki, and H.Kawai, Macromolecules, 1983, **16**, 641.

6 H.L.Snyder, P.Meakin, and S.Reich, Macromolecules, 1983, **16**, 757.

7 T.Hashimoto, in "Current Topics in Polymer Science -1984 vol.2 Polymer Physics", L.A.Utracki ed., Hanser Pub. 1987.

8 M.Okada, and C.C.Han, J. Chem. Phys. 1986, **85**, 5317.

9 P.G. de Gennes, J.Chem.Phys. 1971, **55**, 572.

10 M.Doi, and S.F.Edwards, J.Chem.Soc.Faraday Trans. 2, 1978, **74**, 1789, 1802, 1818.

11 P.G. de Gennes, J.Chem.Phys. 1980, **72**, 4756.

12 P.Pincus, J.Chem.Phys. 1981, **75**, 1996.

13 K.Binder, J.Chem.Phys. 1983, **79**, 6387.

14 R.Gelles, and C.W.Frank, Macromolecules, 1983, **16**, 1448.

15 P.G. de Gennes, "Scaling Concept in Polymer Physics",Cornell Univ. Press, Ithaca and London, 1979.

16 J.D. Ferry, "Viscoelastic Properties of Polymers", 3rd ed., John Wiley & Sons, Inc., N.Y. 1980, pp.374 Table 13-I.

17 T.Hashimoto, and T.Izumitani, Polym. Prepr., Am.Chem.Soc., Div. Polym. Chem. 1985, **26**, 66.

18 T.Hashimoto, T.Izumitani, and M.Takenaka, in preparation, to be submitted to Macromolecules.

Chapter 4 : Effect of Molecular Weight on Later-Stage Spinodal Decomposition -Time-Evolution of q_m and I_m

4-1. Introduction

In chapter 3, the effect of molecular weight on the ealy stage spinodal decomposition (SD) were investigated. In this chapter we will focus on the effect of molecular weight on the later-stage SD. In our previous paper,[10] we reported that the entire process of SD can be divided into three stages called early, intermediate, and late, and referred to the intermediate and late stages combined as the later stage. The early stage is the time interval in which the time evolution of concentration fluctuations follows Cahn's linearized theory,[16] Here, the q-Fourier mode of concentration fluctuation and hence scattering intensity grows exponentially with time t, and the parameters $q_m(0;T)$ and $D_{app}(T)$ characterizing the growth can be evaluated by experiment, where $q_m(0:T)$ is the dominant q-mode of concentration fluctuation at the early stage and $D_{app}(T)$ is the mutual diffusion coefficient, both at the temperature of phase separation T. The later stage is the period in which the nonlinear nature of SD becomes increasingly apparent and the phase-separated structure coarsens with time. The structure coarsening is described by two time functions: $q_m(t;T)$ denoting the peak position of the scattering function at time t and $I_m(t;T)$ denoting the peak intensity of the scattering function at time t. It was shown[10] that if these functions are fitted to the power laws

$$q_m(t;T) \sim t^{-\alpha} \tag{4.1}$$

$$I_m(t;T) \sim t^{\beta}. \tag{4.2}$$

the exponents α and β follow an inequality

$$\beta > 3\alpha \tag{4.3}$$

in the intermediate stage and satisfy the relation

$$\beta = 3\alpha \tag{4.4}$$

in the late stage. This difference allows us to distinguish the late stage from the intermdeiate one.

Previous studies[8-15] have focused on whether the time changes in $q_m(t;T)$ and $I_m(t;T)$ scale with $q_m(0;T)$ and also with the characteristic time $t_c(T)$ defined by

$$t_c(T) \equiv [q_m(0;T)^2 D_{app}(T)]^{-1}. \tag{4.5}$$

If this scaling postulate holds, it follows that a reduced wavenumber $Q_m(\tau)$ and a reduced intensity $\tilde{I}_m(\tau)$ as functions of a reduced time τ should become universal with respect to temperature T, where

$$Q_m(\tau) = q_m(t;T)/q_m(0;T) \tag{4.6}$$

$$\tilde{I}_m(\tau) = I_m(t;T) q_m^3(0;T) \Big/ \int_{q'}^{q''} q^2 I(q,t;T)\,dq \tag{4.7}$$

$$\tau = t/t_c(T) \tag{4.8}$$

with q' and q" being the lower and upper bounds of the wavenumber q beyond which the integrand in Eq. (1.7) becomes effectively zero. The definition of q is as usual, i.e.,

$$q=(4\pi/\lambda)\sin(\theta/2), \tag{4.9}$$

where θ and λ are the scattering angle and the wavelength of the incident beam in the medium, respectively.

Most previous studies[8-14] have substantiated the validity of the above scaling postulate for various pairs of polymers, but it is not yet clear whether the master curves for $Q_m(\tau)$ and $\tilde{I}_m(\tau)$ for a polymer blend are independent of the molecular weights of the constituent polymers. It has already been found for polystyrene/poly(vinylmethylether) that $Q_m(\tau)$ reported by Snyder and Meakin[9] did not coincide with that obtained by Hashimoto et al.[10] This failure of superposition was called the N branch, and it was attributed to the difference in N/Ne between the polymer mixtures examined by the two groups. Here, N and N_e denote the polymerization index of the entire chain and that between adjacent entanglements, respectively, so that N/N_e represents the number of entanglement points per chain.

In this chapter, as a extension of chapter 3, We have investigated the effect of molecular weight on the later stage SD for a binary mixture of poly(styrene-r-butadiene) (SBR) and polyisoprene (PI) in order to deepen our understanding of the scaling postulate.

The chapter consists of the following sections. First, in 4-2, the samples, experimental methods, and phase separation conditions are described. This section is followed by 4-3-1 which presents data from time-resolved light scattering measurements, 4-3-2 which analyzes the early stage SD data by Cahn's linearized theory to evaluate the chatacteristic parameters $q_m(0;T)$ and $D_{app}(T)$, and 4-3-3 which concerns an analysis of the later stage SD data. 4-4 tests the scaling postulate for each of the mixtures studied, and 4-5 compares the master curves obtained in 4-6 with the theoretically predicted molecular weight dependence of coarsening behavior.

TABLE 4-I Sample characterization

Sample	Mw/10^4	Mw/Mn	St(wt%)[a]	Microstructure (%)[b]			
				1,4-cis	1,4-trans	1,2-vinyl	3,4-vinyl
SBR1	11.8	1.1_8	20	16	23	61	-
PI20	20.5	1.1_6	-		35	46	-
PI55	54.6	1.0_2	-	75	16	-	9
PI122	122	1.0_7	-	75	16	-	9
PI273	273	1.2_5	-	79	13	-	8

a) weight percent of styrene monomers in SBR.
b) obtained by IR.

4-2. Experimental Section

4-2-1. Samples and Methods

SBR (coded SBR1) and PI (coded PI20, PI55 PI122, and PI273) were prepared by living anionic polymerization. Their characteristics are given in Table I. Mixtures of SBR1/PI20, SBR1/PI55, SBR1/PI122, and SBR1/PI273 at the composition of 50/50 by weight were dissolved in toluene, and homogeneous solutions containing 7 wt% polymer were filtered through a Milipore film of 0.2 μm pore size. The solutions were then cast to film 0.15 mm-thick in a petri dish by evaporating the solvent at 30C° for several days. The film was further dried in a vacuum oven at room temperature until its weight became constant. The as-cast film thus prepared was opaque because of its internal unmixed structure produced by phase separation via SD during the solvent evaporation. We note that SBR is immiscible with PI so that their blend cannot be made single-phased by temperature elevation without accompanying thermal degradation. Thus we used the method described elsewhere[18] to get their homogeneous mixture. It involved repeated folding and pressing of the film as many times as typically 40 at room temperature at which unmixing

goes more slowly than uniaxial compression in the homogenization process. The homogenized film was sandwiched between thin glass plates and placed in a sample holder. Immediately the sample was heated up to a measuring temperature (50, 60, or 70C°) and the dynamics of its isothermal unmixing was followed in situ by the time-resolved light scattering technique described elsewhere.[19]

4-2-2. Phase-separation conditions

In this work, unmixing via SD was observed for SBR1/PI20 at 50 and 60C°, SBR1/PI55 at 60 and 70C°, SBR1/PI122 at 50, 60, and 70C°, and SBR1/PI273 at 60C°. We may use a parameter ε_T defined by

$$\varepsilon_T = [\chi(T) - \chi_s]/\chi_s, \tag{4.10}$$

as the thermodynamic force that drives SD. Here, $\chi(T)$ is the Flory interaction parameter per monomer for the pair of PI and SBR at temperature T, and χ_s is the value of this parameter at the spinodal temperature T_s and defined by

$$\chi_s = \frac{1}{2}\left(\frac{1}{N_{SBRw}\phi_{SBR}} + \frac{1}{N_{PIw}\phi_{PI}} \right) \tag{4.11}$$

where ϕ_K is the volume fraction of polymer K (SBR or PI) and N_{kw} is the weight-average polymerization index of K. For an approximate estimation of $\chi(T)$ under our phase separation conditions we assume that χ_{SB} and χ_{SI} are much larger than χ_{IB} at each phase separation temperature. Here, for example, χ_{SB} denotes the interaction parameter for the pair of styrene and butadiene monomers. Then $\chi(T)$ may be represented by

$$\chi(T) \equiv \chi_{SI}(1-\varphi) - \chi_{SB}(1-\varphi)\varphi, \tag{4.12}$$

TABLE 4-II Phase separation conditions

Sample	Temperature (°C)	ε_T
SBR1/PI20	50	1.24
SBR1/PI20	60	1.12
SBR1/PI55	60	1.78
SBR1/PI55	70	1.62
SBR1/PI122	50	2.27
SBR1/PI122	60	2.10
SBR1/PI122	70	1.92
SBR1/PI273	60	2.27

where φ is the volume fraction of butadiene units in the SBR chain (actually, 0.814). We use for χ_{SB} and χ_{SI} the empirical expressions:

$$\chi_{SB} = -0.0046 + 30.4/T \quad (4.13)$$

$$\chi_{SI} = 0.0025 + 18.5/T \quad (4.14)$$

which were determined by small-angle X-ray scattering from po]y (styrene-b-butadiene-b-styrene)[20] and poly (isoprene-b-styrene)[21] in the disordered state, respectively.

The values of ε_T calculated with the above set of equations are listed in Table II. They are almost constant over the temperature range covered in our experiment and are larger than unity. Thus, the phase separation temperatures used correspond to deep quench and allow strong segregation to take place.

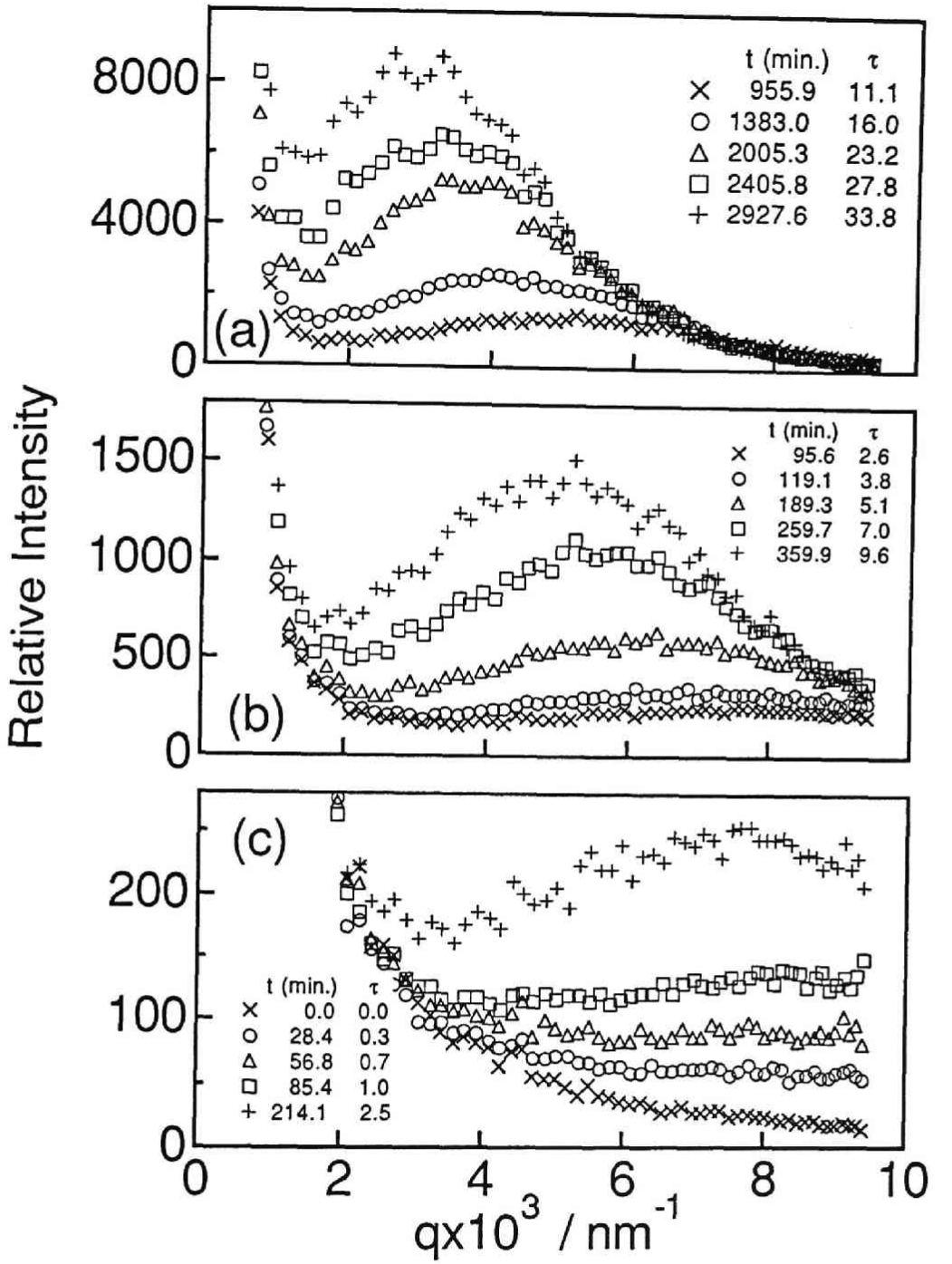

Figure 4-1 Time evolution of the light scattering profile for SBR1/PI273 after onset of unmixing at 60°C.Time elapses in the order from part (c) to (a).

4-3. Results

4-3-1. Time-evolution of the light scattering profile

Figure 1 illustrates how the light scattering profile (scattering intensity I plotted against wavenumber q) for SBR1/PI273 at 60°C changes with time. Similar data were obtained for all other samples studied.

In part (c) of Fig.1, which corresponds to the early stage of SD, the scattering maxima appear at relatively large values of q [$q_m(t;T)$] and their heights $I_m(t;T)$ increase with time while $q_m(t;T)$ remains nearly unchanged. In parts (a) and (b), which cover the later stage of SD, $I_m(t;T)$ keeps growing and $q_m(t;T)$ gets smaller with time. This change in the scatterng profile reflects the progressive coarsening of phase-separated structure. The increase in the peak intensity and the shfit of the peak position for a given mixture went faster as the phase separation temperature was elevated, while those at a given temperature occured at slower rates as the molecular weight of PI in the mixture got higher.

4-3-2. Analysis of the early stage spinodal decomposition

In the early stage SD, if the thermal noise effect is negligible, the scattering intensity I(q, t; T) at given q and T is expected to change with time following Cahn's equation

$$I(q,t;T) = I(q;t=0;T)\exp[2R(q;T)t], \qquad (4.15)$$

where R(q;T) is the growth rate parameter at given q and T. We found that the linear relation between ln I(q,t;T) and t predicted by Eq.(4.15) was obeyed by early stage SD data obtained in all the present experiments, as in previous studies.[22,23] This finding appears to substantiate the neglect of the thermal noise effect in the systems studied. We also found that I(q,0;T) obtained from the ordinate intercept of a linear ln I(q,t;T) vs. t plot satisfied the Ornstein-Zernike formula:[24]

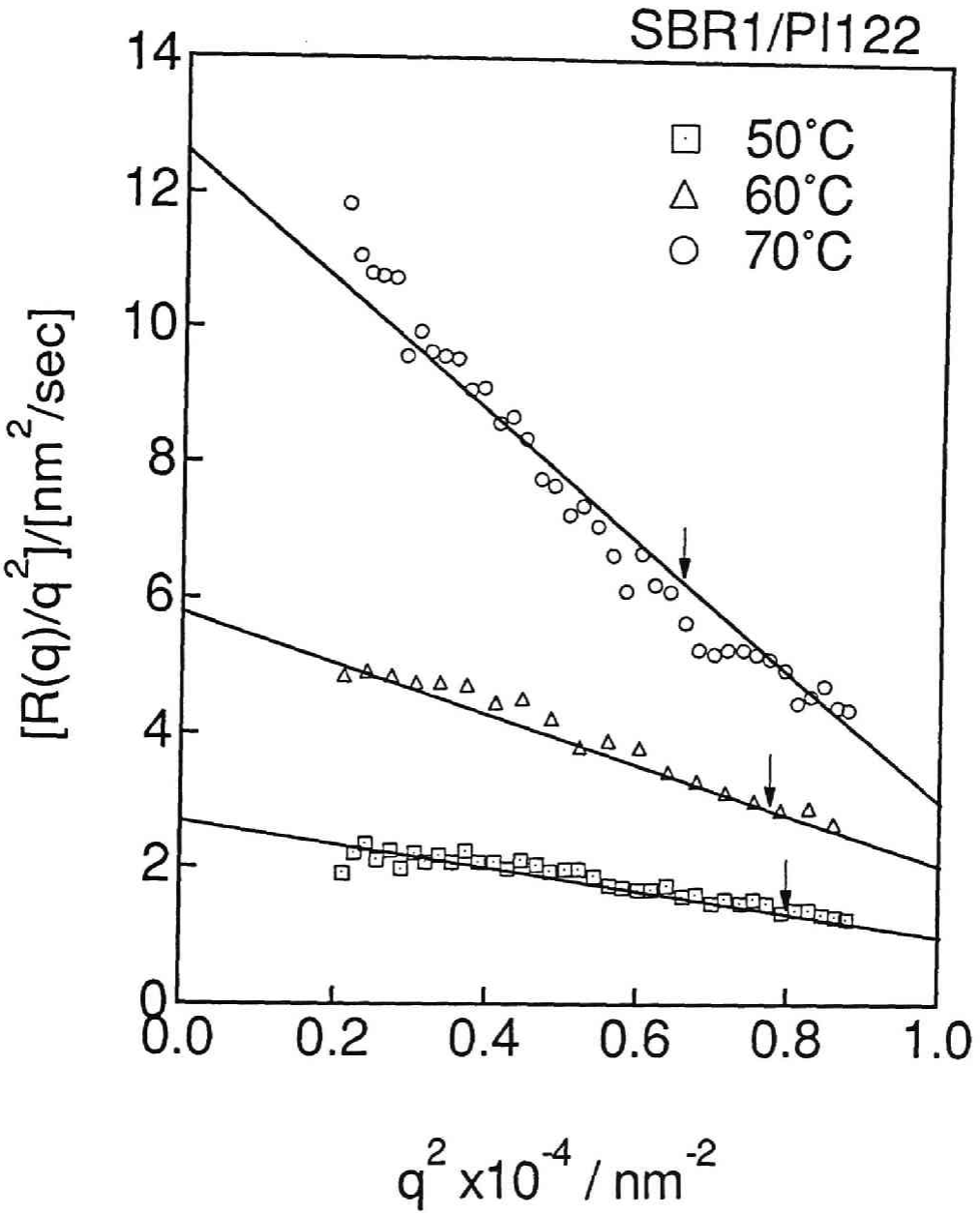

Figure 4-2 $R(q)/q^2$ vs q^2 for the early stage spinodal decomposition of SBR1/PI122 at 50 to 70°C.

TABLE 4-III Parameters characterizing the early stage of spinodal decomposition

Sample	Temperature (°C)	$D_{app}(T)$ (nm^2/sec.)	$q_m \times 10^3$ (nm^{-1})	$t_c \times 10^{-2}$ (sec.)
SBR1/PI20	50	17.0	10.0	5.9
SBR1/PI20	60	31.0	12.0	2.3
SBR1/PI55	60	13.4	9.5	8.4
SBR1/PI55	70	30.0	9.2	3.9
SBR1/PI122	50	2.7	8.1	56.5
SBR1/PI122	60	5.8	8.8	22.4
SBR1/PI122	70	12.6	8.1	12.0
SBR1/PI273	60	2.8	8.4	51.9

$$I(q,t=0;T) = I(q=0)/(1 + q^2\xi^2) \tag{4.16}$$

with large correlation lengths ξ as 75, 119, 171, and 166 nm for SBR1/PI20, SBR1/PI55, SBR1/PI122, and SBR1/PI273, respectively. These ξ values suggest that the initial homogenized samples were in a single-phase state near the spinodal point. As noted above, the phase-separation temperatures used in this work correspond to deep quench. Therefore, the virtual structure factor $I_T(q,T)$ should be such that

$$|I_T(q,T)| << I(q,t=0;T) \tag{4.17}$$

which means that the thermal noise effect is so weak that the time evolution of scattering intensity may be accurately described by Eq.(4.15)[25,26].

According to Cahn's theory, R(q;T) is given by

$$R(q;T) = q^2 D_{app}(T)[1 - q/q_c(T)^2] \quad (4.18)$$

where

$$q_c(T)^2 = 2q_m(0;T)^2, \quad (4.19)$$

with $D_{app}(T)$ being the mutual diffusion coefficient of the system. Thus, both $q_m(0;T)$ and $D_{app}(T)$ can be evaluated from the intercept and slope of a plot $R(q;T)/q^2$ vs. q^2 obtained from early stage SD data. Fig.4-2 shows this plot for SBR1/PI122 at 50, 60, and 70C°, with the solid lines fitting the data points. The other mixtures studied all exhibited similar behavior. Table 4-III summarizes the resulting values of $q_m(0;T)$ and $D_{app}(T)$.

In conclusion, the early stage SD of all the mixtures treated in this work can be described by Cahn's linearized theory with no need for the thermal noise effect taken into account.

4-3-3. Analysis of the later stage spinodal decomposition

Time changes in the peak position $q_m(t;T)$ and the peak intensity $I_m(q;T)$ in the later stage SD of all the four mixtures studied are shown in part (a) to part (d) of Fig. 4-3 on a double logarithmic format. These graphs indicate in common that the higher the temperature the faster the coarsening of phase-separated structure becomes. The arrow attached to each set of data points indicates the time $t_{cr}(T)$ at which SD crossovers from the intermediate to the late stage.

We looked to the long-time behavior of the data in Fig. 4-3 to evaluate the exponents α and β in Eqs. (1.1) and (1.2), respectively. The results are summarized in Table IV, along with the values of $t_{cr}(T)$ and the reduced crossover time $\tau_{cr}(T)$ defined by

TABLE 4-IV Scaling exponents at long time limit and crossover time

Sample	T(°C)	α	β	β/α	t_{cr}(min.)	τ_{cr}
SBR1/PI20	50	0.89	2.7	3.0	144	15
SBR1/PI20	60	0.77	2.3	3.0	65	17
SBR1/PI55	60	0.76	2.4	3.2	410	34
SBR1/PI55	70	0.77	2.4	3.1	196	30
SBR1/PI122	50	0.58	1.7	2.7	559	7.2
SBR1/PI122	60	0.62	1.8	3.0	693	19
SBR1/PI122	70	0.62	1.9	3.1	421	21
SBR1/PI273	60	0.53	1.6	3.0	739	8.5

$$\tau_{cr} \equiv t_{cr}(T)/t_c(T). \tag{4.20}$$

where $t_c(T)$ is defined by Eq. (4.5). The general trend seen from Table 4-IV is that as the molecular weight of PI in the mixture increases, both α and β get smaller while $t_{cr}(T)$ at fixed T gets larger. In the time scale of our experiment, α remains smaller than unity, i.e., SD does not enter Siggia's process.[27] We note that Kawasaki et al.[28] and Furukawa[29] have theoretically predicted 1/2 for the asymptotic value of α.

4-4. Test of the Scaling Postulate on the Peak Position

In this section we subject the later stage data for our four mixtures to a test of the scaling postulate proposed by Chou and Goldburg[17] for $q_m(t;T)$. This postulate requires that when plotted against the reduced time τ, the reduced wavenumber Q_m and the reduced intensity $\tilde{I}_m$ for a given mixture be independent of T. Part (a) to part (d) of Fig. 4-4 show that the data for each of the four mixtures meet this requirement well, as has been found to be the case with other mixtures.[8-14] Thus we can conclude that. in each of the four

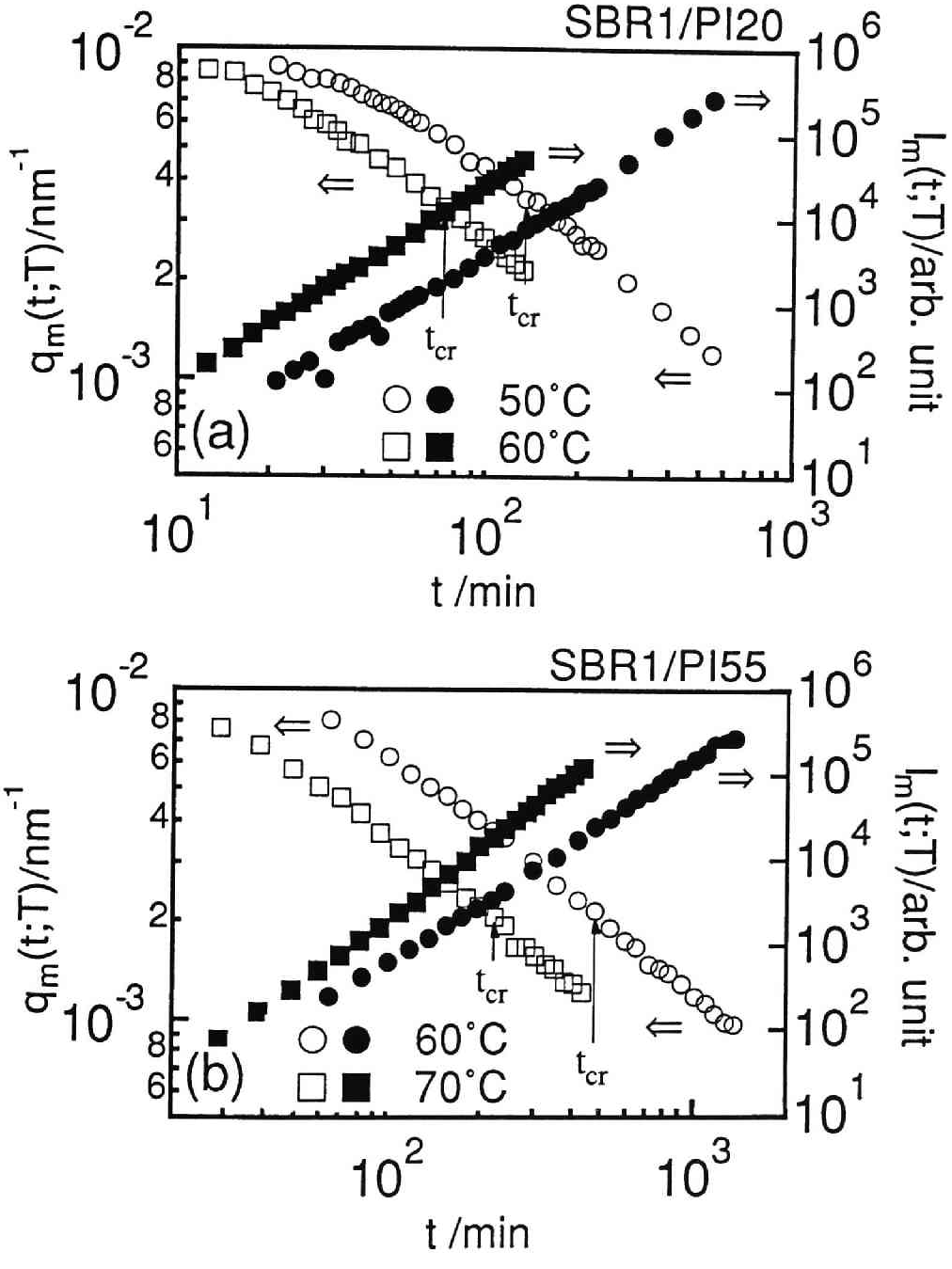

Figure 4-3 Time changes in $q_m(t;T)$ and $I_m(t;T)$ for (a) SBR1/PI20 at 50 and 60°C and (b) SBR1/PI55 at 60 and 70°C. The arrows indicates the crossover time (t_{cr}) from the intermediate stage to late stage.

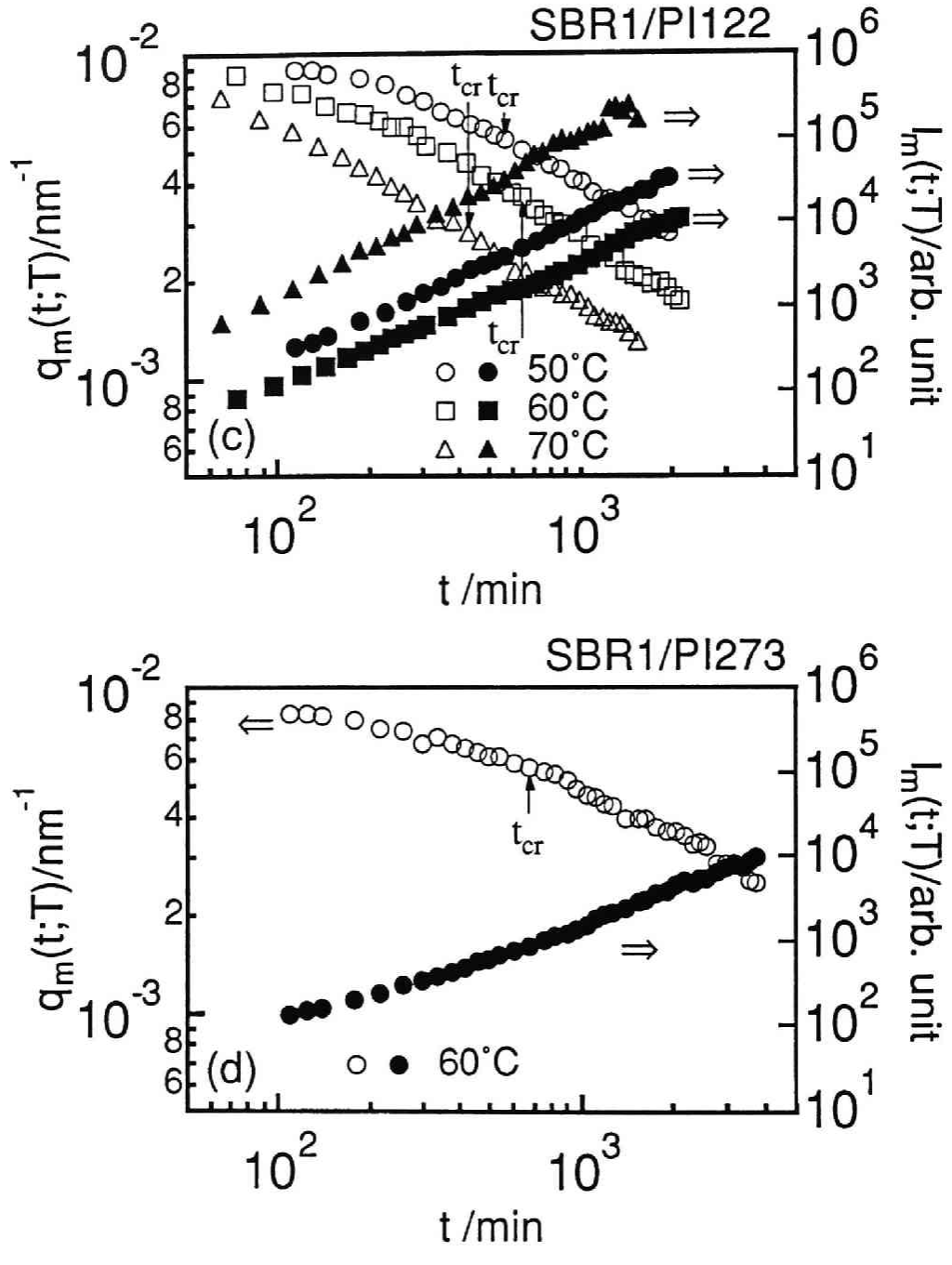

Figure 4-3 Time changes in $q_m(t;T)$ and $I_m(t;T)$ for (c) SBR1/PI122 at 50 to 70°C and (d) SBR1/PI273 at 60°C. The arrows indicates the crossover time (t_{cr}) from the intermediate stage to late stage.

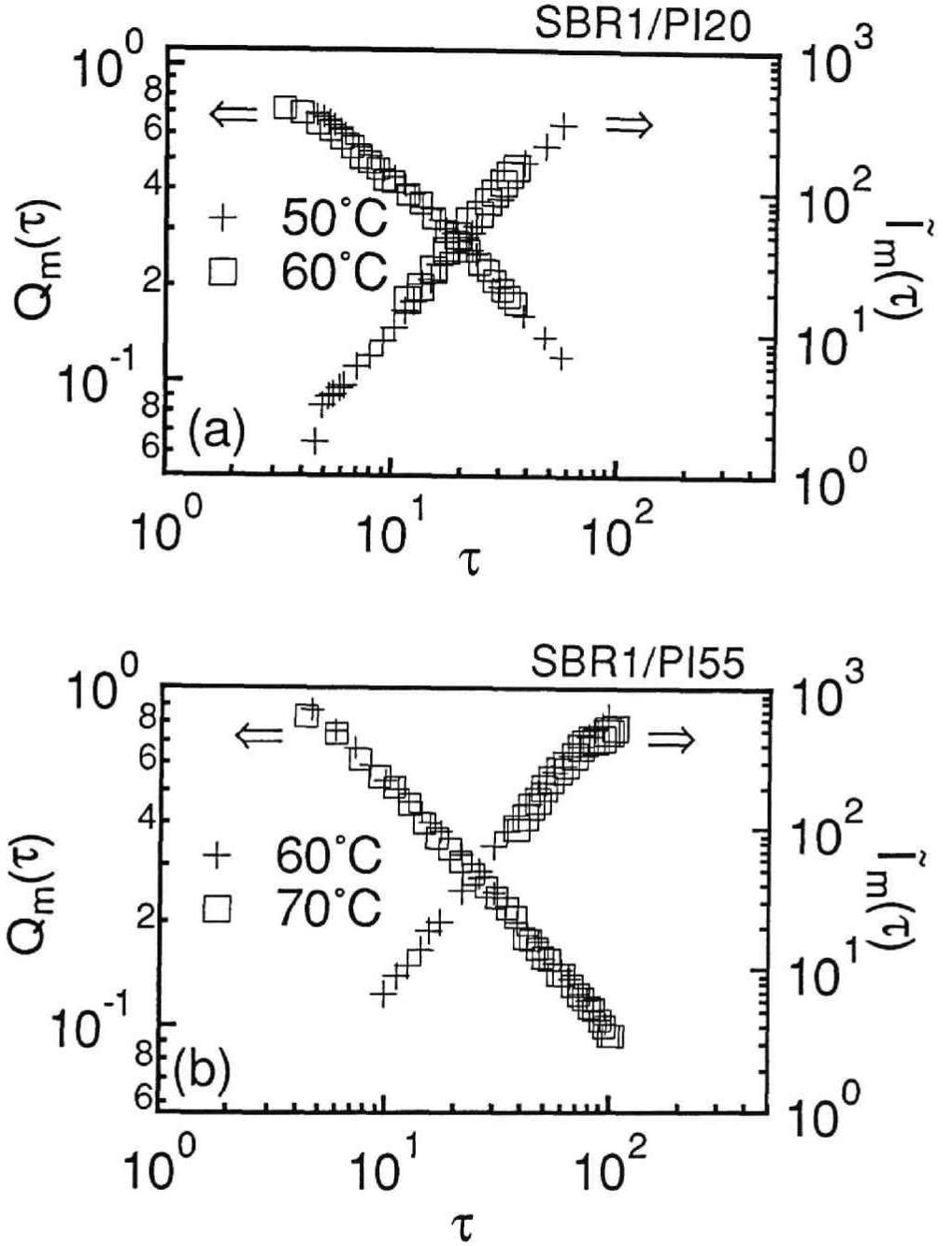

Figure 4-4 Reduced wavenumber $Q_m(\tau)$ and reduced intensity $\tilde{I}_m(\tau)$ plotted against reduced time τ for (a) SBR1/PI20 at 50 and 60°C and (b) SBR1/PI55 at 60 and 70°C.

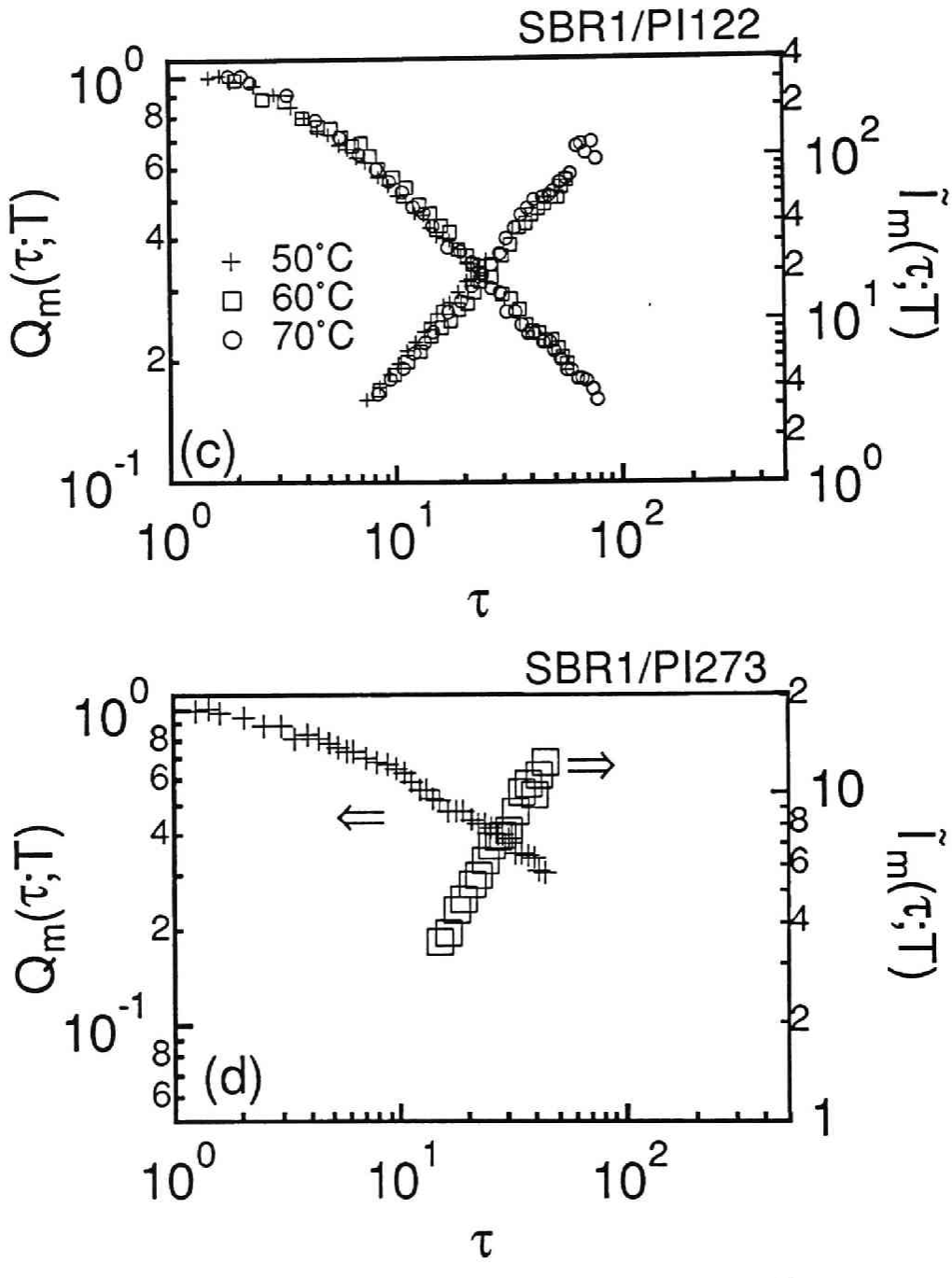

Figure 4-4 Reduced wavenumber $Q_m(\tau)$ and reduced intensity $\tilde{I}_m(\tau)$ plotted against reduced time τ for (c) SBR1/PI122 at 50 to 70°C and (d) SBR1/PI273 at 60°C.

TABLE 4-V Scaling exponents at long reduced time plots

Sample	α	β
SBR1/PI20	0.89	2.7
SBR1/PI55	0.77	2.4
SBR1/PI122	0.62	1.9
SBR1/PI273	0.53	1.6

mixtures, the effect of temperature on the growth of phase-separated structure is simply to change the time scale through t_c and the space scale through $q_m(0;T)$, but not to alter the growth mechanism. Table 4-V lists the values of α and β estimated from the long-time slopes of the reduced plots. We see them to decrease as the molecular weight of PI increases.

4-5. Superposition of the Peak Position Curves for Mixtures with Different Molecular Weights of PI

Figure 4-5 compares the $Q_m(\tau)$ vs. τ plots for the four mixtures. It is seen that the plotted points do not fall on a single curve, showing that structure coarsening proceeds more slowly as the mixture contains a higher molecular weight PI. In other words, the $Q_m(\tau)$ curves for the mixtures with different PI molecular weights are divergent. This is an example of the phenomenon, referred to as the N branch, which has been theoretically predicted by Onuki[30] and proposed by Hashimoto[1,10] on the basis of experimental results.

Onuki's theory is concerned with a symmetric mixture with the chain length larger than that between entanglements and predicts that $Q_m(\tau)$ in the Siggia process after a shallow quench is expressed by

$$Q_m(\tau) \sim (N/N_e)\tau^{-1} \qquad \text{for } N>N_e \tag{4.21}$$

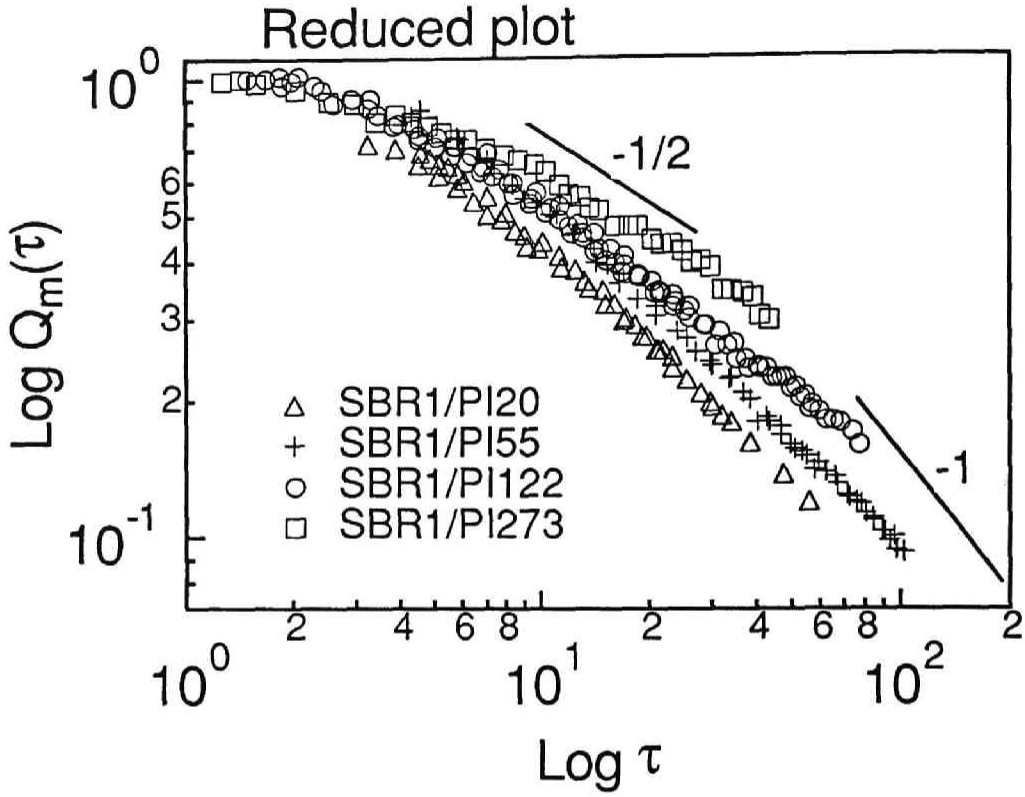

Figure 4-5 Reduced wavenumber $Q_m(\tau)$ plotted as a function of reduced time τ for SBR1/PI20 (open triangle), SBR1/PI55 (cross), SBR1/PI122 (open circle) and SBR1/PI273 (open square).

with N and N_e defined in Sec. 4-1. This relation can be rewritten

$$Q_m(\tau_p) \sim \tau_p^{-1} \tag{4.22}$$

where

$$\tau_p \equiv \tau / a_T(N) \tag{4.23}$$

with

$$a_T(N) = N/N_e, \tag{4.24}$$

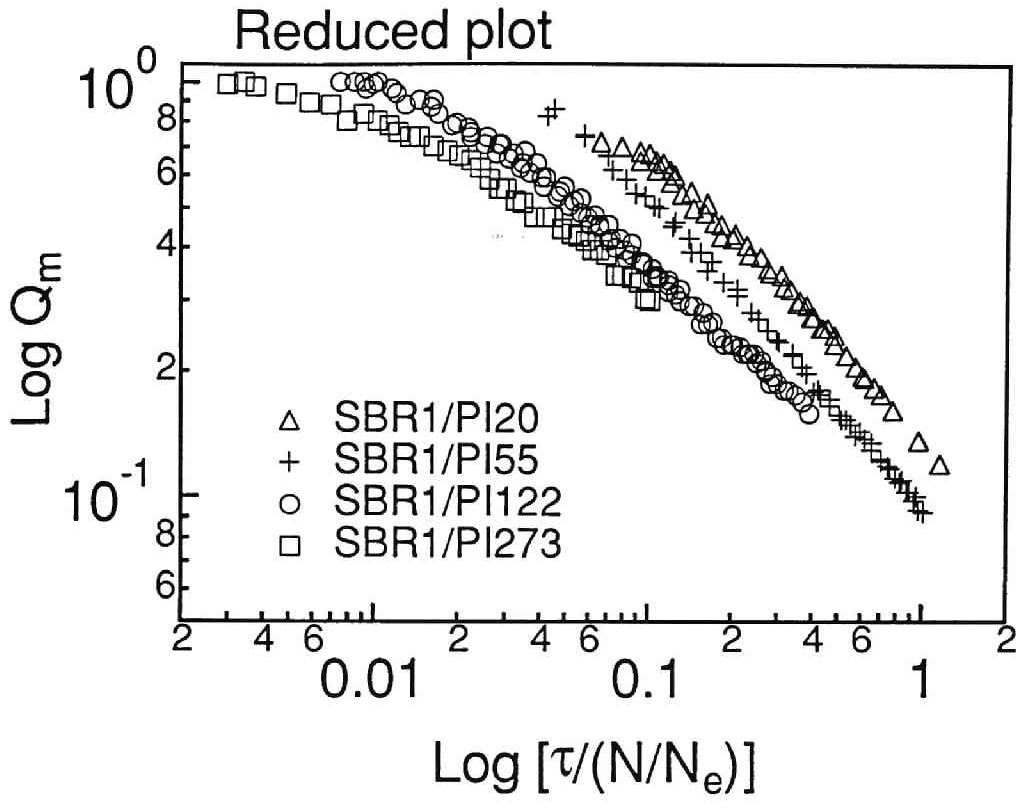

Figure 4-6 Reduced wavenumber Q_m plotted as a function of $\tau_p = \tau/(\overline{N}/\overline{N}_e)$ for four mixtures .

Thus, if Q_m for different molecular weights are replotted against a rescaled reduced time τ_p, the data points should fall on a single curve. This prediction, however, cannot be compared with the present data, because our mixtures are asymmetric ($N_{SBR} \neq N_{PI}$) and, moreover, $N_{e,SBR}$ is not equal to $N_{e,PI}$. Therefore, we attempted the comparison by replacing N/N_e in Onuki's theory with $\overline{N}/\overline{N}_e$, where $\overline{N}$ is the weight-average of N_{SBR} and N_{PI}, and $\overline{N}_e$ is that of $N_{e,SBR}$ and $N_{e,PI}$. Figure 4-6 shows Q_m for the four mixtures plotted against $\tau_p(=\tau/(\overline{N}/\overline{N}_e))$. Evidently, no successful superposition of the data points can be seen.

Next, we extended Onuki's theory for asymmetric mixture under the following assumptions : (i) the mixtures obey the reptation dynamics[31] and (ii) the monometric diffusion coefficient and N_e of both components are identical

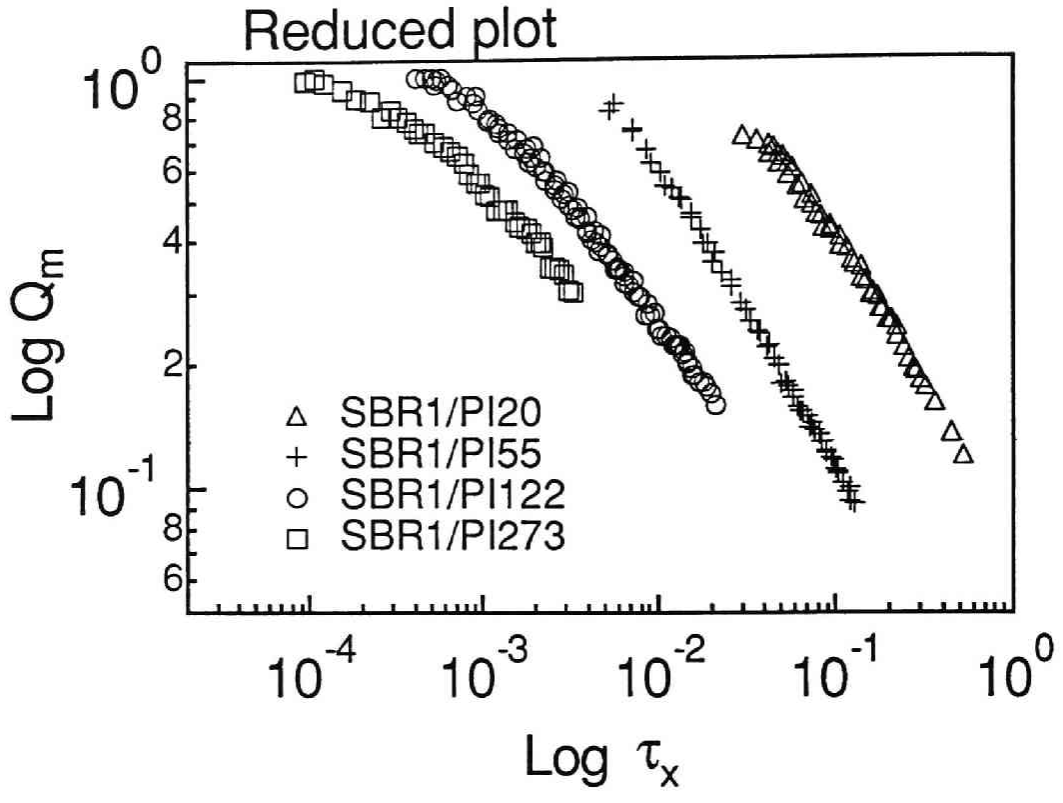

Figure 4-7 Reduced wavenumber Q_m plotted as a function of τ_x for four mixtures .

and (iii) the prefactor of t^{-1} (i.e.,η/σ) in Siggia's eq [Eq(A.1)] is still valid for the asymmetric mixture (see Appendix). The result is

$$Q_m \sim \tau_x^{-1} \tag{4.25}$$

where

$$\tau_x \equiv \tau/a_S(N) \tag{4.26}$$

with

TABLE 4-VI Values of $\bar{N}/\bar{N}_e$ and $a_T(N)$

Sample	$N/\bar{N}_e$	$\frac{N/N_e}{N_{PI20}/N_e}$	$a_T(N)$	$a_F(N)$
SBR1/PI20	49	1	1	1
SBR1/PI55	101	2.1	1.3	1.4
SBR1/PI122	201	4.1	1.7	1.7
SBR1/PI273	428	8.7	2.2	2.5

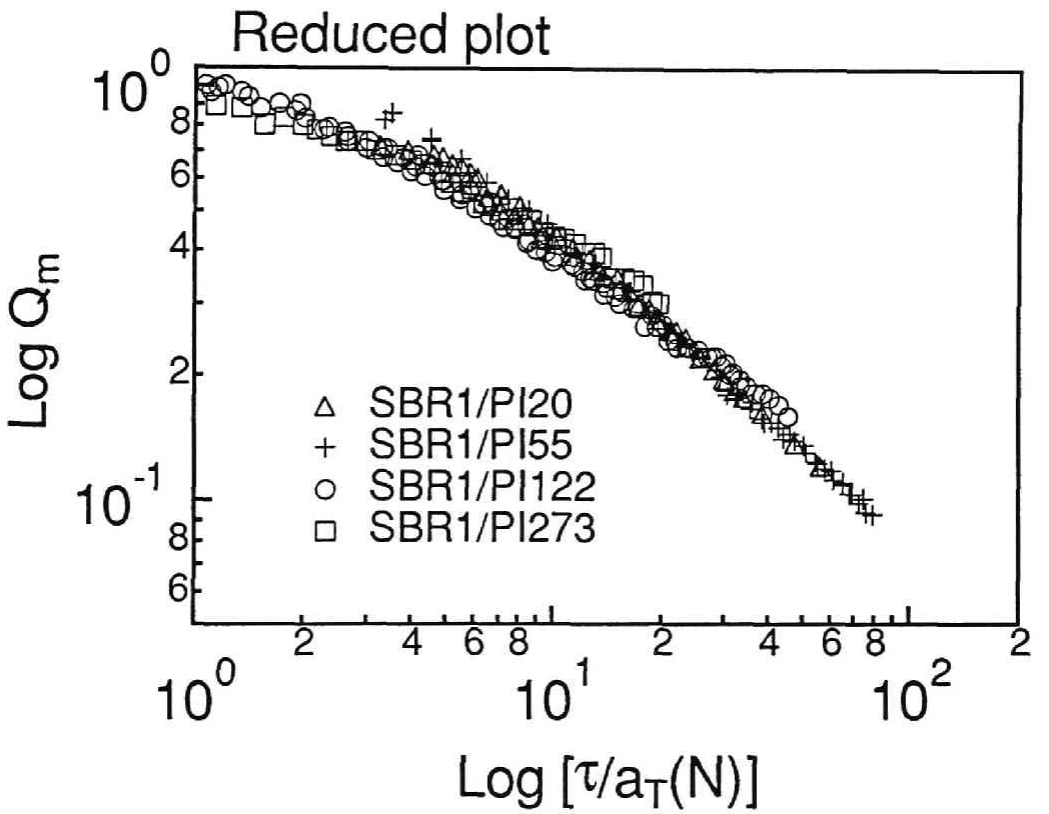

Figure 4-8 Master curve for Q_m reduced to the reference mixture SBR1/PI20 by the horizontal shift with molecular weight-dependent $a_T(N)$.

$$a_S(N) = \frac{\overline{N}_Z \overline{N}_{Z+1}(N_{SBR}\phi_{SBR}^3 + N_{PI}\phi_{PI}^3)}{N_e N_{SBR}\phi_{SBR} N_{PI}\phi_{PI}}, \qquad (4.27)$$

where $\overline{N}_z$ and $\overline{N}_{z+1}$ are z- and z+1 average of polymerization index, respectively. Figure 4-7 shows Q_m for the four mixtures plotted against τ_x. Again we can not superpose the data. We therefore turned to the following empirical attempt.

In Fig. 4-8, we choose SBR1/PI20 as the reference and shift the curves for other mixtures horizontally until they match the curve for the reference as closely as possible. The amounts of shift, denoted by a_T on the linear scale, are given in Table 4-VI, along with the corresponding values of $\overline{N}/\overline{N}_e$ and $(\overline{N}/\overline{N}_e)/(\overline{N}_{PI20}/\overline{N}_e)$. Figure 4-9 (a) shows the a_T values plotted against N/N_e on a double logarithmic format. The plotted points fall well on a straight line, giving

$$a_T \sim (\overline{N}/\overline{N}_e)^{0.37}, \qquad (4.28)$$

which indicates that the shift factor of τ scales with the 0.37 power of N/Ne.

Onuki's theory is concerned with Siggia's regime where Q_m is proportional to τ^{-1}. However, since our measurements did not reach this

Table 4-VII Parameter values in fitting Furukawa's equation.

Sample	A*	B*
SBR1/PI20	0	0.14
SBR1/PI55	0	0.1
SBR1/PI122	0	0.08
SBR1/PI273	0	0.055

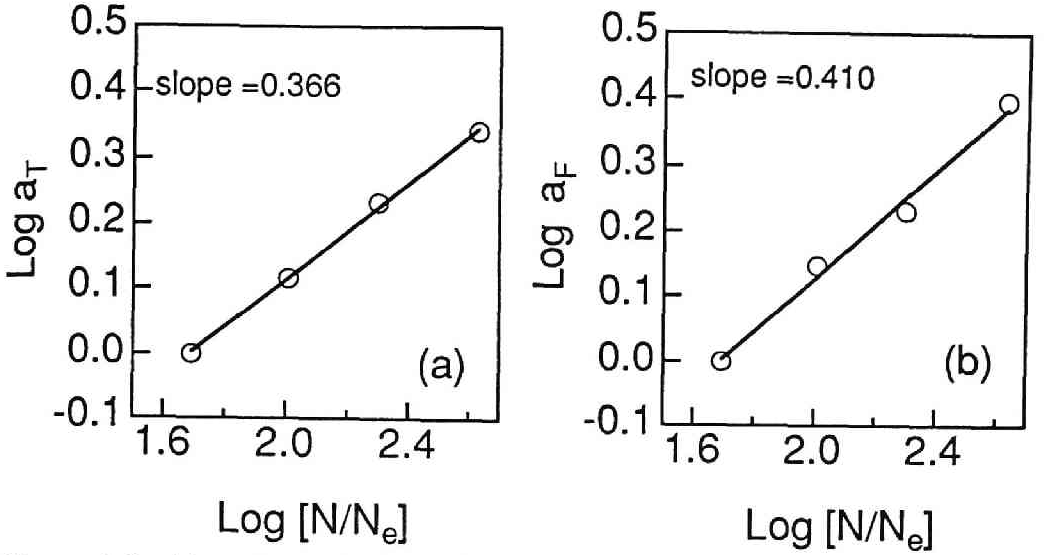

Figure 4-9 (a) $a_T(N)$ and (b) $a_F(N)$ are double logarithmically plotted as a function of $(\overline{N}/\overline{N}_e)$.

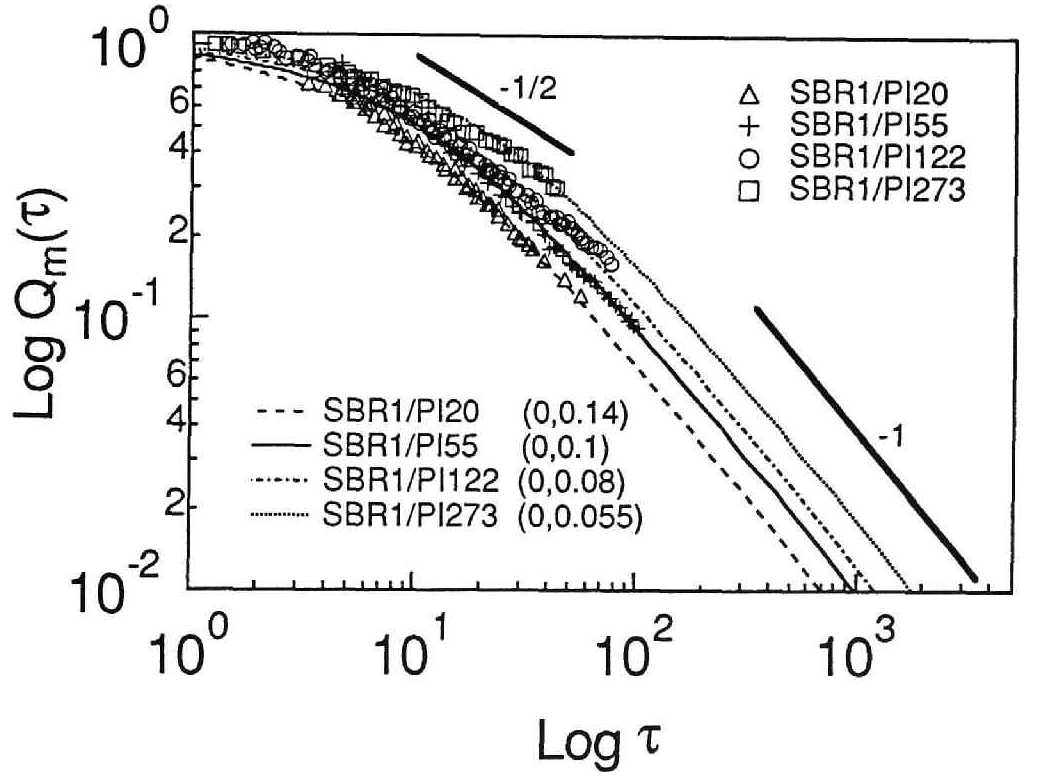

Figure 4-10 $Q_m(\tau)$ extrapolated to Siggia's regime by fitting the data to Furukawa's theory defined by Eq.(6.1).

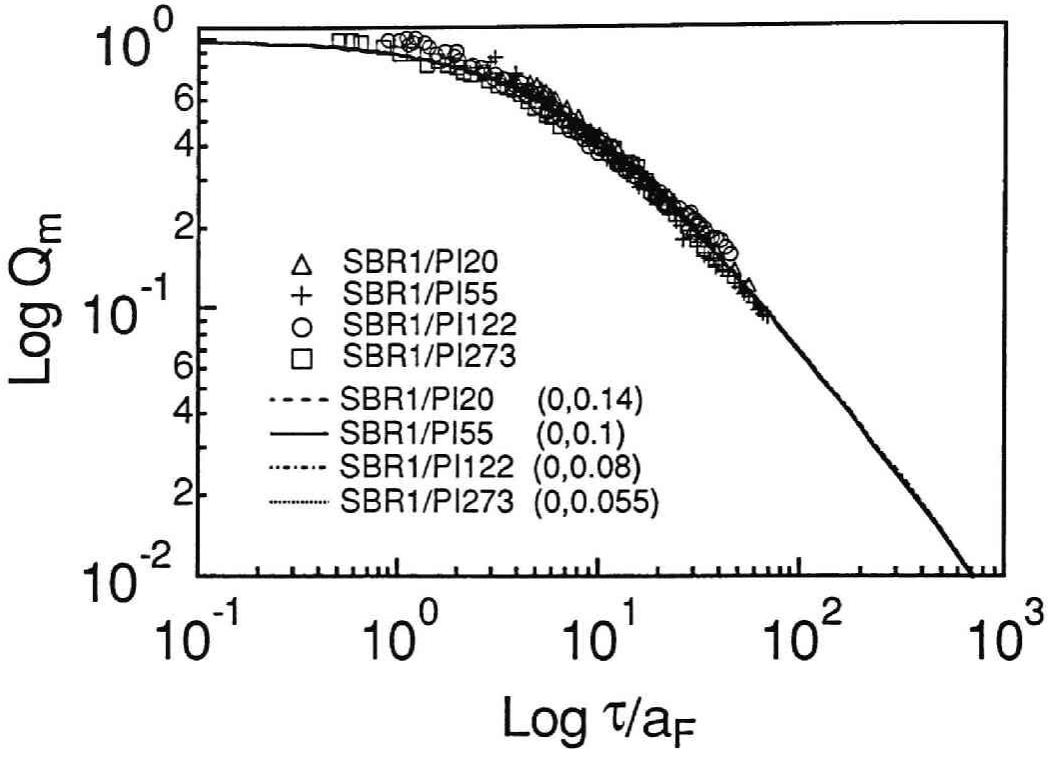

Figure 4-11 Master curve for $Q_m(\tau)$ reduced to the reference mixture SBR1/PI20 by horizontal shift with the amount of molecular weight-dependent $a_F(N)$.

regime, we attempted to extrapolate the data to the Siggia regime by use of Furukawa's theory[32]. This theory gives

$$[Q_m(\tau)^{-1} - 1] - \left\{\left(\frac{A^*}{B^*}\right)^{1/2}\left[\tan^{-1}\left\{Q_m(\tau)^{-1}\left(\frac{B^*}{A^*}\right)^{1/2}\right\} - \tan^{-1}\left\{\left(\frac{B^*}{A^*}\right)^{1/2}\right\}\right]\right\}$$
$$= B^*\tau \qquad (4.29)$$

where A* and B* are adjustable parameters. Figure 4-9 illustrates the best fits of Eq. (4.29) to our data, achieved with the choice of these parameters given

in Table 4-VII. Interestingly, A* is zero for every mixture and B* decreases systematically with increasing PI molecular weight.

The best-fit curves in Fig. 4-10 allow the Siggia regime, where the curve has a slope of unity, to be located for the respective mixtures. They can be superposed to a single curve as shown in Fig. 4-11 by horizontally shifting their parts in the Siggia regime. The amounts of shifting, $a_F(N)$, to the line for SBR1/PI20 are given in Table 4-VI and plotted against $\overline{N}/\overline{N}_e$ in Fig. 4-9 (b) on a double logarithmic format. The data points are well fitted by a straight line, giving

$$a_F(N) \sim (\overline{N}/\overline{N}_e)^{0.41}. \tag{4.30}$$

This exponent is close to that in Eq. (4.28) for a_T. Note also from Table 4-VI that the values of a_F are smaller than those of $(\overline{N}/\overline{N}_e)/(\overline{N}_{PI20}/\overline{N}_e)$. This difference deserves further investigation. In our experiments, the increase of PI molecular weight also causes the increase asymmetry on the phase diagram. Thus the molecular weight effect on $Q_m(\tau)$ is coupled with that of the asymmetry effect. In this connection, it would be of interest to see what happens to $Q_m(\tau)$ when two polymers are kept symmetric having identical chain length and their chain lengths are increased.

4-6. Conclusions

This chapter has dealt with the unmixing process via spinodal decomposition of binary mixtures SBR and PI in which the molecular weight of the former was fixed and that of the latter was varied. The time-evolution of the scattering function after (deep) quenching was followed by the time-resolved light scattering method.

The early stage of spinodal decomposition was found to be described by Cahn's linearized theory, and the parameters $q_m(0;T)$ and $D_{app}(T)$

characterizing it were evaluated. For a given mixture the temperature dependence of the later-stage spinodal decomposition was found to obey the Chou-Goldburg scaling postulate. However, the master curves for different mixtures failed to superimpose, showing the N branch effect. The horizontal shift a_T to reduce them to a single curve had a dependence on PI molecular weight weaker than that predicted by Onuki's theory. The master curves for the reduced peak position $Q_m(\tau)$ were fitted to Furukawa's theory, thereby to extrapolate them to the Siggia time region where Q_m varies as the inverse of the reduced time t. The shift factor a_F needed for superposing the curves in the Siggia regime had a molecular weight dependence comparable to a_T.

Appendix : Derivation of Eqs.(4.25) to (4.27)

We will derive Eqs.(4.25) to (4.27) based on the assumptions that the monomeric diffusion coefficients, D_1, the polymerization indices between entanglement points, N_e, and the statistical segment lengths, a, of both component are identical.

Siggia's equation,

$$q_m(t) \sim (\eta/\sigma)t^{-1} \tag{A.1}$$

can be rewritten, in terms of the reduced variable $Q_m(\tau)$ and τ, by

$$Q_m(\tau) \sim (\eta/\sigma)t_c q_m(0)\tau^{-1}. \tag{A.2}$$

where η and σ are a zero-shear viscosity and a surface tension.

the quantities of $q_m(0;T)$, $t_c(T)$, and σ for asymmetric blends, are given by[25,33]

$$q_m^2(0;T) = \frac{9\bar{N}}{N_{SBR}N_{PI}a^2}\varepsilon_T \tag{A.3}$$

$$t_c(T) = \left[\frac{9\bar{N}^2 D_{SBR}D_{PI}}{N_{SBR}N_{PI}a^2(D_{SBR}N_{SBR}\phi_{SBR} + D_{PI}N_{PI}\phi_{PI})}\varepsilon_T^2\right]^{-1} \tag{A.4}$$

$$\sigma = \frac{2}{3a^2}\left(\frac{1}{N_{SBR}\phi_{SBR}} + \frac{1}{N_{PI}\phi_{PI}}\right)^{3/2}\varepsilon^{3/2}\left(\frac{1}{\phi_{SBR}} + \frac{1}{\phi_{PI}}\right)^{1/2} \times\left(\frac{1}{N_{SBR}\phi_{SBR}^3} + \frac{1}{N_{PI}\phi_{PI}^3}\right)^{-1} \tag{A.5}$$

with ε_T being defined by Eq.(4.10) and $\bar{N}$ by

$$\bar{N} = N_{SBR}\phi_{SBR} + N_{PI}\phi_{PI} \tag{A.6}$$

as in the text. We further assume that η is given by[31]

$$\eta \sim \frac{\bar{N}_w \bar{N}_Z \bar{N}_{Z+1}}{D_1 a N_e^2} \tag{A.7}$$

where N_w, N_z and N_{z+1} are the weight-, z-, and z+1-, average polymerization indecies, respectively. Substituting Eqs.(A.3) to (A.7) into Eq.(A.2), we obtain

$$Q_m(\tau) \sim \frac{\bar{N}_Z \bar{N}_{Z+1}(N_{SBR}\phi_{SBR}^3 + N_{PI}\phi_{PI}^3)}{N_e N_{SBR}\phi_{SBR} N_{PI}\phi_{PI}} \tau^1. \tag{A.8}$$

Reference

1 T. Hashimoto, Phase Transitions **12**, 47 (1988).

2 T. Nose, Phase Transition **8**, 245 (1987).

3 J. D. Gunton, M. San Miguel and P. S. Sahni, *Phase Transition and Critical Phenomena*, edited by C. Domb and J. L. Lebowitz (Academic Press, N.Y., 1983), Vol. 8, p. 269.

4 K. Binder, *Spinodal Decomposition*, edited by P. H. R.W.Cahn E.J.Kramer (VCH, Weinheim, 1990), Vol. 5, p. 405.

5 T. Koga and K. Kawasaki, Phys.Rev.A. **44**, R817 (1991)

6 A. Chakrabarti, A. Toral, J. D. Gunton and M. Muthukumar, Phys.Rev.Lett. **63**, 2072 (1989);A. Chakrabarti, A. Toral, J. D. Gunton and M. Muthukumar, J.Chem.Phys. 92, 6899 (1990).

7 A. Shinozaki and Y. Oono, Phys.Rev.Lett. **66**, 173 (1991).

8 S. Nojima, K. Tsutsumi and T. Nose, Polym.J. **14**, 225 (1982)

9 H. L. Snyder and P. Meakin, J.Chem.Phys. **79**, 5588 (1983).

10 T. Hashimoto, M. Itakura and N. Shimidzu, J.Chem.Phys. **85**, 6773 (1986).

11 H. Yang, M. Shibayama, R. S. Stein, N. Shimidzu and T. Hashimoto, Macromolecules 19, 1667 (1986).

12 T. Kyu and J. M. Saldanha, Macromolecules 21, 1021 (1988).

13 T. Izumitani, M. Takenaka and T. Hashimoto, J.Chem.Phys. **92**, 3213 (1990).

14 H. Fujita, T. Hashimoto and M. Takenaka, Macromolecules **22**, 4663 (1989).

15 F. S. Bates and P. Wiltzius, J. Chem. Phys. **91**, 3258 (1989).

16 J. W. Cahn, J.Chem.Phys. **42**, 93 (1965).

17 Y. Chou and W. I. Goldburg, Phys.Rev.A **20**, 2105 (1979).

18 T. Hashimoto, T. Izumitani and M. Takenaka, Macromolecules **22**, 2293 (1989).

19 T. Hashimoto, J. Kumaki and H. Kawai, Macromolecules **16**, 641 (1983).

20 K.Mori, H.Tanaka, H.Hasegawa and T.Hashimoto, Polymer **30**, 1389 (1989).

21 S.Sakurai, K.Mori, A.Okawara, K.Kimishima, Macromolecules, in press.

22 T. Izumitani and T. Hashimoto, J. Chem. Phys. **83**, 3694 (1985).

23 M. Takenaka, T. Izumitani and T. Hashimoto, Macromolecules **20**, 2257 (1987).

24 L. S. Ornstein and F. Zernike, Proc.Akad.Sci.Amsterdam **17**, 793 (1914).

25 K. Binder, J.Chem.Phys. **79**, 6387 (1983).

26 G. R. Strobl, Macromolecules **18**, 558 (1985).

27 E. D. Siggia, Phys.Rev.A 20, 595 (1979).

28 K.Kawasaki and K.Sekimoto, Europhys.Lett.**4**,339(1987).

29 H. Furukawa, Phys.Rev.A **39**, 239(1989)

30 A. Onuki, J.Chem.Phys. **85**, 1122 (1986).

31 M.Doi and S.F.Edwards J.Chem.Soc.Faraday Trans. **74**, 818 (1978)

32 H. Furukawa, Adv.Phys. **34**, 703 (1985).

33 J. F. Joanny and L. Leibler, J.Phys.(Paris) **39**, 951 (1978).

Chapter 5 : Spontaneous Pinning for Off-Critical Mixtures - Analysis q_m and I_m

5-1. Introduction

In this chapter we present a new feature found in the pattern formation of off-critical polymer mixtures. In a series of our papers[1-4], we presented experimental results on a slow spinodal decomposition of the binary polymer mixtures of polybutadiene (PB) and poly(styrene-random-butadiene) (a random copolymer of styrene and butadiene, coded as SBR) having near critical mixtures. We extended our studies of the spinodal decomposition (SD) for the near critical mixtures to those for off-critical mixtures of the same polymer pair SBR/PB and a similar polymer pair SBR/PI where PI stands for polyisoprene. Similarly to the previous studies, we investigated the coarsening behavior of the mixtures via SD by the time-resolved light scattering method. Time changes of I_m, the maximum scattered intensity, and q_m, the magnitude of the scattering vector at which the intensity becomes maximum, were investigated as a function of composition w of the mixtures and phase separation temperature T, and the results were compared with those obtained for the near critical mixtures. In this paper we shall report a unique phenomenon of "spontaneous pinning" or cessation of the domain growth during SD, found for our off-critical mixtures having high molecular weights. This "spontaneous pinning" should be contrasted with the continuous domain growth which occurs in the comparable time scale for the near critical mixtures of the same polymer pairs.

TABLE 5-I Sample characterization

Sample	M_W	M_W/M_n	St(wt%)[a]	Microstructure (%)[b] 1,4-cis	1,4-trans	1,2-vinyl	3,4-vinyl
SBR1	11.8	1.18	20	16	23	61	-
PB19	19.1	1.16	-	19	35	46	-
PI55	54.6	1.02	-	75	16	9	-

a) weight percent of styrene monomers in SBR.
b) obtained by IR spectroscopy.

TABLE 5-II Phase separation conditions

SBR1/PI55			SBR1/PB19		
Composition (wt./wt.)	T[a] (°C)	ε_T[b]	Composition (wt./wt.)	T[a] (°C)	ε_T[b]
20/80	60	1.1	25/75	50	1.4
30/70	60	2.0		60	1.3
	90	1.8		70	1.3
	120	1.5		110	1.3
50/50	60	3.5	58/42	50	2.8
-	-	-		60	2.7
-	-	-		70	2.6
-	-	-		110	2.4

a) phase separation temperature.
b) rough estimation of the thermodynamic driving force for the phase separation $eT = (\chi - \chi_S)/\chi_S$.

5-2. Exprimental Section

5-2-1. Samples

The samples SBR (coded as SBR1), PB (coded as PB19) and PI (coded as PI55) used in this studies were all prepared by living anionic polymerization. The results of the sample characterization are summarized in Table 5-I where M_w and M_n designate weight average and number average molecular weight, respectively.

5-2-2. Methods

Blends used in this work and their phase separation conditions are summarized in Tables 5-I and 5-II. Each binary mixture, SBR1/PB19 having an off-critical composition of 25/75 wt./wt., SBR1/PB19 having a near critical composition of 58/42 wt./wt., SBR1/PI55 having off-critical compositions of 20/80 and 30/70 wt./wt., and SBR1/PI55 having a near critical composition of 50/50 wt./wt., was dissolved into a homogeneous solution of toluene, containing 10 wt% polymers in total. The solution was placed into a petri dish, which in turn was enclosed in a temperature enclosure controlled at 30°C, and the solvent was allowed to slowly evaporate for one week. The 0.10 mm thick as-cast films thus obtained were further dried in vacuum at room temperature until constant weight was attained.

The as-cast films, which had internal domain structures as a consequence of SD during the solvent evaporation process, could not be brought into a single phase state by raising or lowering the temperature. Instead they were brought into a single phase state by the homogenization process described in detail elsewhere[5]. Immediately after the homogenization at room temperature, the film specimen was subjected to a temperature jump (T jump) to a given phase separation temperature T (see Table II) and an isothermal unmixing process was observed by the time-resolved light scattering technique as described elsewhere[6]. The time t was set zero right after the homogenization. The 0.1 mm thick homogenized film specimen

sandwiched by thin glass slides was set into a small specimen holder, and the T jump was achieved by inserting this holder into a metal block preheated to the phase separation temperature T(see Table 5-II).

A rough estimate of the parameter ε_T which characterizes thermodynamic driving force for the phase separation was also given in Table II for each mixture with a given composition w and at a given phase separation temperature T, where ε_T is defined by

$$\varepsilon_T \equiv [\chi_{eff}(T) - \chi_s]/\chi_s. \qquad (5.1)$$

$\chi_{eff}(T)$ is the effective Flory interaction parameter per segment between the two polymers SBR1 and PB19 or SBR1 and PI55, and χ_s is $\chi_{eff}(T)$ at the spinodal temperature. The method for estimating χ_s and $\chi_{eff}(T)$ were previously described in sec. II-C of ref 3. $\chi_{eff}(T)$ for the SBR1/PI55 mixture was obtained by assuming that the segmental interaction between styrene and isoprene segments is identical to that between styrene and butadiene (χ_{SB}) and that the segmental interaction between butadiene and isoprene segments is negligibly small compared with χ_{SB}.

Time-resolved light scattering intensity distribution was measured as described elsewhere[1]. Since only the relative intensity chnage with time is important in this work, all the intensity levels (in Figs. 5-1 to 5-7, 5-9 and 5-10) are given in a relative intensity unit, but they can be relatively compared one another.

5-3. Results

Time-resolved light scattering profiles measured during the isothermal SD are shown in Fig. 5-1 for the off-critical mixture of SBR1/PI55 30/70 wt./wt. at 60°C and in Fig. 5-2 for the near critical mixture of SBR1/PI55

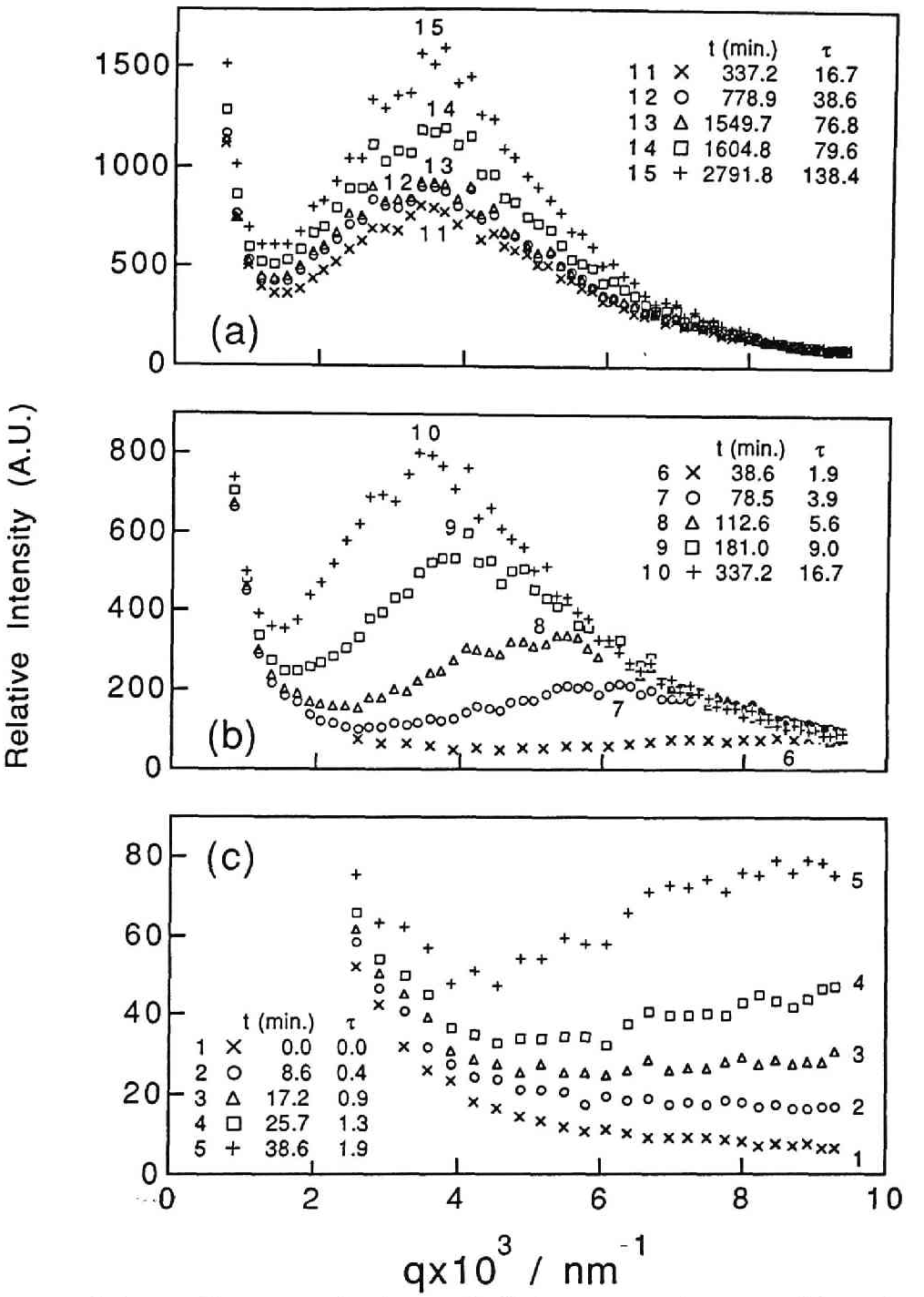

Figure 5-1 Time evolution of light scattering profiles for the SBR1/PI55 30/70 wt./wt. after onset of unmixing at 60°C.

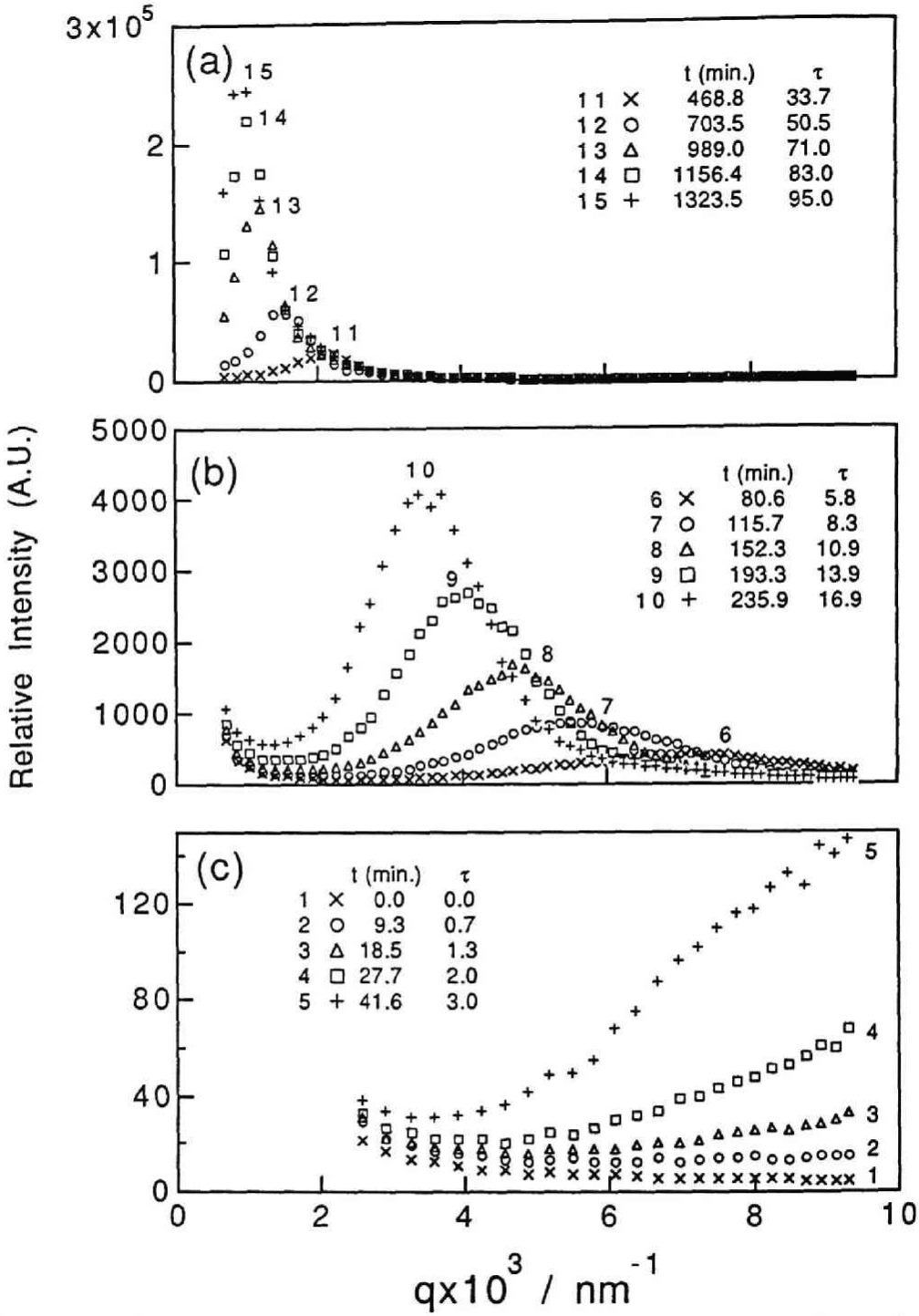

Figure 5-2 Time evolution of light scattering profiles for the SBR1/PI55 50/50 wt./wt. after onset of unmixing at 60°C.

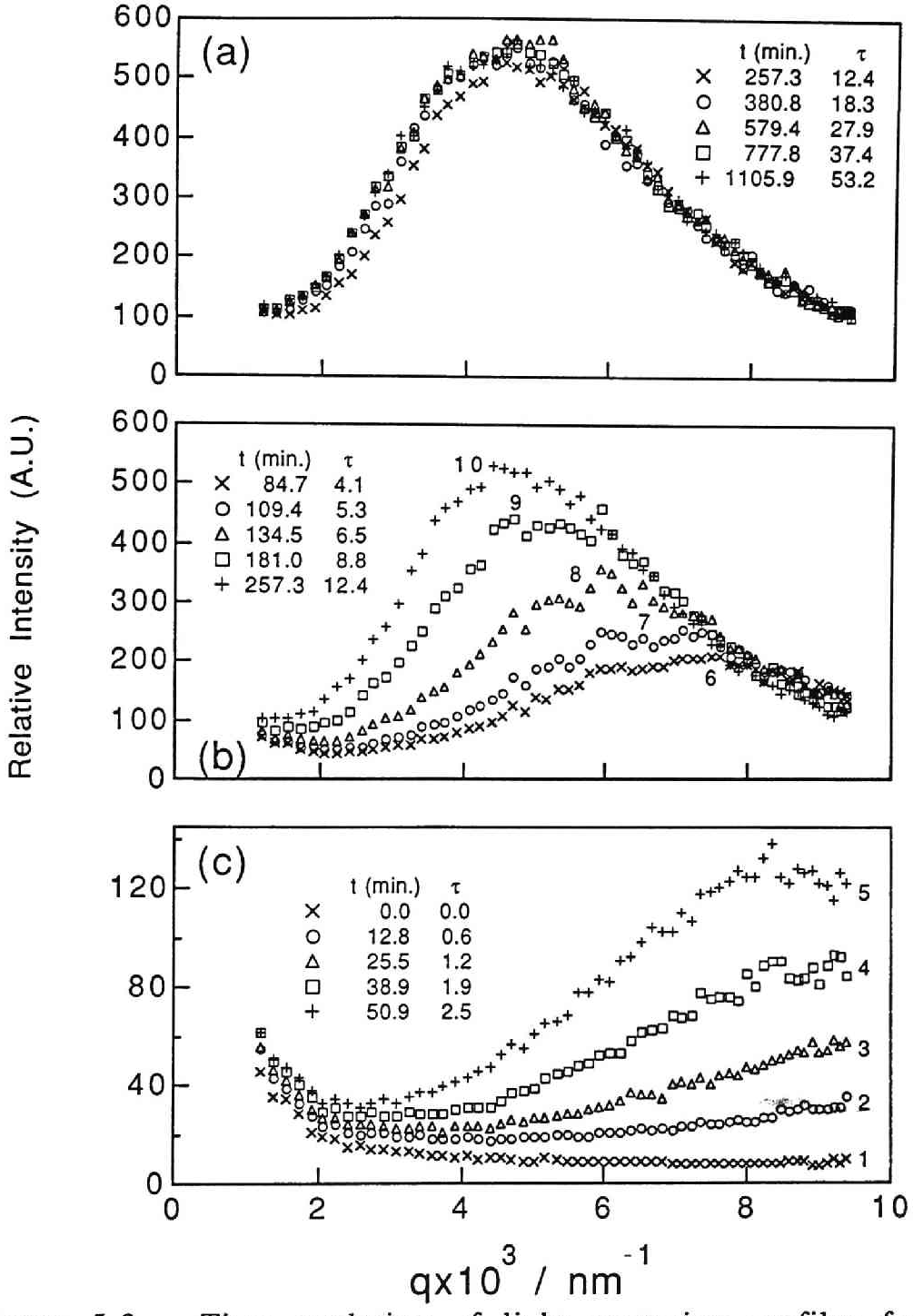

Figure 5-3 Time evolution of light scattering profiles for the SBR1/PB19 25/75 wt./wt. after onset of unmixing at 50°C.

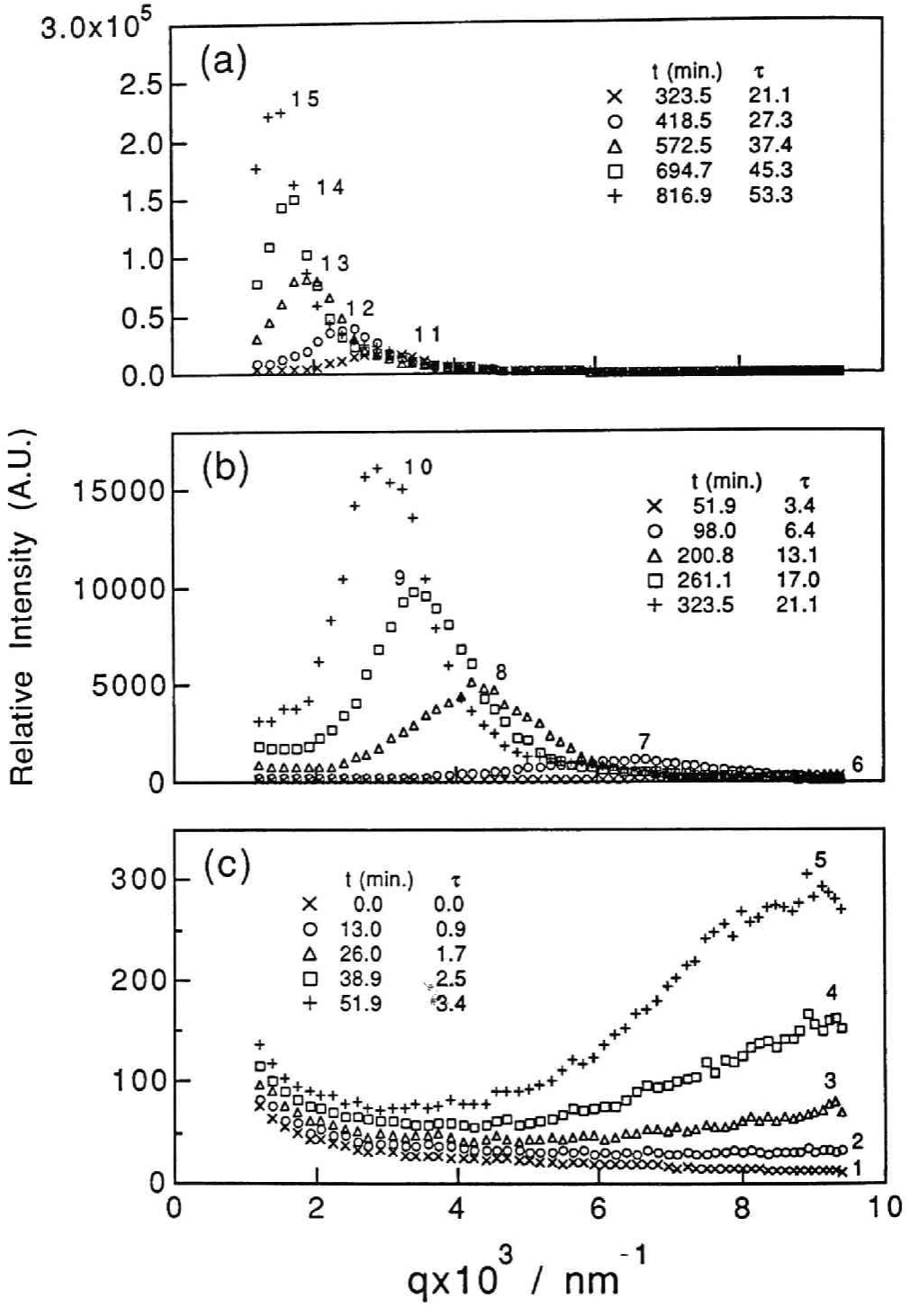

Figure 5-4 Time evolution of light scattering profiles for the SBR1/PB19 58/42 wt./wt. after onset of unmixing at 50°C.

50/50 wt./wt. at 60°C. In each figure the relative scattered intensity is plotted as a function of the magnitude of the scattering vector q

$$q = (4\pi/\lambda)\sin(\theta/2) \qquad (5.2)$$

where λ and θ are the wavelength of the incident light beam and the scattering angle in the medium, respectively. The relative intensity level of the profile taken at a give time can be compared within each figure and between the two figures. In each figure the phase separation time progresses in the order of parts (c) to (a).

Comparisons of the time evolution of the scattering intensity profiles for the off-critical mixture and the near-critical mixture reveal a dramatic difference as well as a close similarity. The similarity is found in the early stage SD; the intensity in the larger q region grows faster than that in the smaller q-region, giving rise to a scattering maximum at $q \cong 8.7\times 10^{-3}$ nm^{-1} [Fig. 5-1(c)] and $q \cong 9.5\times10^{-3}$ nm^{-1} [Fig. 5-2(c)]. Similarity is also found in the later stage in which the peak scattering vector q_m shifts toward smaller values and the peak intensity I_m further increases with time as seen in Figs. 5-1(b) and 5-2(b), implying that the growth of the domain occurs commonly for the two systems up to this time scale.

A dramatic difference in the coarsening behavior of the two systems appears in the much later stage as seen in Fig. 5-1(a) and 5-2(a). The coarsening continues for the near critical mixture, as is obvious from the further increase of I_m and decrease of q_m [Fig. 5-2(a)], while it effectively stops for the off-critical mixture as seen from the cessation of the shift in q_m and from an effective cessation or a dramatic slowing down of the intensity increase in I_m. Note a spectacular difference in the peak intensity I_m in the long time limit, e.g., 1300 to 1500 min.. The increase of the intensity I_m with time for the off-critical mixture is negligibly small compared with that for the

critical mixture. The time evolution of the light scattering profiles during the isothermal SD of the other mixture SBR1/PB19 at 50°C is shown in Fig. 5-3 for the off-critical mixture 25/75 wt./wt. and in Fig. 4 for the near critical mixture 58/42. One can find and confirm that the trends in the similarity and the difference of the coarsening behavior between the off-critical mixture and the near critical mixture of SBR1/PB19 are essentially identical to those found for the SBR1/PI55 .

5-4. Analysis and Discussion

5-4-1. Early stage spinodal decomposition

The early stage SD was analyzed based upon the linearized theory proposed by Cahn[7], according to the method as described in detail elsewhere[1-3]. The effects of the random thermal noise on the time evolution of the scattering profiles were ignored, since our SD experiments were conducted[3,5] far from the spinodal points as manifested by the large values of ε_T in Table 5-II. Nevertheless we should remember that the effects[8] are important in real systems for the time evolution of the concentration fluctuation.

The plots of ln I(q,t) vs t show the linearity over a sufficiently long time interval at all q's and T's covered in this experiments as shown in the earlier works[1-3]. The growth rate of the concentration fluctuation R(q) was obtained from the plots at various q's, T's and w's. The parameters $D_{app}(T,w)$ and $q_m(0;T,w)$ characterizing the early stage SD were determined from the Cahn's plot, $R(q)/q^2$ vs. q^2,

$$R(q)/q^2 = D_{app}(T,w)\{1 - q^2/[2q_m^2(0;T,w)]\} \qquad (5.3)$$

where D_{app} and $q_m(0)$ are the diffusivity and the characteristic wavenumber of the concentration fluctuation which grows at a maximum rate. Both of them are a function of T and w. The results are summarized as a function of

composition w in Table 5-III for the SBR1/PI55 mixtures at 60°C and as a function of T and w for the SBR1/PB19 mixtures. The tables also include t_c, the characteristic time for the blend systems defined by[9,10]

$$t_c^{-1}(T,w) = D_{app}(T,w)q_m^2(0;T,w) \tag{5.4}$$

Composition dependencies of $q_m(0)$ and D_{app} are clearly seen in Tables 5-III and 5-IV in that both $q_m(0)$ and D_{app} at a given T decrease with biasing composition from 50/50 wt./wt., except for the SBR1/PB19 mixture at 50°C. This trend may be interpreted in terms of the linearized theory for asymmetric blends[2,11],

$$q_m^2(0;T,w) = 9\bar{N}(N_A N_B\langle a^2\rangle)^{-1}\varepsilon_T(T,w) \tag{5.5}$$

where

$$\bar{N} \equiv \phi_A N_A + (1 - \phi_A)N_B \tag{5.6}$$

$$\langle a^2\rangle \equiv a_A^2(1 - \phi_A) + a_B^2\phi_A \tag{5.7}$$

and

$$D_{app}(T,w) = D_A D_B[D_A N_A \phi_A + D_B N_B(1 - \phi_A)]^{-1}\varepsilon_T. \tag{5.8}$$

Here N_K, a_K and D_K are the degree of polymerization, the statistical segment length and the self-diffusivity of polymer K (K = A or B), respectively, and ϕ_K is the volume fraction of polymer K (which is related to its weight fraction w). The decrease of $q_m(0)$ with biasing of the composition is primarily attributed to the decrease of ε_T, while the decrease of D_{app} depends upon both

TABLE 5-III Parameters characterizing the early stage SD for various composition of SBR1/PI55 mixtures at 60°C

Blend ratio (wt./wt.)	D_{app} (nm^2/sec.)	$q_m(0)\times10^3$ (nm^{-1})	$t_c\times10^{-2}$ (sec.)
20/80	7.1	8.1	21.5
30/70	12	8.3	12.1
50/50	13.4	9.5	8.3

TABLE 5-IV Parameters characterizing the early stage SD for various composition of SBR1/PB 19 mixtures

Blend ratio (wt./wt.)	Temp. (°C)	D_{app} (nm^2/sec.)	$q_m(0)\times10^3$ (nm^{-1})	$t_c\times10^{-2}$ (sec.)
25/75	50	10.0	8.95	12.5
25/75	60	16.8	8.6	8.0
25/75	70	26.8	8.4	5.3
58/42	50	9.5	10.7	9.7
58/42	60	20.0	10.0	4.9
58/42	70	32	11.4	2.4

ε_T and the transport term (i.e., the prefactor of ε_T in the right hand side of eq. 5.8).

D_{app} increases with increasing T as is clearly seen in Table IV, implying that the SD process studied in this experiment is in the diffusion controlled regime[1]. In other words, the increase of the transport term $D_AD_B[D_AN_A\phi_A + D_BN_B\phi_B]^{-1}$ with T dominates the decrease of the thermodynamic driving force $\varepsilon_T \sim \Delta T$ with T, a phenomenon relevant to SD far from the spinodal point. In this **deep quench** condition, ε_T may not change much with T, though it may change sensitively with w or ϕ. This explains why the temperature dependence of $q_m(0)$ is small and lies within experimental error (see Table 5-IV), though

the composition dependence of $q_m(0)$ is relatively large (see Tables 5-III and 5-IV). Thus the analyses of the early stage SD provide important information as to the state of the mixtures as a function of T and w.

5-4-2. Later stage spinodal decomposition

The coarsening processes in the later-stage SD (i.e., the SD occuring in both the intermediate stage and late stage[10]) of the SBR1/PI55 and SBR1/PB19 mixtures were investigated as a function of composition w and temperature T.

5-4-2-1. Composition dependence

Figure 5-5 shows the coarsening behavior of the SBR1/PI55 mixtures at 60°C as observed by the time evolutions of q_m (part a) and I_m (part b). For the near critical mixture with the composition of 50/50 wt./wt., I_m and q_m continue to increase and decrease, respectively, and hence the coarsening of the phase-separating domains continues over the time period covered in this experiment, i.e., $t < 1200$ min or $\tau \leq 60$ where τ is the reduced time defined by

$$\tau \equiv t/t_c. \tag{5.9}$$

This is consistent with our earlier results[3,10], and $t_{cr,50/50}$ shown in the figure is the crossover time from the intermediate stage to the late stage SD[10] for the 50/50 wt./wt. mixture. This crossover was determined from the change in the time evolution behavior of q_m and I_m as discussed priviously[10],

$$q_m \sim t^{-\alpha} \tag{5.10}$$

and

$$I_m \sim t^{\beta}. \tag{5.11}$$

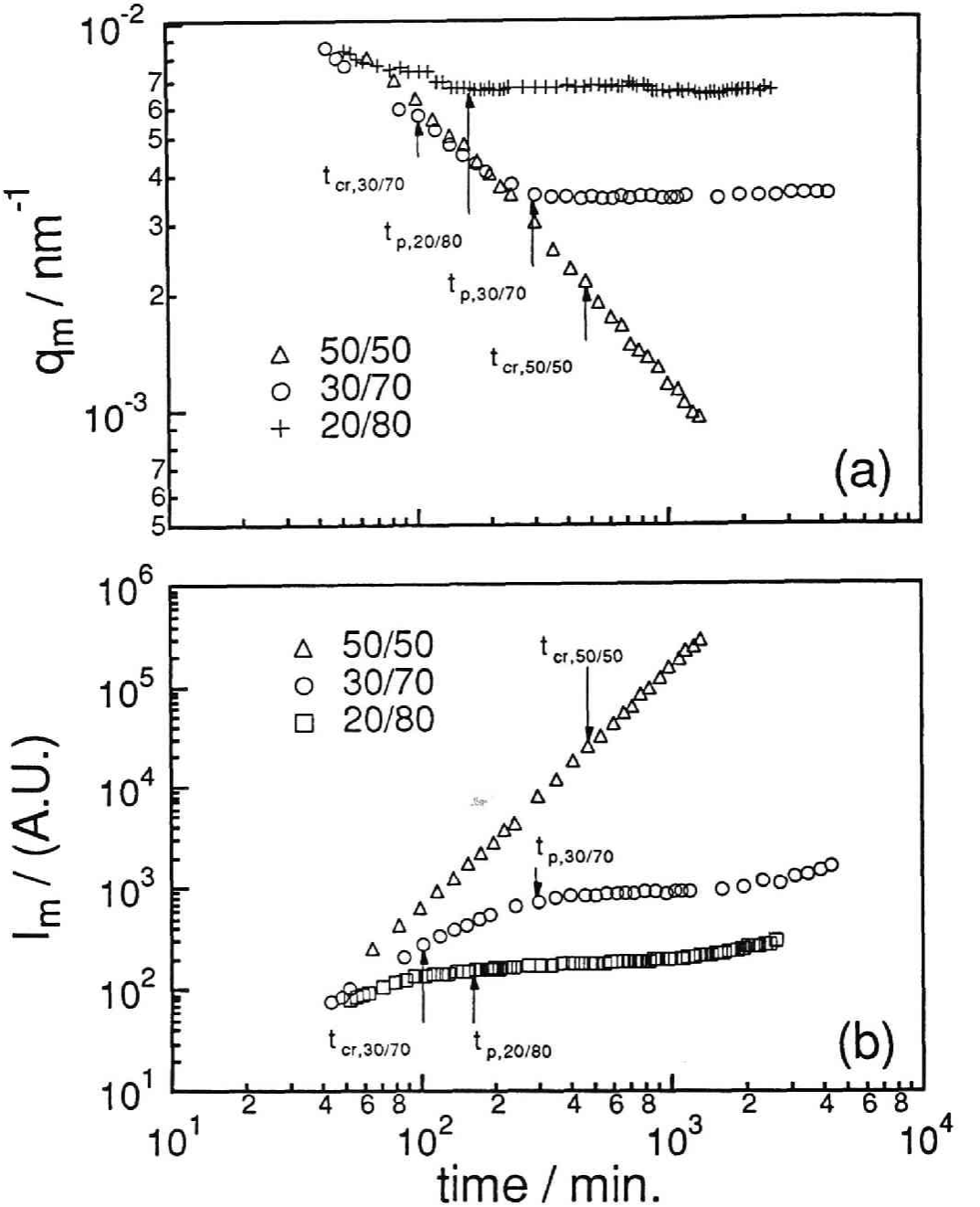

Figure 5-5 Composition dependence of the coarsening behavior for SBR1/PI55 mixtures at 60°C. q_m and I_m are plotted as a function of t in (a) and (b), respectively. t_p and t_{cr} indicate, respectively, the times at which the pinning and the crossover between the intermediate and late stages occur.

TABLE 5-V Summary on the crossover time t_{cr} and the reduced crossover time $\tau_{cr} \equiv t_{cr}/t_c$ between the intermediate and late stage and on the pinning time t_p, the reduced pinning time τ_p and the characteristic wavenumber $q_{m,p}$ at which the pinning occurs for SBR1/PI55

Blend ratio (wt./wt.)	Temp. (°C)	t_{cr} (min.)	τ_{cr}	t_p (min.)	τ_p	$q_{m,p}$ (nm^{-1})
30/70	60	84	4.2	290	14.4	3.53
30/70	90	-	-	110	-	3.92
30/70	120	-	-	33.3	-	3.33
20/80	60	-	-	160	5.4	6.67

In the intermediate stage of $t<t_{cr}$, where the composition difference $\Delta\phi(t)$ of a given component of mixtures in between two coexisting domains increase and the scaled structure factor changes with time, we find that a relationship between the two scaling exponents α and β is given by

$$\beta > 3\alpha. \tag{5.12}$$

On the other hand in the late stageof $t>t_{cr}$, where $\Delta\phi(t)$ reaches an equilibrium value $\Delta\phi_e$ and the global aspect of the scaled structure factor becomes universal with time, we find[10]

$$\beta = 3\alpha. \tag{5.13}$$

The time evolutions of q_m and I_m for the off-critical mixtures with 20/80 and 30/70 wt./wt. compositions are found to be effectively pinned on time scales longer than a composition-dependent pinning time, i.e., $t_{p,20/80}$ or $t_{p,30/70}$. There is definitely a slight increase of I_m even after $t_{p,20/80}$ or $t_{p,30/70}$, but this increase is negligibly small compared with the increase for the 50/50

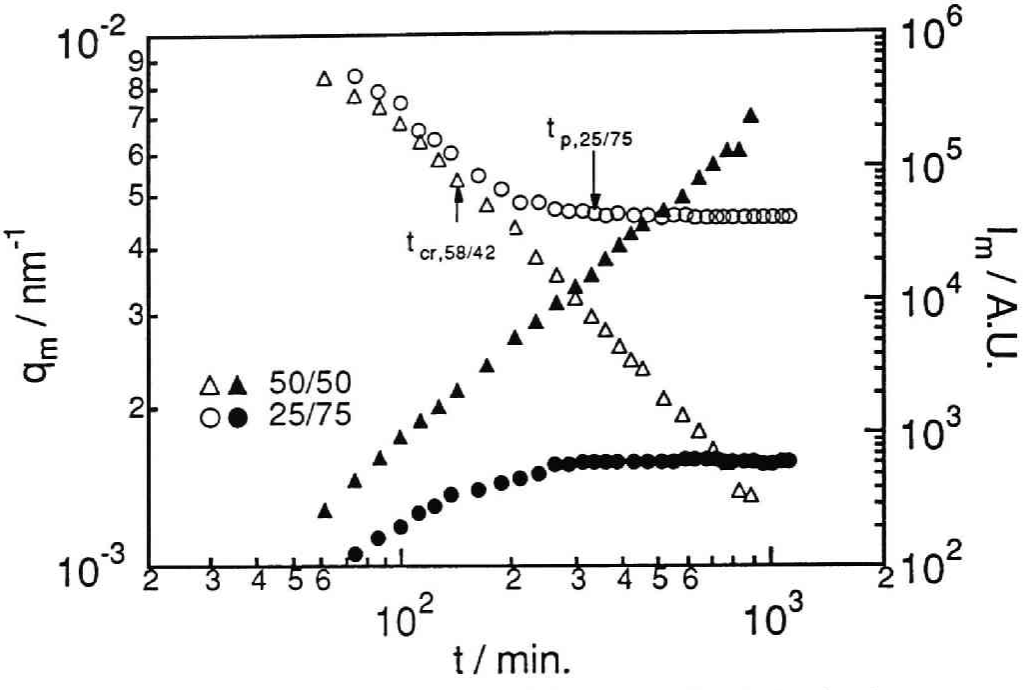

Figure 5-6 Composition dependence of the coarsening behavior for SBR1/PB19 mixtures at 50°C. q_m and I_m are plotted as a function of t.

mixture. It is important to note that the more the composition w is biased away from the 50/50 composition, the earlier is the pinning time and the larger the characteristic wavenumber q_{mp} and hence the smaller the characteristic size $1/q_{mp}$ of the pinned domain. The results are partially summarized in Table 5-V.

The coarsening of the phase-separating domains for the off-critical mixtures is found to be similar to that in the critical mixtures in time scales much shorter than t_p. For the 30/70 mixture, the pinning is found to occur in the late stage, i.e., in the time scale longer than the crossover time $t_{cr,30/70}$ between the intermediate stage and the late stage. However for the 20/80 mixture, the pinning presumably begins to occur in the intermediate stage SD. It should be noted that the crossover time $t_{cr,30/70}$ for the off-critical mixture

appears to be shorter than the crossover time $t_{cr,50/50}$ for the critical mixture. This apparently shorter crossover time will be discussed later in sec. 5-5-3.

Figure 5-6 shows the composition dependence of the coarsening behavior for the SBR1/PB19 at 50°C. The trends found for the SBR1/PI55 are also confirmed for this mixture: (i) the coarsening of the phase-separating domains continues for the near critical mixture but pins at $t > t_{p,25/75}$ and at the level of q_{mp} of 4.6×10^{-3} nm^{-1} for the off-critical mixture, as seen in time evolutions of q_m and I_m, (ii) at $t < t_p$, the coarsening for the off-critical mixture is similar to that for the near critical mixture.

5-4-2-2. Temperature dependence

The pinning behavior for the off-critical mixtures was also investigated as a function of temperature. The results are summarized in Figs. 5-7 and 5-8 for the SBR1/PI55 30/70 wt./wt. mixture and in Figs. 9 and 10 for the SBR1/PB19 25/75 wt./wt. mixture. For interpreting the data, it is important to note that the two mixtures have either the upper critical solution temperature (UCST) or the hour-glass type phase behavior. Even if they have the latter type behavior, an important point for the interpretation is that our experiments were carried out in the temperature regime where ε_T or ΔT tends to decrease slightly with raising temperature, as clarified in sec.5-5-1.

As seen in the time evolutions of q_m [Fig. 5-7(a)] and I_m [Fig. 5-7(b)] for the SBR1/PI55 30/70 wt./wt. mixture at various T's, the coarsening of the phase separating domains takes place before t_p but pins down after t_p. It is found that the higher the temperature the earlier the time for the pinning and the larger the characteristic wavenumber q_{mp} for the pinned structure. The pinning is found to occur either in the intermediate stage, as found for the SD at 90 and 120°C, or in the late stage, as found for the SD at 60°C.

The time evolutions of q_m's at the different temperatures covered in our experiments are expected to fall onto a master curve before the pinning occurs but to split into branches parallel to the abscissa after the pinning when they

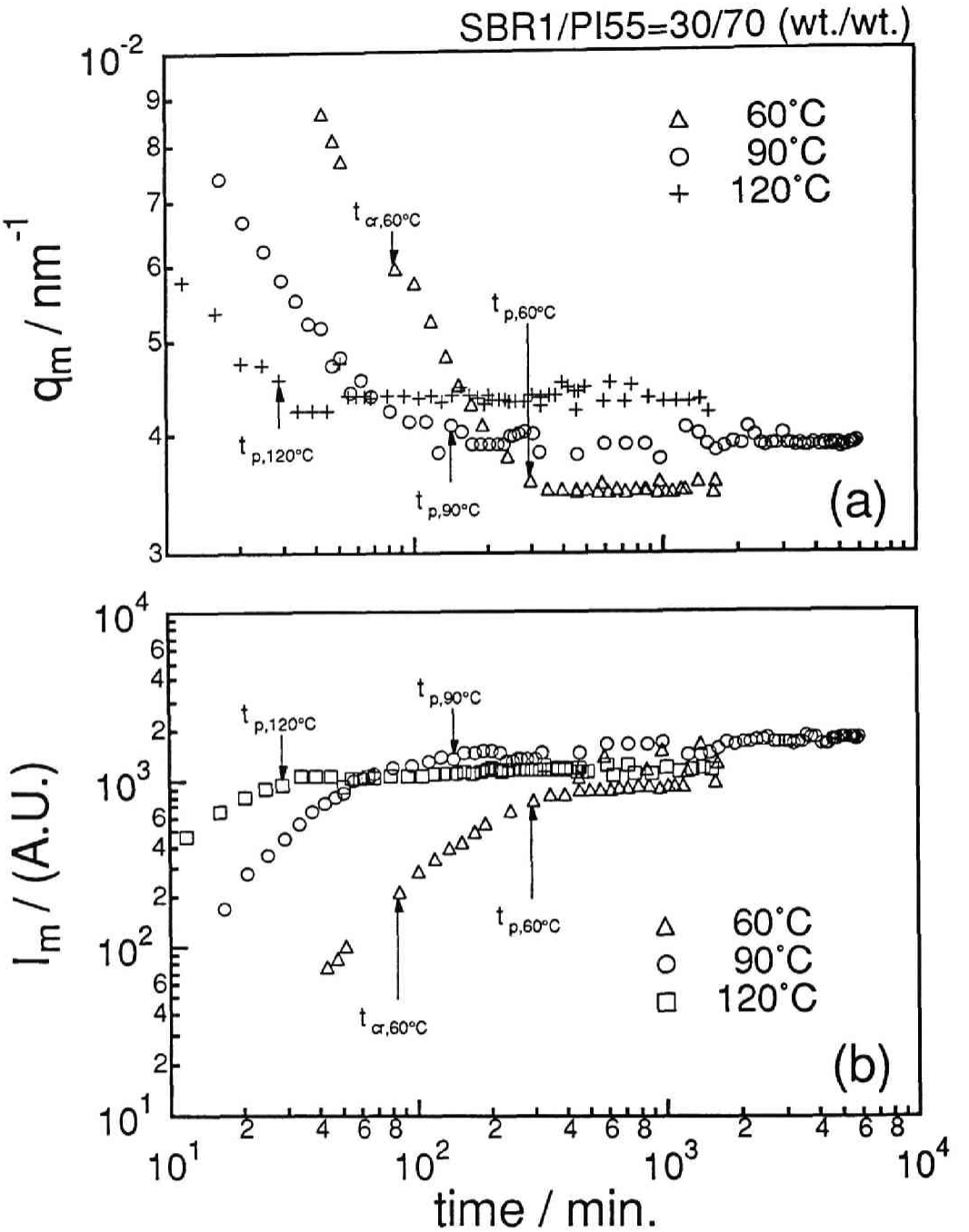

Figure 5-7 Temperature dependence of the pinning behavior for the off-critical mixture of SBR1/PI55 30/70 wt./wt.. q_m and I_m are plotted as a function of t in (a) and (b), respectively.

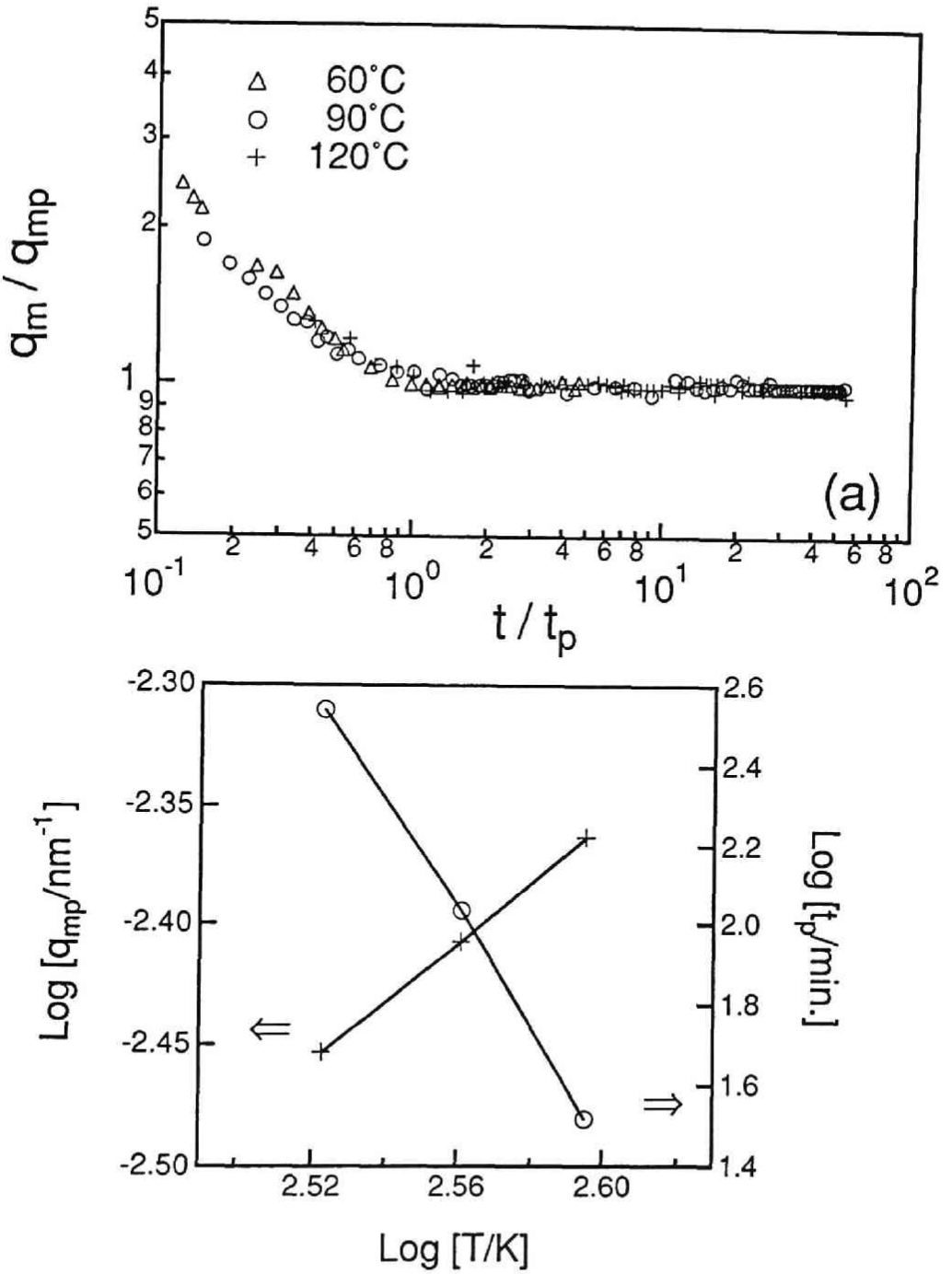

Figure 5-8 Reduced plot of q_m/q_{mp} vs. t/t_p for the off-critical mixture of SBR1/PI55 30/70 wt./wt. at various temperatures (part(a)). part (b) indicates the temperature dependence of t_p and q_{mp} in double logarithmic scale.

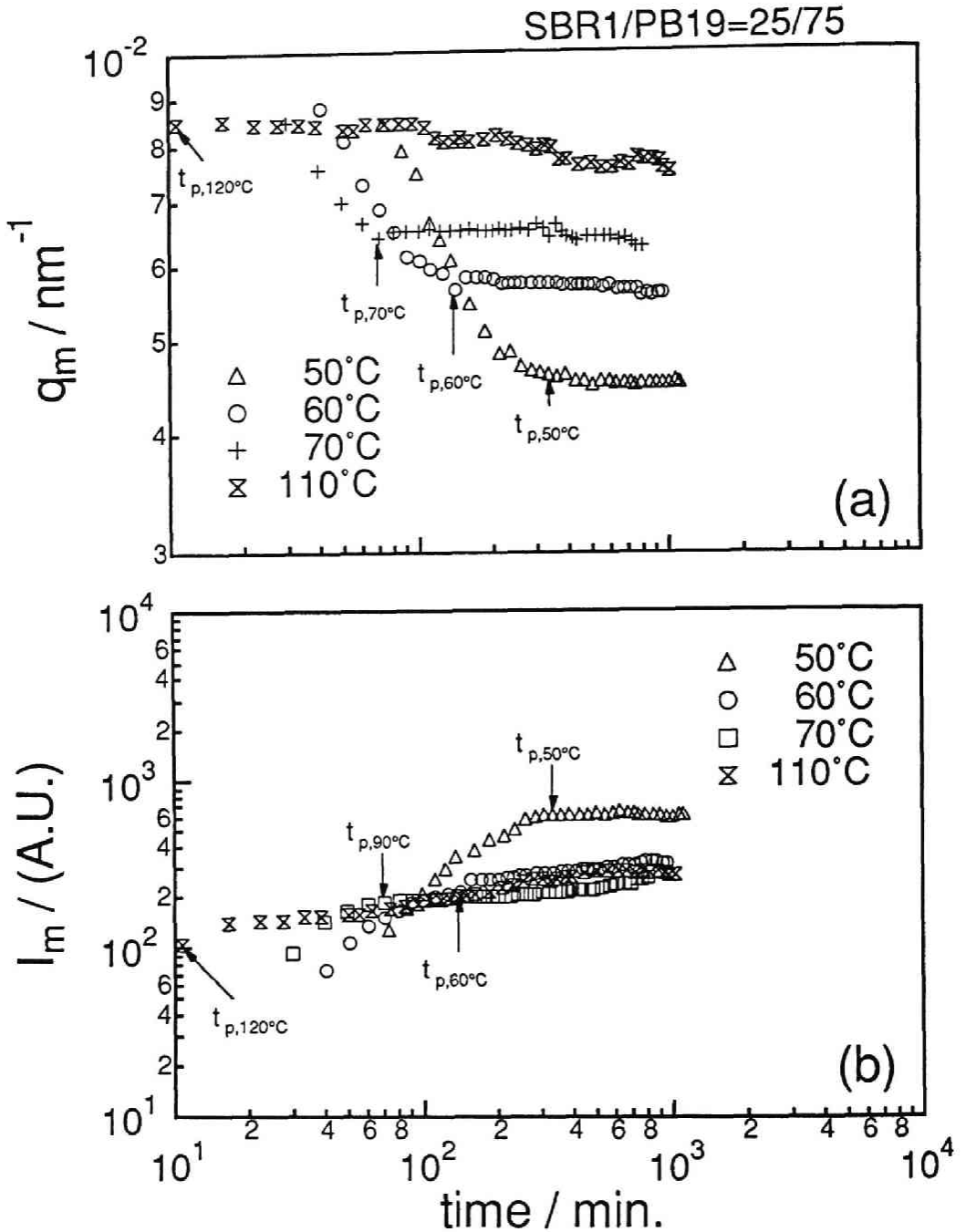

Figure 5-9 Temperature dependence of the pinning behavior for the off-critical mixture of SBR1/PI55 25/75 wt./wt.. q_m and I_m are plotted as a function of t in (a) and (b), respectively.

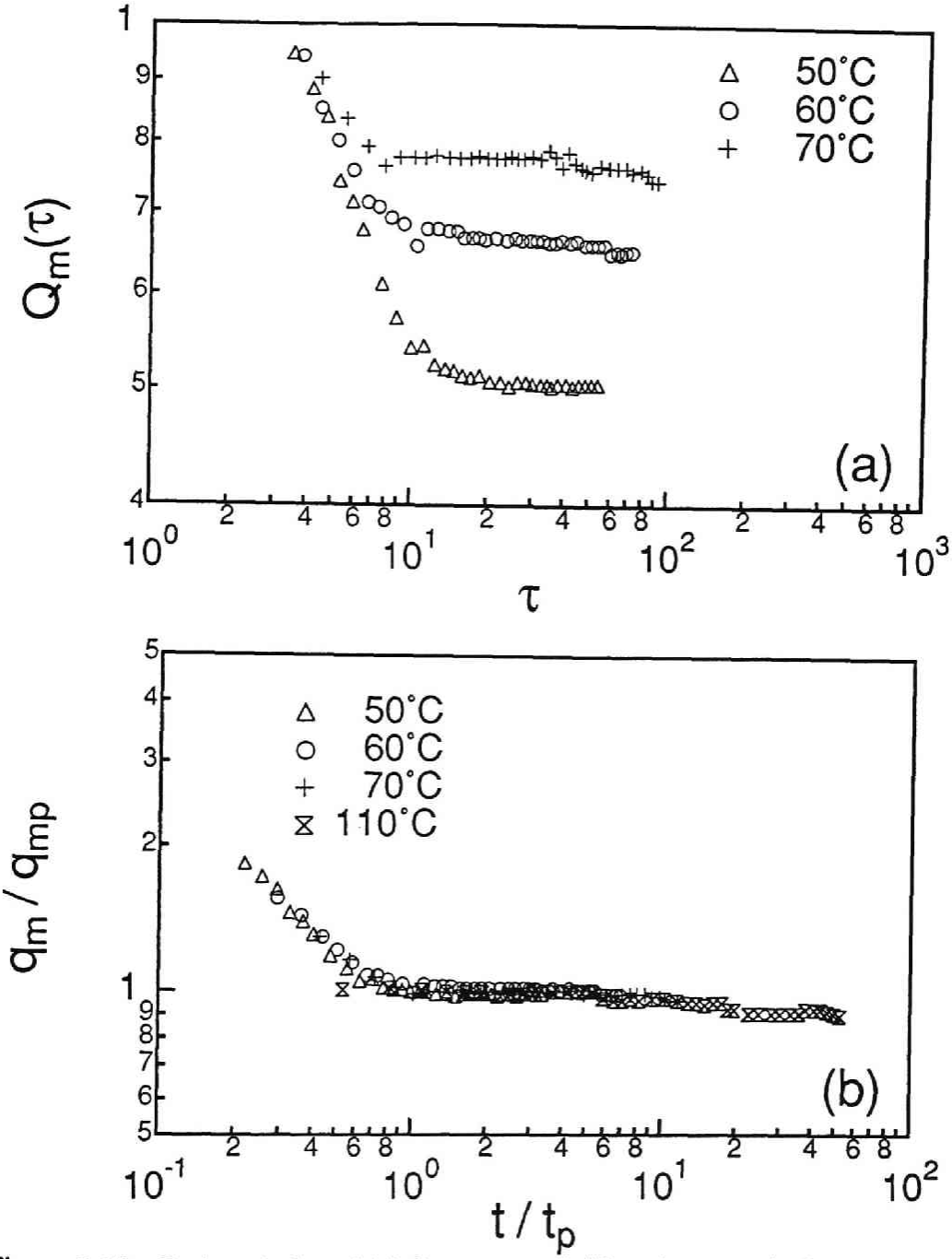

Figure 5-10 Reduced plot of (a) Q_m vs. τ and (b) q_m/q_{mp} vs. t/t_p for SBR1/PB19 25/75 wt./wt. at various temperatures. The diagram inserted at the upper right-hand corner of part b indicates the temperature dependence of t_p and q_{mp} in double logarithmic scales .

are plotted on a reduced plot of Q_m vs τ, based on the Chou-Goldburg scaling postulate[12], as shown in Fig.5.10(a) for the SBR1/PB19 mixture. The quantity Q_m is the reduced characteristic wavenumber defined by

$$Q_m = q_m(t)/q_m(0), \tag{5.14}$$

and the reduced time τ was defined by eq. 9. The reduced pinning time τ_p defined by

$$\tau_p \equiv t_p/t_c \tag{5.15}$$

is not a universal value but depends on composition and temperature as summarized in Tables 5-V and 5-VI.

An attempt was made to check whether or not the time evolutions of q_m's at different T's fall onto a master curve on the reduced plot, as shown in Fig. 5-8, where q_m and t are reduced in terms of q_{mp} and t_p, respectively. Although not excellent, a master curve was approximately obtained, yielding

$$q_m/q_{mp} \sim (t/t_p)^{-\alpha}, \tag{5.16}$$

with $\alpha \fallingdotseq 0$ for $t/t_p < 1$ and $\alpha = 0$ for $t/t_p > 1$. The temperature dependence of t_p and that of q_{mp} are shown in the insert of Fig. 5-8.

A trend essentially identical to that for the SBR1/PI55 mixture is observed in Fig. 5-9 for the temperature dependence of the pinning behavior for the SBR1/PB19 25/75 wt./wt. mixture. A subtle difference is, however, discernible in the two systems in the time scale after the pinning. The SBR1/PB19 mixture shows slightly greater time changes in q_m and I_m than the SBR1/PB55 mixture. For the SBR1/PB19 mixture, the data at 110°C shows

TABLE 5-VI Summary on the pinning time t_p, the reduced pinning time τ_p and the characteristic wavenumber $q_{m,p}$ at which the pinning occurs for SBR1/PB19.

Blend ratio (wt./wt.)	Temp. (°C)	t_p (min.)	τ_p	$q_{m,p}$ (nm^{-1})
25/75	50	339	16.3	4.60
25/75	60	138	10.0	5.65
25/75	70	69.2	7.9	6.52
25/75	110	10.3	-	8.43

the greatest time change at $t > t_p$. Nevertheless this time change should be noted to be negligibly small compared with that for the corresponding critical mixtures at the corresponding temperature range.

Fig. 5-10(a) shows the reduced plot of Q_m vs τ for the SBR1/PB19 25/75 wt./wt. mixture. One can clearly find the *branching* on the reduced plot after the pinning, though a master curve tends to be observed before pinning. Fig. 5-10(b) shows the other reduced plot of q/q_m vs t/t_p. The reduced plot shows a reasonably good master curve among the data obtained at different T's. Tables 5-V and 5-VI summarize the parameters characterizing the coarsening behavior of the off-critical mixtures as a function of temperature and composition.

5-4-3. Change of scaling exponents α and β upon pinning

The time changes of the scaling exponents α and β defined by eqs. 5.10 and 5.11 during the pinning process were investigated for characterizing the time change of the corresponding domain structure. A theoretical basis of this analysis is given by the scattering theory which describes the time evolution of the scattering intensity profile I(q,t) from phase-separating domain systems,

$$I(q,t) \sim \langle \eta^2(t) \rangle \Lambda^3(t) \ \bar{F}(q/\Lambda(t)), \tag{5.17}$$

where $<\eta^2(t)>$, $\Lambda(t)$ and $\overline{F}$ are the mean-square fluctuations for the spatial variation of scattering contrast, the characteristic size of growing domains, and the scaled structure factor[10,13], respectively. The quantities I_m and q_m discussed earlier are related to eq. 5.17,

$$I_m(t) = I(q = q_m, t) \sim <\eta^2(t)> q_m^{-3}(t)\ \overline{F}(1), \tag{5.18}$$

and

$$q_m(t) = 1/\Lambda(t). \tag{5.19}$$

Thus in the intermediate stage where $<\eta^2(t)>$ and $\overline{F}(1)$ grows with time, one expects the inequality given by eq. 5.12. It should be noted that $\overline{F}(1)$ increases with time because the structure factor becomes sharper with time at around $x \equiv q/q_m(t) = 1$, while keeping the invariant $\int \overline{F}(x)x^2dx$ constant with time. On the other hand in the late stage where $<\eta^2(t)>$ effectively reaches an equilibrium value $<\eta^2>_e$ and $\overline{F}(x)$ becomes independent of time, satisfying so called the dynamical scaling hypothesis[13], one expects the equality given by eq. 5.13. A question may be addressed on how these quantities (α and β) change with time during the pinning process. The relationship between α and β is essentially important in answering whether or not the structure changes during the pinning process, and if yes, how it changes. A more direct approach to answer this question is to investigate the time-change of the scaled structure factor $\overline{F}(x)$ during the pinning, which will be discussed elsewhere[14].

Figs. 5-11 and 5-12 show, respectively, the time evolutions of α and α/β at various temperatures for the off-critical (25/75 wt./wt./, dotted lines) and the near critical mixtures (58/42 wt./wt., solid lines) of SBR1/PB19. The figures systematically show the temperature dependence of t_p for the off-

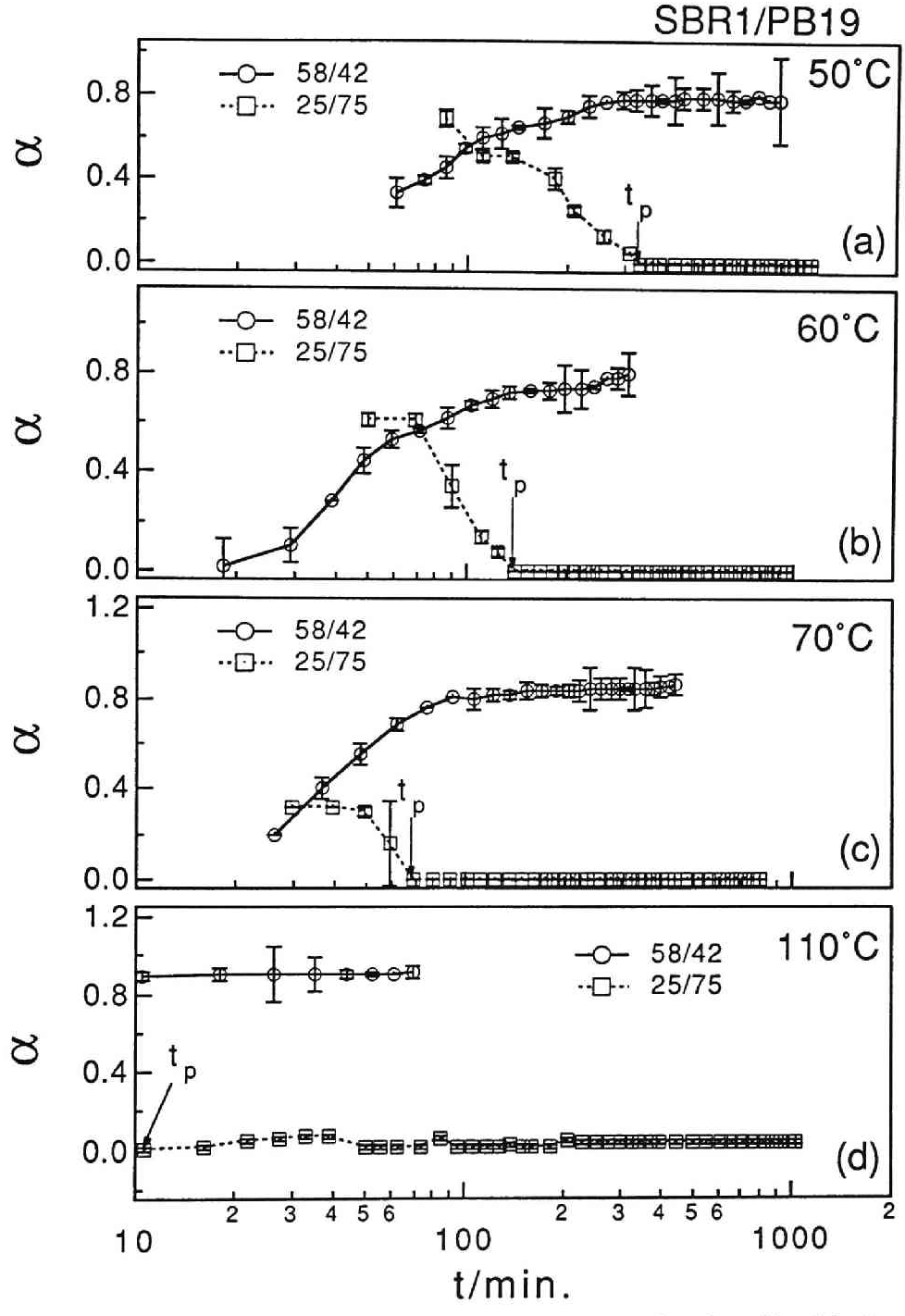

Figure 5-11 Time change of α at various temperatures for the off-critical mixture 25/75 wt./wt. (solid line and open circles) and the critical mixture 58/42 wt./wt. (broken line and squares) of SBR1/PB19.

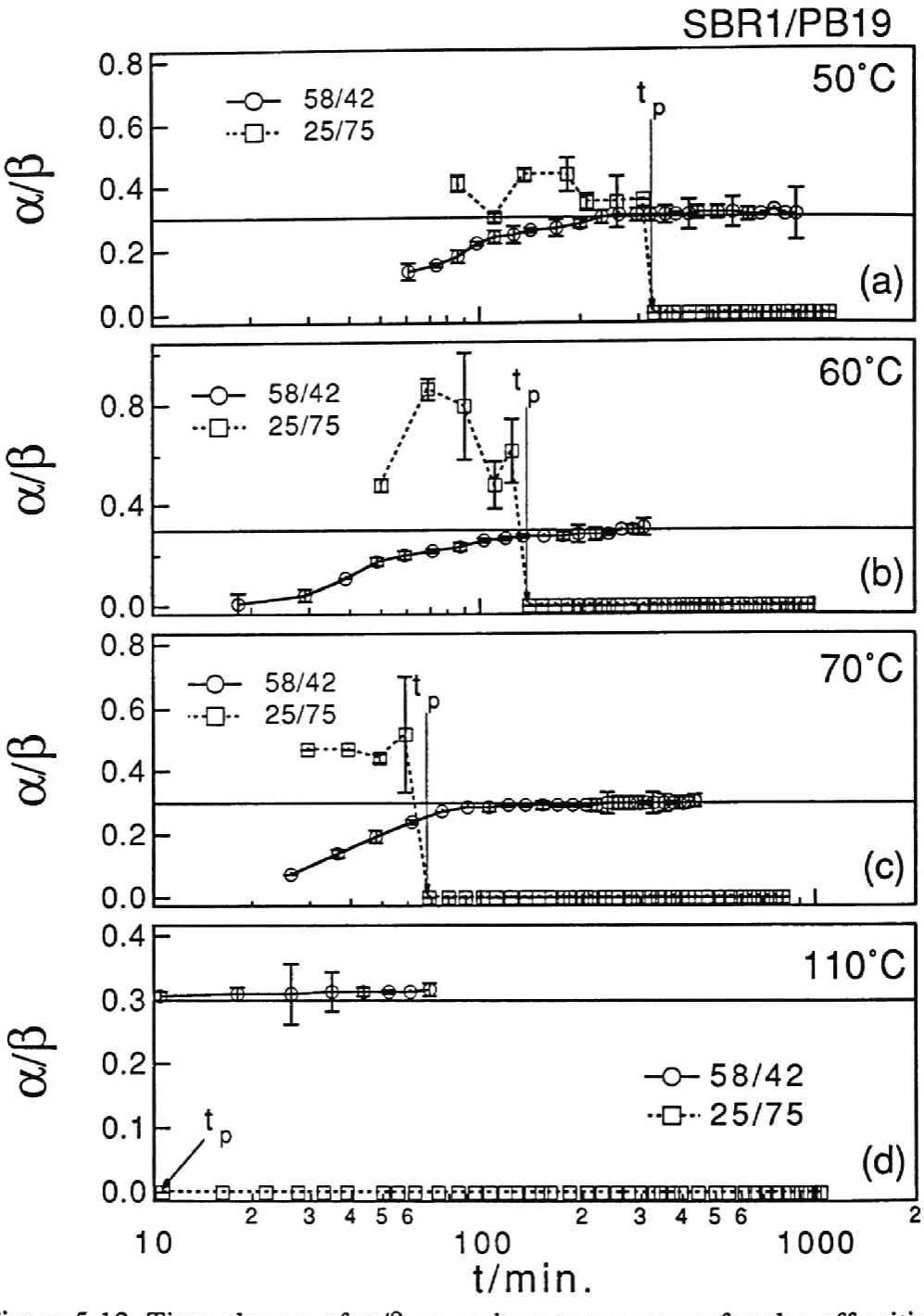

Figure 5-12 Time change of α/β at various temperature for the off-critical mixture (solid line and open circles) and the critical mixture (broken line and squares) of SBR1/PB19 25/75 wt./wt.. The horizontal solid line indicates α/β = 1/3.

critical mixture as discussed in the previous section. For the critical mixtures the value of α tends to increase toward 1 with t, i.e., toward Siggia's limit[15], but for the off-critical mixture it drops to zero at $t > t_p$ (Fig. 5-11). For the off-critical mixture, the time domain where α increases could not be observed. Presumably it exists in the time scale shorter than the time scale covered in our experiment. For the near critical mixture the value α/β increases with t at $t < t_{cr,58/42}$ but reaches 1/3 at $t > t_{cr,58/42}$. as seen in Fig. 5-12 where the horizontal line corresponds to $\alpha/\beta=1/3$. However for the off-critical mixture, the value α/β is close to 1/3 [Fig.5-12(a) for 50°C] or greater than 1/3 [Fig.5-12(b) and (c) for 60°C and 70°C, respectively) at $t<t_p$ (before the pinning) and drops to zero at $t>t_p$. The time domain where α/β increases from zero to 1/3 presumably exists in the scale earlier than that covered in our experiment. The value α/β tends to overshoot the value 1/3 immediately before pinning, as is clearly seen in Fig. 5-12(b) and Fig.5-13. This overshoot implies that

$$\beta<3\alpha \tag{5.21}$$

during the process leading to the pinning, which in turn implies that $\bar{F}(1)$ and/or $\langle\eta^2\rangle$ **decrease** with time during the pinning process. The decrease of $\bar{F}(1)$ appears to be physically more reasonable than the decrease of $\langle\eta^2\rangle$. The decrease of $\bar{F}(1)$, in turn, implies that the structure factor **broadens** during the pinning.

Essentially the same trends as those for SBR1/PB19 were found for SBR1/PI55. The results are summarized in Fig.5-13. The important experimental evidence of the overshoot in the time change of α/β during the pinning can be more clearly confirmed for this mixture than for SBR1/PB19.

Our observation that the crossover time t_{cr} is apparently shorter for the off-critical mixture than that for the near critical mixture (see the discussion

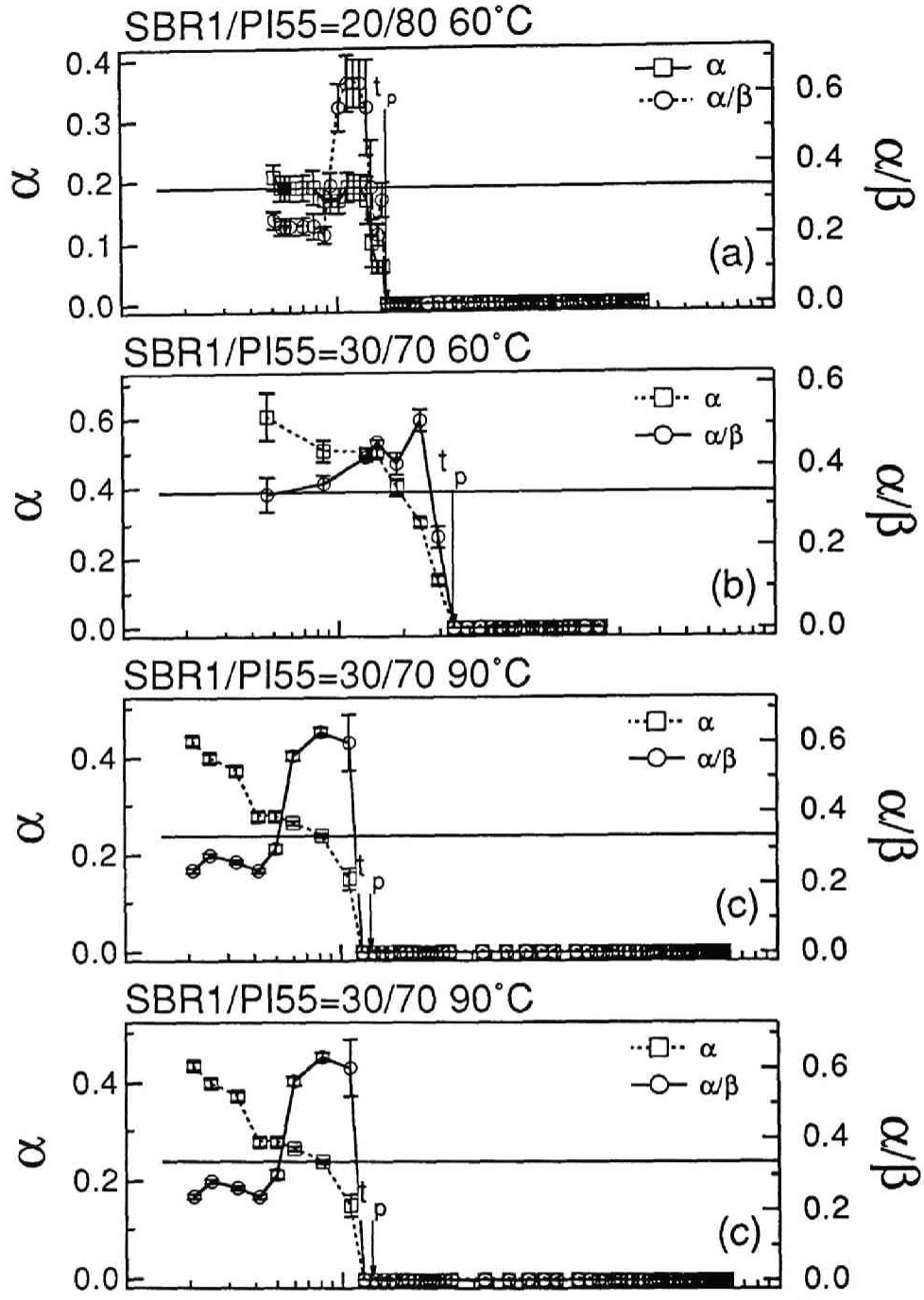

Figure 5-13 Time change of α (broken line and squares) and α/β (solid line and open circles) at various temperature for SBR1/PI55. The horizontal solid line indicates α/β = 1/3.

in sec. 5-5-2-1 and Table 5-V) may be closely related to the decrease of $\overline{F}(1)$ and hence the broadening of the structure factor for the off-critical mixtures which occurs immediately before the pinning process. An alternative interpretation may be given from a view point that the more the composition w is biased toward 0 or 1, motion of only a small number of molecules suffices to increase $\Delta\phi(t)$ toward $\Delta\phi_e$ and hence to generate a large number of smaller domains with equilibrium local compositions at a shorter time t_{cr}.

5-5. Mechanism of spontaneous pinning

Since experimental evidence is not sufficient at present for establishing the pinning mechanism, we present here our conjecture.

The coarsening behavior for the off-critical mixture before the pinning was found to be essentially identical to that for the near critical mixture in sec. 5-4. It was also found earlier that the coarsening of the near critical mixture maintains bicontinuous percolating domains[4]. Thus we can propose for the off-critical mixtures studied here that periodic, bicontinuous, percolating domains are formed via SD and the domains grow with time before the pinning. In sec. 5-4-3 a characteristic structural change was found to occur during the pinning process, which is characterized by a **broadening**, rather than a sharpening, of **the structure factor**. We found also that the structure factor obtained at a long time after the pinning is similar to that for a cluster of discrete domains proposed by Furukawa[16], as will be presented in a companion paper[14]. Thus we conjecture that the spontaneous pinning process originates from a **dynamical percolation-to-cluster (PC) transition.**

Inside the spinodal phase boundary, there may be a region where the percolating domains are maintained until very late stage SD (region B) and a region where the percolating domain structure exists initially but is later broken up into a cluster of discrete domains via the dynamical PC transition (region A) (see Fig. 5-14). Supporting evidence is found in that the pinning

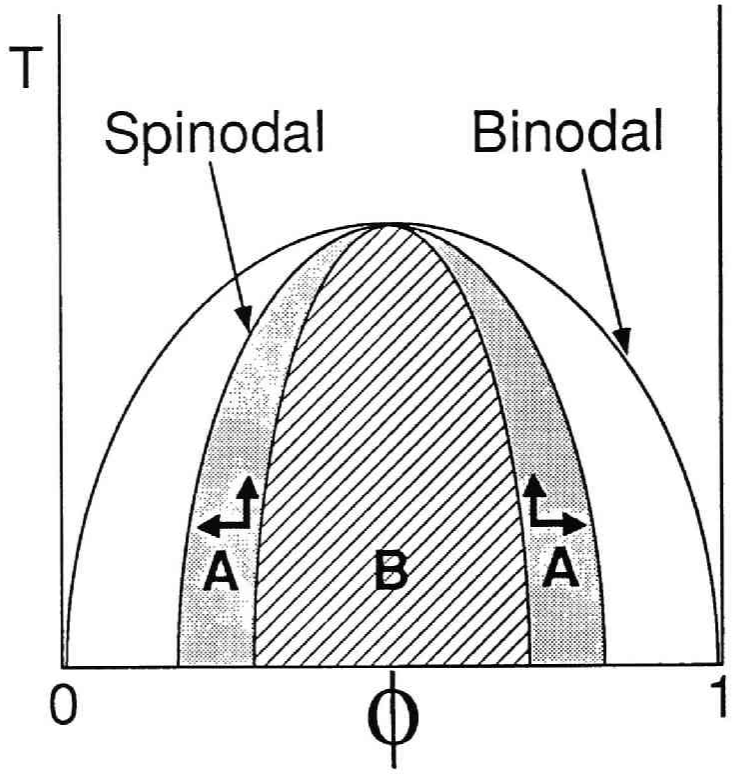

Figure 5-14 Two regions A and B in the spinodal phase boundary. In region A, the pattern is initially percolated but is later transformed into clusters of spheres, due to the dynamical percolation-to-cluster transition. In region B, the percolating pattern is maintained until the very late stage.

occurs earlier as T is raised at a given composition w or as w is biased toward 0 or 1 at a given T, as shown by the arrows in the region A of Fig. 5-14. It should be noted that an increase of T is effectively identical to a biasing w for our mixture.

Although we do not have any direct experimental evidence obtained by a real-space analysis to support the dynamical PC transition for our particular mixtures of SBR1/PB19 and SBR1/PI55, we have it for another mixture of X-7G/PET, as shown in Fig. 5-15, where X-7G and PET stand for a thermotrpic liquid crystalline polymer and polyethylene terepthalate, respectively. Fig. 5-15 shows the time-evolution of the unmixing structure through SD for the 50/50 wt./wt. mixture at 270°C where X-7G and PET are, respectively, anisotropic and isotropic liquids[17]. The series of pictures in Fig. 5-15 follows the structure evolution of the same part of a specimen under crossed polarizers so that the domains rich in X-7G and PET appear to be bright and dark, respectively. In parts (a) and (b), a percolating domain structure of the anisotropic liquid is clearly observed to grow with dynamical self-similarity (percolation regime). Note that both domains are considered to be continuously connected (below and above the plane of the photograph). As the domains grow, the percolating anisotropic domains cannot maintain the macroscopic percolation, for a reason which will be discussed elsewhere[18], resulting in the formation of fragments of the network with a local percolation only as seen in picture (c) in Fig. 5-15 (transition regime). The fragmented network is then degenerated into a cluster of spherical droplets, as seen in part (d) (cluster regime), which is driven by minimizing interfacial free energy. This is the process which we visualize in referring to the PC transition in this chapter.

Our conjecture for the ordering process of the off-critical mixture is as follows. The phase separation via SD develops a periodic domain structure

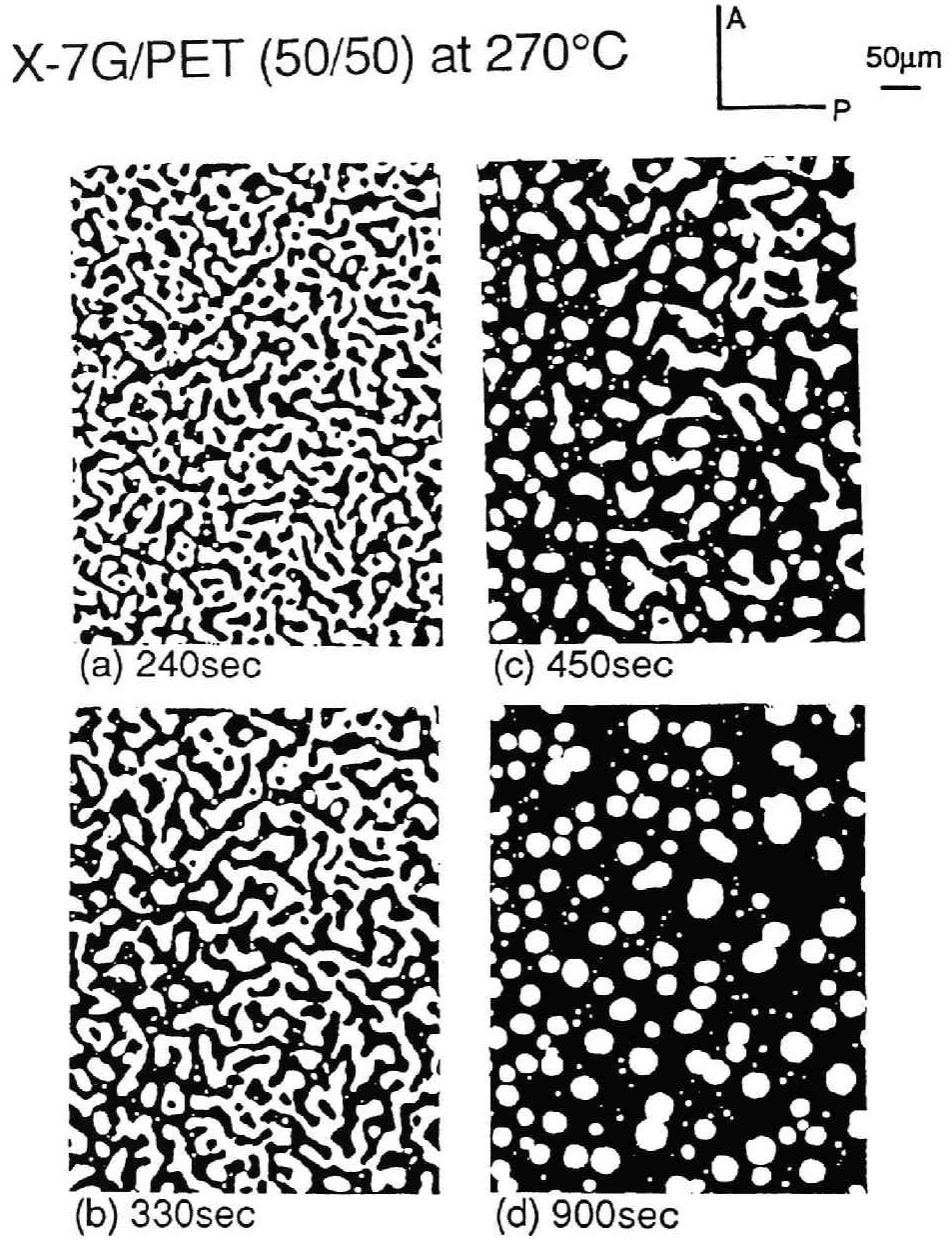

Figure 5-15 Time change of the unmixing structure showing the dynamical percolation-to-cluster transition for PET/X-7G 50/50 wt./wt. at 270°C.

which initially has macroscopic percolation. However as the phase separation proceeds and the domain structure grows, the domains rich in minority component are not able to maintain the macroscopic percolation and transform into a cluster of droplets through the dynamical PC transition. The distribution of the interdroplet distance is sharp enough to give a scattering maximum at a scattering vector q_{mp}, because the droplets originate from the periodic, percolating structure and thus retain memory of the structure before the PC transition. At $t < t_p$ in which the percolating domain pattern exists, the pattern grows via motion of the interface which is spatially continuous. The thermal motion causes instability and breaking up of the network[19,20] into a larger mesh size $\Lambda(t)$ and a thicker percolating network. At $t > t_p$, the growth of the cluster pattern occurs as a consequence of the diffusion and coalescence of droplets, as shown schematically in Fig. 5-16(a) by the transformation of state I into state II.

The diffusion of droplets requires either bulk or surface diffusion of molecules[21]. In bulk diffusion, the diffusion of droplets occurs through a stochastic process such that the molecules forming droplets diffuse out from the droplet to the matrix and condense back into different portion of droplets. This diffusion process has to overcome a kinetic barrier associated with enthalpy of mixing of polymers ΔH_{mix} having repulsive interactions as shown schematically in Fig. 5-16(b). Now ΔH_{mix} per chain is given by,

$$\Delta H_{mix} \sim \chi_{eff} N k_B T, \tag{5.22}$$

where N is the degree of polymerization (DP) of polymers, and the DP's for the two polymers are assumed to be identical to simplify the arguments. Thus when $\chi_{eff}N$ is very large, as is the case for SBR1/PI55 and SBR1/PB19, (i.e., the deep quench condition) the kinetic barrier is too large to be overcome, so that mutual diffusion proportional to $\exp(-\chi_{eff}N)$ is heavily suppressed, and

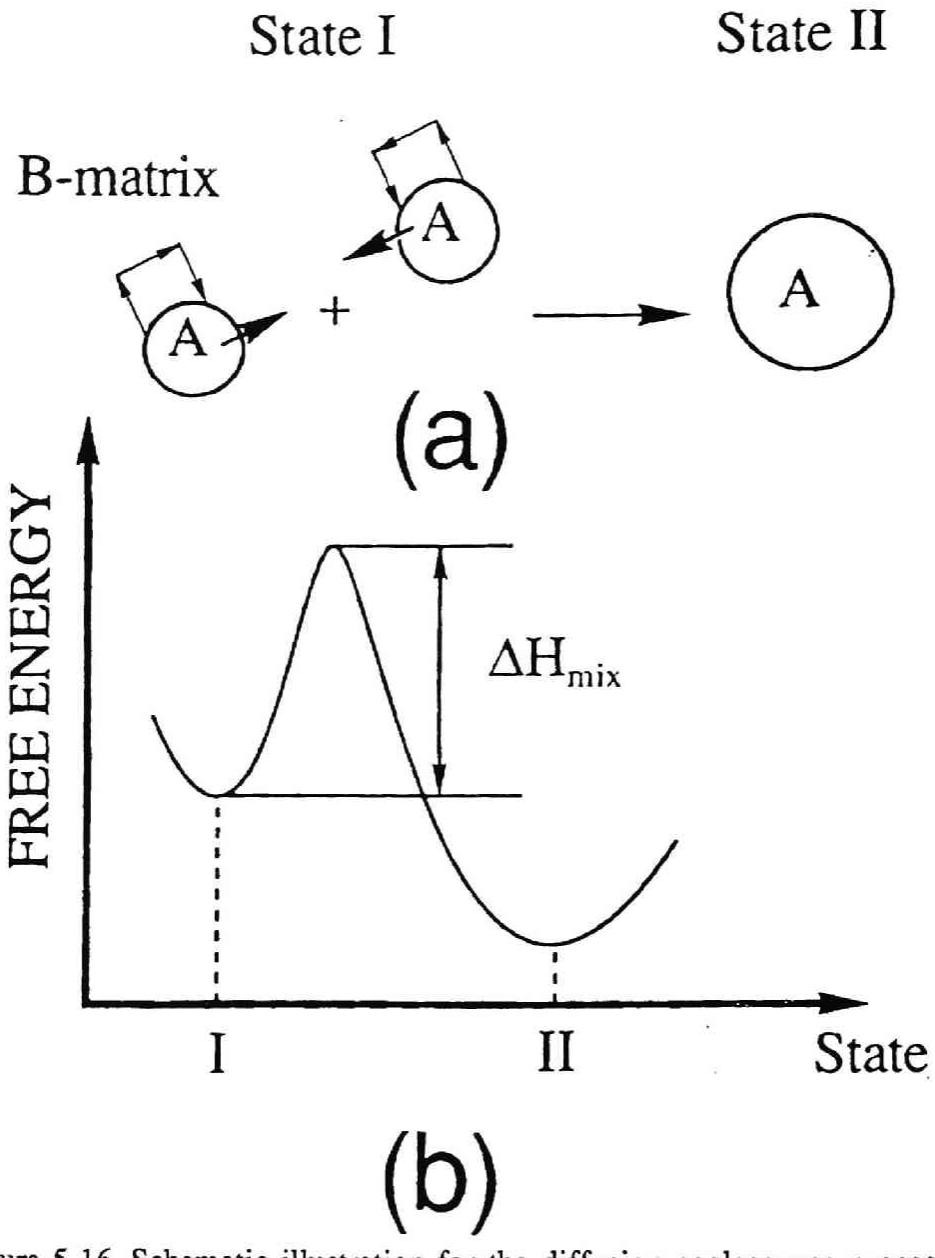

Figure 5-16 Schematic illustration for the diffusion-coalescence process (a) and a kinetic energy barrier for the diffusion-coalescence (b). Since the state I has a higher free energy than the stage II, a transformation from the state I to II is thermodynamically favored. However it must overcome the barrier associated with the heat of mixing ΔH_{mix} of unlike chains in the diffusion-coalescence process

The domain growth is kinetically frozen-in or pinned, though there is a thermodynamical driving force for the domain growth, because the state I having a larger interfacial area has a higher free energy than the state II obtained after the coalescence of droplets. Hence the pinning may be a feature unique to the ordering process of the off-critical mixture with high molecular weights. A similar pinning of the domain growth was reported for the growth of spherical microdomains in block copolymers[22]. For mixtures having smaller molecular weights, $\chi_{eff}N$ is smaller so that the growth of the droplets can always take place. The same argument may be easily extended to the surface diffusion in which ΔH_{mix} may be replaced by an excess surface free energy associated with the change of the interfacial area involved in the surface diffusion process.

A remaining problem exists as to why the dynamical PC transition occurs in the ordering process for off-critical mixtures. A possible interpretation may be given on the basis of an asymmetry in the volume fractions X_{ie}(i=1 or 2) of the two coexisting domains 1 and 2 in equilibrium. In the ordering process, the volume fraction of the domains rich in minority component (e.g., X_1) may decrease with time from 1/2 to the equilibrium value X_{1e} (<1/2). The volume decrease of the minority domains may cause such a symmetry break as envisioned by a transformation from percolating networks to the spherical droplets, i.e., the dynamical PC transition. The percolating network results from the unmixing due to SD. Even in the case when X_1 and X_2 remain unchanged during the coarsening process, such as in the case when the pinning occur in the late stage, the symmetry break and hence the PC transition may occur when the aspect ratio of the network rich in the minority component (or the part of the network between the nearest neighbor branching points) decreases with time. The asymmetry in X_i increases with increasing temperature and with biasing the composition toward 0 or 1 as shown in Fig. 5-14, which may account for the important

piece of experimental evidence that the pinning occurs earlier with increasing temperature and biasing the composition.

In conclusion, the conjecture on the pinning mechanism based on the dynamical PC transition and kinetically frozen diffusion-coalescence process should be confirmed by future experiments, especially by real-space analyses of the domain structure. Such work is in progress in our laboratory.

References

1 T. Izumitani and T. Hashimoto, J. Chem. Phys. **83**, 3694 (1985).

2 M.Takenaka, T. Izumitani, and T.Hashimoto, Macromolecules, **20**, 2257 (1987).

3 T. Izumitani, M. Takenaka, and T. Hashimoto, J. Chem. Phys. **92**, 3213 (1990).

4 M. Takenaka, T. Izumitani, and T. Hashimoto, J. Chem. Phys. **92**, 4566 (1990).

5 T. Hashimoto, T. Izumitani, and M. Takenaka, Macromolecules, **22**, 2293 (1989).

6 T. Hashimoto, J. Kumaki, and H. Kawai, Macromolecules **16**, 641 (1983).

7 J.W. Cahn, J. Chem. Phys. **42**, 193 (1965).

8 H.E. Cook, Acta. Met. **18**, 297 (1970).

9 H.L. Snyder and P. Meakin, J. Chem. Phys. **79**, 5588 (1983).

10 T. Hashimoto, M. Itakura, and N. Shimidzu, J. Chem. Phys. **85**, 6773 (1986). T.Hashimoto, T.Takenaka, and H.Jinnai, J.Appl. Cryst. **24**, 457 (1991).

11 K. Binder, J. Chem. Phys. **79**, 6387 (1983).

12 Y. Chou and W.I. Goldburg, Phys. Rev. A. **20**, 2105 (1979).

13 K. Binder and D. Stauffer, Phys. Rev. Lett. **33**, 1006 (1974); K. Binder, Phys. Rev. B**15**, 4425 (1977).

14 M. Takenaka, T. Izumitani, and T. Hashimoto, in preparation.

15 E.D. Siggia, Phys. Rev. A. **20**, 595 (1979).

16 H. Furukawa, Phys.Rev.Lett. **43**, 136 (1979).

17 H. Hasegawa, T. Shiwaku, A. Nakai, and T. Hashimoto, in "Dynamics of Ordering Processes in Condensed Matter", ed. by S. Komura and H. Furukawa, Plenum Press, N.Y. 1988.

18 A. Nakai, T. Shiwaku, H. Hasegawa, and T. Hashimoto, in preparation.

19 S. Tomotika, Proc. R. Soc. London, Ser. A. **150**, 322 (1935), **153**, 302 (1936).

20 L.P. McMaster, Adv. Chem. Ser. **142**, 43 (1975).

21 K. Binder and D. Stauffer, Phys.Rev.Lett. **33**, 1006 (1974). K.Binder and M.H.Kalos, J.Stat.Phys. **22**, 363 (1980). J. D. Gunton, M. Miguel and P. P. Sahni, *Phase Transition and Critical Phenomena*, edited by C. Domb and J. L. Lebowitz (Academic Press, N.Y., 1983), Vol. 8, p.269.

22 M. Shibayama, T. Hashimoto, and H. Kawai, Macromolecules, **16**, 1434 (1983).

Chapter 6 : Spontaneous Pinning for Off-Critical Mixtures -Analysis of Scaled Structure Factor

6-1. Introduction

In chapter 5, we investigated the spinodal decomposition (SD) of an off-critical mixture of polymers by analyzing time changes in $I_m(t;T)$, the maximum scattered intensity of the scatted intensity profile $I(q,t;T)$ at time t and phase separation temperature T, and $q_m(t;T)$, the magnitude of the scattering vector at which the intensity becomes maximum at t and T. The systems studied were poly(styrene-*ran*-butadiene) (SBR) / polybutadiene (PB) and SBR / polyisoprene (PI). We found that the time changes in q_m and I_m for these off-critical mixtures were pinned at a certain time. This unique phenomenon, which we called "spontaneous pinning",[1] occurred earlier as the composition w was shifted more toward 1 or 0 at a given phase separation temperature T and as T is raised at a given w. We postulated that the spontaneous pinning originates from a "dynamical percolation-to-cluster (PC) transition" and a kinetically frozen diffusion-coalescence process[1]. Recently, Kotnis et.al.[2] computer-simulated the dynamics of off-critical mixtures and found a similar stop of the coarsening process. They gave a similar interpretation to ours on this phenomenon.

In this chapter, we investigated further the scaled structure factor $F(x,t;T)$ as a function of w and T, where $F(x,t;T)$ is defined by

$$F(x,t;T) \equiv q_m(t;T)^3 I(x,t;T) \tag{6.1}$$

with

$$x \equiv q/q_m(t;T). \tag{6.2}$$

It is shown that the dynamical PC transition occurs during the coarsening process before pinning.

Sec. 6-2 describes the samples, the experimental conditions and the phase separation conditions. Sec.6-3 shows results obtained by light scattering experiments. In sec.6-4-1 the time change in the scaled structure factor is presented along with the comparisons between the scaled structure factors for the critical and off-critical mixtures. The temperature dependence of the scaled structure factor and its comparison with a theoretical one are presented in sec. 6-4-2 and 6-4-3. Sec. 6-5 mentions the conclusions from the present study.

6-2. Exprimental section

6-2-1. Samples and sample preparation

The characteristic parameters of the samples SBR (coded SBR1), PB (coded PB19) and PI (coded PI55) are summarized in Table 6-I, where M_w and M_n are weight-average and number-average molecular weight, respectively. Blends used and their phase separation conditions are summarized in Table 6-II. The composition of an off-critical mixture was 25/75 wt./wt. for SBR1/PB19 and 30/70 wt./wt. and 20/80 wt./wt. for SBR1/PI55. Each blend was dissolved in toluene containing the component polymers by 10 wt.% in total. The solutions were cast to films 0.10 mm thick in a petri dish by evaporating the solvent slowly at 30 °C for one week. The films were further dried in a vacuum oven at room temperature until their weight became constant.

6-2-2. Experimental methods

The as-cast films have internal phase-separated structures via SD during the solvent evaporating process. They can not be made single-phased by temperature elevation without thermal degradation. Thus, we prepared single-phased blends by the homogenization process described elsewhere.[3] The homogenized film specimen was sandwiched between thin glass plates in a

TABLE 6-I Sample Characterization

Sample	Mw	Mw/Mn	St(wt%)[b]	Microstructure (%)[a]			
				1,4-cis	1,4-trans	1,2-vinyl	3,4-vinyl
SBR1	11.8	1.1_8	20	16	23	61	-
PB19	19.1	1.1_6	-	19	35	46	-
PI55	54.6	1.0_2	-	75	16	9	-

a) Obtained by IR
b) Weight percent of styrene monomers in SBR.

TABLE 6-II Phase separation conditions

SBR1/PI55			SBR1/PB19		
Composition (wt./wt.)	T[a] (°C)	ε_T[b]	Composition (wt./wt.)	T[a] (°C)	ε_T[b]
20/80	60	1.1	25/75	50	1.4
30/70	60	2.0		60	1.3
	90	1.8		70	1.3
	120	1.5		110	1.3
50/50	60	3.5	48/52	50	2.8
-	-	-		60	2.7
-	-	-		70	2.6
-	-	-		110	2.4

a) Phase separation temperature.
b) Rough estimation of the thermodynamic driving force for the phase separation $\varepsilon_T = [\chi_{eff}(T) - \chi_s]/\chi_s$.

sample holder and then the film specimen was subjected to a jump (T-jump) to a given phase separation temperature T. The dynamics of the unmixing process was observed *in situ* by the time-resolved light scattering method described elsewhere.[4] The time right after the homogenization was taken as the origin of time t.

6-2-3. Phase separation conditions

We estimated the parameter ε_T characterizing the quench depth from the relation

$$\varepsilon_T = [\chi_{eff}(T) - \chi_s]/\chi_s \qquad (6.3)$$

where $\chi_{eff}(T)$ is the effective χ-parameter per segment between the two polymers SBR1 and PB19 or SBR1 and PI55, and χ_s is the value of $\chi_{eff}(T)$ at the spinodal temperature. The method of estimating $\chi_{eff}(T)$ and χ_s has been described in the previous chapter.[1]

As seen in Table 6-II, the values of ε_T for all mixtures studied are larger than unity. This means that our phase separation conditions corresponded to deep quench.

6-3. Results

In our previous paper[1], the time change in the scattered intensity for the off-critical mixture SBR1/PI55 30/70 wt./wt. was compared with that for the critical mixture SBR1/PI55 50/50 wt./wt. at 60°C. Here, in Figures 6-1 and 6-2, we compare the time change for the critical mixture SBR1/PB19 58/42 wt./wt. with that for the off-critical mixture SBR1/PB19 25/75 wt./wt. at 60°C. In each, the relative scattered intensity is plotted as a function of the magnitude of the scattering vector q, i.e.,

$$q=(4\pi/\lambda)\sin(\theta/2) \qquad (6.3)$$

where λ and θ are the wavelength of the incident beam and the scattering angle in the medium, respectively. We introduces a reduced time τ defined by

$$\tau \equiv t/t_c(T) \tag{6.4}$$

where $t_c(T)$ is the characteristic time for the mixture as discussed in our previous paper.[1] Time elapses from part (c) to part (a).

The time changes in the scattered intensity, I(q,t), for the critical mixture and off-critical mixture are similar in the early stage SD corresponding to Figs. 6-1(c) and 6-2(c) and in the later stage SD corresponding to Figs. 6-1(b) and 6-2(b); the intensity increases with time in the indicated q-region and shows a maximum after a certain time. The wavenumber $q_m(t;T)$ of the peak position at t and T then shifts toward smaller q and the peak intensity $I_m(t;T)$ at t and T increases with time reflecting the coarsening of phase separated structure.

However, in a much later stage SD, a marked difference appears in the time changes in the scattered intensity of the two systems, as seen from Figs. 6-1(a) and 6-2(a). For the critical mixture, the increase in $I_m(t;T)$ and the decrease in $q_m(t;T)$ continue, but for the off-critical mixture, $q_m(t;T)$ ceases to decrease and $I_m(t;T)$ turns to increase very slowly after t=138 min. (τ = 10.0). This is the phenomenon we called "spontaneous pinning" in our previous paper.[1]

Figures 6-3 and 6-4 show the time changes in scattering profiles for the off-critical mixture SBR1/PI55 30/70 wt./wt. at 90 and 120°C, respectively. "Spontaneous pinning" is seen in each figure. It is found that the higher the temperature the earlier the pinning time and the larger the characteristic wavenumber for the pinned structure become. The temperature dependence for the off-critical mixture SBR1/PB19 25/75 wt./wt., shown in our previous paper[1], is similar to that for SBR1/PI55 30/70/ wt./wt.

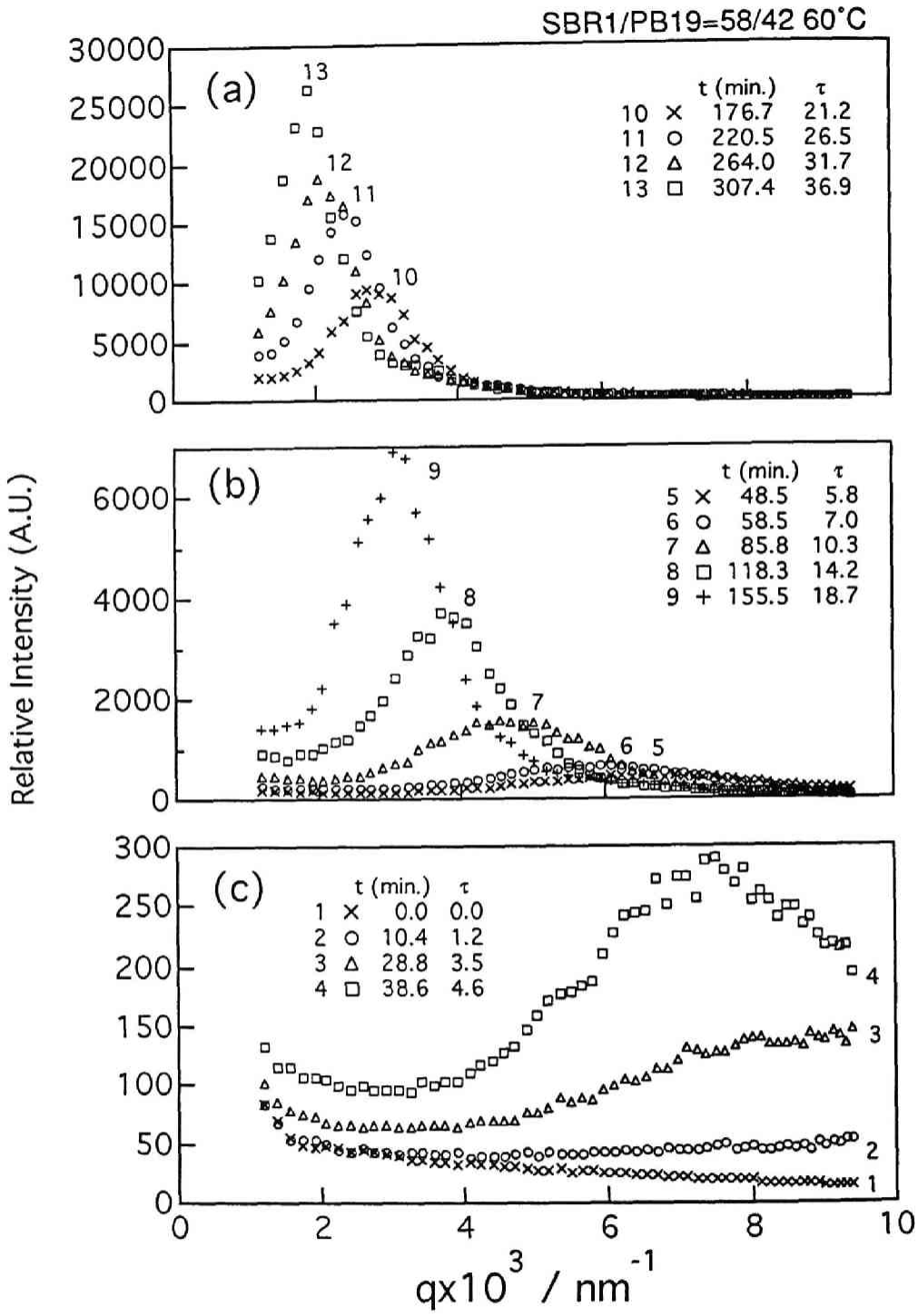

Figure 6-1 Time evolution of the light scattering profile for SBR1/PB19 58/42 wt./wt. after onset of unmixing at 60°C.

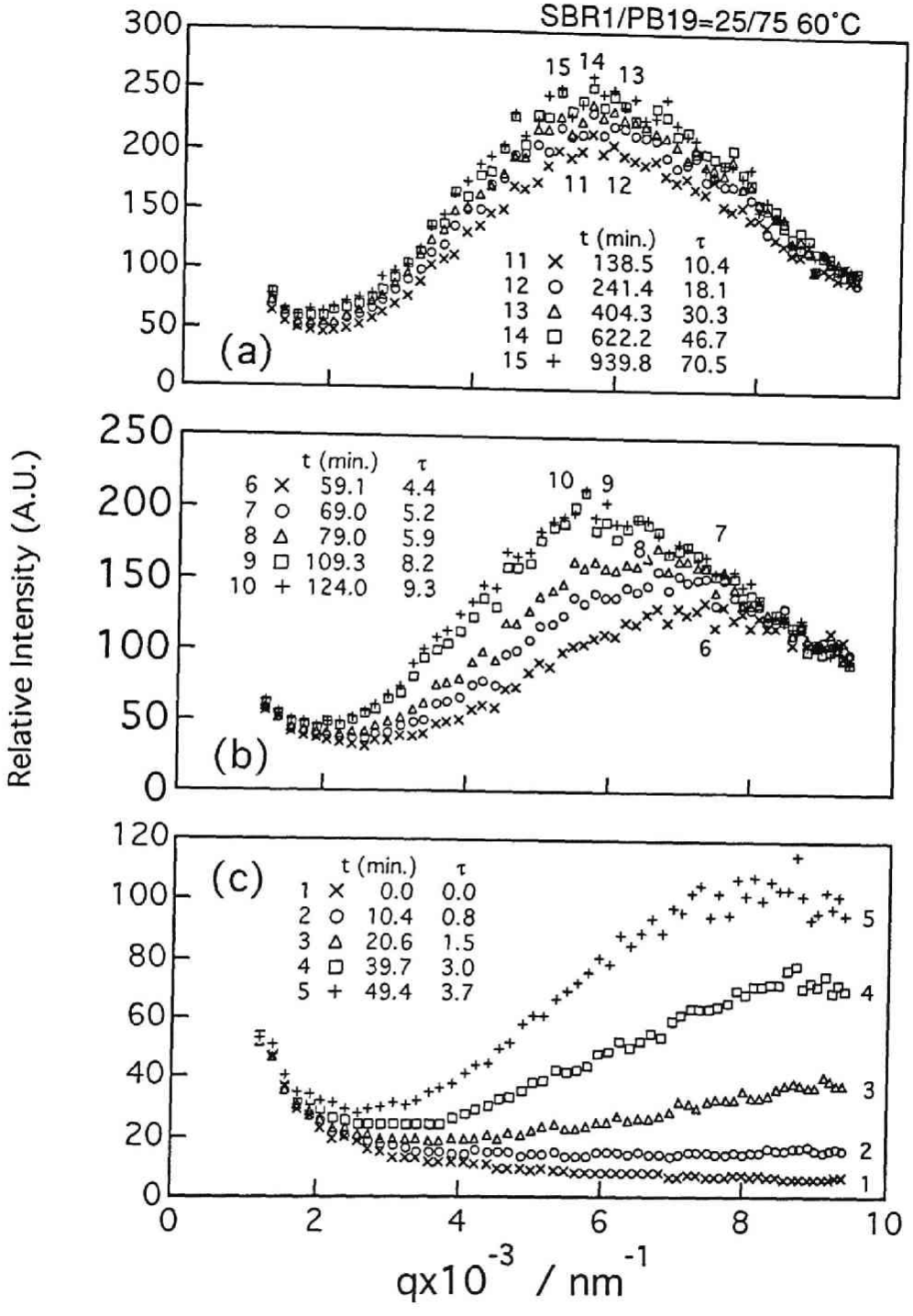

Figure 6-2 Time evolution of the light scattering profile for SBR1/PB19 25/75 wt./wt. after onset of unmixing at 60°C.

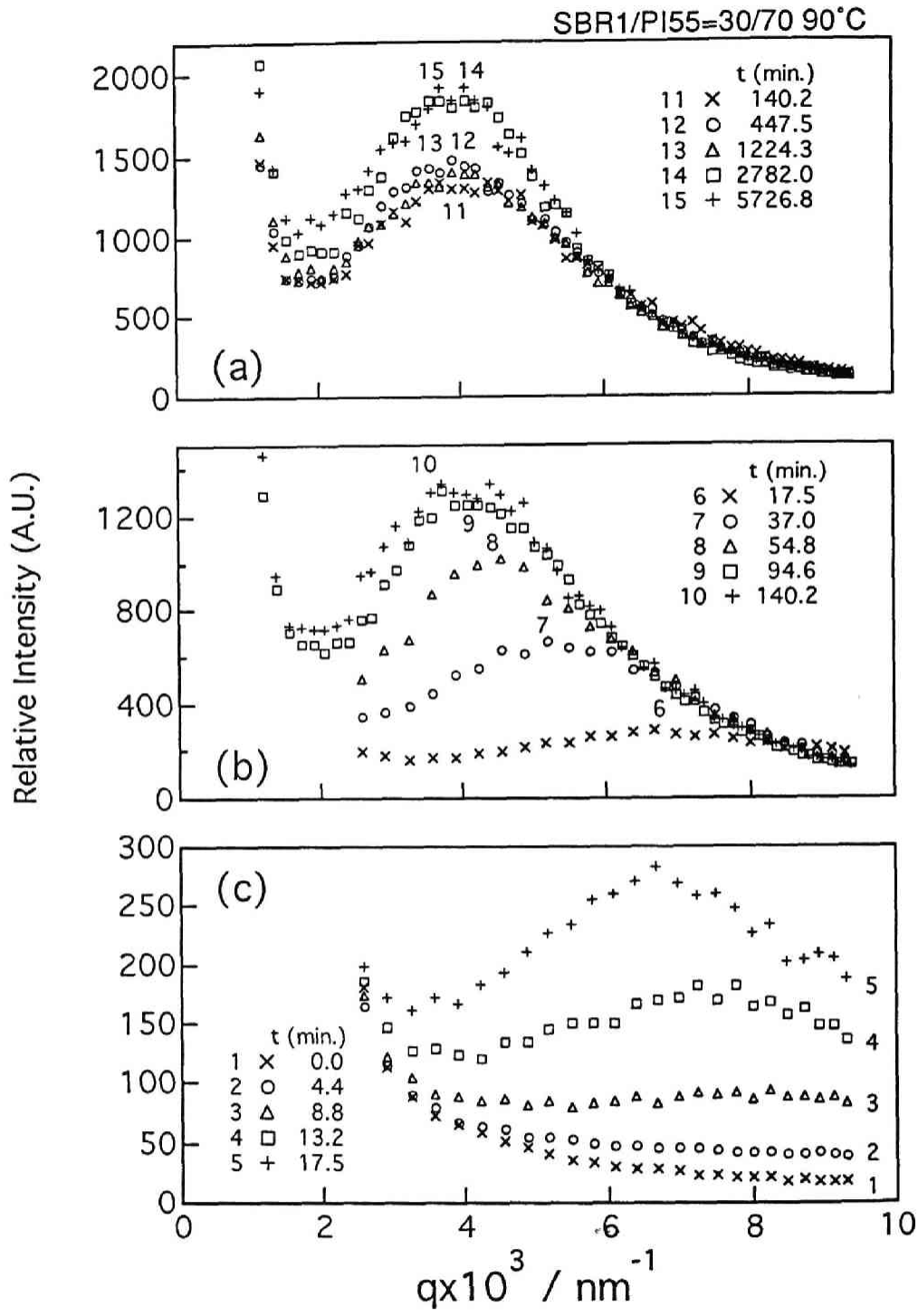

Figure 6-3 Time evolution of the light scattering profile for SBR1/PI55 30/70 wt./wt. after onset of unmixing at 90°C.

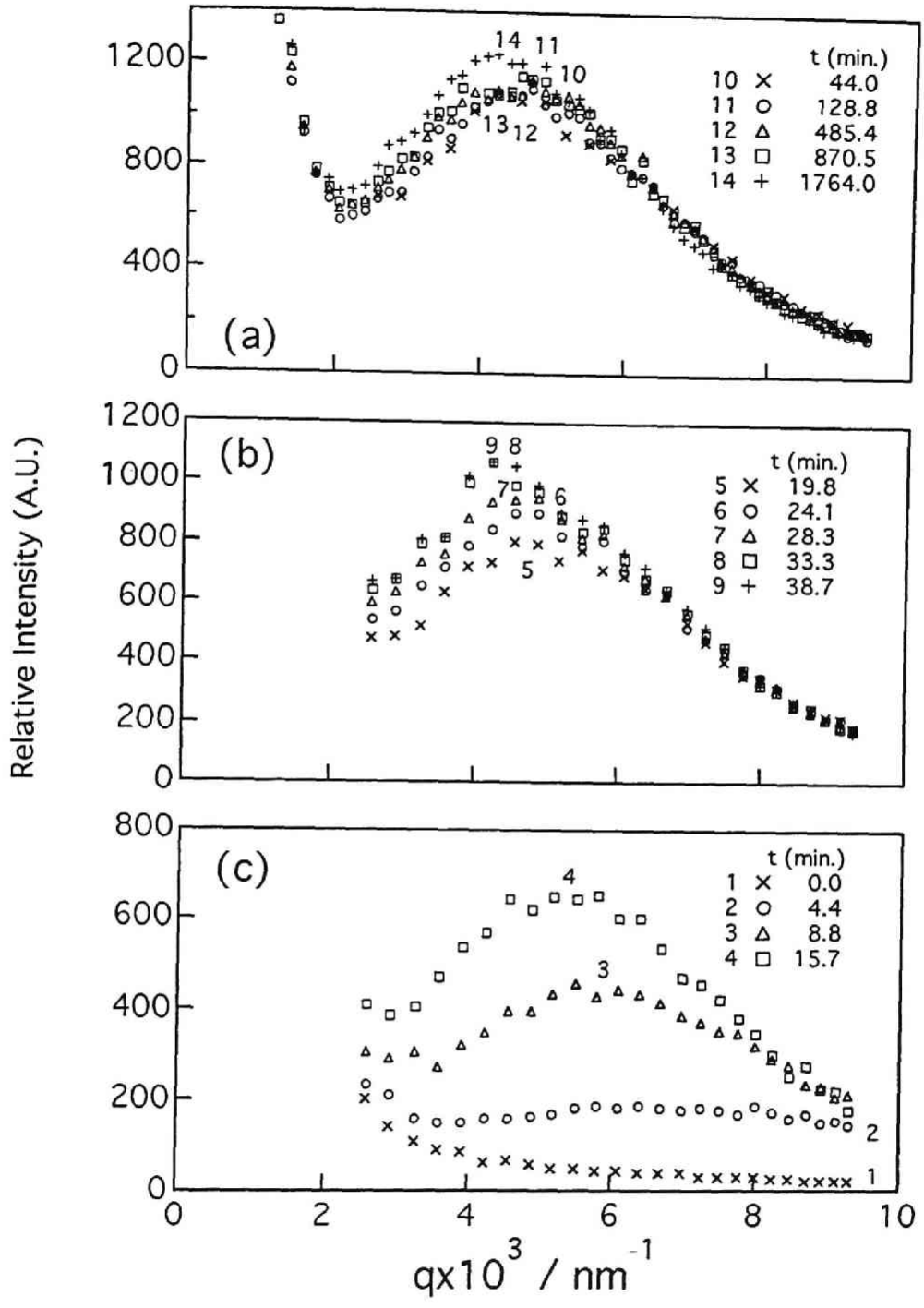

Figure 6-4 Time evolution of the light scattering profile for SBR1/PI55 30/70 wt./wt. after onset of unmixing at 120°C.

6-4. Analysis and discussion

In our previous paper,[1] we analyzed the early stage SD using Cahn's linearized theory[5-7] and investigated the behavior of $q_m(t;T)$ and $I_m(t;T)$ in the later stage SD. In this section, we focus on time changes in the scaled structure factor F(x,t) for SBR1/PB19 and SBR1/PI55 mixtures in the later-stage SD as a function of composition w and phase separation temperature T.

6-4-1. Composition dependence of the time change in the scaled structure factor

6-4-1-1. SBR1/PI55 system

Figures 6-5 and 6-6 show time changes at 60°C in the scaled structure factor F(x,t) plotted as a function of x for the critical mixture SBR1/PI55=50/50 wt./wt. and the off-critical mixture SBR1/PI55 30/70 wt./wt., respectively.

The later-stage for the critical mixture is seen to be divided into two time regions: the intermediate and late stages, as in the previous results.[8-12] In the intermediate stage, $80.6 < t < 468.9$ min. or $5.8 < \tau < 33.7$, the mean squared fluctuations $\langle \eta(t,T)^2 \rangle$ of the refractive index difference between two phases does not yet reach an equilibrium value $\langle \eta(T)^2 \rangle_e$ but increases with time. Hence F(x,t) for different times do not superimpose each other but increase with time as shown in Fig.6-5(a). In addition to the increase in its intensity, the scaled structure factor becomes sharp with time. In Figure 6-5(b), which shows the scaled structure factor F(x,t) in the late stage, $t > 468.9$ min. or $\tau > 33.7$, $\langle \eta(t,T)^2 \rangle$ reaches $\langle \eta(T)^2 \rangle_e$ and the global structure grows in self-similarity and F(x,t) for different times superimpose. According to our previous findings,[1] the time changes in $q_m(t;T)$ and $I_m(t;T)$ are described by

$$q_m(t;T) \sim t^{-\alpha} \tag{6.5}$$

and

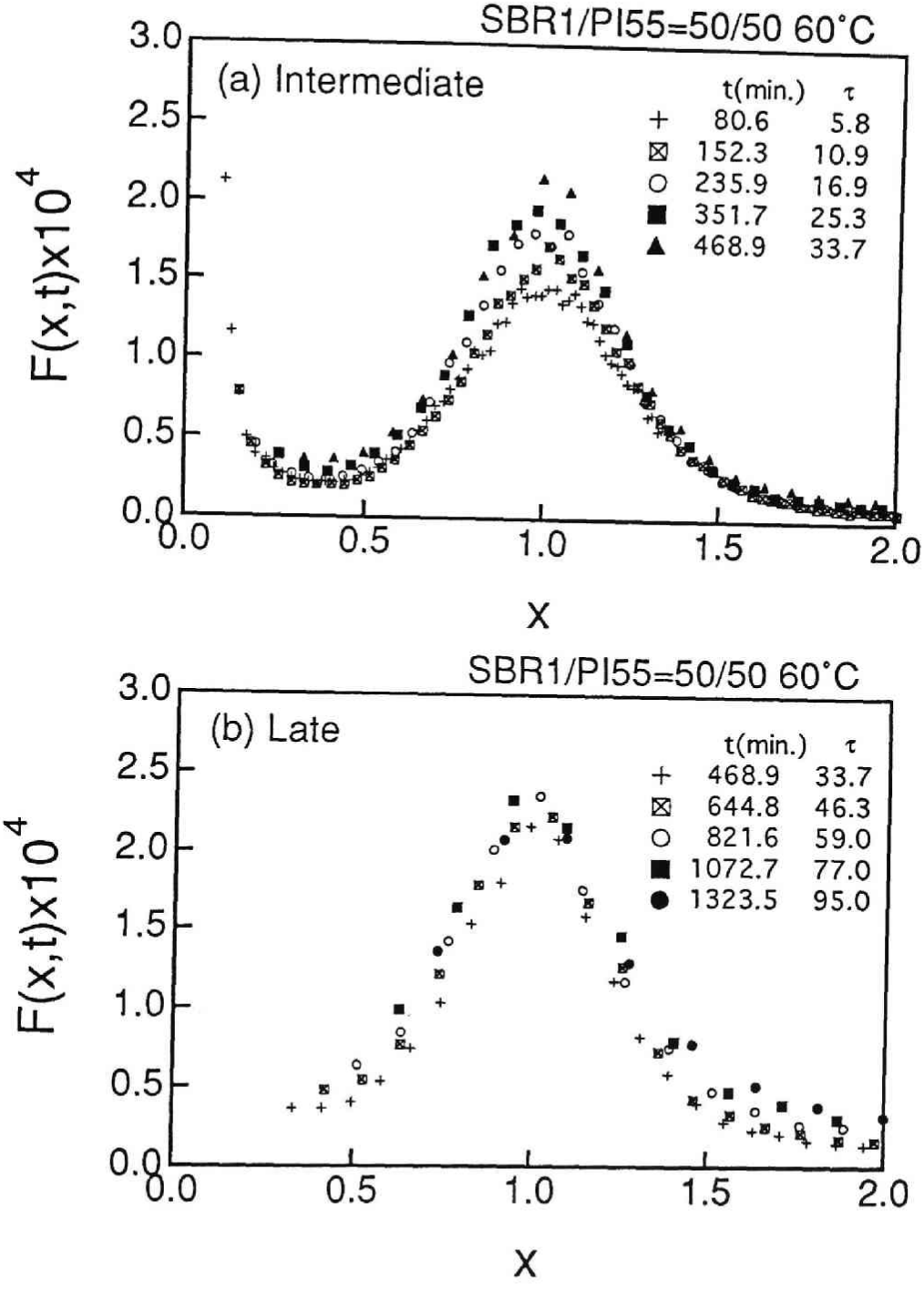

Figure 6-5 Scaled structure factor for SBR1/PI55 50/50 wt./wt. at 60°C in the intermediate stage (a) and the late stage (b).

$$I_m(t;T) \sim t^{\beta} \tag{6.6}$$

with the relationship between α and β changing from

$$\beta > 3\alpha \qquad \text{for } t < 469 \text{ min. or } \tau < 33.7 \tag{6.7}$$

to

$$\beta = 3\alpha \qquad \text{for } t > 469 \text{ min. or } \tau > 33.7. \tag{6.8}$$

The non universal nature of F(x,t) with t in Fig.6-5(a) and the universal nature of F(x,t) with t in Fig. 6-5(b) are consistent with the change from Eqs. (6.7) to (6.8).

The later-stage SD for the off-critical mixture is divided into four stages: *intermediate*, *late*, *transition*, and *pinning*, as (a) to (d) in Fig.6-6.

In the intermediate stage, $46.5 < t < 83.8$ min. or $2.3 < \tau < 4.2$, corresponding to Fig.6-6(a), F(x,t) increases with time, indicating that $\langle \eta(t,T)^2 \rangle$ increases toward the equilibrium value $\langle \eta(T)^2 \rangle_e$. F(x,t) sharpens with time, indicating formation of better defined structure. In the late stage, $83.8 < t < 100.8$ min. or $4.2 < \tau < 5.0$, F(x,t) for different time superpimoses. In this time region, the relation $\beta = 3\alpha$ was found to hold in our previous paper[1]. The late stage for the off-critical mixture starts earlier than that for the critical mixture. This behavior may be explained as follows. The function I(q,t) can be generally expressed by

$$I(q,t) = \langle \eta(t,T)^2 \rangle q_m(t)^{-3} \overline{F}(x,t) \tag{6.9}$$

where $\overline{F}(x,t)$ is the scaling function satisfying

$$\int_0^{\infty} \overline{F}(x,t)\, x^2 dx = 1. \tag{6.10}$$

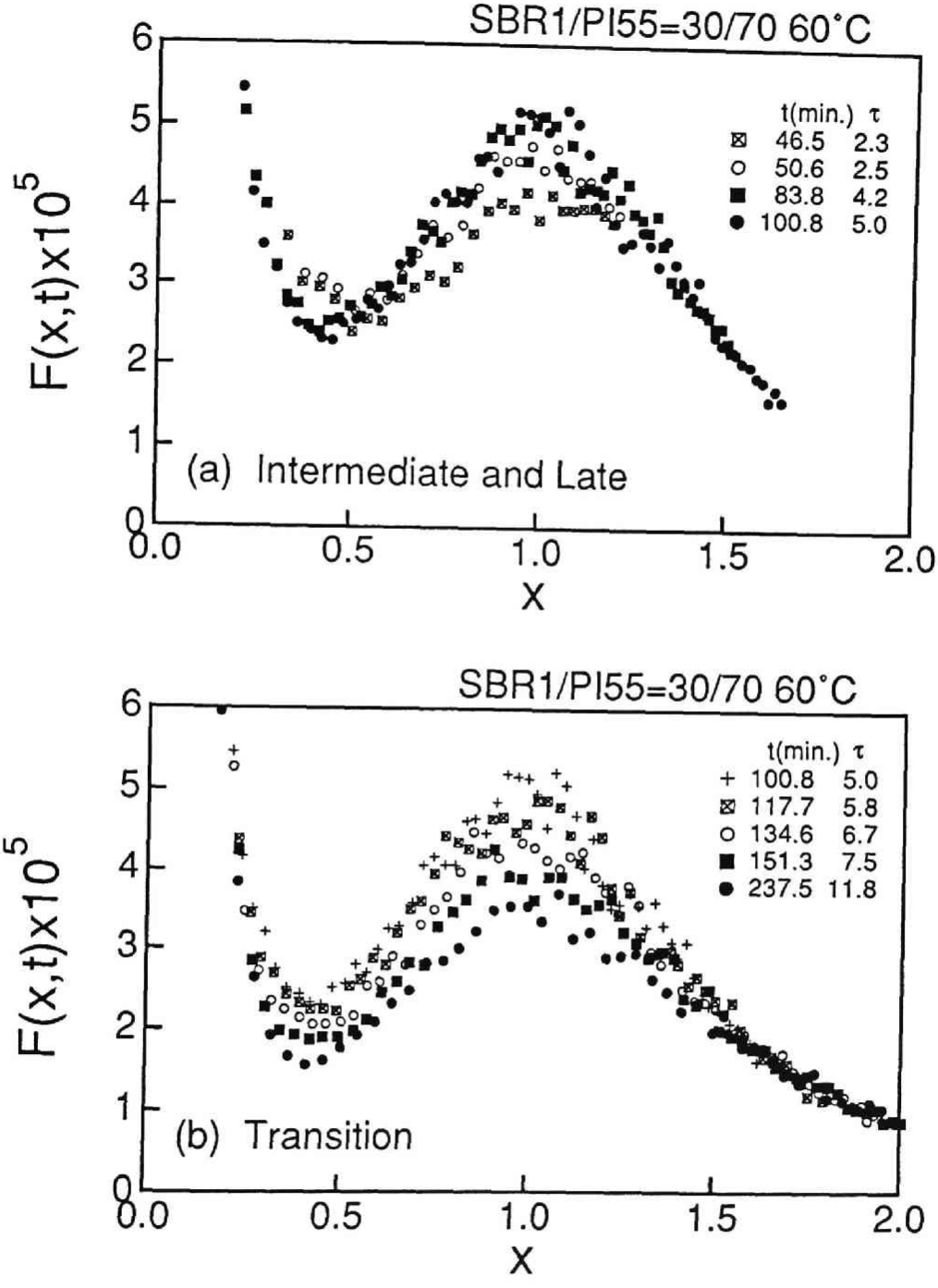

Figure 6-6 Scaled structure factor for SBR1/PI55 30/70 wt./wt. at 60°C. (a) corresponds to the intermediate and late stages and (b) corresponds to the transition stage.

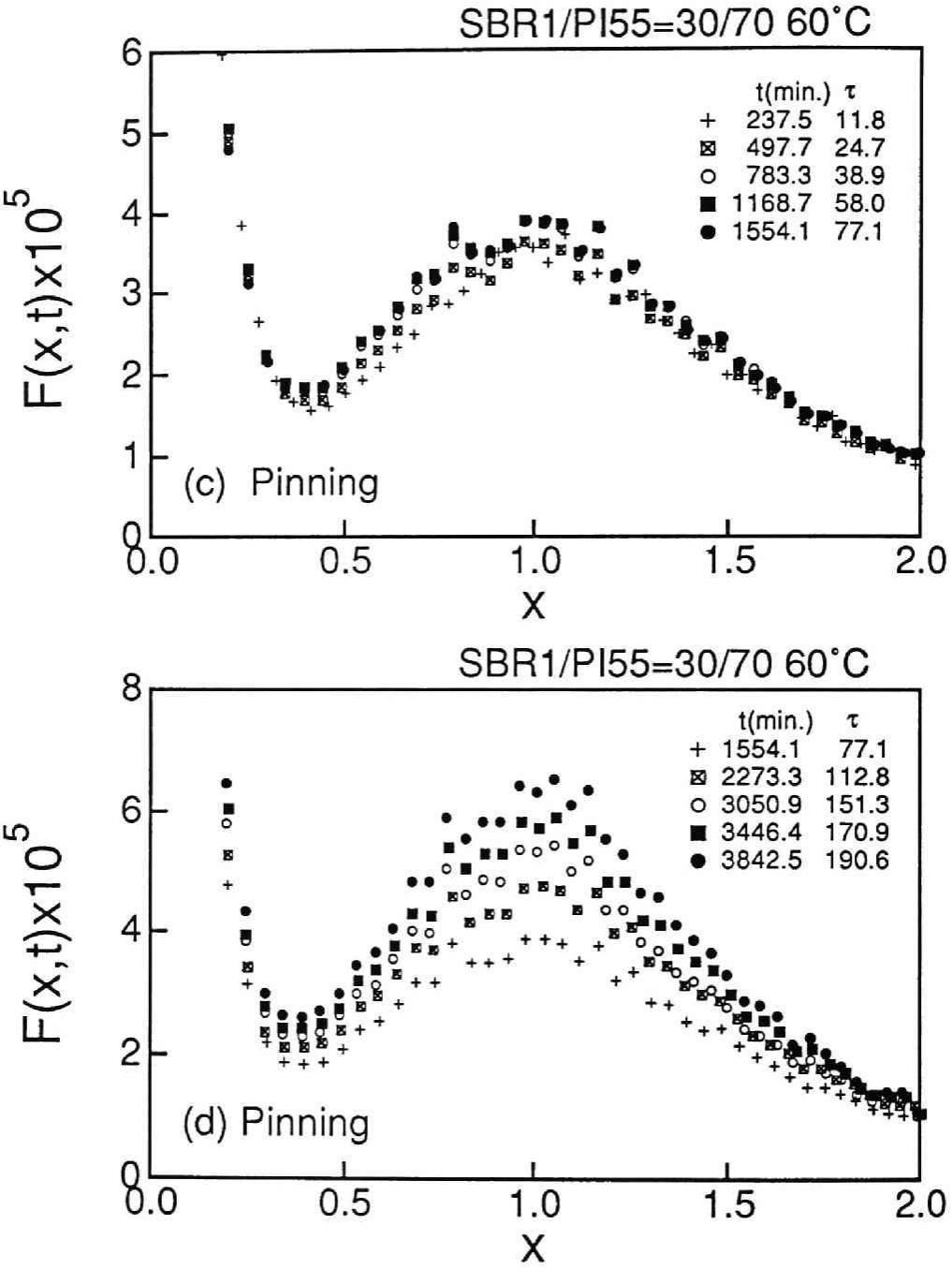

Figure 6-6 Scaled structure factor for SBR1/PI55 30/70 wt./wt. at 60°C. (c) and (d) corresponds to the pinning stage.

$\bar{F}(x,t)$ is related to $F(x,t)$ by

$$F(x,t) = \langle \eta(t,T)^2 \rangle \bar{F}(x,t). \tag{6.11}$$

with $\langle \eta(t,T)^2 \rangle$ given by

$$\langle \eta(t,T)^2 \rangle = \int_0^{\infty} F(x,t)\, x^2 dx. \tag{6.12}$$

The integrand in Eq.(6.12) can be approximated as

$$\int_0^{\infty} F(x,t)\, x^2 dx \approx \int_{x'}^{x''} F(x,t)\, x^2 dx \tag{6.13}$$

where x' and x'' are the lower and upper bounds of x beyond which the integrand effectively becomes zero. From Eqs. (6.11),(6.12) and (6.13), $\bar{F}(x,t)$ can be written

$$\bar{F}(x,t) = F(x,t) \Big/ \int_{x'}^{x''} F(x,t)\, x^2 dx. \tag{6.14}$$

We can analyze time changes in F(x,t) in terms of those in $\bar{F}(x,t)$ [Eq.(6.14)] and $\langle \eta(t,T)^2 \rangle$ [Eqs. (6.12) and (6.13)]. Although not shown here, in the case of critical mixtures, $\bar{F}(x,t)$ becomes sharper and $\langle \eta(t,T)^2 \rangle$ increases with time in the intermediate stage, while $\bar{F}(x,t)$ becomes universal and $\langle \eta(t,T)^2 \rangle$ reaches the constant value $\langle \eta(T)^2 \rangle_e$ in the late stage. Therefore F(x,t) increases with time in the intermediate stage and then becomes invariant with time.[11] In the case of off-critical mixtures, the peak position in the intermediate and late stages exists at so high a q in our experimental q-range that the even

highest x attained by our experiment does not allow the integral in Eq.(6.13) to be computed accurately. Thus it was not possible to determine the time changes in $\langle\eta(t,T)^2\rangle$ and $\overline{F}(x,t)$ in the intermediate and late stages. However, $\langle\eta(t,T)^2\rangle$ is independent of x and F(x,t) is identical in shape to $\overline{F}(x,t)$ on double logarithmic plots. The absolute value for the exponent of x for F(x,t) at x>1 decreases continuously when SD goes from the intermediate to the transition stage, as will be illustrated later in Fig. 6-14. The decrease of the exponents means that $\overline{F}(x,t)$ becomes progressively broader and hence $\overline{F}(x,t)$ around at x=1 decreases as process goes from the intermediate to the transition stage. We believe that this phenomenon is due to the dynamical PC transition which occurs before the spontaneous pinning starts as proposed previously.[1] The increase in $\langle\eta(t,T)^2\rangle$ and the decrease in $\overline{F}(x,t)$ cancel each other, so that F(x,t) remains almost constant at $x \simeq 1$ with time even before $\langle\eta(t,T)^2\rangle$ reaches $\langle\eta(T)^2\rangle_e$ and the late stage for the off-critical mixtures looks as if it starts earlier than that for the critical mixture. Thus we conclude that the origin of the crossover mechanism from the intermediate to the late stage for the off-critical mixture is different from that for the critical mixture.

In the transition stage, $100.8 < t < 237.5$ min. or $5.0 < \tau < 11.8$ (Fig.6(b)), $\langle\eta(t,T)^2\rangle$ almost reaches the equilibrium value $\langle\eta(T)^2\rangle_e$ and the broadening of $\overline{F}(x,t)$ dominates the contribution to F(x,t). Hence, F(x,t) decreases with time. From Eq.(6.9) $I_m(t)$ is given by

$$I_m(t) \equiv I(q_m,t) = \langle\eta(t,T)^2\rangle q_m(t)^{-3}\overline{F}(1,t) \tag{6.15}$$

and $\overline{F}(1,t)$ decreases with time. Therefore, we expect that the relationship

$$\beta < 3\alpha \tag{6.16}$$

holds in the transition stage, as has been confirmed experimentally.[1]

Finally, in the pinning stage, 237.5 min. < t or 11.8 < τ, corresponding to Figs. 6-6 (c) and (d), the coarsening stops and α diminishes to zero.[1] F(x,t) becomes universal in the time interval 273.5 < t < 1554.1 min. or 11.8 < τ < 77.1 (part c), but it increases and sharpens with time after t = 1554.1 min. or τ = 77.1(part d). There may be two possibilities for the interpretation of the time change in F(x,t) shown in Fig. 6-6(d). One possibility is the transformation of the isolated clusters and the other is the equilibration of the composition fluctuations in the two phases.

The scattering function I(q) of a two-phase system, where isolated clusters of component A are dispersed in the matrix of B component, is described by[13]

$$I(q) \sim \langle\eta^2\rangle N\langle|F_J(q)|^2\rangle_{av}\left[1 - \frac{N}{V}\int_0^\infty [1 - P(R)]\frac{\sin qR}{qR}4\pi R^2\, dR\right] \qquad (6.17)$$

Here, N, $\langle\eta^2\rangle$, $F_J(q)$, V and P(R) are, respectively, the total number of the clusters, the mean squared refractive index difference between the A-region and the B-region, the average scattering intensity of the isolated clusters, the total volume of the system and the pair correlation function for the spatial distribution of the centers of clusters. I(q) thus depends on $\langle\eta^2\rangle$, $\langle|F_J(q)|^2\rangle_{av}$ and P(R).

As regards the first possibility mentioned above, the shape change of isolated cluster affects $\langle|F_J(q)|^2\rangle_{av}$ and P(R). Just after the network structure of the minority phase breaks into isolated clusters owing to the dynamical PC transition, the surface of the isolated clusters is tangled as shown in Fig.6-7(a). The wavy interface is then smoothened and the structure of isolated clusters becomes more spherical with time as shown in Fig.6-7(b), thereby to reduce the surface-to-volume ratio.

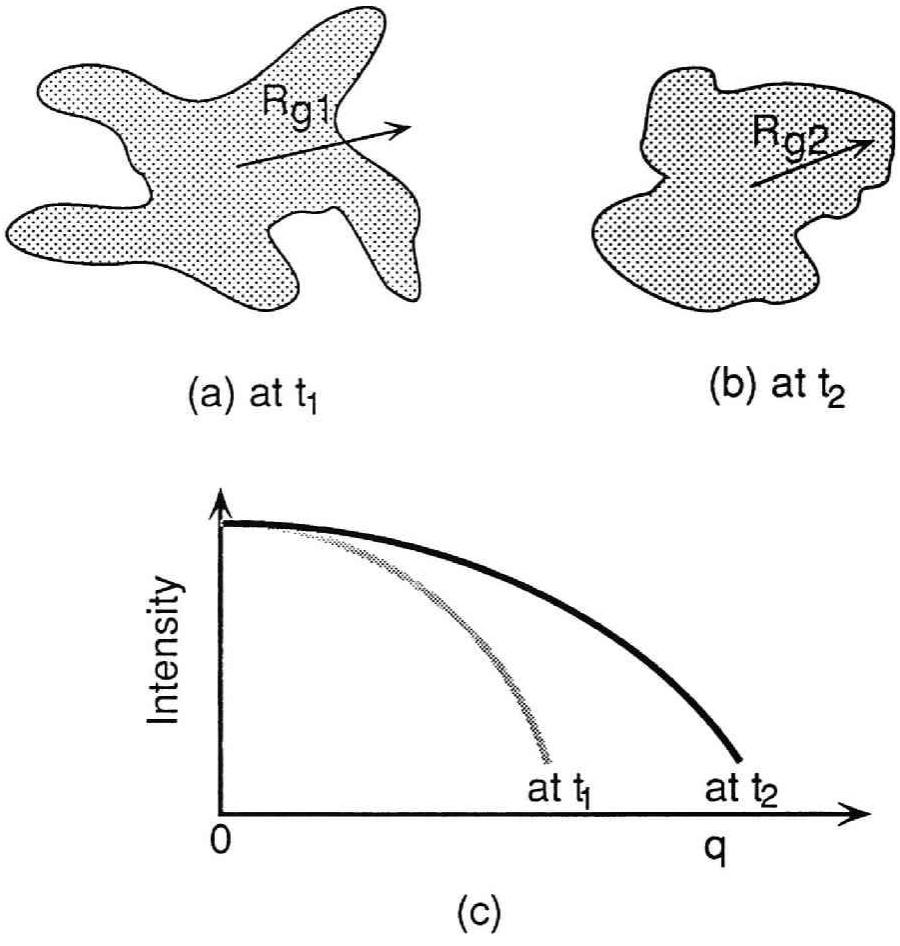

Figure 7 Schematic illustration of the clusters for the off-critical mixture in the early time of the pinning stage (a) and the late time of the pinning stage (b). (c) shows their scattered intensity.

We first consider a simplified case in which the transformation doesn't essentially change the the location of the clusters but makes their average radius of gyration R_g smaller. When this is the case, only $\langle|F_J(q)|^2\rangle_{av}$ varies but $\langle\eta^2\rangle$ and the term inside [ ] in Eq.(6.17) does not change with time. The average scattering intensity of the cluster $I_p(q) \equiv \langle|F_J(q)|^2\rangle_{av}$ is approximated by

$$I_p(q) = I_p(0)\exp(-q^2R_g^2/3) \qquad (6.18)$$

with the condition

$$qR_g<<1, \tag{6.19}$$

where R_g is the z-average radius gyration of clusters. The volumes of the clusters are conserved during the transformation process, so that $I_p(0)$ remains constant. Hence, I(q) at a given q depends only on R_g and increases with time, because R_g decreases with time, as shown in Fig.6-7(c). This explains why F(x,t) increases with time in Fig.6-6(d). Let us next consider why F(x,t) becomes sharper as the transformation progresses. We also consider the case when the transformation makes not only R_g smaller but also the location of the clusters more periodical, accompanied by the change in the cluster shape. In this case, the distribution P(R) of the distances between clusters becomes narrow and the increase in F(x,t) can be explained in terms of a change in P(R). The narrowing of P(R) also causes F(x,t) to sharpen.

As for the second possibility, the equilibration of the composition fluctuation in the two phases affects $\langle\eta^2\rangle$. This phenomenon appears when the dynamical PC transition occurs before $\langle\eta^2\rangle$ reaches equilibrium, and it causes $\langle\eta^2\rangle$ in Eq. (6.17) to increase, so that both I(q) and F(x,t) increase with time. However, the shape of F(x,t) does not change during the equilibration process.

Figure 6-8 shows the composition dependence of $\tilde{F}(x,\tau) \equiv F(x,\tau)/F(x=1,\tau)$ for SBR1/PI55 50/50 wt./wt. at 60°C where $\tilde{F}(x,\tau)$ for the off-critical mixture 30/70 wt./wt. and 20/80 wt./wt. at 60°C were compared with that for the critical mixture 50/50 wt./wt. First, we compare $\tilde{F}(x,\tau)$ at $\tau \simeq 5$, corresponding to the intermediate stage SD for both the critical mixture and the off-critical mixtures [Fig.6-8(a)]. $\tilde{F}(x,\tau)$ for the critical mixture is sharper than those for the off-critical mixtures and $\tilde{F}(x,\tau)$ for the latter are identical except for $x<0.7$. The shapes of $\tilde{F}(x,\tau)$ for 30/70 wt./wt. and 50/50 wt./wt. for $1.3 < x < 1.5$ are represented by

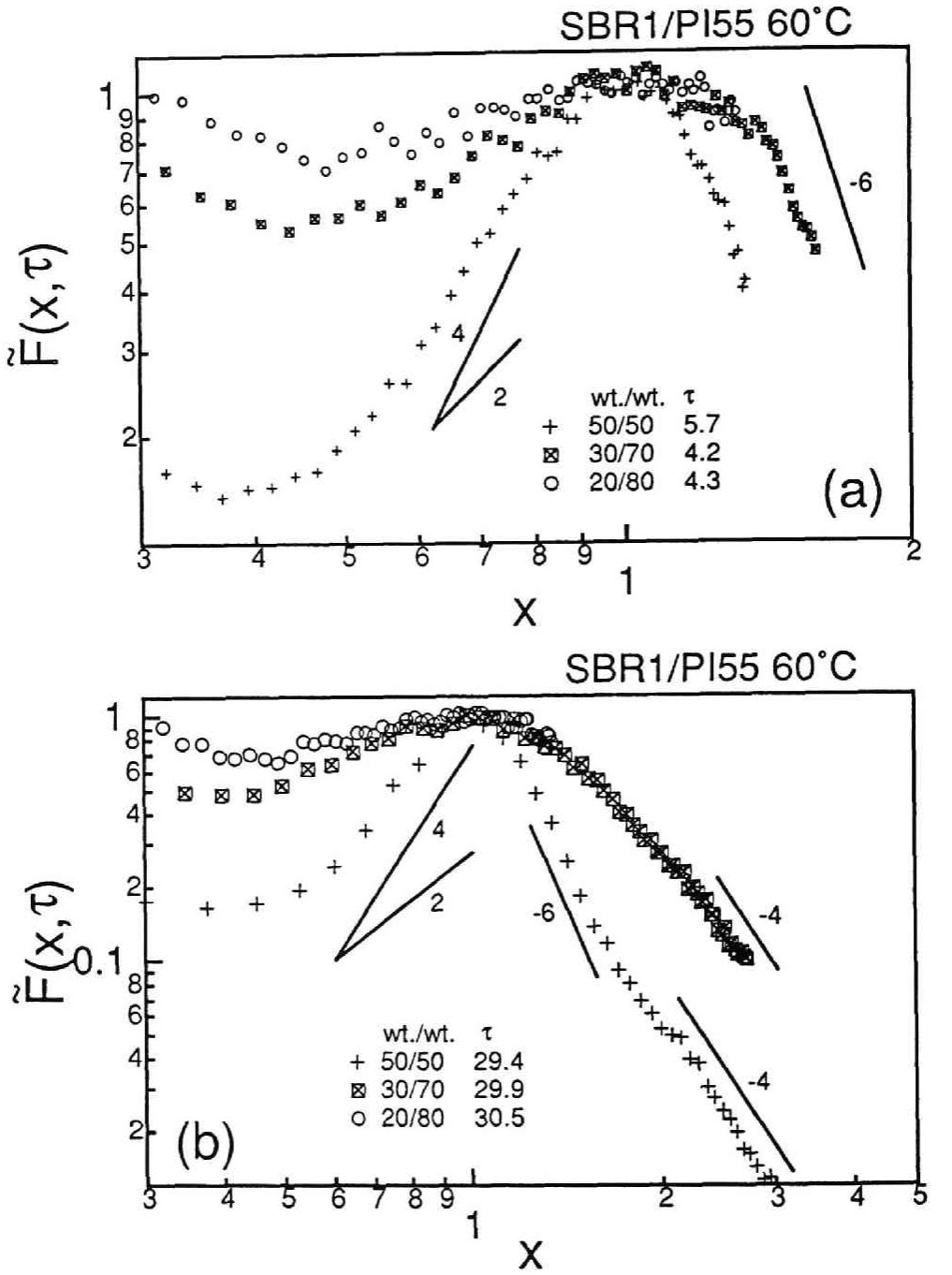

Figure 6-8 Composition dependence of the scaled structure factor for SBR1/PI55 mixtures at 60°C in double logarithmic scale. (a) and (b) corresponds to about τ=5 and τ=30, respectively.

$$\tilde{F}(x,\tau) \sim x^{-6}. \qquad (6.20)$$

According to Furukawa's theory[14] and Tomita's theory[15], the regime of the x^{-6} dependence is expected for bicontinuous percolated networks. Thus the x^{-6} dependence of $\tilde{F}(x,\tau)$ for the off-critical mixture suggests that a bicontinuous percolated network is formed in the intermediate stage of its SD process. $\tilde{F}(x,\tau)$ at $0.5<x<0.8$ is represented by

$$\tilde{F}(x,\tau) \sim x^{3.3} \quad \text{for 50/50 wt./wt.,} \qquad (6.21)$$

$$\tilde{F}(x,\tau) \sim x^{1.6} \quad \text{for 30/70 wt./wt.,} \qquad (6.22)$$

and

$$\tilde{F}(x,\tau) \sim x^{1.2} \quad \text{for 20/80 wt./wt.} \qquad (6.23)$$

With shifting the composition toward 0 or 1 at $\tau \cong 4.2$-4.3, before but close to the dynamical PC transition, the percolation network tends to be less perfect. The grain size ξ of the network ξ within which the network is percolated tends to decrease with the increasing bias of the composition. As the percolation network becomes less perfect and the grain size ξ decreases, compensation of intra-grain and inter-grain correlation of the network becomes less perfect, giving rise to an enhanced excess scattering at $q<1/\xi$. The $x^{3.3}$-dependence of the critical mixture is close to the x^4-dependence obtained theoretically by Furukawa[16] and by Yeung[17] with computer simulation. The $x^{1.6}$-dependence obtained for the off-critical mixture is not very much different from the x^2-dependence predicted theoretically by Furukawa.[14]

In Fig.6-8(b), we compare $\tilde{F}(x,\tau)$ at $\tau \simeq 30$ for the off-critical mixture and the critical mixture; $\tau=30$ corresponds to the pinning stage [Fig.6-6(c)] for the off-critical mixture and the late stage for the critical mixture. $\tilde{F}(x,\tau)$ at $1<x$ for the critical mixture is expressed by

$$\tilde{F}(x,\tau) \sim x^{-6} \qquad \text{for } 1.0 < x < 1.8 \tag{624}$$

and

$$\tilde{F}(x,\tau) \sim x^{-4} \qquad \text{for } 1.8 < x. \tag{6.25}$$

On the basis of Tomita's theory[15] we proposed that the change in the x-dependence from Eq.(6.24) to (6.25) is due to the spatial crossover from the tangled to the smooth interface.[11,12] The Porod regime[18] is realized for $x > x_c = q_c/q_m$, where $q_c \cong 1/R_m$, is the mean interfacial curvature. A shoulder appears at $x \cong 2$ which may be due to the formation of local lamellae.[11,12] On the other hand, $\tilde{F}(x,\tau)$ for the off-critical mixtures in the regime $1 < x$ is given by

$$\tilde{F}(x,\tau) \sim x^{-3} \qquad \text{for } 1.0 < x < 2.2 \tag{6.26}$$

and

$$\tilde{F}(x,\tau) \sim x^{-4} \qquad \text{for } 2.2 < x. \tag{6.27}$$

The x^{-3} dependence reflects the correlation of the cluster-cluster separation and the x^{-4}-dependence characterizes the Porod regime.[18] The behavior of $\tilde{F}(x,\tau)$ for $x<1$ is almost the same as that at $\tau=4.7$ for both the critical mixture and the off-critical mixtures. For the latter, the large length scale concentration fluctuations of the order of ξ are generated in the earlier stage of $\tau \cong 4.2$-4.3 and they persist up to a later stage of $\tau \cong 30$.

6-4-1-2. SBR1/PB19

Figures 6-9 and 6-10 show time changes in F(x,t) at 50°C for the critical mixture SBR1/PB19 58/42 wt./wt. and for the off-critical mixture SBR1/PI55 25/75 wt./wt., respectively. The time change in F(x,t) for the critical mixture is again divided into two regions : the intermediate stage ($72.8 < t < 200.9$ min. or $4.8 < \tau < 13.1$) corresponds to Fig.6-9(a) and the late stage ($200.8 < t$ or $13.1 < \tau$) corresponds to Fig.6-9(b), which shows behavior is similar to that of

SBR1/PI55 50/50 wt./wt. These time changes in F(x,t) are consistent with the previous results[1] with respect to the relation between α and β, Eqs.(6.7) and (6.8), respectively.

The time change in F(x,t) for the off-critical mixture in the later-stage SD is divided into two stages : transition and pinning as shown in Fig.6-10. In the transition stage, $97.2 < t < 208.0$ min. or $4.7 < \tau < 10.0$ (Fig.6-10(a)), the broadening of $\overline{F}(x,t)$ causes F(x,t) to broaden with time and the relationship between α and β approximately obeys Eq.(6.16). This tendency is the same as that observed in the transition stage of SBR1/PI55 30/70 wt./wt. The intermediate and late stages are not observed for SBR1/PB19 25/75 wt./wt., differing from SBR1/PI55 30/70 wt./wt. The difference may be attributed to the broadening of $\overline{F}(x,t)$ that dominates the increase in $\langle \eta(t,T)^2 \rangle$ even at early times in the intermediate stage.

In the pinning stage, 208.0 min. $< t$ or $10.0 < \tau$, corresponding to Fig. 6-9 (b), the coarsening stops and α is zero.[1] Here, F(x,t) is independent of time for $208.0 < t < 1106.0$ min. or $10.0 < \tau < 53.1$. The observable reduced time for SBR1/PB19 25/75 wt./wt., i.e. τ=53.1 was smaller than τ= 77.1 at which F(x,t) for SBR1/PI55 30/70 wt./wt.[Fig.6-6(d)] started to increase. If we measured up to the reduced time larger than 53.1, we would observe the increase in F(x,t) even for SBR1/PB19 25/75 wt./wt.

Figure 6-11 compares $\widetilde{F}(x,\tau)$ at 50°C for SBR1/PB19 25/75 wt./wt. with that for SBR1/PB19 58/42 wt./wt. Similar to SBR1/PI55, the scaled structure factor for each of these off-critical mixtures is broader than that for the critical mixture.

In Fig.6-11(a), the comparison is made at about τ=7.5 , corresponding to the intermediate stage and the transition stage for the critical and off-critical mixtures, respectively. The behavior of $\widetilde{F}(x,\tau)$ for the critical mixture at high x is expressed by Eq.(6.20), which is similar to that of SBR1/PI55 50/50 wt./wt. On the other hand, the high x behavior of the off-critical mixtures is fitted by

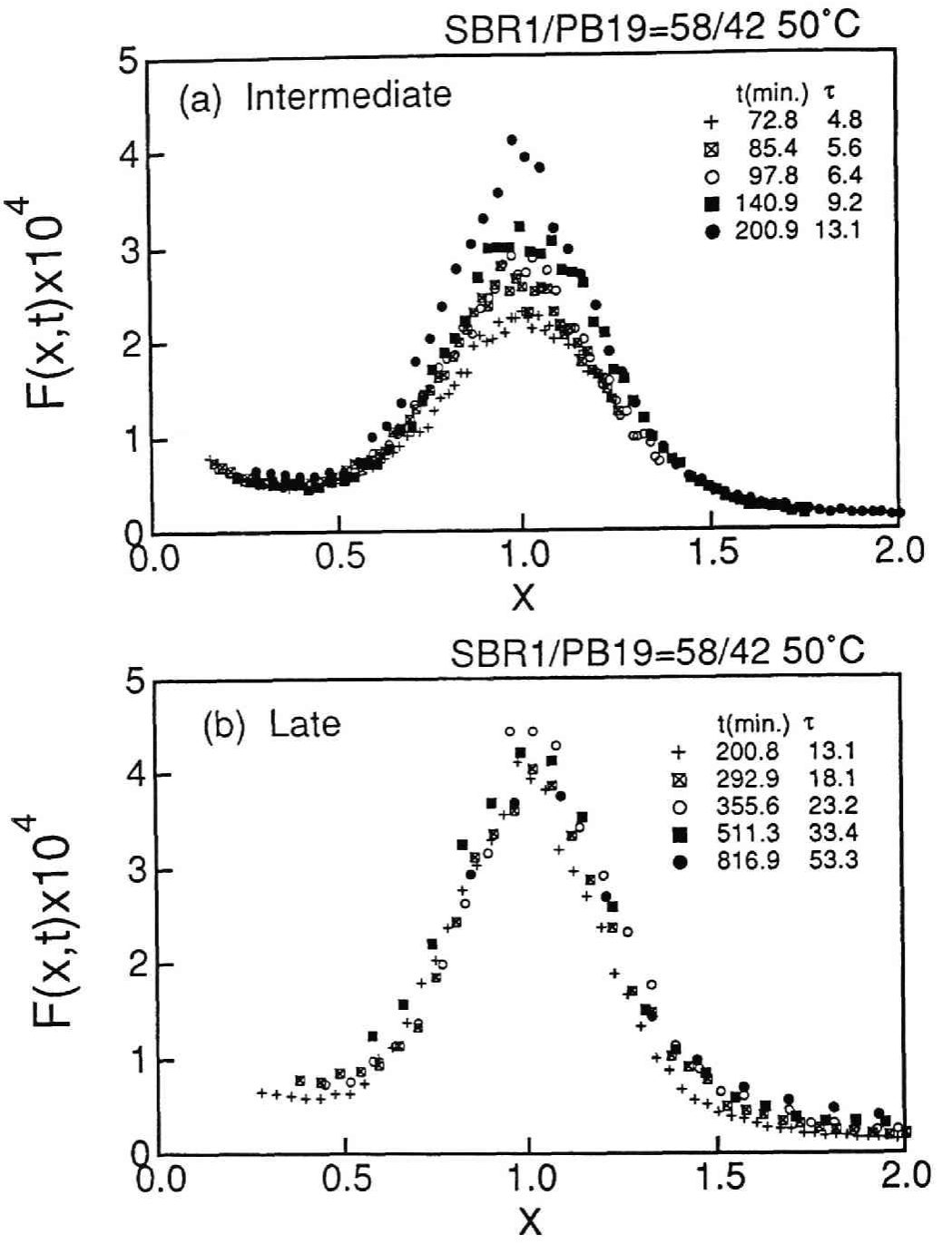

Figure 6-9 Scaled structure factor for SBR1/PB19 58/42 wt./wt. at 50°C in the intermediate stage (a) and the late stage (b).

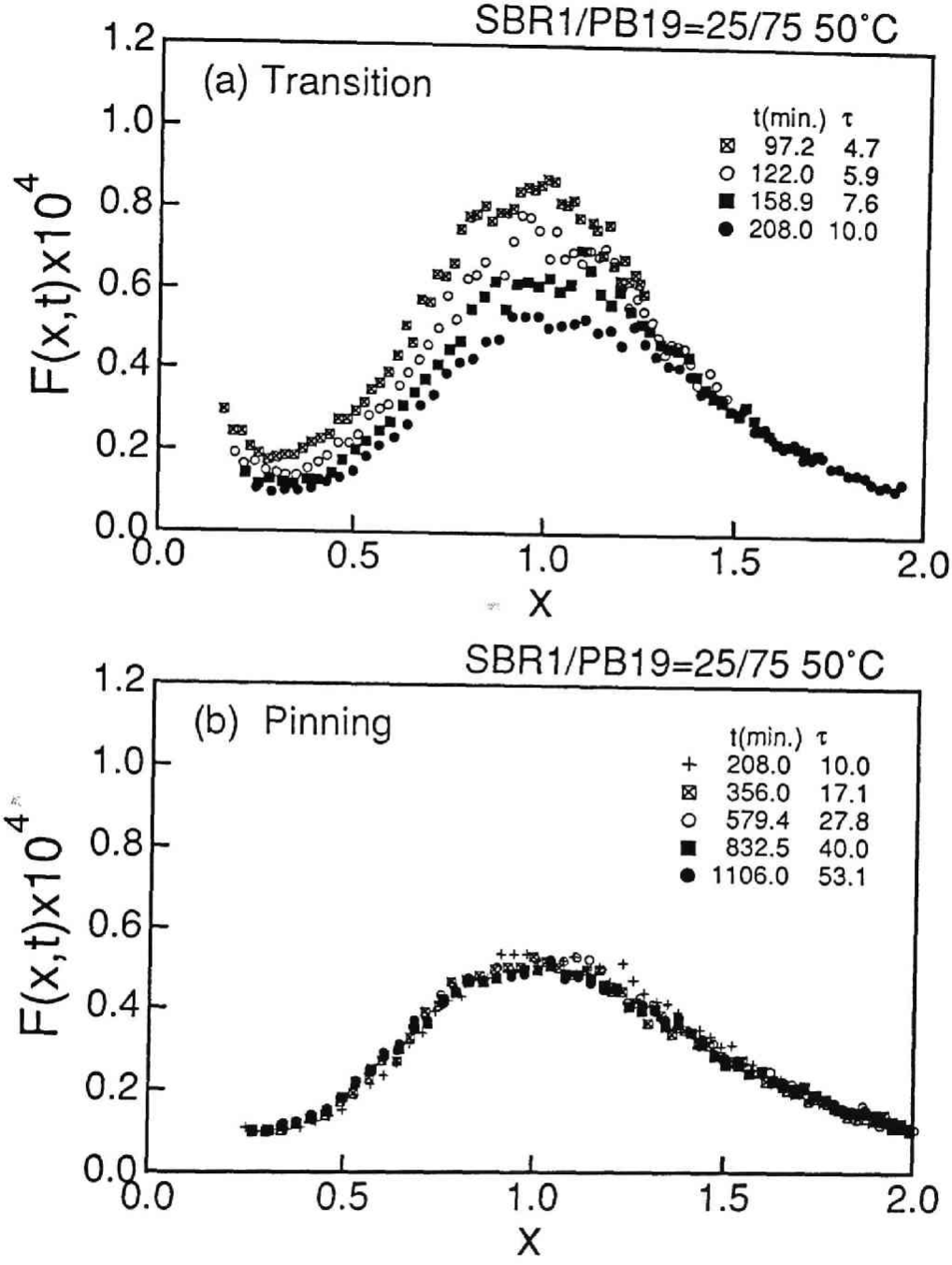

Figure 6-10 Scaled structure factor for SBR1/PB19 25/75 wt./wt. at 50°C in the transition stage (a) and the pinning stage (b).

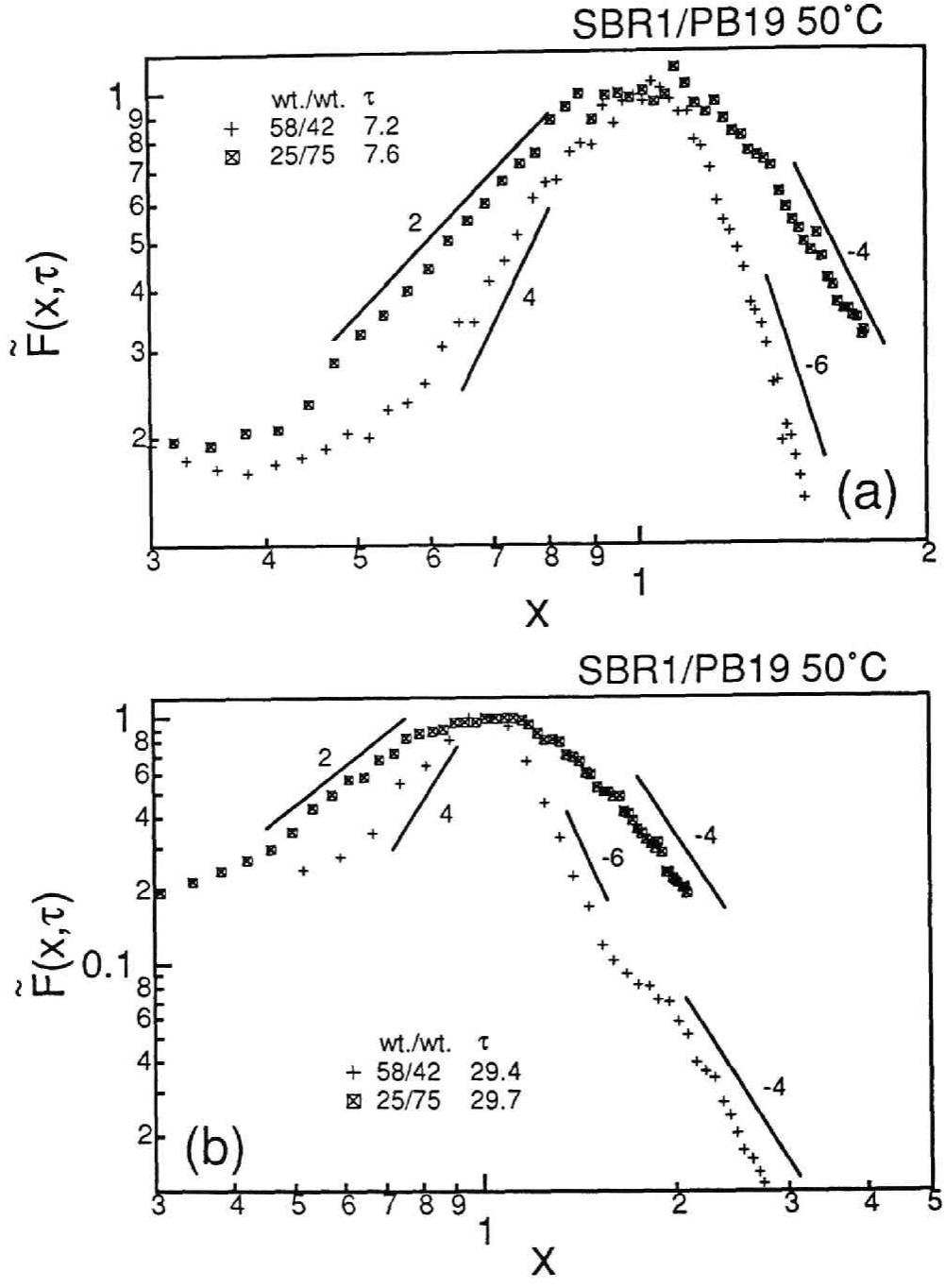

Figure 6-11 Composition dependence of the scaled structure factor for SBR1/PB19 25/75 wt./wt. at 50°C in double logarithmic scale. (a) and (b) corresponds to about τ=7 and τ=30, respectively.

$$\tilde{F}(x,\tau) \sim x^{-4}, \qquad (6.28)$$

which is different from that for SBR1/PI55 30/70 wt./wt. mixtures [Fig.6-8(a)]. The difference results from the difference in the time scale of observation. τ=4.2 for SBR1/PI55 30/70 wt./wt. in Fig.6-8(a) corresponds to the late stage, where the phase-separated structure still keeps bicontinuous network. On the other hand, τ=7.6 for SBR1/PB19 25/75 wt./wt. in Fig.6-11(a) corresponds to the transition stage where most of the bicontinuous network has already been broken into the clusters as result of the dynamical PC transition. The x-dependence of $\tilde{F}(x,\tau)$ for x<1 for the critical mixture is fitted by

$$\tilde{F}(x,\tau) \sim x^{4}, \qquad (6.29)$$

which agrees with Furukawa's result[16] and Yeung's one.[17] $\tilde{F}(x,\tau)$ for x<1 for the off-critical mixture is fitted by

$$\tilde{F}(x,\tau) \sim x^{2} \qquad (6.30)$$

which also agrees with Furukawa's theory.[14]

In Fig.6-11(b), the comparison is made at about τ=30, corresponding to the late stage and the pinning stage for the critical and off-critical mixtures, respectively. The behavior of $\tilde{F}(x,\tau)$ for the critical mixture in the region 1 < x is characterized by Eqs.(6.24) and (6.25). It is found that the spatial crossover from the x^{-6} to x^{-4} dependence is similar to that observed with SBR1/PI55 50/50 wt./wt. The behavior of $\tilde{F}(x,\tau)$ for the off-critical mixture is fitted by

$$\tilde{F}(x,\tau) \sim x^{-3.3} \qquad \text{for } 1.0<x<1.6 \qquad (6.31)$$

and

$$\tilde{F}(x,\tau) \sim x^{-4} \qquad \text{for } 1.6 < x, \tag{6.32}$$

which is similar to that for SBR1/PI55 30/70 wt./wt.. The behavior of $\tilde{F}(x,\tau)$ for $x<1$ at τ =30 are almost the same as those at τ=7.2 for 58/42 wt./wt and, τ=7.6 for 25/75 wt./wt.

6-4-2. Temperature dependence of the scaled structure factor

Figure 6-12 shows $\tilde{F}(x,\tau)$ at $t/t_p(T)$= 15 for the off-critical mixture SBR1/PI55 30/70 wt./wt. at 60, 90 and 120 °C, where $t_p(T)$ is the pinning time defined in our previous paper,[1] i.e., the time at which the spontaneous pinning occurs. $\tilde{F}(x,\tau)$ at various temperatures show the following common features: (i) $\tilde{F}(x,\tau)$ for $x<1$ has the $x^{1.6}$ dependence and (ii) $\tilde{F}(x,\tau)$ at the high x-limit exhibits the x^{-4} dependence. However, the upturn of $\tilde{F}(x,\tau)$ at the low x limit becomes more marked with increasing temperature. Its origin is large length scale concentration fluctuations comparable in size to ξ discussed in sec. 6-4-1-1. The excess scattering increases with increasing T. SBR1/PI55 has a UCST phase diagram, so that the volume fraction of the cluster phase decreases with increasing temperature. This decrease enhances large length scale concentration fluctuations. In other words, the osmotic compressibility associated with the number density fluctuations of clusters increases.

Figure 6-13 shows $\tilde{F}(x,\tau)$ at $t/t_p(T)$ = 3.2 for the off-critical mixture SBR1/PB19 25/75 wt./wt. at 50, 60, 70 and 110°C. The accessible q-range was too limited to observe the behavior of $\tilde{F}(x,\tau)$ in the high x region at 60,70 and 110°C because the coarsening is pinned down at a high value of q_m. However, $\tilde{F}(x,\tau)$ even at the low x limit is independent of temperature, differing from the case of SBR1/PI55 30/70 wt./wt.

6-4-3. Time change in the interfacial structure due to the dynamical PC transition

The dynamical PC transition affects the interfacial structure or the scaled structure factor for $1<x<2$. As mentioned above, Furukawa predicted that the

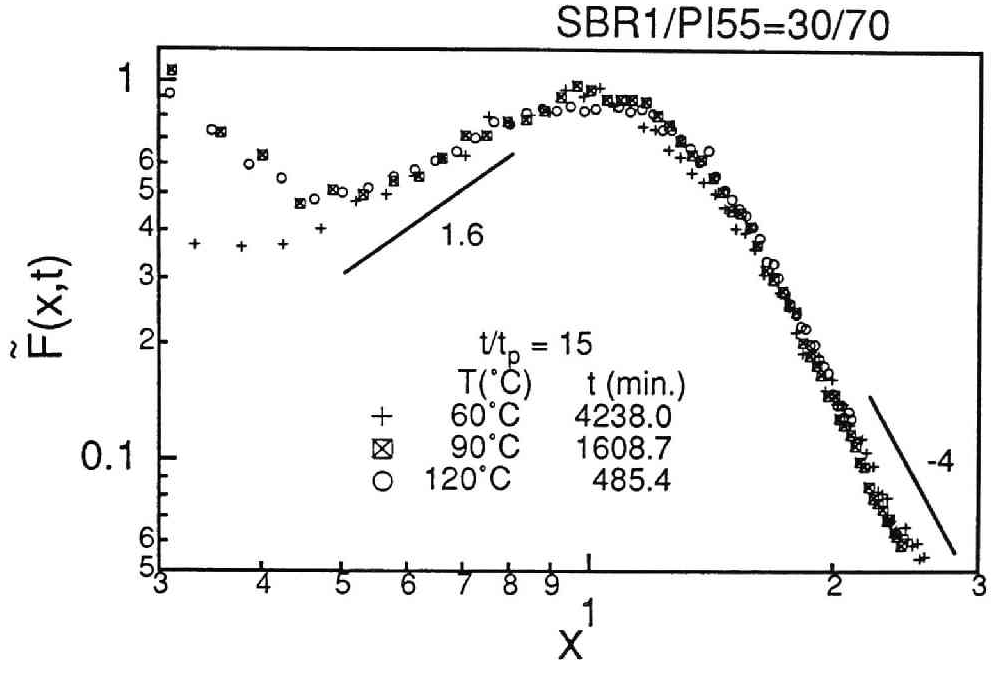

Figure 6-12 Temperature dependence of the scaled structure factor at $t/t_p(T)$ = 15 for SBR1/PI55 30/70 wt./wt. at 60, 90 and 120°C.

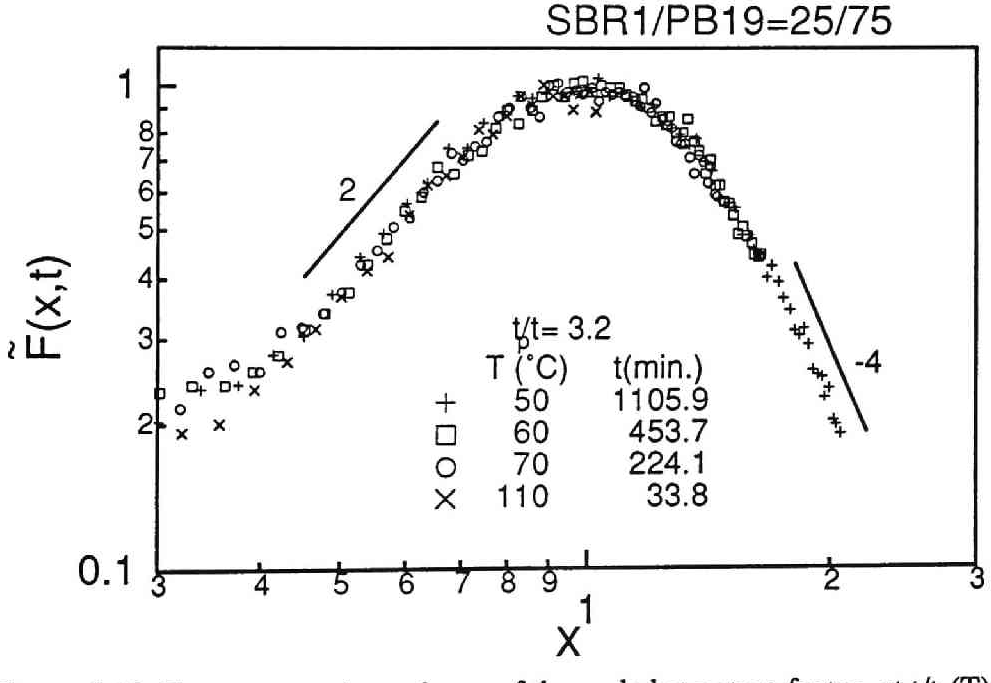

Figure 6-13 Temperature dependence of the scaled structure factor at $t/t_p(T)$ = 3.2 for SBR1/PB19 25/75 wt./wt. at 50,60, 90 and 110°C.

scaled structure factor in this range of x is proportional to x^{-6} for the percolated structure and to x^{-4} for the cluster structure. Here we consider how the interfacial structure changes with time owing to the dynamical PC transition before the pinning stage.

Figure 6-14 shows the time change in $F(x,\tau)$ for $1.0<x$ for the off-critical mixture SBR1/PI55 30/70 wt./wt. at 60°C in the transition stage. $F(x,\tau)$ in this x range is described by

$$F(x,\tau) \sim x^{-n} \tag{6.33}$$

with n decreasing from 6.0 to 3.3 with time, as shown in Fig.6-15(b). Figure 6-15(a) shows the time change in $q_m(t)$ and Fig.6-15(b) also shows the time variation of the exponent m in $F(x,\tau)\sim x^m$ for $0.5<x<0.8$. The values of m are about 1.6 at all stages but those of n change with time, decreasing from 6.0 to 3.3 in the transition stage. This change in n is caused by progress of the dynamical PC transition which produces isolated clusters and broadens the distribution of the intercluster separation. The broader this distribution, the broader the scattering intensity distribution and hence the smaller n becomes. Thus in the transition stage the x^{-6}-dependence of $F(x,\tau)$ which reflects the tangled interface of the bicontinuous percolated network changes to the $x^{-3.3}$-dependence which reflects the distribution of intercluster distance as the dynamical PC transition proceeds. In this stage (84 min. < t < 300 min.), the mean curvature q_c of the interface is still so large that the spatial crossover[11] from $F(x,\tau) \sim x^{-n}$ (n= 6 to 3.3) relevant to the phase-separated domains as a whole to $F(x,\tau) \sim x^{-4}$ relevant to the interfacial structure (Porod's law) occurs at a large value of x equal to $x_c \equiv q_c/q_m(t;T)$. Therefore the Porod's law can not be discerned in the region of x covered in this experiment ($1<x<2.6$) but should rather be found in the region of x greater than 2.6. As time elapses, especially in the late period of the pinning stage (200 min.< t < 4300 min.), however, q_c

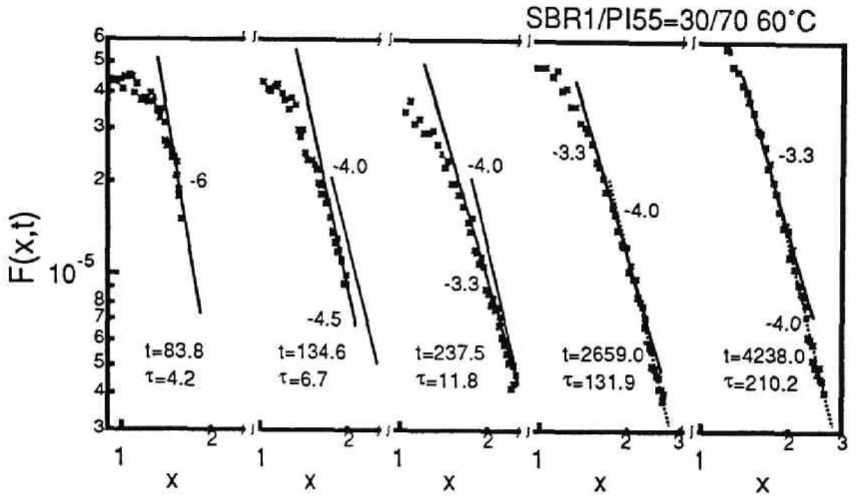

Figure 14 Time change in $F(x,\tau)$ for $1.0 < x < 3.0$ for SBR1/PI55 30/70 wt./wt. at 60°C in double logarithmic scale.

or x_c above which the Porod's law can be observed becomes so small that the Porod's law region x comes within our window of observation, i.e., for $2<x<3$. This explains the value n which decreases to about 3.3 in the transition stage and remains unchanged during the early period of the pinning stage comes back to 4 in the late period of the pinning stage [see Fig.6-15(b)].

Figure 6-16(a) and (b) show the time change in $q_m(t)$ and those in n and m, respectively, for the critical mixture SBR1/PI55 50/50 wt./wt. at 60°C. The values of n and m are almost constant 6.0 and 3.3 respectively, suggesting that the bicontinuous percolation network is formed even in the intermediate stage in which concentration fluctuation are not yet to reach equilibrium. In the late time of the late stage, both n and m decreases and these phenomenon can be attributed to the appearance of a higher order shoulder at x=2 and the zero order scattering, i.e., the excess scattering at $q<1/\xi$, as discussed in sec. IV-A-1, respectively.

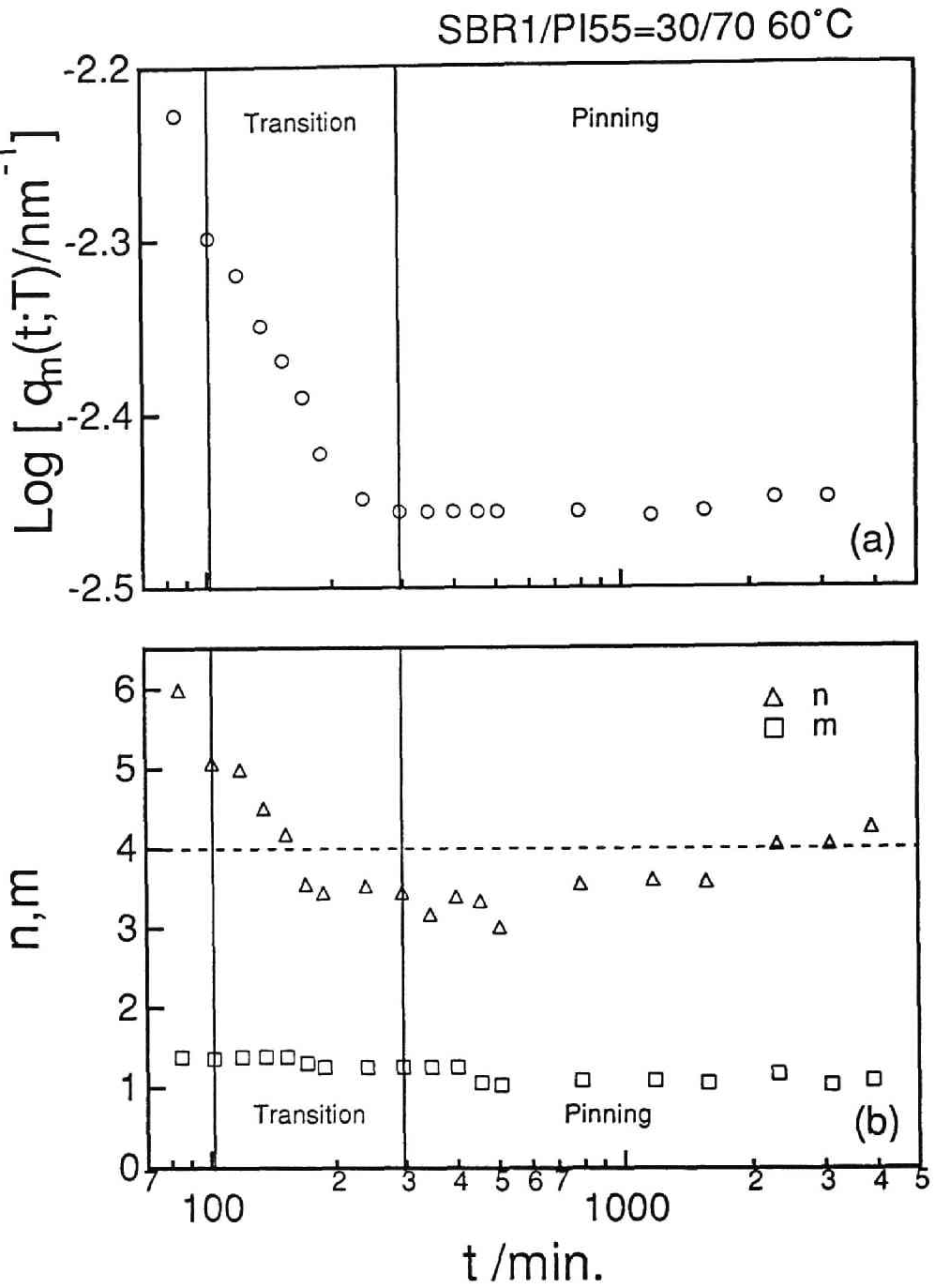

Figure 6-15 Time changes in $q_m(t)$ (a) and n,m (b) for SBR1/PI55 30/70 wt./wt. at 60°C in double logarithmic scale.

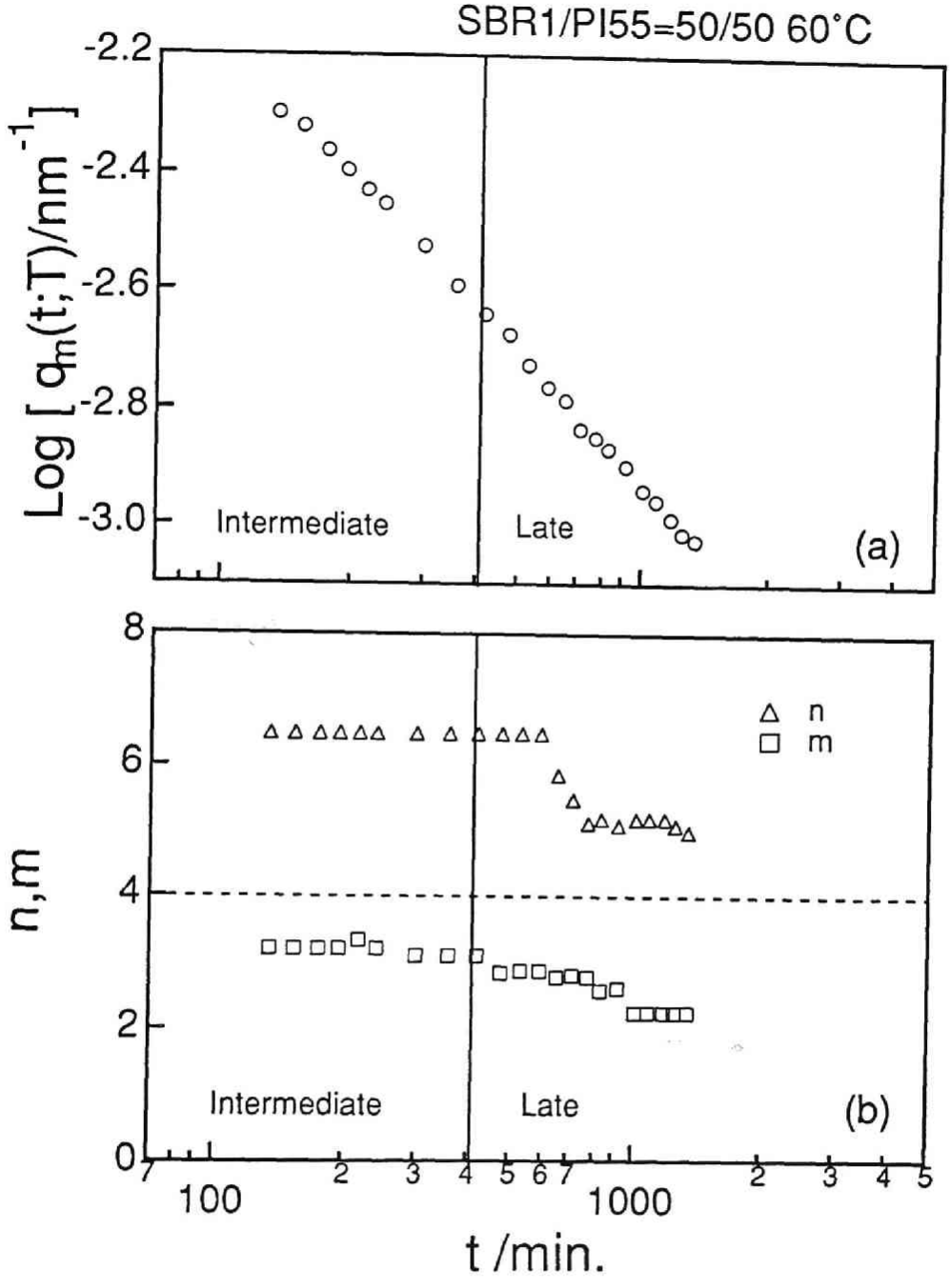

Figure 16 Time changes in $q_m(t)$ (a) and n,m (b) for SBR1/PI55 50/50 wt./wt. at 60°C in double logarithmic scale.

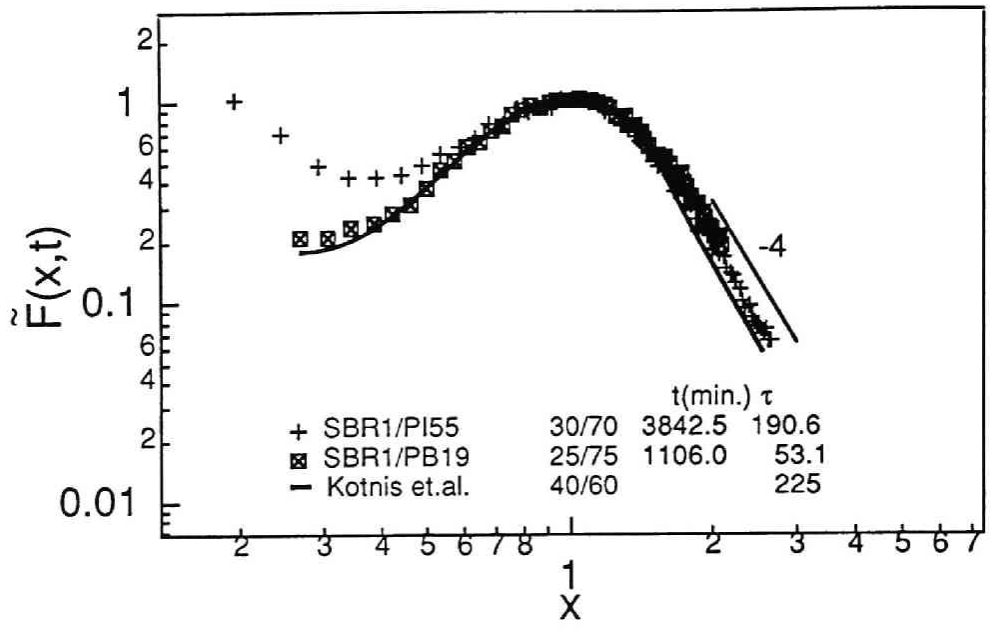

Figure 6-17 Comparison between our experimental scaled structure factors and Kotnis et.al.'s .

6-4-4. Comparison with the scaled structure factors obtained by computer simulation

From computer simulations with Flory-Huggins-de Gennes free energy functional, Kotnis et.al.[2] have found the transnodal region in the phase diagram of a symmetric polymer mixture at an off-critical composition. i.e., the region where the coarsening process is suppressed owing to an entropic barrier for chain transport across the interface. In Figure 6-17, our $\tilde{F}(x,\tau)$ for SBR1/PI55 30/70 wt./wt. at 60°C at t= 3842.5 min. or τ= 190.6 and for SBR1/PB19 25/75 wt./wt. at 50°C and t= 1106.0 min. τ= 53.1 are compared with $\tilde{F}(x,\tau)$ in the pinning stage (τ=225) obtained by Kotnis et.al. The initial composition ϕ_0 and the phase separated temperature T which they used are 0.4 and 35°C, respectively. This temperature corresponds to a quench depth 27K. Although their phase separation condition and the systems are different from ours, our $\tilde{F}(x,\tau)$ is quite similar to one of Kotnis et.al. at τ=225. They[2] also showed the real space image of the scaled structure factor at ϕ_0=0.4 and T=35°C, which is

that of isolated clusters at τ=200 (see Fig.6b in ref.2). Unfortunately they did not show $F(x,\tau)$ at τ=2, where we observed a percolated network.

6-5. Conclusion

Unmixing processes via spinodal decomposition (SD) in off-critical mixtures SBR1/PI55 and SBR1/PB19 were investigated as a function of temperature and the composition of SBR by applying the time-resolved light scattering method.

From analyses of the scaled structure factor F(x,t), the SD process for the off-critical mixture SBR1/PI55 30/70 wt./wt. was found to consists of the five stages: *early, intermediate, late, transition, and pinning*. The dynamics of the early stage SD can be approximated by Cahn's linearized theory as discussed in our previous paper. In the intermediate stage, the scaled structure factor F(x,t) increases with time and the relationship between α and β is given by $\beta>3\alpha$. In the late stage SD, the scaled structure factor F(x,t) becomes invariant with time and $\beta=3\alpha$ holds. The crossover from the intermediate to the late stage for the off-critical mixtures occurs as a result of cancellation between the increase in $\langle\eta(t,T)^2\rangle$ and the broadening in $\overline{F}(x,t)$ and hence the decreasing in $\overline{F}(x,t)$ at x=1. The latter results from the dynamical percolation-to-cluster (PC) transition. In the transition stage, the contribution of $\overline{F}(x,t)$ to F(x,t) becomes important owing to this transition. Thus, F(x,t) at x=1 decreases but $\langle\eta(t,T)^2\rangle$ remains to be the constant value $\langle\eta(T)^2\rangle_e$ independent of t, the relationship between α and β becomes $\beta<3\alpha$ and the power to x in F(x,t) for 1<x decreases. In the pinning stage, the coarsening process stops and α becomes zero, In its early stage, F(x,t) remains unchanged but in its late stage F(x,t) at x=1 increases and sharpens with increasing time. The increase in F(x,t) arises from the change in the cluster shape (Fig.6-7) and from the equilibration of the composition fluctuation, while the sharpening in F(x,t) arises from the change in the distribution function of the cluster-cluster separation.

The SD process for the off-critical mixture SBR1/PB19=25/75 wt./wt. is classified into three stages: *early*, *transition* and *pinning*. Since the contribution of the broadening of $\overline{F}(x,t)$ to F(x,t) becomes significant even at early times of the intermediate stage, we were unable to observe such intermediate and late stages as found previously.[8-12]

The asymmetry in the volume fraction of the two phases increases with either increasing temperature or shifting the initial composition toward 0 or 1, and generates large scale fluctuations. The excess scattering due to such fluctuations becomes dominant, giving rise to a marked upturn of F(x,t) with decreasing x toward 0 for $x<0.5$. The upturn was composition-dependent, but its the temperature dependence was not clear enough to be observed for both SBR1/PI55 30/70 wt./wt. and SBR1/PB19 25/75 wt./wt.

References

1 T.Hashimoto, M.Takenaka and T.Izumitani, J.Chem.Phys. in press; M.Takenaka, K.Tanaka and T.Hashimoto, in "Contemporary Topics in Polymer Sicence, vol.6 Mlultiphase Macromolecular Systems," B.M. Culberston, Ed., Plenum, N.Y. 1989.

2 M.A.Kotnis and M.Muthukumar, Macromolecues **25**, 1716(1992).

3 T. Hashimoto, T. Izumitani and M. Takenaka, Macromolecules **22**, 2293 (1989).

4 T.Hashimoto, J.Kumaki and H.Kawai, Macromolecules **16**, 641 (1983).

5 J. W. Cahn, J.Chem.Phys. **42**, 93 (1965).

6 P. G. de Gennes, J.Chem.Phys. **72**, 4756 (1980).

7 K. Binder, J.Chem.Phys. **79**, 6387 (1983).

8 T. Hashimoto, M. Itakura and H. Hasegawa, J.Chem.Phys. **85**, 6118 (1986).

9 T. Hashimoto, M. Itakura and N. Shimidzu, J.Chem.Phys. **85**, 6773 (1986).

10 T. Izumitani, M. Takenaka and T. Hashimoto, J.Chem.Phys. **92**, 3213 (1990)

11 M. Takenaka, T. Izumitani and T. Hashimoto, J.Chem.Phys. **92**, 4566 (1990).

12 T. Hashimoto, M. Takenaka and H. Jinnai, J.Apply.Cryst. **24**, (1991).

13 F.Zernike and J.A. Prins, Z.Pysik, **41**, 184(1927).

14 H. Furukawa, Physica A **123**, 497 (1984).

15 H.Tomita, Progr. Theor. Phys. Progr. Lett. **72**,656 (1984); Progr. Theor. Phys. **75**, 482 (1986).

16 H. Furukawa, Phys.Rev.B **40**, 2341 (1989); J.Phys.Soc.Jpn. **58**, 216 (1989).

17 C. Yeung, Phys.Rev.Lett. **61**, 1135 (1988).

18 G. Porod, Koll. Z.,**124**,83(1951); ibid,**125**,51(1952); ibid,**125**,108(1952).

Summary

In chapter 1 structure self-assembling in the spinodal decomposition (SD) of polymer blends in its late stage was explored for a near critical mixture of polybutadiene (PB) and polyisoprene (PI) by a time-resolved light scattering technique, with a particular emphasis on the time-evolution of the interface structure. By analyzing a scaled structure factor $F(x,t)\equiv I(q,t)q_m(t)^3$ over wide ranges of a reduced scattering vectors $x \equiv q/q_m(t)$ and time, it was found relevant to divide the late stage of SD into two stages, I and II. Here, I(q,t) denotes the scattered intensity as a function of the scattering vector q and time t. In the intermediate stage preceding the late one, F(x,t) became sharper with its peak at x=1 increasing with t. However, as time elapsed, F(x,t) turned to be universal for t, first in the range of x smaller than about 2 and then over the entire range of x accessible by the present experiment. The time interval in which the former occurred is defined as the late stage I, and the one in which the latter was realized called the late stage II. In the late stage I, the average thickness of phase-phase interfaces decreases toward an equilibrium value and the time-evolution of the interfacial area density $\Sigma(t)$ does not scale with $q_m(t)$, i.e., the exponents γ and α in the power laws $\Sigma(t) \sim t^{-\gamma}$ and $q_m(t) \sim t^{-\alpha}$ do not coincide (actually, $\alpha < \gamma$). The late stage II corresponds to the process in which these exponents become equal and the interface thickness reaches equilibrium. Such conditions probably ensure SD the establishment of a complete dynamical scaling law.

In chapter 2 the studies in chapter 1 on time-evolution of the interfacial structure for a critical mixture of PB and PI undergoing SD was extended to explore the behavior as a function of T again using the time-resolved light scattering method. The study involved the investigation of the time-evolutions of various characteristic parameters such as the wavenumber $q_m(t;T)$ of the dominant mode of the concentration fluctuations, the maximum scattered

intensity $I_m(t;T)$, the scaled structure factor $F(x,t)$, the interfacial area density $\Sigma(t;T)$, and the characteristic interfacial thickness $t_I(t;T)$ from the early-to-late stage, SD where t refers to time after the onset of SD and x refers to the reduced scattering vector defined by $x = q/q_m(t;T)$; q is the magnitude of the scattering vector. The results confirm the model previously proposed at a given T over a wider temperature range corresponding to the quench depth $\Delta T = T - T_s = 5.5$ to 34.5 K or $\varepsilon_T = (\chi-\chi_s)/\chi_s = 4.50\times10^{-2}$ to 2.79×10^{-1} where T_s is the spinodal temperature, and χ and χ_s are the Flory interaction parameter at T and T_s, respectively.

In chapter 3 the early stage of the spinodal decomposition of binary polymer mixtures of PI and styrene-butadiene random copolymer (SBR) at a composition of 50/50 wt/wt was studied by time-resolved light scattering as a function of molecular weight of SBR at 60°C, which is well above the glass transition temperature of both components, thus the two components being in liquid state. The early stage of the spinodal decomposition of the mixtures was found to be described with a good approximation by the linearized theory of Cahn, the analyses of which yielded characteristic parameters for the early stage of the spinodal decomposition. The parameter $q_m(0)^2/D_{app}$ shows the molecular weight dependence of M^1 at the high molecular weight limit, supporting that the decomposition involves mutual diffusion of center-of-mass of polymer molecules via reptation ($q_m(0)$ is the wavenumber of the dominant mode of the fluctuations, and D_{app} is the mutual diffusivity of the mixture).

In chapter 4 the unmixing process via spinodal decomposition of SBR/PI mixtures was investigated by the time-resolved light scattering method to see how it is affected by the temperature of phase separation T and by the molecular weight of PI with that of SBR fixed. Time changes in $q_m(t;T)$ and $I_m(t;T)$ were followed to explore the coarsening process in the later stage of spinodal decomposition. For each mixture the observed changes at different T were reduced to a master curve when plotted against a reduced time τ. This

finding is consistent with the Chou-Goldburg scaling postulate. The master curves for mixtures with different PI molecular weights were divergent, showing the phenomenon called the N branch. However, it was possible to bring them to a master curve when τ was multiplied by a shift factor depending on the average number of entanglements per chain. The dependence was weaker than that predicted theoretically by Onuki.

In chapter 5 SD of off-critical mixtures of SBR with PI or PB was investigated as a function of the composition w of the mixtures and of the phase separation temperature T by time-resolved light scattering. The coarsening behavior of the mixtures was characterized in terms of the time change in the maximum intensity $I_m(t;T)$ and that in the magnitude of the scattering vector $q_m(t;T)$ at which the intensity becomes maximum. It was found that the time changes of $I_m(t;T)$ and $q_m(t;T)$ for the off-critical mixtures studied here are effectively pinned at a certain time defined here as the "pinning" time. This spontaneous pinning of the growth of the unmixing structure was found to occur earlier when w is biased toward 0 or 1 at a given T and when the phase separation temperature is raised at a given w, for these systems which seemingly have upper critical solution temperature behavior.

In chapter 6 the later-stage SD of off-critical mixtures of SBR/PI or SBR/PB was investigated by the time-resolved light scattering method. Time changes in the scaled structure factor F(x,t) were determined as a function of the composition w of the mixture and of the phase separation temperature T. It was found that the later-stage SD for the off-critical mixture is divided into four stages : intermediate, late, transition and pinning. The time change in the interfacial structure of the phase-separated structure showed that the dynamical percolation-to-cluster transition occurs before the pinning stage.

List of Publications

1. "Slow Spinodal Decomposition in Binary Liquid Mixtures of Polymers. 2. Effects of Molecular Weight and Transport Mechanizm", Macromolecules **20**, 2257(1987)
   Coauthors: T.Hashimoto and T.Izumitani
   (Chapter3)

2. "Sharp scaled structure factor observed for late stage spinodal decomposition of polymer mixtures", Polymer Commun.**30**,45(1989)
   Coauthors: T.Hashimoto and T.Izumitani
   (not included in the dissertation)

3. "Morphology control of polymer blends by a chemical pinning of spinodal decomposition", Polymer Commun. **30**, 177(1989)
   Coauthors: T.Hashimoto and H.Jinnai
   (not included in the dissertation)

3. "Homogenization of Immiscible Rubber/Rubber Polymer Mixtures by Uniaxial Compression", Macromolecules, **22**, 2293(1989)
   Coauthors: T.Hashimoto and T.Izumitani
   (not included in the dissertation)

4. "Mechanism and Ordering Process of Polymer Blends at Phase Transition", Contemporary Topics in POLYMER SCIENCE, Vol.6, 363(1989)
   Coauthors: T.Hashimoto and Kyozi Tanaka
   (related to Chapters 5 and 6)

5. "Time Change in the Maximum of Scattering Intensity during Spinodal Decomposition", Macromolecules **22**,4663(1989)
Coauthors: H,Fujita and T.Hashimoto
(not included in the dissertation)

6. "Slow Spinodal Decomposition in Binary Liquid Mixtures of Polymers. III. Scaling analyses of later-stage unmixing", J.Chem.Phys.**92,** 3213(1990)
Coauthors: T.Hashimoto and T.Izumitani
(not included in the dissertation)

7. "Slow Spinodal Decomposition in Binary Liquid Mixtures of Polymers. IV. Scaled Structure Factor for later-stage unmixing", J.Chem.Phys. **92**, 4566(1990)
Coauthors: T.Hashimoto and T.Izumitani
(not included in the dissertation)

9. "Small-Angle Neutron Scattering and Light Scattering Studies on the Miscibility of Protonated Polyisoprene/Deuterated Polybutadiene Blends", Macromolecules **24**, 1813(1991)
Coauthors: T.Hashimoto, C.C.Han, H.Hasegawa, S.Sakurai
(not included in the dissertation)

10. "Scattering Studies of Self-Assembling Processes of Polymer Blends in Spinodal Decomposition", J.Appl.Cryst. **24**, 457(1991)
Coauthors: T.Hashimoto and H.Jinnai
(Chapter 1)

11. "Scattering studies of self-assembling processes of polymer blends in spinodal decomposition. II. Temperature dependence", J.Chem.Phys. **96**, 6177(1992)
Coauthors: T.Hashimoto
(Chapter 2)

12. "Slow Spinodal Decomposition in Binary Liquid Mixtures of Polymers. V. Molecular Weight dependence in the later-stage unmixing", J.Chem.Phys. in press
Coauthors: T.Hashimoto and T.Izumitani
(Chapter 4)

13. "Spontaneous Pinning of Domain Growth during Spinodal Decomposition of Off-Critical Polymer Mixtures", J.Chem.Phys. in press
Coauthors: T.Hashimoto and T.Izumitani
(Chapter 5)

13. "Spontaneous Pinning of Domain Growth during Spinodal Decomposition of Off-Critical Polymer Mixtures. II. Scaling Analysis", J.Chem.Phys. in press
Coauthors: T.Hashimoto and T.Izumitani
(Chapter 6)

14. "Dynamics and Self-Organization of Polymer Mixtures at Phase Transition" Kobunshi **38**, 882(1989)
Coauthor: T.Hashimoto
(not included in the dissertation)

15 "Interface of Polymer Blends and Its Time-evolution in Phase Separation Process" Kobunshi **41**, 330(1992)
Coauthor: T.Hashimoto
(related to Chapter 1)

16. "SANS Studies of Phase Separation Process in Polymer Mixtures" BUTSURI, **46**, 1032(1991)
Coauthor: T.Hashimoto
(not included in the dissertation)

17. "Soshiki-Keiseiron" in "Kouseinou Polymer Alloy", J.Furukawa. ed., Chapter 4, **83**(1991)
Coauthor: T.Hashimoto
(not included in the dissertation)

18. "Self-Diffusion of Block Copolymer Chains in Lamellar Microdomains and Disordered Melts" Macromolecules, in press.
Coauthors: T.Hashimoto and D.Ehlich
(not included in the dissertation)

19. "Direct determination of anisotropic diffusion in a bulk block copolymer by FRS", Macromolecules, in press.
Coauthors: T.Hashimoto and D.Ehlich
(not included in the dissertation)

20. "Molecuar Weight Dependence of the Mobility in Polymer Blends" Polymer, in press.
Coauthors: Yi. Feng, C.C.Han and T.Hashimoto
(not included in the dissertation)

Acknowledgements

The present thesis is based upon the study carried out under the auspices of Professor Sueo Kawabata, at the Department of Polymer Chemistry, Faculty of Engineering, Kyoto University, from 1986 to 1992.

The author wishes to express his sincere gratitude to Professor Sueo Kawabata for his continuous interest and encouragement throughout the study.

He also wishes to express his thanks to Professor Takeji Hashimoto, at Department of Polymer Chemistry, Faculty of Engineering, Kyoto University, for his constant guidance, encouragement, valuable suggestions and comments in the course of the study.

He wishes to express his thanks to Mr. Tatsuo Izumitani, Daicel co. Ltd., for his valuable suggestions, discussions and collaborations.

Thanks are also due to Professor Kyozi Kawasaki, Dr. Toshihiro Kawakatsu and Mr. Tsuyoshi Koga, the Department of Physics, Kyusyu University, Kyusyu, and Mr. Hiroshi Jinnai, Department of Polymer Chemistry, Faculty of Engineering, Kyoto University, for their valuable discussions and collaboration.

He acknowledges to Drs. Hirokazu Hasegawa, Shoji Suehiro, Mr. Kenji Saijo Miss Akemi Nakai for useful suggestions and co-operation.

He acknowledges also to Drs. Hideaki Tanaka, Tomoaki Takebe and Shinichi Sakurai for valuable comments and help.

Finally, the author express his heartfelt thanks to his parents Michio Takenaka and Sumako Takenaka, and his wife Yoshiko Takenaka, for their care and constant encouragements during the study.

November, 1992 Mikihito Takenaka